Fluctuations and Phase Transitions in Quantum Ising Systems

by

Ryan McKenzie

B.Sc. Math and Physics Honours, The University of British Columbia, 2008

A THESIS SUBMITTED IN PARTIAL FULFILLMENT
OF THE REQUIREMENTS FOR THE DEGREE OF

Doctor of Philosophy

in

THE FACULTY OF GRADUATE AND POSTDOCTORAL STUDIES
(Physics and Astronomy)

The University of British Columbia
(Vancouver)

August 2016

Abstract

The quantum Ising model is perhaps the simplest possible model of a quantum magnetic material. Despite its simplicity, its versatility and wide range of applications, from quantum computation, to combinatorial optimization, to biophysics, make it one of the most important models of modern physics. In this thesis, we develop a general framework for studying quantum Ising systems with an arbitrary single ion Hamiltonian, with emphasis on the effects of quantum fluctuations, and the quantum phase transition between paramagnetic and ferromagnetic states that occurs when a magnetic field is applied transverse to the easy axis of the system.

The magnetic insulating crystal $LiHoF_4$ is a physical realization of the quantum Ising model, with the additional features that the dominant coupling between spins is the long range dipolar interaction, and each electronic spin is strongly coupled to a nuclear degree of freedom. These nuclear degrees of freedom constitute a spin bath environment acting on the system. In this thesis, we present an effective low temperature Hamiltonian for $LiHoF_4$ that incorporates both these features, and we analyze the effects of the nuclear spin bath on the system. We find the lowest energy crystal field excitation in the system is gapped at the quantum critical point by the presence of the nuclear spins, with spectral weight being transferred down to a lower energy electronuclear mode that fully softens to zero at the quantum critical point. Furthermore, we present a toy model, the spin half spin half model, that illustrates the effects of an anisotropic hyperfine interaction on a quantum Ising system. We find the critical transverse field is increased when the longitudinal hyperfine coupling is dominant, as well as an enhancement of both the longitudinal electronic susceptibility and an applied longitudinal field.

In addition, we present a field theoretic formalism for incorporating the effects of fluctuations beyond the random phase approximation in general quantum Ising systems. We find that any regular on site interaction, such as a nuclear spin bath, does not fundamentally alter the critical properties of a quantum Ising system. This formalism is used to calculate corrections to the magnetization of $LiHoF_4$.

Preface

In this thesis, we study fluctuations and phase transitions in quantum Ising systems, of which the fascinating magnetic material $LiHoF_4$ is a particular example. The study of $LiHoF_4$, in particular, the study of the effect the nuclear degrees of freedom have on the system, was suggested by Dr. Philip Stamp. All the research carried out in this thesis, and the tools developed for that purpose, are the work of the author.

Table of Contents

List of Tables

List of Figures

Acknowledgments

I would like to acknowledge the support of my thesis supervisor, Dr. Philip Stamp. His breadth of knowledge is remarkable. I would also like to thank the friends and family, too numerous to name, who have helped and supported me over the years.

Dedication

This thesis is dedicated to my mother, whose love and support have made my life possible.

Chapter 1

Introduction

Magnetic materials have a venerable history. They were of interest to Thales, often considered the first known philosopher, in the 6th century BC. However, according to Aristotle, Thales believed a magnet's ability to attract iron filings was due to its soul [1]. Although magnets were put to practical use as compass needles as early as 1000AD, there was little improvement in the understanding of magnetism for over two millennia. This changed during the scientific revolution, starting in 1600 with the publication of William Gilbert's book, *De Magnete*. This book is remarkable for its reliance on empiricism, and for Gilbert's contempt for some of the established beliefs of his time. Gilbert looked for truth "in things themselves," rather than relying on the beliefs of his predecessors. The magnetic field of the earth is perhaps the best known of Gilbert's discoveries [2].

Over the following centuries, many of the world's best scientists developed the theory of electricity and magnetism, and shed light on the connection between the two, relying on experiment to be their guide. This culminated with the publication of the electromagnetic field equations of James Clerk Maxwell in 1873. These equations explained light as an electromagnetic phenomenon, a discovery that was fully illuminated by Einstein's special theory of relativity at the start of the 20th century. Despite the success of Maxwell's electromagnetic theory, an understanding of magnetic materials remained elusive.

In the early part of the 19th Century, André-Marie Ampere, building on Hans Christian Oersted's discovery in 1820 that a current carrying wire could deflect a compass needle, proposed that the magnetic properties of materials may be due to continually flowing microscopic electric currents inside the material [2]. In the latter part of the 19th century, through experiments, Pierre Curie deduced that each atom in certain magnetic materials (paramagnets) that lack a spontaneous magnetization, behaves like a little magnet whose orientation may be altered by an applied magnetic field, or, the collective behaviour of which, may be altered by a change in temperature. This led Pierre Weiss to propose that in certain materials with a permanent mag-

netization (ferromagnets) there was an internal field responsible for aligning each little magnet. However, at the time, there was no known mechanism that could produce the field necessary in most materials. In 1926, the quantum mechanical exchange interaction was discovered by Heisenberg and Dirac [3, 4]. This interaction proved to be typically responsible for the dominant interactions between the atomic magnetic moments in magnetic materials, and is strong enough to account for the fields observed in a ferromagnet. Although the exchange interaction is the dominant interaction in most magnetic materials, there exist exceptions. In magnetic materials where the electrons are tightly bound to their host atoms, the exchange interaction will be weak. In this case, the dominant interaction may be the dipole-dipole interaction between the magnetic moments at each atomic site. This thesis will deal with a material in which dipolar interactions are dominant, viz., the magnetic insulating crystal $LiHoF_4$.

Weiss' mean field (MF) approximation, in which each atomic magnet, or spin (the magnetic moment of a particle is proportional to its intrinsic quantum property of spin), responds to the average field produced by all other spins in the material, is of primary importance in the study of magnetic materials because, at a qualitative level, it produces many of the features of a magnetic substance, such as the phase diagram, the magnetization, and the susceptibility. In order to obtain quantitative agreement between theory and experiment, or to understand the behaviour of a magnetic system as it undergoes a phase transition, it is often necessary to go beyond MF theory. Much of this thesis will be devoted to systematically determining corrections to the MF approximation.

The simplest correction to MF theory is known as the Gaussian approximation, or equivalently, the random phase approximation (RPA). As discussed in many textbooks, for example [5], phenomenological Landau theory involves writing down an energy functional for the magnetization of a system

$$L = \int d^3\vec{r}\left[\mathscr{L}[M(\vec{r})] + \frac{\gamma}{2}(\nabla M(\vec{r}))^2\right], \tag{1.1}$$

where $\mathscr{L}[M(\vec{r})]$ is a function of the magnetization, and the gradient term represents the energy cost of the spatial variation of the magnetization. In the MF approximation, we assume $M(\vec{r}) = M$ is constant, and minimize $\mathscr{L}(M)$ to find the mean field. In the Gaussian approximation, we expand $\mathscr{L}[M(\vec{r})]$ for small $M(\vec{r})$, and truncate at quadratic order. The free energy of the system may then be calculated from

$$F = -\beta \ln\left(\int \mathscr{D}M(\vec{r})\; e^{-\beta L}\right), \tag{1.2}$$

where β is the inverse temperature, and $\int \mathscr{D}M(\vec{r})$ denotes a functional integral is to be per-

formed over every configuration of the magnetization. In this thesis we will use $\int \mathscr{D}x$ to denote a functional integral, and we will use $\int dx$ to denote ordinary integration. The Gaussian approximation allows for a system to fluctuate around its MF; however, these fluctuations are treated as non-interacting. In this thesis, we will rigorously derive equations such as (1.2), starting from a microscopic model, and we will systematically determine corrections to the Gaussian approximation.

The Ising model, in its simplest guise, is a microscopic model of a magnetic material in which the spins are arranged on a lattice, and each spin may only point up or down. There is an energy associated with every configuration of the spins depending on the interaction energy between neighbours. This is perhaps the simplest possible microscopic model of a magnetic material. The model was given to Ising, by Lenz, in an attempt to better understand ferromagnetism and phase transitions. Ising solved the model in one dimension in his 1924 thesis, and found no evidence of a phase transition to a ferromagnetic state. He concluded that this held true in higher dimensions; however, this was shown to be false by an argument made by Peierls [6]. Peierls divided a two dimensional square lattice into postive and negative regions corresponding to spin up and spin down. He then showed that at a low enough temperature the area encapsulated by one region may be smaller than the area encapsulated by the opposite region, which leads to the conclusion there will be an excess of one spin or another. In 1944, a rigorous solution to a two dimensional Ising model was published by Onsager [7]. This solution clearly showed a transition from a paramagnetic to a ferromagnetic state at a critical temperature T_c, and showed the specific heat of the system is divergent at the critical point in the thermodynamic limit, i.e., there is a continuous phase transition. The deceptively simple Ising model is able to exhibit complex behaviour.

The Ising model will be a central topic of this thesis. However, we will not be concerned with the classical Ising model discussed above, in which each spin points up or down $S^z \in \{1,-1\}$. Instead, we will be concerned with the quantum Ising model in which we promote S^z to a quantum spin operator. In, for example, a transverse magnetic field, this allows for spins to be in a superposition of states. At low temperatures ($T \sim 1K$), the magnetic insulating crystal $LiHoF_4$ is a physical realization of the quantum Ising model. The anisotropy of the system is a result of the crystal electric field, due to the surrounding ions (the ligands), that mixes and splits the $J = 8$ electronic multiplet of the holmium ion. In the absence of an applied magnetic field, spectroscopy and susceptibility experiments find a degenerate ground state separated from the first excited state by a gap of around $11K$ [8–10]. $LiHoF_4$ has the additional feature that the observed ferromagnetic order stems from the dominant dipolar interaction between the electronic spins, rather than the exchange interaction. Furthermore, each Ho^{3+} ion is strongly coupled to its spin $I = \frac{7}{2}$ nucleus [11]. The interaction between the electronic and nuclear

degrees of freedom is known as the hyperfine interaction, and is of primary interest in this thesis.

In this thesis, we will focus on $LiHoF_4$. However, we note that many of the procedures carried out on the $LiHoF_4$ Hamiltonian, and the tools developed for the study of the system, are applicable to the rest of the $LiReF_4$ series (Re=rare earth), and to other quantum Ising systems. Large single crystals of materials in the $LiReF_4$ series (of very high quality in the case of $LiHoF_4$) can be grown from a melt, making them well suited for research [12]. The $LiReF_4$ series displays a range of interesting behaviour. Both $LiHoF_4$ and $LiTbF_4$ are dipolar coupled Ising ferromagnets; however, in $LiTbF_4$ the lowest two MF energy levels are gapped even in zero transverse field and the hyperfine interaction is roughly half as strong as in $LiHoF_4$ [13, 14]. The material $LiErF_4$ is a dipolar coupled XY antiferromagnet [15]. The rare earth elements in $LiReF_4$ compounds may be mixed, or replaced by non-magnetic yttrium, leading to interesting spin glass behaviour [16], in which the magnetic moments freeze in a random manner.

The dipolar coupling between spins caused a great deal of early interest in $LiHoF_4$, as the upper critical dimension (the dimension above which there is MF critical behaviour) of a dipolar coupled Ising system is three, whereas in an exchange coupled system the upper critical dimension is four. The properties of a magnetic system near a phase transition obey power laws because of the scale invariance of the underlying theory. For example, the magnetization of an Ising system varies as $m \sim (T_c - T)^\beta$ for $T < T_c$. Above the critical dimension, this behaviour may be understood using Landau MF theory, in which case we find $\beta = \frac{1}{2}$; below the critical dimension, fluctuations play a key role. The renormalization group provides a method for systematically determining the effect of fluctuations, and can be used to determine critical exponents such as β [5]. A system at its critical dimension is known as marginal.

In 1969, Larkin and Khmel'nitzkii showed that a dipolar coupled Ising system in three dimensions is expected to have MF critical exponents with logarithmic corrections [17]. Renormalization group calculations later established this as the marginal critical behaviour of such systems [18–20]. In the thermodynamic limit, the Fourier transform of the longitudinal dipolar interaction (the dipole wave sum) in the long wavelength limit has the form

$$D_k = D_0 + a_1 \frac{k_z^2}{k^2} + a_2 k^2 + a_3 k_z^2 + \cdots , \tag{1.3}$$

where the coefficients depend on details of the underlying lattice, and, due to the nature of the long range dipolar interaction, the zero momentum summation depends on the sample shape. The a_1 term in the dipole wave sum is not well defined in the zero momentum limit. This ambiguity is removed if a finite sized sample is considered, in which case the dipole wave sum

becomes

$$D_k = D_0 + \widetilde{a}_2 k^2 + \widetilde{a}_3 k_z^2 + \cdots \tag{1.4}$$

It is the a_1 term in equation (1.3) that leads to the dipolar fixed point, with logarithmic corrections to MF critical behaviour, in a renormalization group treatment of a dipolar coupled system. Carrying out renormalization on a term that is not well defined in the long wavelength limit seems like a questionable procedure, nevertheless, the dipolar fixed point has been observed in experiments [21].

In 1978, Beauvillain *et al.* investigated the critical behaviour of the dipolar coupled material $LiHoF_4$ using magnetic susceptibility measurements; however, they were unable to differentiate between MF critical behaviour and the logarithmic corrections expected at the marginal dimension [22]. Magnetization measurements made by Griffin *et al.* in 1980 definitively showed evidence for the logarithmic corrections to MF behaviour [23]. The marginality of the critical behaviour of $LiHoF_4$ is reviewed in a 2001 paper of Nikkel and Ellman, in which they present further evidence for marginality based on specific heat measurements [21].

It is the marginal critical behaviour that sparked early interest in $LiHoF_4$; however, in this thesis, our focus won't be on the marginal critical behaviour due to the dipolar interaction, rather, we will concern ourselves with $LiHoF_4$'s other main feature, the coupling to the nuclear degrees of freedom. Furthermore, we will be primarily interested in $LiHoF_4$ in an applied transverse magnetic field that splits the degenerate ground state.

The degenerate ground state doublet of $LiHoF_4$ may be split by the application of a magnetic field transverse to the easy axis of the crystal, making $LiHoF_4$ a physical realization of the transverse field quantum Ising model (TFIM). This model was introduced by de Gennes in 1963 to account for protons tunneling between two different states in the ferroelectric phase of KH_2PO_4, and is discussed in a somewhat more general context in a 1966 paper of Brout *et al.* [24, 25]. The TFIM has a wide range of applicability beyond ferroelectric and ferromagnetic materials. For example, in a Jahn-Teller system spin up and spin down states may correspond to different distortions of the crystal lattice. The coupling between "spins", and the effective transverse field, are due to the crystal electric field of the system. For a list of real systems to which the TFIM model can be applied see [26]. A transverse field applied to a quantum Ising system is able to destroy the ordered phase of the system at any temperature. At zero temperature, a transverse magnetic field of about $4.9T$ applied to $LiHoF_4$ is able to destroy the ferromagnetic order of the system in a quantum phase transition [27].

A quantum phase transition (QPT) is a zero temperature phase transitions driven by quantum fluctuations between competing quantum ground states, whose energy depends on some

control parameter such as magnetic field, pressure, or doping. These differ from classical phase transitions, which are driven by thermal fluctuations. In a classical system the kinetic and potential parts of the Hamiltonian, $H(p,q) = H_{kin}(p) + H_{pot}(q)$, commute (we use p and q to represent the three dimensional momenta and positions of all N particles in the system). This means that static thermodynamic properties of a classical system, which follow from the partition function

$$Z_{classical} = \frac{1}{N!} \int dp e^{-\beta H_{kin}(p)} \int dq e^{-\beta H_{pot}(q)}, \tag{1.5}$$

may be studied without considering the dynamics. In a quantum system the kinetic and potential parts of the Hamiltonian are operators that might not commute. Therefore, the dynamical behaviour of the system must be included when studying its static thermodynamic properties. This is an essential part of the study of QPTs.

Phase transitions are generally classified as either first order, or continuous. In a first order transition, such as the transition between water and ice, the two phases may coexist at the transition point. In a continuous phase transition, this ceases to be the case. The ferromagnetic to paramagnetic transition of the TFIM is an example of such a transition. The study of continuous QPTs is interesting, as they are prevalent in nature, occurring in materials such as high T_c superconductors, and heavy fermion systems, and the effects of a QPT on the properties of a material extend to regions of the phase diagram away from the quantum critical point [28–30]. The TFIM is perhaps the simplest system that undergoes a continuous QPT.

A system that undergoes a continuous phase transition can often be characterized by an order parameter. An order parameter is a thermodynamic quantity that is non-zero in one phase, and zero in the other. For example, the longitudinal magnetization serves as an order parameter in the ferromagnetic to paramagnetic transition of the TFIM. Close to a critical point, spatial correlations between fluctuations of the order parameter are characterized by the correlation length ξ, which diverges at the critical point. Likewise, temporal fluctuations are characterized by a correlation time ξ_τ. The correlation time is related to the correlation length by $\xi_\tau = \xi^z$. The dynamic critical exponent z follows from an anisotropy in the scaling of space and time under scale transformations (renormalization) of a system. It is model dependent, for example, the TFIM has $z = 1$, meaning that time effectively acts as an extra spatial dimension in the quantum critical regime, whereas for an itinerant antiferromagnet $z = 2$. In general, the effective dimensionality of a system near a quantum critical point will be $d_{eff} = d + z$, with the additional dimensions stemming from temporal fluctuations. For more details on the dynamic critical exponent and the effective dimensionality of a system near a quantum critical point, see the original work of Hertz [31].

The partition function of the TFIM at zero temperature has been mapped to a classical model in one higher dimension by Suzuki [32]. This is an explicit example of the shift in effective dimensionality of a quantum system due to temporal fluctuations. More generally, we may write the partition function of a quantum system as

$$Z = \int \mathscr{D}M(\vec{r},\tau) \exp\left(- \int d\vec{r} \int_0^{\hbar\beta} d\tau \, \mathscr{L}[M(\vec{r},\tau)] \right), \tag{1.6}$$

where $\mathscr{L}[M(\vec{r},\tau)]$ is the Lagrangian of the (fluctuating) order parameter of the system. We work with imaginary time $\tau = it$. Written in this way, it appears that time manifests itself in the quantum partition function as an additional dimension with a domain determined by β, the inverse temperature. This is misleading because under renormalization space and time might not scale isotropically leading to a dynamical critical exponent $z \neq 1$. Suzuki's mapping clearly demonstrates that for the TFIM the dynamic critical exponent is $z = 1$. The transverse Ising system $LiHoF_4$ also has $z = 1$; however, the complicated single ion Hamiltonian make an explicit mapping to a higher dimensional classical system impracticable, and it is necessary to deal with the quantum Hamiltonian.

Despite the fact that temporal fluctuations in a quantum system effectively manifest themselves as additional spatial dimensions, with $d_{eff} = d + z$, QPTs are of fundamental interest because their behaviour can be qualitatively different from that of their classical counterparts. There are many reasons for this. For example, in a system with random disorder in space, the disorder will be infinitely correlated in time. Typically, this causes the effects of disorder to be stronger in quantum systems. See the book of Sachdev for further discussion of this point [28]. Another example, discussed in the reviews of Vojta, Belitz and Kirkpatrick [29, 33, 34], is that the presence of soft modes in a quantum system (not including the order parameter fluctuations) may fundamentally alter its critical behaviour. This is due to long range dynamical interactions between the order parameter fluctuations not necessarily present in classical systems.

In $LiHoF_4$, where the upper critical dimension of the classical phase transition is three, we expect MF critical behaviour in the quantum regime where, due to the quantum to classical correspondence, the effective dimensionality is four. Such behaviour is observed in the 1996 susceptibility measurements of Bitko *et al.*, where the quantum regime is accessed by varying the transverse field near zero temperature [27]. In this thesis, we will investigate the effect of the nuclear degrees of freedom on this QPT.

Bitko *et al.* note that, due to the strong hyperfine interaction, the nuclear degrees of freedom in $LiHoF_4$ have a significant impact on the system's phase diagram. At low temperatures, the hyperfine interaction stabilizes the ferromagntic phase against the effects of the transverse magnetic field [27]. The hyperfine interaction also manifests itself in specific heat measure-

ments. Each electronic eigenstate is split into eight electronuclear levels by the $I = \frac{7}{2}$ nuclear spin, and, as discussed in a 1983 paper of Mennenga *et al.*, these electronuclear degrees of freedom exhibit themselves as a Shottky type contribution (a significant increase) to the low temperature specific heat [35]. The electronic excitation spectrum of $LiHoF_4$ is also strongly affected by the hyperfine interaction. In a continuous quantum phase transition, the energy required for order parameter fluctuations is expected to soften to zero at the quantum critical point. The TFIM undergoes such a transition. In 2005, Rønnow *et al.* published neutron scattering experiments that show that what should have been the electronic soft mode in $LiHoF_4$ is gapped by the presence of the nuclear spins [36]. Although the soft mode is gapped, the longitudinal magnetization of the system, which serves as an order parameter, goes to zero continuously at the critical point, which is characteristic of a continuous phase transition. An analysis of this behaviour based on an effective low temperature Hamiltonian for $LiHoF_4$ is an important part of this thesis. Much of the physics of $LiHoF_4$ discussed so far is illustrated in Figure 1.1, taken from [36].

Our analysis of $LiHoF_4$ begins in Chapter 2, where we present the Hamiltonian of the system with a discussion of each term, and the expected domain formation in the material. We then derive a low temperature effective Hamiltonian for $LiHoF_4$ that fully incorporates the nuclear degrees of freedom. No such model exists in the literature. We find that the effective transverse magnetic field acting directly on the nuclear spins is quite large, a fact that has been overlooked by past researchers. This field originates from a shift in the $4f$ electron cloud surrounding each holmium ion due to the applied transverse magnetic field. In Chapter 3, we take the Fourier transform of the long range dipolar interaction present in $LiHoF_4$. Although our focus is not on the dipolar coupling between the electronic spins, and the resultant critical behaviour, the dipolar interaction is an important aspect of the material, so the interaction is dealt with in detail.

An alternative effective Hamiltonian for $LiHoF_4$ has been developed by Schechter and Stamp [37, 38]. In their work, a set of eight pseudospin operators are introduced to account for transitions between low energy electronuclear eigenstates. When compared to the Hamiltonian derived in this thesis, this pseudospin Hamiltonian is rather cumbersome to work with. Furthermore, the pseudospin Hamiltonian does not make clear that the hyperfine interaction leads to a significant effective transverse magnetic field that acts directly on the nuclear spins, as discussed in the previous paragraph. This field plays a crucial role in determining the behaviour of the system near its quantum critical point.

After discussing the Hamiltonian of real $LiHoF_4$ in Chapters 2 and 3, we turn to a toy model that elucidates some of the physics of quantum Ising systems coupled to nuclear degrees of freedom in Chapter 4. The toy model consists of an exchange coupled spin half Ising system,

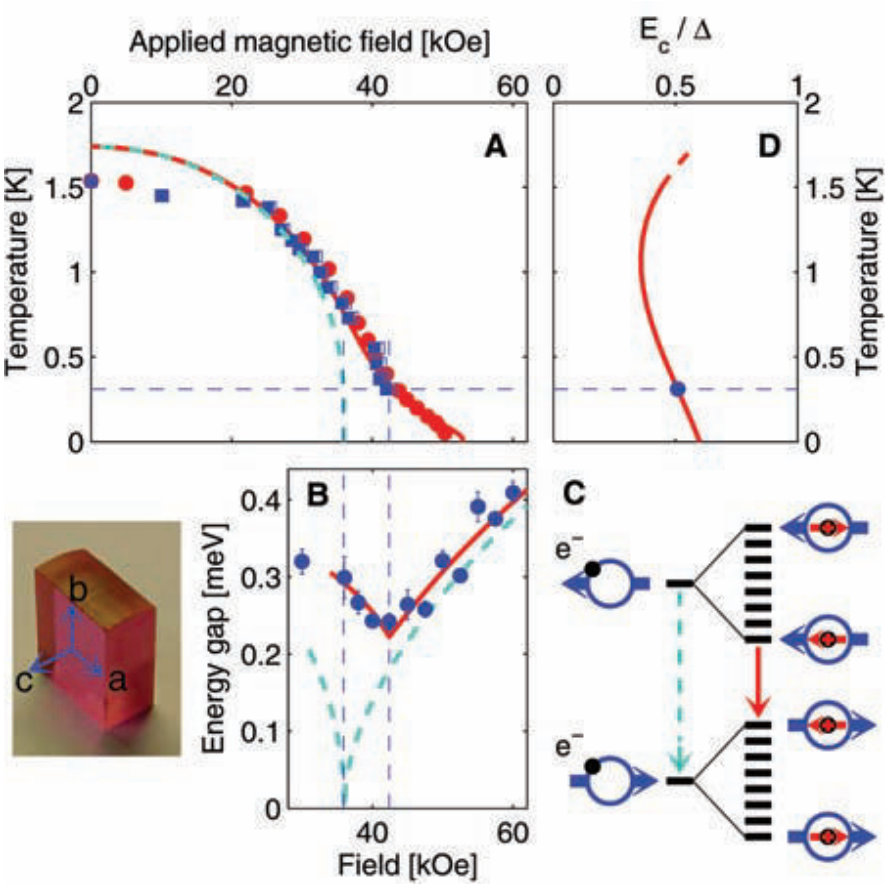

Figure 1.1: The above figure, taken from the paper of Rønnow *et al.*, illustrates many aspects of the magnetic insulating crystal $LiHoF_4$. In A, we see the phase diagram as determined by magnet susceptibility (circles) and neutron scattering (squares). At low temperatures, we see that the ferromagnetic phase is stabilized by the hyperfine interaction. In B, we see the gap in the spectrum at what would be the electronic soft mode in the absence of hyperfine interactions. The dashed line shows the soft mode in the absence of the hyperfine interaction. Diagram C is a schematic illustration of the electronic eigenstates split into multiplets by the nuclear degrees of freedom. Finally, in D, we see the ratio of the energy gap E_c shown in diagram B, to the splitting of the two lowest MF electronic energy levels (Δ), plotted as a function of temperature.

coupled to a spin half nuclear spin with an anisotropic hyperfine interaction, in the presence of a transverse magnetic field. This spin half spin half model (SHSH) shows that an anisotropic hyperfine interaction, with a dominant longitudinal component, leads to an enhancement of the longitudinal susceptibility of an Ising system, as well as an enhancement of an applied longitudinal field. Furthermore, this model clearly illustrates the gap in the electronic spectrum caused by the nuclear spins. We see that spectral weight of the gapped mode is transferred to a low energy electronuclear mode that fully softens to zero at the quantum critical point. In Chapter 5, we apply what we have learned studying the toy model to the effective low temperature Hamiltonian of $LiHoF_4$.

Above, we have introduced the quantum Ising system $LiHoF_4$, and discussed two of its key features: the dipolar interaction, and the strong coupling to the nuclear degrees of freedom. As mentioned, our primary interest in the system is due to the hyperfine interaction. This stems from the fact that the nuclear spins in $LiHoF_4$ can be viewed as a spin bath environment acting on the electronic degrees of freedom. The physics of such an environment has been elucidated in the work Prokof'ev and Stamp [39]. Early work on quantum systems coupled to environmental degrees of freedom was carried out by Feynman and Vernon in their seminal 1963 paper on influence functionals, in which they considered a quantum system coupled to an environment consisting of a bath of harmonic oscillators [40]. Performing an average over the oscillator bath degrees of freedom yields the influence functional, which encodes the effects of the environment on a quantum system. This approach was further developed by Caldeira and Leggett to make quantitative predictions about macroscopic systems of practical importance such as SQUIDs [41]. Caldeira and Leggett consider a single two state system coupled to a bath of harmonic oscillators. If all but one of the holmium ions in $LiHoF_4$ are replaced with non-magnetic yttrium ions, the resulting crystal is a physical realization of the Caldeira-Leggett model, with the oscillators being the phonons in the crystal. More accurately, as the electronic holmium spin is coupled to a nuclear spin, the model consists of a pair of interacting spins coupled to an environmental sea (PISCES). The PISCES model was considered in a 1998 paper by Dubé and Stamp [42], although, because the coupling between the nuclear spin and the phonons in a holmium ion embedded in $LiYF_4$ is very weak, it is a poor realization of the model studied in [42].

We have discussed both a spin bath environment and an oscillator bath environment. Perhaps the best way of clarifying the difference between the two is with a representative model

$$H = -\frac{J}{2}\sum_{\langle ij\rangle} S_i^z S_j^z - \Delta\sum_i S_i^x + \sum_i\sum_n A^n \vec{I}_i^n \cdot \vec{S}_i + c\sum_i S_i^z(a_i^\dagger + a_i) + \sum_k \varepsilon_k a_k^\dagger a_k. \qquad (1.7)$$

Here we consider an exchange coupled transverse Ising system, coupled at each site to addi-

tional degrees of freedom $\vec{I}$. We consider a diagonal coupling, but this does not necessarily have to be the case. The $\vec{I}$s could be nuclear spins, or they could equally well be a collection of crystal defects, or other impurities, that couple to the Ising spins. The final two terms represent a bath of harmonic oscillators (bosons) with a longitudinal coupling to each spin. Again, the coupling does not necessarily have to take this form. This bath of bosons could represent phonons in a crystal. If a set of N environmental modes is weakly coupled to the system of interest, it is possible to map them to an oscillator bath type environment consisting of delocalized modes belonging to an infinite dimensional Hilbert space. As discussed by Prokof'ev and Stamp [39], if the coupling to the environmental modes is strong (independent of the number of modes in the system), no such mapping to an oscillator bath environment is possible. These environmental modes constitute the spin bath environment $\{I_i^n\}$, each element of which belongs to a finite dimensional Hilbert space, and couples to the system in a manner independent of the number of spin bath modes.

The result of an environment acting on a quantum system is decoherence. The state of a quantum system may be specified by its wavefunction $|\Psi\rangle = \sum_i c_i|\phi_i\rangle$, with the corresponding density operator being $\widehat{\rho} = |\Psi\rangle\langle\Psi| = \sum_{ij} c_i c_j^*|\phi_i\rangle\langle\phi_j|$. Performing an average over the environmental degrees of freedom in the density matrix yields the reduced density matrix of the system alone. If the system is entangled with its environment (this means the wavefunction of the system plus the environment can't be written as a simple product $|\Psi\rangle = |\phi\rangle_{env} \otimes |\theta\rangle_{sys}$), averaging over environmental degrees of freedom causes phase relations between different components of the system to be lost. This is because the system's phase information may be distributed amongst the environmental degrees of freedom. This causes the reduced density matrix to become a mixed state obeying the laws of classical probability rather than being a pure quantum state. Decoherence lies at the heart of the quantum to classical transition and, possibly, the measurement paradox in quantum mechanics, as well as being of great practical importance for the development of quantum computation. In a quantum computation, entanglement between quantum states must be maintained long enough to carry out meaningful manipulations. Decoherence destroys this entanglement, and it is necessary to mitigate, or control, the effects of decoherence in order to carry out meaningful quantum computations.

The spin bath environment is a particularly inimical source of decoherence because it persists down to zero temperature. At zero temperature, precession of the bath spins between spin flips in the system of interest, as well as exchange of phase information between the system and the bath when a system spin flips, leads to dechorence [39]. Controlling decoherence due to a spin bath environment is essential in the effort to build a quantum computer.

Quantum annealing is a method of quantum computation that takes advantage of quantum tunneling to facilitate finding the (approximate) ground state of a system with an energy land-

scape consisting of many local minima separated by high and narrow energy barriers. In a frustrated quantum Ising model,

$$H = -\sum_{ij} V_{ij} S_i^z S_j^z, \tag{1.8}$$

there may be no single ground state consisting of an orderly arrangement of the spins. Frustration stems from V_{ij} assuming positive and negative values, or from certain underlying lattices, for example, a triangular lattice, in antiferromagnetic systems. A frustrated Ising system is often referred to as the Ising spin glass model because it may have a spin glass ground state. A frustrated quantum Ising system may have an energy landscape amenable to quantum annealing. Quantum annealing involves applying a strong transverse field to a quantum Ising system, then weakening the field so that the system can attempt to settle into its ground state. A quantum system may tunnel out of local minima in the energy landscape allowing the system to achieve its ground state faster than if energy barriers are overcome by repeatedly heating and cooling the system, as in thermal annealing. Many problems with significant practical applications, such as the traveling salesman, and the graph partition problem, can be mapped to a an Ising spin glass model [43]; however, the energy landscape of these problems does not necessarily give quantum annealing an advantage when trying to find their ground state. Finding problems with industrial significance that map to the Ising spin glass model, and have an energy landscape amenable to quantum annealing, is a major challenge facing those interested in the commercial development of the field.

Quantum annealing has received a great deal of media attention in the past several years due to the commercial development of a quantum annealer by D-Wave Systems. D-Wave artificially engineers systems with an Ising spin glass Hamiltonian by making use of superconducting flux qubits, in which the qubits (Ising spins) are superconducting loops in which the current can circulate clockwise, or counterclockwise. Recently, D-Wave has achieved the remarkable feat of linking over 1000 of these flux qubits, and the resulting quantum annealer is benchmarked in [44]. The D-Wave annealer clearly demonstrates that quantum tunneling is being utilized to find the ground state of a certain realization of the Ising spin glass model. However, due to limited connectivity between the qubits, and rapid decoherence times, it is unclear whether or not the machine will offer a practical advantage over a classical computer. A superconducting flux qubit quantum annealer with longer coherence times, and better connectivity, than the D-Wave machine is under development by John Martinis' group. Martinis hopes to have a functioning quantum annealer consisting of about 100 qubits as soon as 2017. More information can be found in the following MIT technology review article [45].

The development of a superconducting flux qubit quantum annealer is seriously hindered

by the problem of achieving high connectivity between the constituent qubits. One possibility for circumventing this difficulty is to engineer Ising spin glass systems by trapping atoms in an optical lattice. Different states of the trapped atoms serve as the Ising spins, and the interactions between the spins are mediated by phonons whose interactions can be tuned through the optical lattice [46]. Two dimensional lattices consisting of up to 350 trapped atoms have been achieved [47]. There have been recent proposals of how to make use of trapped atoms in an optical lattice as a quantum annealer to solve the number partition problem, which is a problem that maps to the Ising spin glass model, and that may have an energy landscape amenable to quantum annealing [48].

When $LiHoF_4$ is doped with non-magnetic yttrium, the frustrated nature of the long range dipolar interaction leads to an energy landscape amenable to quantum annealing. It was in $LiHo_xY_{1-x}F_4$ that, in 1999, Brooke *et al.* first demonstrated the practicality of quantum annealing [49]. The study of $LiHo_xY_{1-x}F_4$ is interesting in its own right as the system has many interesting features. For example, as discussed by Schechter, off diagonal dipolar couplings in the doped material effectively induce a longitudinal random field [50]. The critical behaviour of a dipolar coupled Ising model in the presence of a random field is discussed for Mn_{12} acetates by Millis *et al.* [51]. The Mn_{12} acetate system is quite similar to the doped $LiHoF_4$ system; however, Mn_{12} is simpler because hyperfine interactions play no role in the thermodynamics. Also, $LiHo_xY_{1-x}F_4$ will undergo a spin glass transition below a critical value of the doping of at most $x_c = 0.46$, as discussed by Reich *et al.* [52, 53]. A spin glass is a system where the spins freeze in a randomly aligned manner with a transition that may be characterized by the divergence of the non-linear susceptibility χ_3, where, expanding the magnetization about small applied fields, χ_3 is defined by $M(H) = \chi H + \chi_3 H^3 + \chi_5 H^5 + \cdots$, as discussed in a 1977 paper of Suzuki [54]. The theoretical analysis of spin glass in dilute magnetic materials such as $LiHo_xY_{1-x}F_4$ is complicated by the quenched nature of the disorder, that is, the non-magnetic impurities are not in thermodynamic equilibrium, and it is necessary to consider a set of replicas of the system, where a different realization of the disorder may be present in each replica, in order to obtain meaningful results [43]. The spin glass phase of $LiHo_xY_{1-x}F_4$ has been of particular interest because the dynamic susceptibility of dilute samples appeared to exhibit anomalous (antiglass) behaviour [55]. Evidence for this anomalous behaviour has not been borne out in more recent experiments [56]; however, the role of the nuclear spins on the dynamics of the doped system remains an interesting problem [37, 38]. A review of the physics of $LiHo_xY_{1-x}F_4$ is available in [57].

Our focus in this thesis is on fluctuations and phase transitions in quantum Ising models, rather than on decoherence and the other challenges facing the development of quantum computation, or the interesting behaviour of $LiHo_xY_{1-x}F_4$. The prevalence of quantum Ising

systems in nature make this an interesting topic in its own right, particularly when the system is coupled to additional degrees of freedom. In Chapters 2, 4, and 5, we have analyzed $LiHoF_4$, and the spin half spin half model, within the random phase approximation (RPA), thus elucidating the effects of the nuclear degrees of freedom. As mentioned in the opening paragraphs of this introduction, a goal of this thesis is to systematically determine corrections to the RPA. We do so by developing a field theoretic formalism for quantum Ising systems. The inclusion of the effects of fluctuations beyond the RPA is important for model determination, particularly in dipolar coupled systems where, due to the frustrated long range nature of the interaction, the effects of fluctuations can be significant. Furthermore, the field theoretic formalism that we develop in Chapter 6 of this thesis has a great deal of versatility, and applications beyond model determination, such as the spin glass problem discussed above, and the behaviour of systems with time dependent parameters. Future applications of the field theoretic formalism are discussed in the closing chapter of this thesis.

We develop the field theoretic formalism by making use of the well known Hubbard-Stratonovich transformation to decouple the interaction between spins in the partition function for the system. We then proceed to integrate over all the microscopic spin degrees of freedom leaving an effective theory for the Hubbard-Stratonovich field. This procedure was used by Young in 1976 to discuss the quantum phase transition in the spin half transverse field Ising model [58]; however, Young does not calculate the coefficients of the resulting theory beyond quadratic order. In this thesis, we develop the formalism to all orders, and we provide explicit expressions for the coefficients of the theory to quartic order for a system with an arbitrary single ion Hamiltonian. We note that this procedure has been extensively developed for itinerant magnetic systems, beginning with the work of Hertz [31], and is discussed in the recent review of Brando *et al.* [59]. Alternative methods for incorporating the effects of fluctuations in quantum Ising systems that do not make use of an effective field theory are discussed in the introduction to Chapter 6. We think that the development of the field theoretic formalism is important because it allows for a treatment of a system's critical behaviour via the renormalization group.

We use the field theoretic formalism of Chapter 6 to develop a diagrammatic perturbation theory for including the effects of fluctuations in quantum Ising systems, and, in Section 6.3.3, we show that it is equivalent to the high density approximation (an expansion in the inverse coordination number) introduced by Brout [60, 61], and presented for the spin half transverse field Ising model by Stinchecombe [26, 62, 63]. In Chapter 7, we apply the field theoretic formalism to the calculation of corrections to the MF magnetization of various quantum Ising systems.

We close this introduction with a brief summary of what we think are the most significant

accomplishments of this thesis. These are:

1. A derivation of a low temperature effective Hamiltonian for $LiHoF_4$ in a transverse magnetic field that fully incorporates the nuclear degrees of freedom in Chapter 2. No such model exists in the literature. This Hamiltonian shows that the dominant mixing of the nuclear degrees of freedom is due to an effective transverse field acting directly on the nuclear spins due to a shift in each Ho^{3+} ions $4f$ electron cloud. In Chapter 3, a detailed analysis of the long range dipolar interaction between the electronic spins is provided.

2. In Chapter 4 we introduce a toy model with exactly solvable single ion eigenstates that elucidates the effect of an anisotropic hyperfine interaction on a quantum Ising system. We find that a dominant longitudinal hyperfine interaction stabilizes the system against the disordering effects of an applied transverse field, as well as enhancing both the longitudinal susceptibility of the system, and the effect of a longitudinal field. The enhancement of a longitudinal field has not been previously noted.

3. In Chapters 4 and 5, an RPA analysis of the toy model and $LiHoF_4$ is provided. The RPA results clearly show that the effect of the nuclear spins is to gap what would have been the electronic soft mode in a system with no hyperfine coupling, with spectral weight being transferred down to a low energy electronuclear mode that fully softens to zero at the quantum critical point. This explains the neutron scattering experiments carried out on $LiHoF_4$ by Rønnow *et al.* [36].

4. In Chapter 6, a general field theoretic formalism for quantum Ising systems that allows for the effect of fluctuations beyond the RPA is developed. This field theory is used to derive a diagrammatic perturbation theory, with the perturbation parameter being the inverse coordination number, equivalent to the theory introduced by Brout [60, 61], and applied to the spin half transverse field Ising model by Stinchcombe [26, 62, 63]. We use the theory to derive corrections to the magnetization of $LiHoF_4$ in Chapter 7.

5. We find that a regular nuclear spin bath, that is, a single species of nuclear spin coupled to each electronic degree of freedom, will have no effect on the quantum critical behaviour of a quantum Ising system.

Despite the fundamental importance of quantum Ising systems, and of the transverse field Ising model in particular, there has been no significant improvements in Stinchcombe's work since its publication in 1973 [26, 62, 63]. Thermodynamic research on quantum Ising systems has been largely focused on critical behaviour [28], rather than on the more general problem of the inclusion of the effects of fluctuations beyond the random phase approximation in real

magnetic systems. In this thesis, we generalize Stinchcombe's work to systems with an arbitrary single ion Hamiltonian, and, by using the field theoretic approach, we provide a derivation of the diagrammatic perturbation theory that offers a great deal of clarity and simplicity when compared to past approaches. If the work here becomes more widely appreciated, we hope to see it applied to Ising systems doped with non-magnetic impurities, antiferromagnets, systems coupled to an oscillator bath environment, and systems with time dependent parameters. We think that these topics, in particular the study of disordered systems and non-equilibrium dynamics, are among the most important problems of 21^{st} century condensed matter physics, and believe that the formalism presented here is well suited to the study of such problems.

Chapter 2

The LiHoF4 Hamiltonian

The rare earth magnetic insulating crystal $LiHoF_4$ is a central topic of this thesis. At low temperatures, $LiHoF_4$ is a physical realization of the magnetic dipole coupled quantum Ising model; however, there is the additional feature that each electronic spin is strongly coupled to a nuclear degree of freedom. The system undergoes a phase transition from a paramagnetic to a ferromagnetic state, induced by the long range dipolar interaction, below a critical temperature of 1.53K [11]. The ferromagnetic order may be destroyed by the application of a magnetic field transverse to the easy axis of the system. At zero temperature, the ferromagnetic order is destroyed in a quantum phase transition at a critical value of the transverse field of about 4.9T. The experimental phase diagram, taken from Bitko *et al.* [27], is shown in Figure 2.1. In this chapter, we introduce the Hamiltonian of $LiHoF_4$, and derive an effective low temperature Hamiltonian that includes the nuclear degrees of freedom. The truncation procedure used here to obtain the low energy Hamiltonian was first employed by Chakraborty *et al*. [64]; however, this is the first time the nuclear spins have been fully incorporated. In addition to the derivation of the low temperature effective Hamiltonian, this chapter includes a discussion of domain formation in $LiHoF_4$. We note that the Hamiltonian for $LiHoF_4$ has many free parameters (the CF parameters, and the exchange interaction). As these parameters may be tuned in theoretical calculations, or numerical simulations, claims regarding quantitative agreement between theory and experiment should be treated with some suspicion. A challenge facing experimentalists is to better determine the free parameters in $LiHoF_4$.

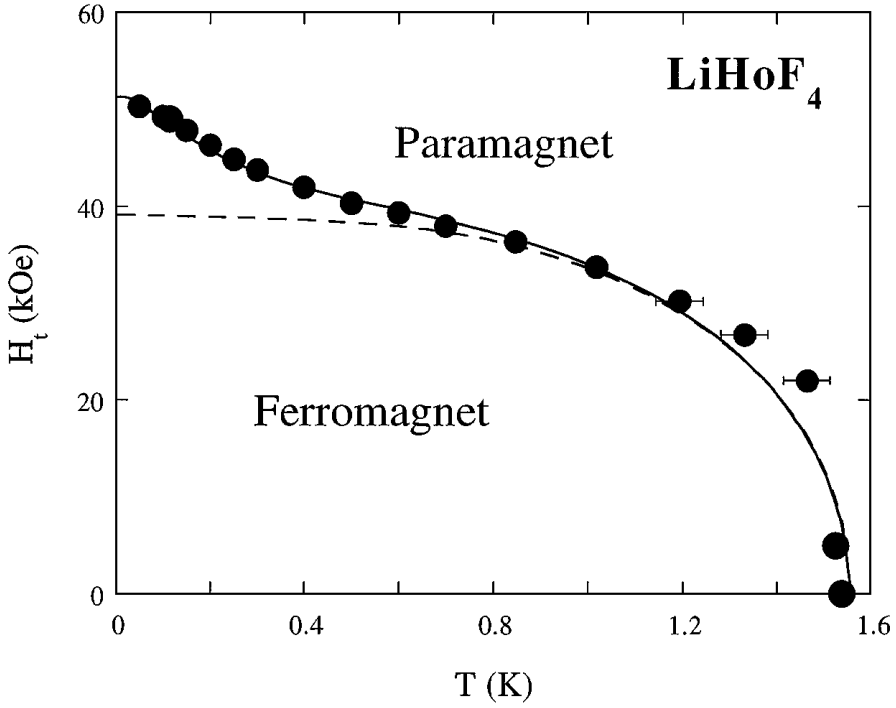

Figure 2.1: The above figure shows the phase diagram of $LiHoF_4$, measured by Bitko *et al.* via magnetic susceptibility (solid circles). The vertical axis is the applied transverse field, and the horizontal axis is the temperature. The dashed line is the phase diagram calculated using mean field theory, neglecting the hyperfine interaction. The solid line is calculated using mean field theory, with the hyperfine interaction included. There are several free parameters in the MF calculations which lead to the apparently good agreement between the experimental data and the MF results. In reality, fluctuations in the MF have a significant impact on the phase diagram of $LiHoF_4$ due to the dominant long range dipolar coupling between electronic spins.

The Hamiltonian

The magnetic properties of $LiHoF_4$ are due to the partially filled $4f$ shells of the Ho^{3+} ions. Trivalent rare earth ions shed their two outer $6s$ electrons, and a single $5d$ electron, leaving a core with the electronic configuration of xenon, and a partially filled $4f$ shell. In the ground state of Ho^{3+}, there are ten $4f$ electrons that fill the orbital angular momentum eigenstates, $L_z \in \{-3,-2,-2,0,1,2,3\}$, in accord with Hund's rules. That is, the total spin of the electrons is maximized, thereby minimizing the exchange energy between electrons, leading to $S = 2$; the total orbital angular momentum is maximized, minimizing the coulomb interaction energy between electrons, leading to $L = 6$; and the total angular momentum is given by $J = L+S = 8$, thereby minimizing the spin orbit interaction energy. Hund's rules follow from the Russell-Saunders coupling scheme, which is known to be accurate for $4f$ electrons. The term symbol,

$^{2S+1}L_J$, for the Ho^{3+} ion is $^5I_8$. A discussion of the physics of rare earth atoms may be found in [65].

If we take $U(r_i) = -eV(r_i) = -\frac{Ze^2}{4\pi\varepsilon_0 r_i}$ to be the radially symmetric potential of the i^{th} $4f$ electron in a rare earth element, the spin orbit interaction due to the $4f$ electrons is

$$H_{so} = \sum_i \frac{1}{2m_e^2c^2}\frac{1}{r_i}\frac{\partial V(r_i)}{\partial r_i}\vec{l}_i\cdot\vec{s}_i = \pm\lambda(LS)\vec{S}\cdot\vec{L} = \pm\frac{\lambda(LS)}{2}(\vec{J}^2 - \vec{L}^2 - \vec{S}^2), \tag{2.1}$$

where $\vec{L} = \sum_i \vec{l}_i$ and $\vec{S} = \sum_i \vec{s}_i$, and the $+$ $(-)$ sign refers to a less (more) than half full $4f$ shell. In order to obtain the spin orbit coupling λ, we express the spin orbit interaction in a basis of states of total orbital and spin angular momentum, L^2, L_z and S^2, S_z. It is a consequence of the Wigner-Eckart projection theorem that $\lambda(LS)$ is a function of only $||L^2|| = L(L+1)$ and $||S^2|| = S(S+1)$, and not of L_z and S_z. Holmium's large atomic number leads to a significant spin orbit interaction; therefore, we work in a basis of states of the operators L^2, S^2, J^2, and J^z. With the gyromagnetic ratio of the electron taken to be exactly two, the Zeeman energy of a holmium ion in a magnetic field will be given by

$$H_Z = -\mu_B(\vec{L} + 2\vec{S})\cdot\vec{B} = -\mu_B g_L \vec{J}\cdot\vec{B}, \tag{2.2}$$

where the Bohr magneton is given by $\mu_B = 0.6717K/T$, and we have made use of the Wigner-Eckart projection theorem in the form

$$\langle L\ S\ J\ J^z|\vec{L} + 2\vec{S}|L\ S\ J\ J^{z'}\rangle = g_L\langle J\ J^z|\vec{J}|J\ J^{z'}\rangle \tag{2.3}$$

to obtain the final expression. The Landé g factor, with $L = 6$ and $S = 2$, is given by

$$g_L = 1 + \frac{J(J+1) - L(L+1) + S(S+1)}{2J(J+1)} = \frac{5}{4}. \tag{2.4}$$

More intuitively, noting that the time average of the spin angular momentum will lie along the total angular momentum vector

$$\vec{S}_{avg} = \frac{\vec{S}\cdot\vec{J}}{||J^2||}\vec{J}, \tag{2.5}$$

we may write $\langle\vec{L} + 2\vec{S}\rangle = \langle\vec{J} + \vec{S}_{avg}\rangle$ which leads to the Landé g factor given in equation (2.4).

After our brief discussion of the electronic configuration of a holmium ion, and the spin orbit interaction, we move on to the magnetic insulator $LiHoF_4$. The following Hamiltonian

may be used to model $LiHoF_4$,

$$H = \sum_i V_C(\vec{J}_i) - g_L \mu_B \sum_i B_x J_i^x - \frac{1}{2} J_D \sum_{i \neq j} D_{ij}^{\mu\nu} J_i^\mu J_j^\nu + \frac{1}{2} J_{nn} \sum_{<ij>} \vec{J}_i \cdot \vec{J}_j + A \sum_i \vec{I}_i \cdot \vec{J}_i, \tag{2.6}$$

where $V_C(\vec{J}_i)$ is the crystal field, which will be discussed in Section 2.1.1, and B_x is an applied transverse magnetic field. The dipolar interaction between electronic spins,

$$D_{ij}^{\mu\nu} = \frac{3(r_i^\mu - r_j^\mu)(r_i^\nu - r_j^\nu) - |\vec{r}_i - \vec{r}_j|^2 \delta_{\mu\nu}}{|\vec{r}_i - \vec{r}_j|^5}, \tag{2.7}$$

has strength $J_D = \frac{\mu_0}{4\pi}(g_L \mu_B)^2$. The summation is over a tetragonal Bravais lattice with four Ho^{3+} ions per unit cell. The lattice spacing in the *xy* plane is $a = 5.175$Å, and the longitudinal lattice spacing is $c = 10.75$Å. The holmium ions have the Scheelite structure, with fractional coordinates $(0,0,\frac{1}{2})$, $(0,\frac{1}{2},\frac{3}{4})$, $(\frac{1}{2},\frac{1}{2},0)$ and $(\frac{1}{2},0,\frac{1}{4})$ [66]. In Figure 2.2, taken from the thesis of Kraemer [16], the structure of $LiHoF_4$ is illustrated including all atoms in the unit cell. Using the in plane lattice spacing as a reference, we find the strength of the dipolar interaction to be $\frac{J_D}{a^3} = 7mK$. Estimates of the antiferromagnetic exchange interaction vary, as will be discussed in Section 2.1.1. Throughout this thesis, unless otherwise noted, we will use the estimate of Rønnow *et al.*, $J_{nn} = 1.16mK$ [67]. The net spin of the holmium nucleus is $I = \frac{7}{2}$, and the hyperfine interaction is $A = 39mK$. A discussion of the nuclear interactions is provided in Section 2.1.2.

Due to the frustrated long range nature of the dipolar interaction, fluctuations have a significant impact on the properties of $LiHoF_4$. The validity of the Hamiltonian given in equation (2.6), taking into consideration the effect of fluctuations, has been tested via Monte Carlo simulations, and through the application of a high density approximation (an expansion in the inverse coordination number). The high density approximation was carried out by Rønnow *et al.* in [67]. They diagonalize the full 136×136 electronic plus nuclear single ion Hamiltonian in the presence of a transverse magnetic field, and make use of the formalism of Jensen, presented in [68], to include the effects of fluctuations. By tuning the crystal field parameters, and the antiferromagnetic exchange interaction, Rønnow *et al.* are able to obtain agreement between theory and experiment for most of the phase diagram; however, no single choice of parameters was found to account for the entire phase diagram. At low temperatures, Rønnow *et al.* are also able to obtain a good fit to the (gapped) lowest energy crystal field excitation, apart from an overall scaling factor of 1.15. Magnetoelastic interactions are suggested as a

possible source of the discrepancy in the excitation energy; however, they appear insufficient to account for the discrepancies observed in the phase diagram.

Quantum Monte Carlo simulations have been carried out on an effective low temperature Hamiltonian for $LiHoF_4$ in a transverse magnetic field by Chakraborty *et al.* [64]. In their paper, Chakraborty *et al.* ignore the hyperfine interaction in their low temperature effective Hamiltonian, choosing instead to incorporate its effects through a sytematic renormalization of the transverse magnetic field. At a fixed temperature, with $T < T_c = 1.53K$, the experimental critical transverse field is upto 30% larger than the value predicted by Monte Carlo simulations using the same parameters as the work of Rønnow *et al.* [67] discussed in the previous paragraph. Chakraborty *et al.* attribute the discrepancy to uncertainties in the crystal field parameters. They find the results of their calculations become increasingly sensitive to the crystal field parameters as the transverse field is raised. The work of Chakraborty *et al.* has been revisited by Tabei *et al.* in a paper in which classical Monte Carlo is used to analyze the $B_x/T_c \ll 1$ regime. Effects due to quantum fluctuations are included in their work perturbatively. The deviation between experimental and theoretical phase diagrams in increasing transverse field persists in Tabei *et al.*'s work, and, by comparing several numerical techniques, they conclude it is most likely not of computational origin. Tabei *et al.* test a single set of alternative crystal field parameters, and, provided the antiferromagnetic exchange interaction is adjusted to obtain the correct zero transverse field critical temperature, they find little difference in the experimental phase diagram. This leads them to tentatively conclude that in weak transverse fields the crystal field parameters are not the source of the difference between theory and experiment. Tabei *et al* suggest anisotropic exchange, higher order multipolar interactions, or magnetoelastic couplings as possible sources of the discrepancy.

We note that in Chakraborty *et al.*'s work the hyperfine interaction is incorporated as a renormalization of the effective transverse field, and in Tabei *et al.*'s work the hyperfine interaction is left out altogether because it is thought to be irrelevant in the regime of interest $\frac{B_x}{T_c} \ll 1$ [64, 69]. As will be shown in Section 2.2, in zero transverse field the longitudinal hyperfine interaction has a significant magnitude. One might expect that it will stabilize the $LiHoF_4$ system against the effects of fluctuations, in a way not accounted for by a renormalization of the effective transverse field. We suggest this as a possible source of the discrepancy between the theoretical and experimental phase diagrams determined by Monte Carlo simulations.

In Section 2.2, we derive an effective low temperature Hamiltonian for the $LiHoF_4$ system that fully incorporates the effects of the nuclear spins. This Hamiltonian will be used to perform an analysis of the sytem in the random phase approximation in Chapter 5. In Chapter 6, we will develop a field theoretic formalism that leads to a high density approximation (an expansion in the inverse coordination number) to include the effects of fluctuations in quantum Ising

systems such as $LiHoF_4$. We will defer further discussion of the high density approximation, and a comparison to the formalism of Jensen used in the paper of Rønnow *et al.* [67, 68], to that chapter.

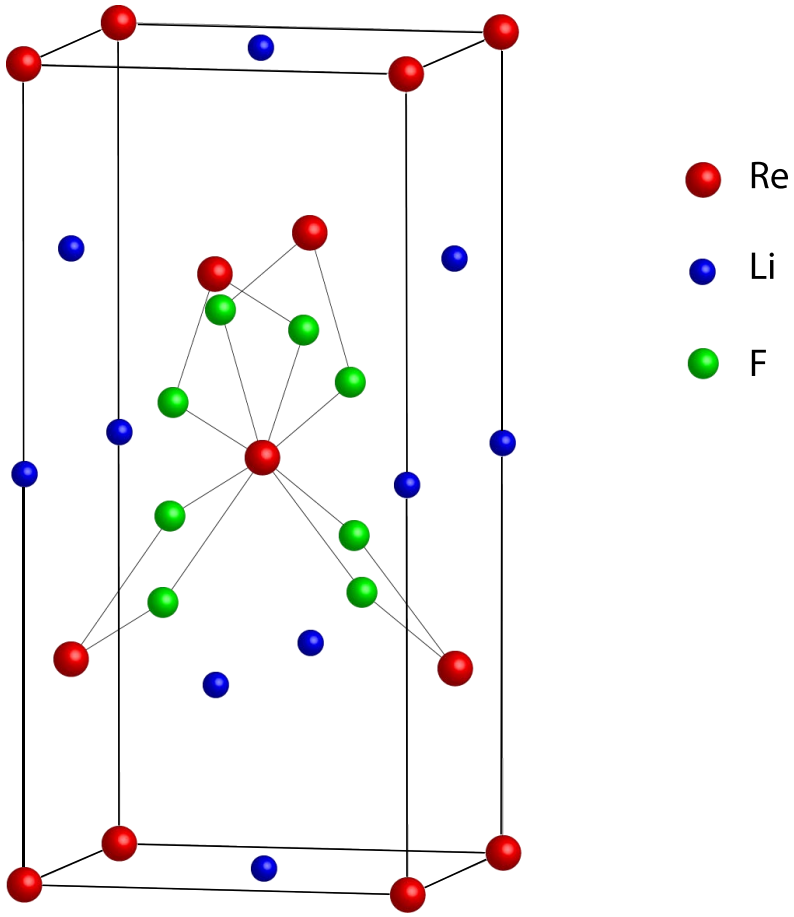

Figure 2.2: The figure above, taken from the thesis of Kraemer [16], shows the structure of materials in the $LiReF_4$ series, where Re is a rare earth atom.

The Crystal Field and Exchange Interaction

The high electronegativity of the fluorine ions in $LiHoF_4$ leads to a distortion of the of the $4f$ electron cloud surrounding each holmium ion, lifting the 17-fold degeneracy of the $J = 8$ magnetic moment. This perturbation is accounted for by the inclusion of the crystal electric field $V_C(\vec{J}_i)$. The physics of the crystal field, which we will review here, is discussed in [70, 71].

The crystal field Hamiltonian due to the ions surrounding each holmium ion (the ligands), is given by

$$V_C = -\frac{e^2}{4\pi\varepsilon_0}\sum_{kj}\frac{Z_j}{|\vec{R}_j - \vec{r}_k|}, \tag{2.8}$$

where e is the electron charge, Z_j is the effective charge of the j^{th} ligand, and $\vec{R}_j$ and $\vec{r}_k$ are the positions of the j^{th} ligand and k^{th} electron in the $4f$ cloud, respectively. We may expand equation (2.8) in spherical harmonics to obtain

$$V_C = \sum_{n=0}^{\infty}\sum_{m=-n}^{n} A_n^m \sum_k r_k^n Y_n^m(\theta_k, \phi_k). \tag{2.9}$$

This Hamiltonian may be put in a form more amenable to calculation by writing the spherical harmonics in terms of their Cartesian coordinates, $\sum_k Y_n^m(\theta_k, \phi_k) = f_n^m(x, y, z)$, and replacing the functions f_n^m with spin operators sharing all the same symmetries. This is known as the Stevens' operator equivalents method [72–74], and leads to the following expression for the crystal field Hamiltonian

$$V_C(\vec{J}) = \sum_{n=0}^{\infty}\sum_{m=-n}^{n} B_n^m O_n^m(\vec{J}). \tag{2.10}$$

The operator equivalents O_n^m corresponds to sums or differences of the spherical harmonics $Y_n^{\pm m}$. In practice, the crystal field parameters B_n^m are determined by experiments. In rare earth materials, the summation over n is restricted to $n = 2, 4, 6$, and the possible values of m are restricted by the point group of the crystal in question. For an extensive review of the crystal field Hamiltonian in rare earth compounds, see [75]. For $LiHoF_4$, the symmetry of the tetragonal crystal (scheelite, or space group $C_{4h}^6 - I4_{1/a}$) leads to a crystal field given by

$$V_C(\vec{J}) = B_2^0 O_2^0 + B_4^0 O_4^0 + B_6^0 O_6^0 + B_4^4(C) O_4^4(C) + B_6^4(C) O_6^4(C) + B_4^4(S) O_4^4(S) + B_6^4(S) O_6^4(S), \tag{2.11}$$

where the Stevens' operators are

$$
\begin{aligned}
O_2^0 &= 3J_z^2 - J(J+1) \qquad (2.12)\\
O_4^0 &= 35J_z^4 - 30J(J+1)J_z^2 + 25J_z^2 - 6J(J+1) + 3J^2(J+1)^2\\
O_6^0 &= 231J_z^6 - 315J(J+1)J_z^4 + 735J_z^4 + 105J^2(J+1)^2J_z^2 - 525J(J+1)J_z^2 + 294J_z^2\\
&\quad - 5J^3(J+1)^3 + 40J^2(J+1)^2 - 60J(J+1)\\
O_4^4(C) &= \frac{1}{2}(J_+^4 + J_-^4)\\
O_6^4(C) &= \frac{1}{4}(J_+^4 + J_-^4)[11J_z^2 - J(J+1) - 38] + h.c.\\
O_4^4(S) &= \frac{1}{2i}(J_+^4 - J_-^4)\\
O_6^4(S) &= \frac{1}{4i}(J_+^4 - J_-^4)[11J_z^2 - J(J+1) - 38] + h.c.
\end{aligned}
$$

We use $h.c.$ to denote the Hermitian conjugate.

In $LiHoF_4$, the crystal field induces strong anisotropy leading to the Ising nature of the material. Typically, in a crystal with tetragonal symmetry, the $n = 2$ terms are dominant. It is easy to see how this leads to anisotropy by considering only the O_2^0 term and the Zeeman energy of the mean field

$$H = B_2^0 O_2^0 - g_L \mu_B \vec{J} \cdot \vec{B}. \qquad (2.13)$$

By diagonalizing the Hamiltonian above, we find that with $B_2^0 < 0$ the ground state energy of the system is minimized if the mean field (MF) is in the z direction (the long axis of the tetragonal crystal), and if $B_2^0 > 0$ the preferential direction for ordering is in the xy plane. The sign of B_2^0 depends on whether the $4f$ electron cloud of the rare earth element is flattened in the z direction ($B_2^0 < 0$), or elongated in the z direction ($B_2^0 > 0$). In $LiHoF_4$, $B_2^0 < 0$ and there is strong Ising anisotropy.

The crystal field parameters (CFPs) of $LiHoF_4$ have been measured via a number of experimental techniques, by many different groups; however, no consensus has been reached regarding their values. An early estimate of the parameters, based on susceptibility measurements, was made by Hansen *et al.* in 1975 [10]. In 1980, the CFPs were again determined via magnetic susceptibility measurements by Beauvillain *et al.* [76]; however, Beauvillain *et al.* make no reference to the work of Hansen *et al*. Optical spectroscopy was used to determine the CFPs by Christensen, and by Gifeisman *et al.*, in the late 1970s [77, 78]. Electron paramagnetic resonance was used by Shakurov *et al.* to estimate the CFPs in 2005 [79]. Around the same time, numerical estimates of the CFPs, based on neutron scattering data, were made by

CFP (K)	Ref. [10]	Ref. [76]	Ref. [78]	Ref. [77]	Ref. [79]	Ref. [67]	Ref. [80]
B_2^0	-0.754	-0.853	-0.609	-0.606	-0.609	-0.696	-0.672
$10^3 B_4^0$	4.94	5.55	3.25	3.75	3.75	4.06	3.58
$10^6 B_6^0$	1.16	1.16	8.41	6.06	6.05	4.64	6.26
$10^2 B_4^4(C)$	5.26	5.44	4.29	4.16	3.15	4.18	4.07
$10^4 B_6^4(C)$	9.92	9.99	8.17	7.95	6.78	8.12	7.32
$10^2 B_4^4(S)$	0	0	0	0	2.72	0	0
$10^4 B_6^4(S)$	1.96	1.37	0	0	4.14	1.14	1.98

Table 2.1: In this table, we list various estimates of the crystal field parameters of $LiHoF_4$ in units of Kelvin. References [10, 76] are based on the susceptibility measurements of Hansen *et al.* and Beauvillain *et al.*, respectively. References [77, 78] are, respectively, the optical light scattering experiments of Gifeisman *et al.* and Christensen. Reference [79] contains the estimates based on Shakurov *et al.*'s EPR experiments. In [67], we have the numerical estimates of Rønnow *et al.*, and in [80], we have the estimates of Babkevich *et al.* based on neutron scattering experiments.

Rønnow *et al*. [67]. More recently, in 2015, neutron scattering was used by Babkevich *et al.* to determine the CFPs [80]. In Table 2.1, we list these values of the CFPs. In this thesis, we use the crystal field parameters of Rønnow *et al*. [67] because, in the low temperature regime that we will be primarily concerned with, they provide a good fit to the experimental phase diagram of $LiHoF_4$. $LiHoF_4$ provides an arena for testing many aspects of fundamental physics, as discussed in the introduction to this thesis, therefore it is crucial that these parameters are determined with greater accuracy.

The antiferromagnetic exchange interaction has not been directly determined. An estimate of its strength has been made by Rønnow *et al* [67], based on inelastic neutron scattering data. Using the crystal field parameters listed above, they find an exchange interaction of $J_{nn} = 1.16mK$ provides a good fit to the experimental phase diagram, except in the vicinity of the zero transverse field critical temperature ($T_c^0 = 1.53K$), that is, their fit is good when when $\frac{T_c}{g_L \mu_B B_x} > 1$, where T_c is the critical temperature in an applied transverse field B_x. By taking $B_6^4(S) = 0.87 \times 10^{-5} K$ and $J_{nn} = 3.13mK$ they are able to obtain a better fit to the experimental phase diagram near $T_c^0 = 1.53K$; however, there are now significant discrepancies between the experimental and calculated phase diagram at intermediate temperatures of about $0.4K$ to $1.5K$.

Another estimate of the exchange interaction was made by Tabei *et al.*, based on zero transverse field Monte Carlo simulations [69]. The exchange interaction is used to tune the critical temperature to the correct experimental value. These simulations neglect the effect of the hyperfine interaction; however, they note that prior Monte Carlo simulations [64], which incor-

porated the effect of the hyperfine interaction via a renormalization of the effective transverse field, indicate that the effect of the hyperfine interaction is unimportant when the transverse field is zero. We are skeptical of this result as a renormalization of the transverse field fails to account for any stabilizing effect the longitudinal hyperfine interaction might have against the disorder caused by fluctuations. Using the crystal field parameters of [67], Tabei *et al.* find the exchange interaction to be $J_{nn} = 3.91mK$. The parameters in Tabei *et al.*'s work are tuned to obtain the correct experimental value for the zero transverse field critical temperature; however, the tuned parameters fail to produce the experimental phase diagram away from $B_x = 0$. They suggest that magnetoelastic couplings, higher order multipolar interactions, or anisotropic exchange, may be sources of the discrepancy [69].

In this thesis, we will use the crystal field parameters of [67], and take $J_{nn} = 1.16mK$ unless otherwise noted. These parameters have been demonstrated to provide a good fit to the experimental phase diagram in the low temperature regime.

The electronic energy levels in the crystal field are mixed and split by the applied transverse magnetic field. In the absence of the applied field, the system has a degenerate ground state separated from the first excited state by about 11K. The degenerate ground state is split by the transverse field leading to the effective transverse Ising nature of the system. As the transverse field is increased towards the quantum critical point, there is also significant mixing with the higher lying levels that cannot be included perturbatively. In Figure 2.3, we plot the energy levels of the electronic single ion Hamiltonian,

$$H_e = \sum_i V_C(\vec{J}_i) - g_L \mu_B \sum_i B_x J_i^x, \tag{2.14}$$

as a function of the transverse field. The inset shows the splitting of the lowest two energy levels, relevant to the effective transverse field Ising Hamiltonian used to model the system, and the next highest excited state. This higher lying state is separated from the lower lying doublet by at least $10K$.

Group theoretic considerations determine the general structure of the ground state doublet to be a mixture of the odd electronic eigenstates. The applied transverse field breaks the symmetry of the ground state, and mixes even eigenstates of the J^z operator into the ground state Hamiltonian. The mixing of the eigenstates of the J^z operator, $J^z|j\rangle = j|j\rangle$, in the ground state and the first excited state of equation (2.14),

$$|\Psi^{1,2}\rangle = \sum_{j=-7}^{7} \alpha_j^{1,2} |j\rangle, \tag{2.15}$$

is illustrated in Figures 2.4 and 2.5.

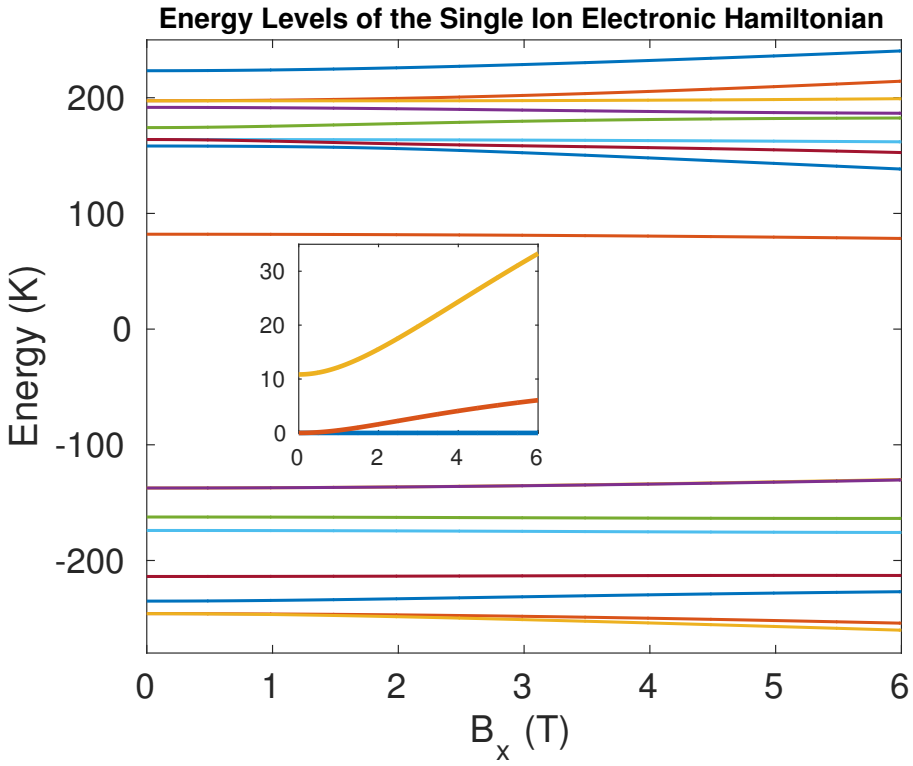

Figure 2.3: In this figure, we show the energy levels of the crystal field component of the $LiHoF_4$ Hamiltonian (in Kelvin) as a function of an applied transverse field B_x (in Tesla). The inset shows the lowest three energy levels with the ground state taken as zero energy. We see that the second excited state is seperated from the low energy doublet by a gap of over $10K$.

The Hyperfine Interactions

The Ho^{3+} ions in $LiHoF_4$ consist of a single nuclear isotype with nuclear spin $I = \frac{7}{2}$. As discussed by Mennenga *et al.* in their paper on the specific heat of $LiHoF_4$ [35], the nuclear part of the Hamiltonian for a Ho^{3+} ion may be written as

$$\mathscr{H}_n = A\vec{I}\cdot\vec{J} + g_n\mu_n\vec{I}\cdot\vec{H}_n + \mathscr{H}_Q. \tag{2.16}$$

The first term, which we will refer to as the hyperfine interaction, is the most significant. It is due primarily to the magnetic interaction between each holmium ion's $4f$ electron cloud and its nucleus. The final two terms have been dropped from the $LiHoF_4$ Hamiltonian given in equation (2.6) because they are expected to be small. The second term includes any externally applied field, or mean field (MF), due to the neighbouring holmium ions. It also includes nuclear dipole-dipole interactions between the holmium nucleus and neighbouring nuclear spins, and Fermi contact interactions other than core polarization effects. Any core polarization ef-

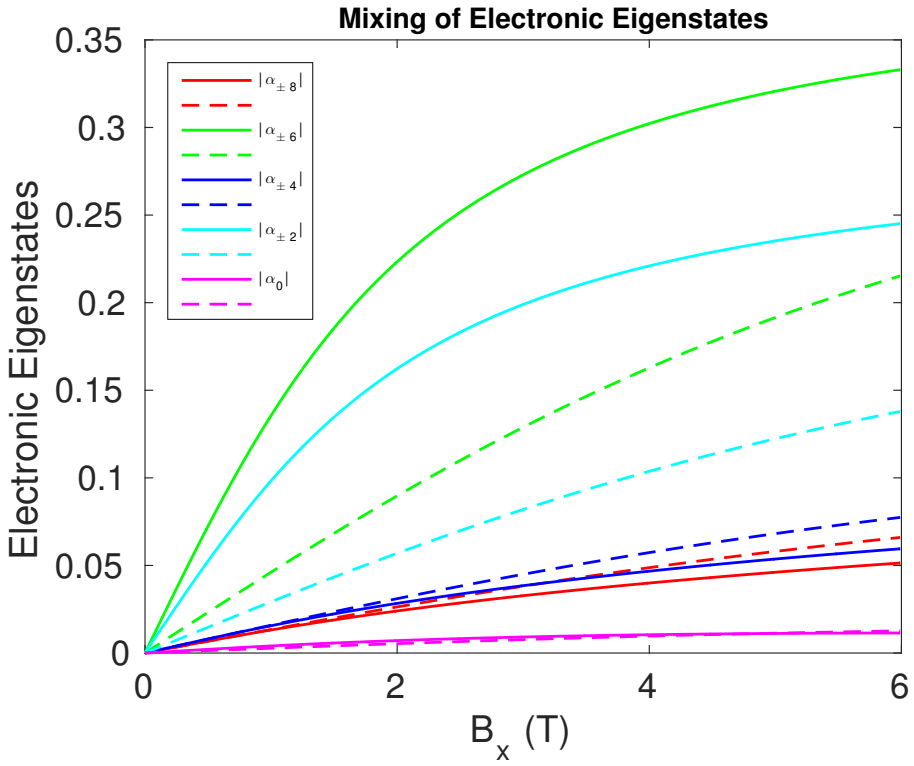

Figure 2.4: In this figure, we show the mixing of the even electronic eignestates of the J^z operator by the crystal field as a function of an applied transverse field for the ground state (solid line) and first excited state (dashed line) of the electronic component of the single ion Hamiltonian for $LiHoF_4$. Each α_j corresponds to the electronic eigenstate such that $J^z|j\rangle = j|j\rangle$

fects are included in the first term. The nuclear magneton is $\mu_n = 3.66 \times 10^{-4} K/T$ and the nuclear g factor for holmium is $g_n = 4.17$ [81]. The final term is the nuclear electric quadrupole interaction at the holmium nucleus. In addition, there will be hyperfine terms involving only the lithium and fluorine nuclei $\mathscr{H}_{n'}(\vec{I}_F, \vec{I}_{Li})$. The most significant parts of $\mathscr{H}_{n'}(\vec{I}_F, \vec{I}_{Li})$ are the transferred hyperfine interactions due to the Fermi contact interaction between the holmium electrons, and the lithium and fluorine nuclei. We will discuss each of these terms in turn below, beginning with the most significant, the hyperfine interaction. For a more detailed discussion of hyperfine interactions in rare earth atoms see the review by Bleaney [82]. Here we provide a brief review of what we deem to be most significant.

The hyperfine interaction may be written as

$$\mathscr{H}_A = A\vec{I}\cdot\vec{J} = -g_n\mu_n\vec{I}\cdot\vec{H}_{4f}, \tag{2.17}$$

where $\vec{H}_{4f}$ is the magnetic field at the nucleus of a Ho^{3+} ion due primarily to its $4f$ electron cloud. We say primarily because we allow this term to include small corrections due to the

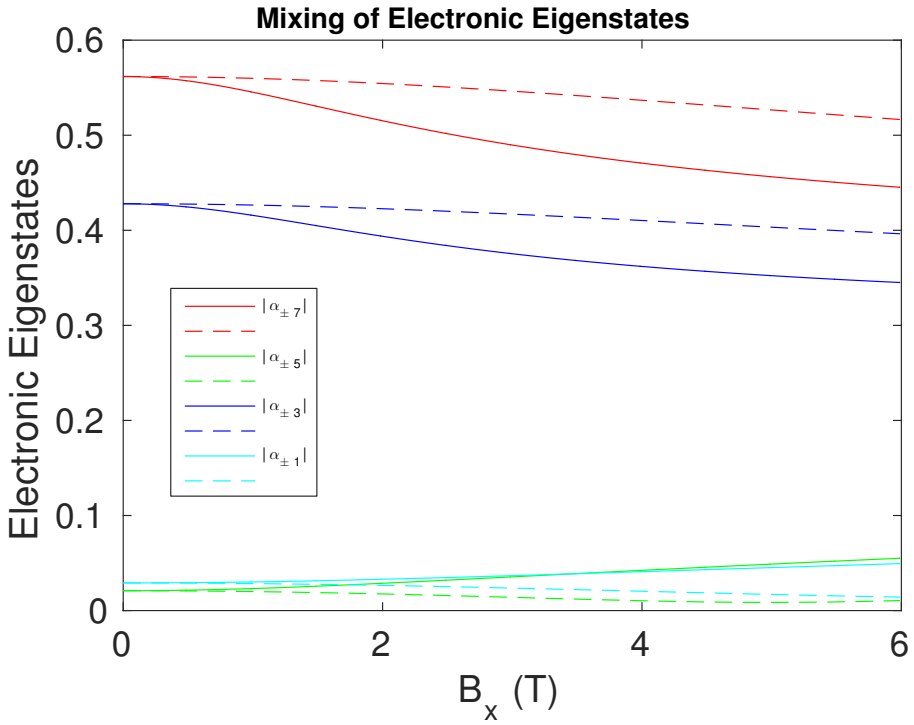

Figure 2.5: In this figure, we show the mixing of the odd electronic eignestates of the J^z operator by the crystal field as a function of an applied transverse field for the ground state (solid line) and first excited state (dashed line) of the electronic component of the single ion Hamiltonian for $LiHoF_4$. Each α_j corresponds to the electronic eigenstate such that $J^z|j\rangle = j|j\rangle$

atom's core electrons. The largest contribution to $\vec{H}_{4f}$ comes from the orbital angular momentum of the $4f$ electrons, and is given by

$$\vec{H}_L = -2\mu_B \sum_i \langle r_i^{-3}\rangle \vec{l}_i = -2\mu_B \langle r^{-3}\rangle \vec{L}, \tag{2.18}$$

where we have assumed that each orbital has the same average radius to obtain the final expression. The next largest contribution is due to the dipolar field of the electron spins, and may be written as

$$\vec{H}_s = 2\mu_B \sum_i \langle r_i^{-3}\rangle [\vec{s}_i - 3(\vec{s}_i \cdot \vec{r}_i)\vec{r}_i] = 2\mu_B \langle r^{-3}\rangle \xi [L(L+1)\vec{S} - 3(\vec{L}\cdot\vec{S})\vec{L}]. \tag{2.19}$$

The final expression is obtained by using the Steven's equivalent operator method, the details of which are found in [73]. For Ho^{3+} the numerical factor is $\xi = -\frac{1}{990}$. The orbital and spin angular momentum vectors precess rapidly around the (conserved) total angular momentum vector $\vec{J} = \vec{L} + \vec{S}$. Projecting onto $\vec{J}$, we find the time averaged field felt by the nucleus to be

given by

$$\vec{H}_{4f} = -2\mu_B\langle r^{-3}\rangle\left[\vec{L}\cdot\vec{J} - \xi\left(L(L+1)\vec{S}\cdot\vec{J} - 3(\vec{L}\cdot\vec{S})(\vec{L}\cdot\vec{J})\right)\right]\frac{\vec{J}}{J(J+1)}. \tag{2.20}$$

This expression is subject to several corrections, such as the Fermi contact interaction due to the polarization of core s electrons. These corrections are discussed by Bleaney in [82], and will not be discussed here. The hyperfine field $\vec{H}_{4f}$ is largest for Ho^{3+} and Er^{3+} with fields approaching 800 Tesla. This, in conjunction with with holmium's large (relative to the other rare earths elements) nuclear g factor, $g_n = 4.17$, and large nuclear spin, $I = \frac{7}{2}$, lead to the significant hyperfine coupling in $LiHoF_4$.

We now consider the second term in equation (2.16), $\mathscr{H}_{ext} = g_n\mu_n\vec{I}\cdot\vec{H}_n$, which we take to be the energy of a holmium nuclear spin due to the field generated by all sources external to the holmium ion itself. This term includes any externally applied magnetic field, as well as the MF caused by the neighbouring holmium ions. It also includes the dipolar fields due to the nuclear moments of neighbouring ions. All these interactions are suppressed by a factor (or factors) of $\frac{\mu_N}{\mu_B}$ relative to the interaction of these fields with a holmium electronic spin, or the dipole-dipole interaction between holmium electronic spins. This term may also include Fermi contact interactions between the holmium nucleus and electrons belonging to neighbouring ions. Spectroscopy experiments carried out by Magariño *et al.* on $LiHo_xY_{1-x}F_4$, where most of the holmium has been replaced by non-magnetic yttrium, are presented in [9], and spectroscopy experiments in pure $LiHoF_4$ are presented in [13]. They found a spacing between hyperfine resonance lines of $A = 479G\frac{1T}{10^4G} * g_L * \mu_B = 40.2mK$ in the dilute sample, and in the pure sample they found $A = 39.8mK$. This shows neighbouring holmium atoms in the pure sample have little impact on the spacing of the lines in the hyperfine spectrum. Assuming that Fermi contact interactions with the lithium and fluorine electrons are small, we are justified in dropping $\mathscr{H}_{ext} = g_n\mu_n\vec{I}\cdot\vec{H}_n$ from the thermodynamic analysis of the $LiHoF_4$ Hamiltonian.

The most significant part of $\mathscr{H}_{n'}(\vec{I}_F, \vec{I}_{Li})$ is the transferred hyperfine interaction due to the Fermi contact interaction between the holmium electrons and the lithium and fluorine nuclei. NMR experiments carried out by Hansen and Nevald have determined these interactions [83]. They found that for fluorine, the transferred hyperfine interaction is of the same order of magnitude as the dipole-dipole coupling between the fluorine nuclear spin and the holmium electonic spin. For lithium, the transferred hyperfine interaction is five times smaller than the lithium-holmium dipolar coupling. These terms may be safely dropped when performing a thermodynamic analysis of the $LiHoF_4$ Hamiltonian; however, we note that, as pointed out by Schechter and Stamp [38], they may still have an impact on the relaxational dynamics, and decoherence, in $LiHoF_4$.

The final term in equation (2.16) is the nuclear electric quadrupole interaction $\mathscr{H}_Q$. Recall that the energy of a charge distribution, $q = \int \rho(r) d\vec{r}$, placed in an electric field may be expanded as [84]

$$\mathscr{H}_{multipole} = qV(0) - \vec{P}\cdot\vec{E}(0) - \frac{1}{6}\sum_{ij} Q^{ij}\frac{\partial E_j}{\partial r_i}(0) + \cdots, \tag{2.21}$$

where $\vec{E} = -\nabla V$ is the electric field, and $\vec{P}$ and Q^{ij} are, respectively, the dipole and quadrupole moments of the charge distribution. We are interested in the charge distribution of each holmium nucleus in the presence of the electric field created by its surroundings. The first term corresponds to a constant shift in the ground state energy and may be ignored, and the dipolar term is zero because the electric field is zero at the nucleus (otherwise the nucleus would move). The final term, the quadrupolar term, may be non-zero because derivatives of the electric field may be non-zero at the nucleus. In terms of equivalent spin operators, we may write the quadrupolar operator as

$$Q^{ij} = \int \rho(r)(3r_i r_j - r^2\delta_{ij}) d\vec{r} = \frac{Q}{I(2I-1)}\left[\frac{3}{2}(I^i I^j + I^j I^i) - I(I+1)\delta_{ij}\right], \tag{2.22}$$

with $Q \equiv Q^{zz}$. With an appropriate choice of axes $V_{ij} = \partial^i E^j = 0$ for any $i \neq j$, and, for a system with axial symmetry about the z axis such that $V_{xx} = V_{yy}$, the quadrupolar interaction will take the form

$$\mathscr{H}_Q = P[I_z^2 - \frac{1}{3}I(I+1)]. \tag{2.23}$$

Such is the case in $LiHoF_4$. The value of Q for a holmium atom is $Q = 2.4$ barns, which is unremarkable when compared to the Q values of the neighbouring rare earth atoms in the periodic table. Specific heat measurements have been used to find the value of P for $LiHoF_4$ by Mennenga *et al.* [35]. We note that in Mennenga *et al.* $A_\parallel = A\frac{g_\parallel}{g_L}$, where an effective g factor of $g_\parallel = 13.5$ has been introduced to account for the systems crystal field. They fit their data to the Shottky anomaly in the specific heat due to the nuclear spins, and allow in their model a contribution from the hyperfine interaction, and a nuclear quadrupole field. For the hyperfine interaction they find $A = 38.8mK$, and for the nuclear electric quadrupole interaction they find $P = 2mK$, which is very close to the value for the free ion which they state is $P = 1.7mK$. This indicates that the electric field gradient is due primarily to the $4f$ electron cloud, and the effect of the crystal electric field is relatively small. We will find, after performing the truncation to obtain the low energy Hamiltonian, that the effective longitudinal hyperfine interaction is enhanced to $A_z \approx 200mK$, whereas the quadrupole coupling is left unchanged, so neglecting

the quadrupole term introduces errors on the order of about 1% to the Hamiltonian. Errors of the same order of magnitude are incurred when the transverse dipolar interactions are dropped from the effective theory. In the remainder of this thesis, the nuclear quadrupole interaction will be neglected, and we will take $A = 39mK$.

Domains in LiHoF4

In order to discuss domains in $LiHoF_4$, we begin by discussing the local field felt by each holmium ion inside the crystal. We follow closely the discussion of Mennenga *et al.* in [35]. The local field will be given by

$$\vec{h}_{loc} = \vec{h}_a + \frac{4\pi}{3}\vec{M} + \lambda_{dip}\vec{M} - \vec{N}\cdot\vec{M} + \lambda_{ex}\vec{M}, \tag{2.24}$$

where $\vec{M}$ is the magnetic moment per unit volume, which, for the sake of simplicity, we take to be constant. This corresponds to assuming our sample is a uniformly magnetized ellipsoid, in which case the demagnetizing field, to be discussed shortly, is uniform [85]. There is an externally applied magnetic field $\vec{h}_a$, and $\vec{h}_{ex} = \lambda_{ex}\vec{M}$ is the field due to the exchange interaction. The dipolar field is $\vec{h}_{dip} = \frac{4\pi}{3}\vec{M} + \lambda_{dip}\vec{M} - \vec{N}\cdot\vec{M}$. The three terms in the dipolar field are, respectively, the Lorentz local field due to the exclusion of the origin in the dipolar sums, a contribution due strictly to the structure of the lattice, and the demagnetizing field, which depends on the external shape of the sample [8, 35]. The dipolar interaction will be dealt with in detail in Chapter 3.

From Maxwell's equations, we know the total magnetostatic energy of our sample will be given by

$$E = -\frac{\mu_0}{2}\int \vec{M}\cdot\vec{h}\, d^3\vec{r}, \tag{2.25}$$

where the integral is over the volume of our sample, and $\vec{h} = \vec{h_a} - \vec{N}\cdot\vec{M}$ is the macroscopic field given by Maxwell's equations. In the case of a uniformly magnetized ellipsoid considered so far, the integrand is constant and we simply have $E = -\frac{\mu_0}{2}V\vec{M}\cdot\vec{h}$. In the ferromagnetic phase of the system, the analysis is no longer as simple. The system may arrange itself into domains in order to minimize its total energy, in which case the macroscopic field and magnetization will be non-homogenous.

As discussed in [35], there is experimental evidence indicating that in the ferromagnetic phase of $LiHoF_4$, in a field applied along the easy axis of the crystal, the macroscopic average

field,

$$\overline{h^z} = \frac{1}{V}\int_V h^z = h_a^z - N^z\overline{M^z}, \tag{2.26}$$

will be zero up to the saturation value of the magnetization, i.e. $h_a^z = N^z\overline{M^z}$, where $\overline{M^z} = M_+^z + M_-^z$ is now the difference between the contributions of the spins in the up and down domains. In zero applied field, we are led to the conclusion that the system forms long needle like domains, in which case the demagnetization factor for each domain is $N^z = 0$, or that the net magnetization of the system is zero (or both!). As discussed by Tabei *et al.* [69], according to Griffiths' theorem [86] the magnetization of the sample must be zero in the thermodynamic limit. Griffiths' theorem states that spins on a lattice with magnetic dipole-dipole interactions, exchange, and anisotropy energy, possess a well defined bulk free energy, independent of sample shape, in the thermodynamic limit, in the absence of an externally applied magnetic field. This implies the net magnetization of the system must be zero, otherwise, magnetic moments on the surface of the sample would couple to the dipolar moments in the sample, causing shape dependence [35]. Mennenga *et al.* note that their specific heat measurements in zero applied field are independent of sample shape, which can also be understood as a result of Griffiths' theorem. We note that because Griffiths' theorem is only applicable in the thermodynamic limit, the question remains as to how large a system must be in order to have zero net magnetization, and, if there are impurities pinning domain walls, how long it will take the system to reach a state of zero magnetization.

Mennenga *et al.* [35] provide an interesting argument for the vanishing of the macroscopic average field, $\overline{h^z}$, that we reproduce here. They begin by defining the measured susceptibility $\overline{M^z} = \chi_a^{zz} h_a^z$, and the internal susceptibility $\overline{M^z} = \chi_{med}^{zz}\overline{h^z}$, where the internal susceptibility is the response of the medium to the macroscopic average field. As the domain structure is macroscopic, the field to which it will respond is $\overline{h^z}$, so χ_{med}^{zz} measures the susceptibility of the domains. We find that the measured susceptibility may be written as

$$\chi_a^{zz} = \frac{\overline{M^z}}{h_a^z} = \frac{1}{N^z + \frac{\overline{h^z}}{\overline{M^z}}} = \frac{1}{N^z + (\chi_{med}^{zz})^{-1}}. \tag{2.27}$$

In order for the macroscopic average field to vanish in the ferromagnetic phase of the system, we must have $\chi_a^{zz} = \frac{1}{N^z}$, which implies the internal susceptibility of the medium must diverge. This means that the domain walls must have high mobility. As Mennenga *et al.* put it [35] , in equilibrium, we have $\overline{h^z} = 0$. A change in h_a^z will produce a non-zero $\overline{h^z}$; the domain structure will immediately readjust itself so as to keep $\overline{h^z} = 0$. We note that this argument was presented in an earlier paper of Cooke *et al.* [11], in which they verify that $\chi_a^{zz} = \frac{1}{N^z}$ in the ferromagnetic

phase of $LiHoF_4$. They also note that no hysteresis effects are present in $LiHoF_4$, which is another effect of the mobile domain walls.

Experimental evidence for the domain structure of $LiHoF_4$ from optical light scattering is presented in [8], where they found evidence of needle like domains with the extension of one domain perpendicular to the easy axis of the crystal being about $5\mu m$, at a temperature of $0.92T_c$ ($T_c = 1.54K$), in cylindrical samples with the z-axis parallel to the easy axis of the material. In addition, Cooke *et al.* argue in favour of the formation of needle like domains based on energy considerations [11].

Further evidence for the formation of needle shaped domains in $LiHoF_4$ has been found by Kjønsberg and Girvin using Monte Carlo simulations [87]. Considering a spherical sample consisting of 215 dipoles, they see evidence of needle shaped domains. Domains are also considered by Biltmo and Henelius in [88]. Based on energy considerations in a finite cylinder with non-zero demagnetization factor, they predict the formation of parallel sheet domains in the system's ground state. Unfortunately, there is no experimental evidence to support this prediction, so, in this thesis, we will consider a long thin uniformly magnetized cylinder with zero demagnetization field, or a system divided into needle like domains, as has been observved near the zero transverse field phase transition [8].

As noted by Chakraborty *et al.* in [64], in $LiHoF_4$, at low temperatures, the transverse dipolar interaction is negligible compared to the longitudinal dipolar interaction. This means a spin pointing in a direction transverse to the easy axis is unaware of the orientation of its neighbours. Hence, an applied transverse field polarizes spins uniformly in the x direction, or, as Chakraborty *et al.* put it [64], the magnetization M^x is unaware of the domain structure formation in $LiHoF_4$.

Within a single domain away from the domain wall, where the macroscopic field is $h^z = 0$, the local field acting on a spin will be

$$\vec{h}_{loc} = \left(\frac{4\pi}{3} + \lambda_{dip} + \lambda_{ex} \right) \vec{M}. \tag{2.28}$$

The anisotropy energy in $LiHoF_4$ is large, leading to domain walls with a very narrow width; hence, most of the spins will experience the same local field. In what follows, we will consider a long thin cylindrical sample with zero demagnetizing field. Such a sample should consist of a single domain. It also reflects the local field felt by a spin in a sample of $LiHoF_4$ that is divided into needle shaped domains, as discussed above.

The Effective Low Temperature Hamiltonian

We now derive an effective low temperature Hamiltonian for the $LiHoF_4$ system. Following [64], we diagonalize the electronic part of the single ion Hamiltonian $\widetilde{H}_e = UH_eU^\dagger$, with

$$H_e = \sum_i V_C(\vec{J}_i) - g_L\mu_B \sum_i B_x J_i^x. \tag{2.29}$$

We apply the same rotation to the spin operators $\widetilde{J^\mu} = UJ^\mu U^\dagger$, and truncate the operators down to the two by two subspace that mixes the lower two eigenstates of H_e

$$J^\mu = C_\mu(B_x) + \sum_{\nu=x,y,z} C_{\mu\nu}(B_x)\tau^\nu. \tag{2.30}$$

The lower two electronic eigenstates of H_e are well separated from the rest of the electronic eigenstates as illustrated in Figure 2.3. The hyperfine interaction, and the interaction energy between holmium ions, is too weak to cause significant mixing with the higher lying eigenstates, which justifies the truncation procedure. We apply a second rotation in order to diagonalize the J^z operator in the two by two subspace so that $J^z = C_{zz}\tau^z$. In terms of the two lowest eigenstates of H_e, $|\alpha\rangle$ and $|\beta\rangle$, our basis is $|\uparrow\rangle = \frac{1}{\sqrt{2}}[|\alpha\rangle + \exp i\theta|\beta\rangle]$ and $|\downarrow\rangle = \frac{1}{\sqrt{2}}[|\alpha\rangle - \exp i\theta|\beta\rangle]$, where the phase is fixed such that the coefficient of the lowest eigenstate $|\alpha\rangle$ is real and positive. We note that, contrary to the recent claim made in [89], the Ising nature of the electronic degrees of freedom is maintained in an applied transverse field, with the relevant Ising eigenstates, $|\uparrow\rangle$ and $|\downarrow\rangle$, being a mixture of all the J^z eigenstates, given in Figures 2.4 and 2.5. In Figure 2.6, we plot the non-zero matrix elements of the effective spin half operators as a function of the transverse field.

In terms of the effective spin operators, the Hamiltonian H_e may be written in the two by two subspace as

$$\begin{aligned} H_e \approx & \sum_i E_{CM,i}(B_x) - \frac{1}{2}\Delta(B_x)\sum_i \tau_i^x \\ & - \frac{1}{2}J_D C_{zz}^2(B_x)\sum_{i\neq j} D_{ij}^{zz}\tau_i^z\tau_j^z + \frac{1}{2}J_{nn}C_{zz}^2(B_x)\sum_{<ij>}\tau_i^z\tau_j^z, \end{aligned} \tag{2.31}$$

where E_{CM} is the average of the two lowest electronic energy levels, and Δ is their difference. The terms neglected in this approximation either vanish due to symmetry considerations, or they are significantly smaller ($\sim 1\%$) than the terms given in equation (2.31). For a discussion of these terms see [69]. The Ising nature of the system is apparent in the truncated Hamiltonian.

We now reintroduce the nuclear spins by truncating the hyperfine interaction, $H_{hyp} = A\sum_i \vec{I}_i \cdot$

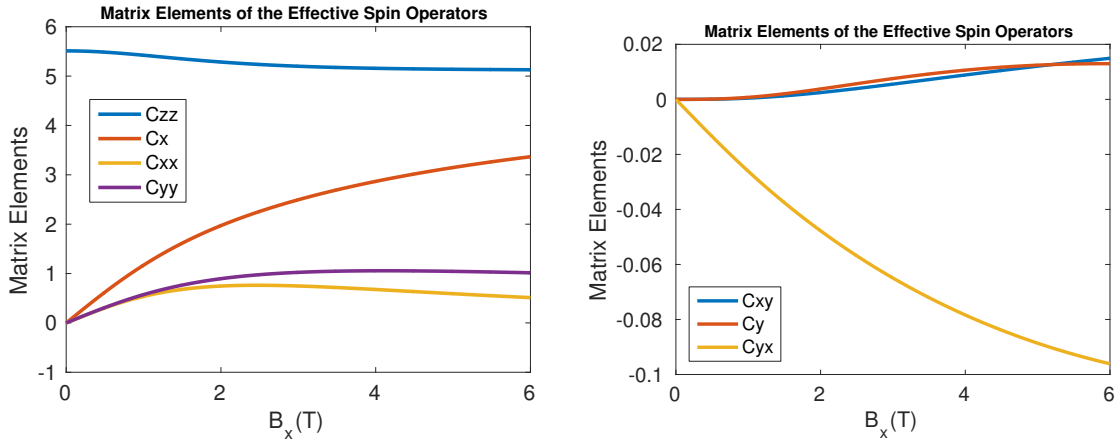

Figure 2.6: In the figures above, we plot the non-zero matrix elements of the effective spin half operators, $J^{\mu} = C_{\mu}(B_x) + \sum_{\nu=x,y,z} C_{\mu\nu}(B_x)\tau^{\nu}$, for the truncated $LiHoF_4$ Hamiltonian. The plot on the left shows the larger matrix elements, with the upper most matrix element being C_{zz}. Below C_{zz}, in descending order, we have C_x, C_{xx} and C_{yy}. The matrix elements in the right hand plot are much smaller than those on the left. In descending order, we have C_y, C_{xy}, and C_{yx}.

$\vec{J}_i$, down to the lowest two electronic levels (we replace $\vec{J}_i$ with the effective spin half operator for the two by two subspace). The result for the hyperfine interaction is

$$\begin{aligned} H_{hyp} = & AC_x \sum_i I_i^x + AC_y \sum_i I_i^y \\ & + AC_{zz} \sum_i \tau_i^z I_i^z + AC_{xz} \sum_i \tau_i^z I_i^x + AC_{yz} \sum_i \tau_i^z I_i^y \\ & + A\frac{C_{xx} + C_{yy} + i(C_{yx} - C_{xy})}{4} \sum_i \tau_i^+ I_i^- + A\frac{C_{xx} + C_{yy} - i(C_{yx} - C_{xy})}{4} \sum_i \tau_i^- I_i^+ \\ & + A\frac{C_{xx} - C_{yy} + i(C_{yx} + C_{xy})}{4} \sum_i \tau_i^- I_i^- + A\frac{C_{xx} - C_{yy} - i(C_{yx} + C_{xy})}{4} \sum_i \tau_i^+ I_i^+ . \end{aligned} \tag{2.32}$$

Dropping the energy shift E_{CM}, and keeping only nonzero terms in the hyperfine interaction, we find our effective low temperature Hamiltonian to be (suppressing the field dependence of our operators)

$$\begin{aligned} H_{eff} = & -\frac{\Delta}{2} \sum_i \tau_i^x - \frac{1}{2} J_D C_{zz}^2 \sum_{i \neq j} D_{ij}^{zz} \tau_i^z \tau_j^z + \frac{1}{2} J_{nn} C_{zz}^2 \sum_{<ij>} \tau_i^z \tau_j^z \\ & + \sum_i \vec{\Delta}_n \cdot \vec{I}_i + A_z \sum_i \tau_i^z I_i^z + A_{\perp} \sum_i \tau_i^+ I_i^- + A_{\perp}^{\dagger} \sum_i \tau_i^- I_i^+ \\ & + A_{++} \sum_i \tau_i^+ I_i^+ + A_{++}^{\dagger} \sum_i \tau_i^- I_i^- , \end{aligned} \tag{2.33}$$

where

$$\vec{\Delta}_n = (AC_x, AC_y, 0) \tag{2.34}$$

and

$$\begin{aligned} A_z &= AC_{zz} \\ A_\perp &= A\frac{C_{xx}+C_{yy}+i(C_{yx}-C_{xy})}{4} \\ A_{++} &= A\frac{C_{xx}-C_{yy}-i(C_{yx}+C_{xy})}{4} \end{aligned} \tag{2.35}$$

Incorporating the nuclear spins into the model by applying the trunctation procedure for the electronic spins to the hyperfine interaction was suggested by Chakraborty et al. in [64]; however, it was never carried out in their work. This is the first time such a procedure has been used to analyze $LiHoF_4$.

In Figure 2.7, we show the effective transverse field acting on the electronic spins as a function of the physical transverse field B_x (in Tesla). The inset shows the next two largest parameters in the effective Hamiltonian, the transverse field acting directly on the nuclear spins, and the longitudinal hyperfine interaction. We see that the effective transverse field acting on the nuclear spins is rather large, and should not be neglected. The remaining parameters in our model, the magnitudes of which are illustrated in Figure 2.8, are significantly smaller.

The important point to take from the low energy effective Hamiltonian is the anisotropy of the hyperfine interaction, and the large effective transverse magnetic field acting directly on the nuclear spins. We see that the effective longitudinal hyperfine interaction is about $A_z = 200mK$, and the transverse component, $A_\perp$, is over ten times smaller. As for the electronic dipole-dipole interaction, the source of the anisotropy is the deformation of the electronic $4f$ orbitals due to the crystal electric field. The effective transverse field acting on the nuclear spins, Δ_n^x, is roughly $100mK$ when the real transverse field, B_x, is between 3T and 6T. It is this effective transverse field that is responsible for the dominant mixing of the nuclear spins, rather than the transverse hyperfine interaction. This effective field is a result of the strong hyperfine interaction in $LiHoF_4$, viz., the physical transverse field shifts the electronic $4f$ orbitals leading a significant effective field acting directly on the nuclear spins via the hyperfine coupling. The dominant longitudinal hyperfine interaction is well known, and was considered by Mennenga et al. in their specific heat measurements in 1983 [35]; however, the large effective field acting on the nuclear spins has not been previously noted.

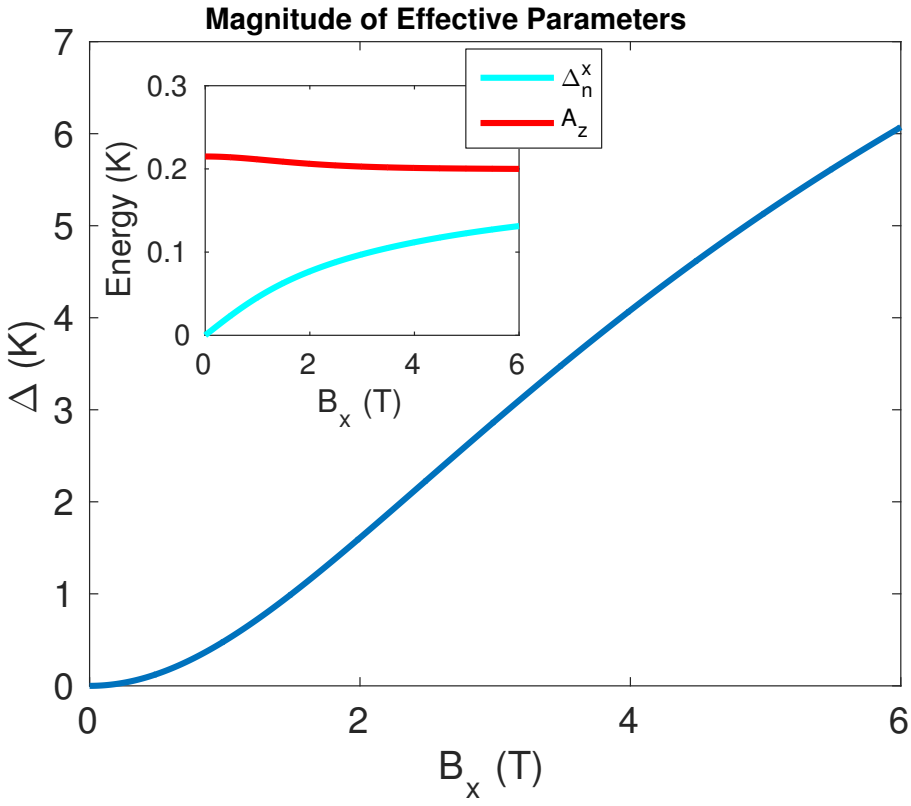

Figure 2.7: In this figure, we plot the effective transverse field, Δ (in Kelvin), acting on the effective Ising spins in $LiHoF_4$, as a function of the physical transverse field B_x (in Tesla). The inset shows the next largest parameters in the $LiHoF_4$ Hamiltonian, these being the effective transverse field acting directly on the nuclear spins, Δ_n^x, and the longitudinal hyperfine coupling, A_z.

Summary

In this chapter, we discussed the rare earth insulating magnet $LiHoF_4$, and its effective low temperature Hamiltonian. At low temperatures, this system is a physical realization of the dipolar coupled Ising model. In Section 2.1, we introduced the Hamiltonian thought to model the material and illustrated its crystal structure. The crystal field, which leads to the Ising anisotropy of the system, and the exchange interaction, are then discussed in Section 2.1.1. In $LiHoF_4$, each electronic degree of freedom is strongly coupled to a nuclear spin. The physics of this hyperfine interaction is discussed in Section 2.1.2. Before turning to the low temperature effective Hamiltonian, we discussed domain formation in $LiHoF_4$ in Section 2.1.3. We relayed the fact that the material forms needle like domains (near its it critical point at least), and that the domain walls have high mobility, dominating the susceptibility in the ordered phase.

In Section 2.2, we truncated the Hamiltonian obtaining a low temperature effective model that fully incorporates the nuclear degrees of freedom. The nuclear spins have not been in-

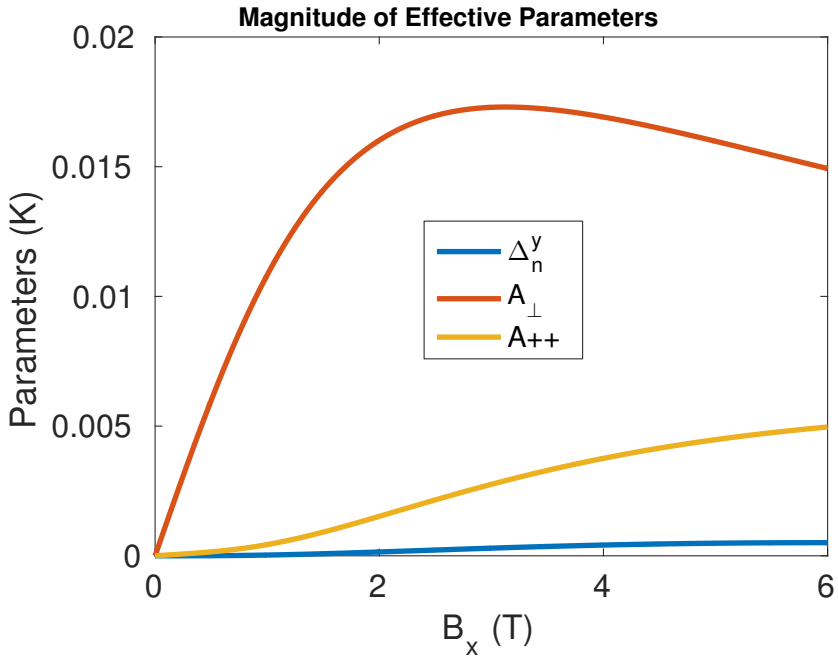

Figure 2.8: In this figure, we plot the magnitudes of the transverse hyperfine parameters, $A_\perp$ being the uppermost line, and A_{++} being the middle line, in the effective low temperature Hamiltonian for $LiHoF_4$ as a function the applied transverse magnetic field B_x. The lowest line is the stray field, Δ_n^y, acting on the nuclear spins in the direction transverse to the easy axis and the direction of the applied transverse field. All these parameters are about an order of magnitude smaller than the other parameters in the model in the vicinity of the critical transverse field $B_x = 4.9T$.

cluded as part of the truncation procedure in previous work. We saw that this effective Hamiltonian is essentially the Ising model, with a hyperfine interaction that is anisotropic, and an effective transverse magnetic field acting on the nuclear spins with a magnitude that is comparable to that of the longitudinal hyperfine interaction. Although the effective anisotropic hyperfine interaction is well known, the effective transverse field acting on the nuclear spins has not been pointed out previously. It is this field that is primarily responsible for the mixing of the nuclear degrees of freedom at low temperatures.

Chapter 3

Dipolar Interaction

In $LiHoF_4$, one must take into consideration the long range dipolar interaction between spins. Recall that in the low temperature effective hamiltonian for $LiHoF_4$ the dipolar component is given by

$$H_{dip} = -\frac{1}{2} J_D C_{zz}^2(B_x) \sum_{i \neq j} D_{ij}^{zz} \tau_i^z \tau_j^z, \tag{3.1}$$

where $\frac{J_D}{a^3} = 7mK$, with $a = 5.175$Å being the transverse lattice spacing. The effective spin half operator is given by $J^z = C_{zz}(B_x)\tau^z$, with $C_{zz}(B_x)$ plotted in Figure 2.6. The spatial dependence of the longitudinal component of the dipolar interaction strength is given by

$$D_{ij}^{zz} = \frac{1}{r_{ij}^3}\left(\frac{3z_{ij}^2}{r_{ij}^2} - 1\right), \tag{3.2}$$

where $r_{ij} = |\vec{r}_i - \vec{r}_j|$, and $z_{ij} = z_i - z_j$.

An analysis of the long range dipolar interaction, taking into account the underlying crystal structure of $LiHoF_4$, is an essential part of understanding the system. This analysis has not been presented explicitly in the literature, so we do so here. We analyze the longitudinal component of the dipolar interaction in Fourier space, performing a dipole wave sum to obtain each Fourier component of the dipolar interaction.

Dipole wave sums were calculated in the continuum limit by Holstein and Primakoff, in 1940, in a paper in which second quantization was used to derive the spin wave spectrum of a dipole-dipole coupled Heisenberg ferromagnet [90]. Working in the continuum limit corresponds to assuming the underlying lattice structure of the sample is simple cubic, and fails to produce the correct result for crystals with a more complicated lattice. Furthermore, Holstein and Primakoff neglect any boundary effects; boundary effects are important for momenta with

wavelengths on the order of the system size, and have a significant impact on the zero momentum summation. In Section 3.1, we reproduce Holstein and Primakoff's results for a spherical sample, and incorporate the effects of the system's boundary. We then repeat the calculation for a long, thin, finite cylinder, which corresponds to the dipolar field felt by a spin within a needle shaped domain. In Section 3.2, we perform the discrete dipole wave sum for small momenta by brute force numerically, and compare with the continuum results.

Dipole wave sums in primitive cubic lattices (simple cubic, body centered cubic, and face centered cubic) were carried out by Cohen and Keffer in a 1955 paper [91]. Cohen and Keffer consider boundary effects in their work, and a key result is that the system's boundary is only significant for momenta such that $kR < 10$, with R being the system size. They also find that the dipole wave sum is independent of position unless $kR < 10$, with the exception of the point at $k = 0$. At $k = 0$, the shaped dependent dipole wave sum is completely independent of the choice of origin, except for origins immediately next to the sample surface. The results of Cohen and Keffer were obtained using the Ewald summation method, which we apply to $LiHoF_4$ in Section 3.3.

The Ewald summation method divides a sum into a short range part, and a long range part. Performing the long range part of the summation in Fourier space leads to rapid convergence of what might otherwise be a slowly converging series. In $LiHoF_4$, the Ewald summation is complicated by the underlying lattice. Ewald summation for a lattice with a basis (the set of atoms associated with each lattice point) has been considered by Bowden and Clark [92]. Bowden and Clark sum over a set of sublattices to account for each atom in the crystal. Rather than sum over sublattices, we prefer to introduce a geometric factor to account for the basis. The calculation is essentially the same. In Section 3.3, we perform the dipole wave sum using Ewald summation in a spherical sample of $LiHoF_4$. In Section 3.3.1, we redo the calculation in a long cylindrical sample of $LiHoF_4$, relevant to a system with needle like domains. No such calculation appears to exist in the literature.

Dipolar Interaction in the Continuum Limit

We begin by calculating the Fourier transform of the dipolar interaction in the continuum limit. This calculation follows the work published in 1940 by Holstein and Primakoff [90]. The

Fourier transform of the dipolar interaction is given by

$$D_k = \frac{1}{N}\sum_{i\neq j} D_{ij} e^{ik(r_i - r_j)} = \frac{1}{N}\sum_{i\neq j}\frac{1}{r_{ij}^3}\left(\frac{3z_{ij}^2}{r_{ij}^2} - 1\right)e^{ikr_{ij}} \tag{3.3}$$
$$= \frac{N}{V}\int_{r\neq 0}\frac{1}{r^3}\left(\frac{3z^2}{r^2} - 1\right)e^{i\vec{k}\cdot\vec{r}}d^3\vec{r}.$$

We exclude the origin ($\int_{r\neq 0}$) from the integral on the final line because the summation excludes the term $i = j$. Clearly, the dipole wave sum on a discrete lattice will depend on the structure of the underlying lattice. In the continuum limit, any information regarding the structure of the lattice is lost. Explicit calculations show that the continuum result is equivalent to performing the discrete summation over a simple cubic lattice [91]. This may be understood as a reflection of the fact that the simple cubic lattice contains a homogeneous distribution of points. In, for example, a tetragonal crystal, one of the spatial directions is stretched. This leads to the discrepancy between the lattice summation over a tetragonal crystal and the continuum result.

We may rewrite equation (3.3) as

$$D_k = \frac{N}{V}D(0) + \frac{N}{V}\int_{r\neq 0}\frac{1}{r^3}\left(1 - \frac{3z^2}{r^2}\right)\left(1 - e^{i\vec{k}\cdot\vec{r}}\right)d^3\vec{r} \tag{3.4}$$
$$= \frac{N}{V}D(0) + \frac{Nk_z}{V}\frac{\partial}{\partial k_z}\int\frac{1}{r^3}e^{i\vec{k}\cdot\vec{r}}d^3\vec{r} + \frac{N}{V}\left[\frac{z}{r^3}\left(1 - e^{i\vec{k}\cdot\vec{r}}\right)\right]_{\partial z} dxdy,$$

where an integration by parts is performed on the z component of the integral, and $D(0) = \int_{r\neq 0}\frac{1}{r^3}\left(\frac{3z^2}{r^2} - 1\right)d^3\vec{r}$. The above manipulations separate the zero wavevector component of the sum, which contains the divergence at the origin, from the rest.

The zero wavevector component of the sum is given by

$$\frac{N}{V}D(0) = -\frac{N}{V}\int_{r\neq 0}\frac{1}{r^3}\left(1 - \frac{3z^2}{r^2}\right)d^3\vec{r} \tag{3.5}$$
$$= -\frac{N}{V}\int_{in}\frac{z}{r^3}\hat{z}\cdot\vec{n}d\Sigma - \frac{N}{V}\int_{out}\frac{z}{R^3}\hat{z}\cdot\vec{n}d\Sigma,$$

where *in* denotes a small sphere centered at the origin, and *out* denotes the outer surface of the specimen. We exclude the origin and use Gauss' theorem to obtain the second line from the first. The first term is a surface integral, oriented towards the origin, over a small sphere, which gives us the Lorentz local field. The second term is an integral over the outer surface of the sample, oriented towards infinity, which gives us the demagnetizing field

$$H_D = -\frac{N}{V}\int_{out}\frac{z}{R^3}\hat{z}\cdot\vec{n}d\Sigma. \tag{3.6}$$

Ignoring the demagnetizing field for the moment, we find the Lorentz local field to be

$$\begin{aligned}\frac{N}{V}D(0)\Big|_{in} &= -\frac{N}{V}\int_{in}\frac{z}{r^3}\hat{z}\cdot\vec{n}d\Sigma \\ &= \frac{N}{V}\int_0^{2\pi}\int_0^{\pi} sin(\theta)cos^2(\theta)d\theta d\phi = \frac{N}{V}\frac{4\pi}{3}.\end{aligned} \tag{3.7}$$

Given a spherical sample of a simple cubic crystal, the demagnetizing field is equal and opposite to the Lorentz local field, and the zero wavevector sum vanishes. With a more complicated underlying lattice, or a more complicated sample shape, the contributions will not cancel. In a uniformly magnetized ellipsoid, the demagnetizing field is constant; however, the demagnetizing field of a non-ellipsoidal sample may be a rather complicated function of the specimen's shape that likely needs to be worked out numerically [85]. We will deal with lattices more complicated than simple cubic later in Sections 3.2 and 3.3.

We now turn to the momentum dependent part of the dipole wave sum. We consider a spherically shaped sample with radius R, and perform the first integral in equation (3.4) in spherical coordinates

$$I_1 = \frac{Nk_z}{V}\frac{\partial}{\partial k_z}\int\frac{1}{r^3}e^{i\vec{k}\cdot\vec{r}}d^3\vec{r} = \frac{4\pi Nk_z}{V}\frac{\partial}{\partial k_z}\int_0^R\frac{\sin(kr)}{kr^2}dr. \tag{3.8}$$

In Section 3.1.2, we will consider a long cylindrical sample, relevant to materials that form needle like domains. We now perform the $\frac{\partial}{\partial k_z}$ derivative and integrate to get

$$I_1 = -\frac{4\pi N}{V}\frac{k_z^2}{k^2}\Big[1 - j_0(kR)\Big], \tag{3.9}$$

where j_0 is a spherical Bessel function of the first kind. In an infinite sample $j_0(kR) \to 0$, and we're left with only the term to the left of the square brackets.

The boundary term in equation (3.4) from the integration by parts can be evaluated as follows (assuming a spherical sample)

$$\begin{aligned}I_2 &= \frac{N}{V}\int\left[\frac{z}{r^3}(1-e^{i\vec{k}\cdot\vec{r}})\right]_{\partial z}dxdy \\ &= \frac{N}{V}\frac{2}{R^3}\int_{-R}^{R}\int_{-\sqrt{R^2-y^2}}^{\sqrt{R^2-y^2}}\sqrt{R^2-r^2}\left[1-e^{i\vec{k}_\perp\cdot\vec{r}_\perp}\cos\left(k_z\sqrt{R^2-r^2}\right)\right]dxdy\end{aligned} \tag{3.10}$$

where $\vec{r}_\perp = (x,y)$ and $r = |\vec{r}_\perp|$. In polar coordinates, the integral becomes

$$\begin{aligned} I_2 &= \frac{N}{V}\frac{2}{R^3}\int_0^R \int_0^{2\pi} r\sqrt{R^2-r^2}\left[1-e^{ik_\perp r\cos\theta}\cos\left(k_z\sqrt{R^2-r^2}\right)\right]drd\theta \\ &= \frac{N}{V}4\pi\int_0^1 x^2\left[1-J_0(k_\perp R\sqrt{1-x^2})\cos\left(k_z Rx\right)\right]dx, \end{aligned} \tag{3.11}$$

where $J_0(x)$ is a Bessel function of the first kind. In the limit of infinite sample size ($k_\perp R \gg 1$), we find

$$I_2 = \frac{N}{V}\frac{4\pi}{3} - \frac{N}{V}4\pi\int_0^1 y\sqrt{1-y^2}J_0(k_\perp Ry)\cos\left(k_z R\sqrt{1-y^2}\right)dy \tag{3.12}$$

Numerical integration indicates the integral on the right vanishes as we take the limit of an infinite sized system. This is expected because as $R\to\infty$, J_0 and the cosine become rapidly varying functions that average to zero.

Our final result, for a spherical sample with cubic symmetry in the limit of infinite sample size, is

$$D_k = \begin{cases} \frac{N}{V}\frac{4\pi}{3} + H_D & : k = 0 \\ \frac{N}{V}\frac{4\pi}{3} + H_D + \frac{N}{V}\frac{4\pi}{3}\left(1-3\frac{k_z^2}{k^2}\right) & : k \neq 0 \end{cases}$$

Recall that in a spherical sample the Lorentz local field and the demagnetizing field are equal and opposite and will sum to zero. We leave them in the expressions above as a reminder that they may not cancel in a system with a more complicated shape, or a more complicated underlying lattice. In such a sample, the zero frequency dipole wave sum is given by $D_0 = \frac{N}{V}\left(\frac{4\pi}{3}+\lambda_{dip}\right)+H_D$, where λ_{dip} accounts for the lattice structure. Note that in the limit $k\to 0$, the term $\frac{k_z^2}{k^2}$ can take on any value in the interval $[0,1]$. This ambiguity is removed when we take into consideration corrections due to the finite size of the spherical sample.

Finite Sized Spherical Sample

We now consider the dipole wave sum for a finite sized spherical sample in the continuum limit. This calculation is performed in the 1955 work of Cohen and Keffer [91], in which they perform dipole wave sums for primitive cubic lattices taking into account finite size effects. Cohen and Keffer find that boundary effects are negligible outside the region $kR < 10$. For momenta inside this region, the dipole wave sum will have strong position and shape dependence, except at $k = 0$. At $k = 0$, the dipole wave sum is independent of the choice of origin; however, it will still be dependent on the shape of the sample.

The boundary contributes three additional terms to the dipolar sum, $\partial D_k = H_D + \partial D_k^2 +$

∂D_k^3. The first term, which stems from the zero wavevector sum, is the demagnetization field

$$H_D = -\frac{N}{V}\int_{out}\frac{z}{R^3}\hat{z}\cdot\vec{n}d\Sigma = -\frac{N}{V}\frac{4\pi}{3}. \tag{3.13}$$

In a spherical sample with cubic symmetry, this is equal and opposite to the Lorentz local field given by equation (3.7). The second term comes from the boundary of the integral in equation (3.9). We get an additional contribution to the dipole sum of

$$\partial D_k^2 = \frac{N}{V}\frac{4\pi k_z^2}{k^2}j_0(kR). \tag{3.14}$$

In the limit $kR \ll 1$, the Bessel function may be approximated as $j_0(kR) \approx 1 - \frac{1}{6}(kR)^2$, and

$$I_1 = -\frac{4\pi N}{V}\frac{k_z^2}{k^2}\left[1 - j_0(kR)\right] \approx -\frac{N}{V}\frac{2\pi}{3}(k_zR)^2. \tag{3.15}$$

The third boundary term comes from (3.11), which we consider in the small k limit, where

$$J_0(k_\perp R\sqrt{1-x^2}) \approx 1 - \frac{(k_\perp R)^2}{4}(1-x^2) \qquad \cos(k_zRx) \approx 1 - \frac{(k_zRx)^2}{2}. \tag{3.16}$$

We find

$$\begin{aligned}\partial D_k^3 &= -\frac{N}{V}4\pi\int_0^1 x^2 J_0(k_\perp R\sqrt{1-x^2})\cos(k_zRx)dx \\ &\approx -\frac{N}{V}4\pi\left[\frac{1}{3} - \frac{(k_zR)^2}{10} - \frac{(k_\perp R)^2}{30}\right].\end{aligned} \tag{3.17}$$

This gives us

$$I_2 \approx \frac{N}{V}\frac{4\pi}{3}\left[\frac{(kR)^2}{10} + \frac{(k_zR)^2}{5}\right], \tag{3.18}$$

which leads to the following expression for the dipole wave sum at small wavevectors ($\lambda \gg R$) in a spherical sample with simple cubic symmetry

$$D_k = \frac{N}{V}\frac{4\pi}{3} + H_D + \frac{N}{V}\frac{4\pi}{3}\frac{R^2}{10}[k_\perp^2 - 2k_z^2]. \tag{3.19}$$

In a spherical sample, the first two terms cancel, but we leave them in as a reminder that there may be a zero frequency contribution to the sum for other sample shapes, or with an underlying lattice that is not simple cubic. In a ferromagnet, a system will order at a wavevector such that D_k is a maximum. From the above expression, we see that it is energetically favourable for the

system to order at $k = k_\perp \neq 0$. It is energetically favourable for a spherically sample to order at wavevectors slightly away from zero.

In a sample that is large enough, the system will rearrange itself, forming domains, in order to minimize its free energy. In such a system, it no longer makes sense to consider the shape of the sample, rather, it is the shape of the domains that is important. Stray fields from neighbouring domains are negligible because the system forms domains in order to eliminate these fields. In Section 3.1.2, we turn to a long thin cylindrical sample, consistent with a system that forms needle like domains.

Finite Sized Cylindrical Sample

We now consider the dipole wave sum, in the continuum limit, for a long thin cylindrical sample. This sample shape has been considered by Cohen and Keffer [91]; however, they did not publish their results. The expansion in plane waves presented here is straightforward; however, an expansion in cylindrical waves may prove useful for obtaining analytic results. We leave the cylindrical wave calculation as a subject of future work. The calculation most likely exists elsewhere in the literature, but the time required to track it down far exceeds the time required to carry out the calculation.

We begin with the expression

$$D_k = \frac{N}{V}D(0) + \frac{Nk_z}{V}\frac{\partial}{\partial k_z}\int \frac{1}{r^3}e^{i\vec{k}\cdot\vec{r}}d^3\vec{r} + \frac{N}{V}\int\left[\frac{z}{r^3}(1-e^{i\vec{k}\cdot\vec{r}})\right]_{\partial z} dxdy. \tag{3.20}$$

In a long thin cylinder, magnetized along its longitudinal axis, the demagnetizing field is approximately zero. This is because the magnetic surface charge (unpaired dipoles) lie at the top and the bottom of the cylinder. As the length of the cylinder is increased, the interaction energy of these dipoles goes to zero [85]. This means

$$\frac{N}{V}D(0) = \frac{N}{V}\frac{4\pi}{3}. \tag{3.21}$$

We perform the first integral in cylindrical coordinates

$$\begin{aligned} I_1 &= \frac{Nk_z}{V}\frac{\partial}{\partial k_z}\int \frac{1}{r^3}e^{i\vec{k}\cdot\vec{r}}d^3\vec{r} \\ &= \frac{Nk_z}{V}\frac{\partial}{\partial k_z}\int_{-h}^{h}\int_0^{2\pi}\int_0^R \frac{r}{(r^2+z^2)^{\frac{3}{2}}}e^{ik_\perp r\cos\theta}e^{ik_z z}drd\theta dz \\ &= -\frac{N4\pi k_z}{V}\int_0^h\int_0^R \frac{rzJ_0(k_\perp r)}{(r^2+z^2)^{\frac{3}{2}}}\sin(k_z z)drdz, \end{aligned} \tag{3.22}$$

where, in the final line, we have performed the angular integral and reduced the z domain to $[0,h]$. In the long wavelength limit, $k_z h \ll 1$ and $k_\perp R \ll 1$, we find

$$\begin{aligned} I_1 &\approx -\frac{N4\pi k_z^2}{V}\int_0^h\int_0^R \frac{rz^2}{(r^2+z^2)^{\frac{3}{2}}}drdz \\ &= -\frac{N2\pi k_z^2}{V}\left[h^2 - h(R^2+h^2)^{\frac{1}{2}} + R^2\ln\left(\frac{h+(R^2+h^2)^{\frac{1}{2}}}{R}\right)\right]. \end{aligned} \tag{3.23}$$

Assuming a long thin cylinder, we find

$$I_1 \approx -\frac{N}{V}2\pi(k_z h)^2\left[\frac{R^2}{h^2}\ln\left(\frac{2h}{R}\right) - \frac{R^2}{2h^2} + \cdots\right]. \tag{3.24}$$

For the second integral we have

$$\begin{aligned} I_2 &= \frac{N}{V}\int\left[\frac{z}{r^3}(1-e^{i\vec{k}\cdot\vec{r}})\right]_{\partial z} dxdy \\ &= \frac{N}{V}\int_0^{2\pi}\int_0^R \frac{hr}{(r^2+h^2)^{\frac{3}{2}}}\left[2-2e^{ik_\perp r\cos\theta}\cos(k_z h)\right]drd\theta \\ &= \frac{N}{V}4\pi h\int_0^R \frac{r}{(r^2+h^2)^{\frac{3}{2}}}\left[1-J_0(k_\perp r)\cos(k_z h)\right]dr \end{aligned} \tag{3.25}$$

Expanding in the long wavelength limit we find

$$I_2 \approx \frac{N}{V}4\pi h\left[\frac{k_\perp^2}{4}\left(\frac{R^2+2h^2}{(R^2+h^2)^{\frac{1}{2}}} - 2h\right) + \frac{k_z^2 h^2}{2}\left(\frac{1}{h} - \frac{1}{(R^2+h^2)^{\frac{1}{2}}}\right)\right]. \tag{3.26}$$

For a long thin cylinder, $R \ll h$, the expression becomes

$$I_2 \approx \frac{N}{V}2\pi k_z^2 h^2\frac{R^2}{2h^2} - \frac{N}{V}2\pi k_\perp^2 R^2\frac{R^2}{4h^2} + \cdots. \tag{3.27}$$

The dipole sum is then given by

$$D_k \approx \frac{N}{V}\frac{4\pi}{3} - \frac{N}{V}2\pi k_z^2 h^2\left[\frac{R^2}{h^2}\ln\left(\frac{2h}{R}\right) - \frac{R^2}{h^2}\right] - \frac{N}{V}2\pi k_\perp^2 R^2\frac{R^2}{4h^2} + \cdots. \tag{3.28}$$

Recall that for a long thin cylinder we have $H_D \approx 0$. We see that in a cylindrical sample, the quadratic term will depend on the aspect ratio, with the longitudinal momentum component becoming more dominant as the length of the cylinder is increased. Unlike the spherical sample, in the case of a long thin cylinder, we see that D_k has a maximum at $k = 0$. Hence, a long thin cylindrical sample will order at zero wavevector.

Direct Summation of the Dipolar Interaction in LiHoF4

In this section, we resort to direct summation to obtain the dipole wave sums in $LiHoF_4$. This summation converges at a reasonable rate in the long wavelength limit $kR \ll 1$; however, it takes an unreasonably long time to converge for momenta belonging to the rest of the Brillouin zone. In Section 3.3, we will perform perform the summation over the entire Brillouin zone using the Ewald summation method. The work here, which is valid at small momenta, can be used to verify the Ewald summation results.

We will consider the cases of a spherical sample and a long cylindrical sample, or needle shaped domain. The summations are complicated by the fact that the underlying lattice of the system is not simple cubic. We will sum over four sublattices to account for each atom in the $LiHoF_4$ crystal. The dipolar sum is given by

$$D_{\vec{k}}^{zz} = \frac{1}{N}\sum_{i\neq j} D_{ij} e^{i\vec{k}\cdot(\vec{r}_i-\vec{r}_j)} = \sum_{l\neq 0} \frac{1}{r_l^3}\left(\frac{3z_l^2}{r_l^2} - 1\right) e^{i\vec{k}\cdot\vec{r}_l}, \tag{3.29}$$

where $\vec{r}_l = \vec{r}_i - \vec{r}_j$. The positive and negative components of the dipole wave sums are not independent, they are related by $D_{\vec{k}}^{zz} = (D_{-\vec{k}}^{zz})^*$. Upon summation over the Brillouin zone, the positive and negative momentum components of the imaginary part of the dipole wave sum will cancel, and may be neglected from the subsequent analysis. For the real component, we have $\mathrm{Re}[D_{\vec{k}}^{zz}] = \mathrm{Re}[D_{-\vec{k}}^{zz}]$; hence, all terms odd in $\vec{k}$ will vanish.

Note that D_{ij} is a function of an atom's distance from the origin. We will group the terms in the sum accordingly. We divide the sum into four parts, $D_{\vec{k}}^{zz} = D_k^1 + D_k^2 + D_k^3 + D_k^4$, where the four terms correspond to the following atoms:

$$\begin{aligned}
&\vec{r}_l{}^1 = (ma, na, pc) && \vec{r}_l{}^2 = (m+\frac{1}{2}, n+\frac{1}{2}, p+\frac{1}{2}) \\
&\vec{r}_l{}^3 = (\pm m, \pm(n+\frac{1}{2}), p+\frac{1}{4}) \quad \text{and} && \vec{r}_l{}^3 = (\pm(n+\frac{1}{2}), \pm m, -p-\frac{1}{4}) \\
&\vec{r}_l{}^4 = (\pm(m+\frac{1}{2}), \pm n, p+\frac{3}{4}) \quad \text{and} && \vec{r}_l{}^4 = (\pm n, \pm(m+\frac{1}{2}), -p-\frac{3}{4}).
\end{aligned} \tag{3.30}$$

We introduce

$$D(m,n,p) = \frac{1}{[(m^2+n^2)a^2 + (pc)^2]^{\frac{3}{2}}}\left[\frac{3(pc)^2}{(m^2+n^2)a^2+(pc)^2} - 1\right] \tag{3.31}$$

for notational compactness.

First, we consider $\vec{r}_l{}^1 = (ma, na, pc)$, and, to avoid overcounting lattice sites, we treat the

axes, planes, and bulk of the sample separately. Along the axes we find

$$D_k^1|_{\text{axes}} = \sum_{m=1}^{\infty} \left[\cos(k_x ma) + \cos(k_y ma)\right] 2D(m,0,0) + \sum_{p=1}^{\infty} 2\cos(k_z pc) D(0,0,p) \tag{3.32}$$
$$\approx \sum_{m=1}^{\infty} \left[4D(m,0,0) - k_\perp^2 (ma)^2 D(m,0,0)\right] + \sum_{p=1}^{\infty} \left[2D(0,0,p) - k_z^2 (pc)^2 D(0,0,p)\right],$$

where $k_\perp^2 = k_x^2 + k_y^2$. We are careful to distinguish between the summation along the transverse axes and the summation along the easy axis, as these terms will contribute differently depending on whether we are considering a sphere or a cylinder. Along the planes we find

$$D_k^1|_{\text{planes}} = \sum_{m,n=1}^{\infty} 4\cos(k_x ma)\cos(k_y na) D(m,n,0) \tag{3.33}$$
$$+ \sum_{m,p=1}^{\infty} \left[\cos(k_x ma)\cos(k_z pc) + \cos(k_y ma)\cos(k_z pc)\right] 4D(m,0,p)$$
$$\approx \sum_{m,n=1}^{\infty} \left[4D(m,n,0) - 2k_\perp^2 (ma)^2 D(m,n,0)\right]$$
$$+ \sum_{m,p=1}^{\infty} \left[8D(m,0,p) - 2k_\perp^2 (ma)^2 D(m,0,p) - 4k_z^2 (pc)^2 D(m,0,p)\right],$$

and in the bulk we find

$$D_k^1|_{\text{bulk}} = \sum_{m,n,p=1}^{\infty} 8\cos(k_x ma)\cos(k_y na)\cos(k_z pc) D(m,n,p) \tag{3.34}$$
$$\approx \sum_{m,n,p=1}^{\infty} \left[8D(m,n,p) - 4k_\perp^2 (ma)^2 D(m,n,p) - 4k_z^2 (pc)^2 D(m,n,p)\right].$$

For compactness, we now introduce, for example, $m + \frac{1}{2} \equiv m_{\frac{1}{2}}$, or $p + \frac{3}{4} \equiv p_{\frac{3}{4}}$. For the atoms at $\vec{r}_l{}^2 = (m_{\frac{1}{2}}, n_{\frac{1}{2}}, p_{\frac{1}{2}})$, we only need to consider the bulk. We find

$$D_k^2 = \sum_{m,n,p=0}^{\infty} 8\cos\left(k_x m_{\frac{1}{2}} a\right)\cos\left(k_y n_{\frac{1}{2}} a\right)\cos\left(k_z p_{\frac{1}{2}} c\right) D(m_{\frac{1}{2}}, n_{\frac{1}{2}}, p_{\frac{1}{2}}) \tag{3.35}$$
$$\approx \sum_{m,n,p=0}^{\infty} \left[8D(m_{\frac{1}{2}}, n_{\frac{1}{2}}, p_{\frac{1}{2}}) - 4k_\perp^2 m_{\frac{1}{2}}^2 a^2 D(m_{\frac{1}{2}}, n_{\frac{1}{2}}, p_{\frac{1}{2}}) - 4k_z^2 p_{\frac{1}{2}}^2 c^2 D(m_{\frac{1}{2}}, n_{\frac{1}{2}}, p_{\frac{1}{2}})\right].$$

Next, we consider the atoms at $\vec{r}_l{}^3 = (\pm m, \pm n_{\frac{1}{2}}, p_{\frac{1}{4}})$ and $\vec{r}_l{}^3 = (\pm n_{\frac{1}{2}}, \pm m, -p_{\frac{1}{4}})$. We must

consider the planes and the bulk of the sample separately. In the planes, where $m = 0$, we find

$$D_k^3|_{\text{planes}} = \sum_{n,p=0}^{\infty} 2\left[\cos\left(k_x n_{\frac{1}{2}} a\right)\exp\left(-ik_z p_{\frac{1}{4}} c\right) + \cos\left(k_y n_{\frac{1}{2}} a\right)\exp\left(ik_z p_{\frac{1}{4}} c\right)\right] D(0, n_{\frac{1}{2}}, p_{\frac{1}{4}}) \tag{3.36}$$

$$\approx \sum_{n,p=0}^{\infty}\left[4D(0,n_{\frac{1}{2}},p_{\frac{1}{4}}) - k_\perp^2 n_{\frac{1}{2}}^2 a^2 D_{(0,n_{\frac{1}{2}},p_{\frac{1}{4}})} - 2k_z^2 p_{\frac{1}{4}}^2 c^2 D(0,n_{\frac{1}{2}},p_{\frac{1}{4}})\right],$$

and in the bulk we have

$$D_k^3|_{\text{bulk}} = \sum_{\substack{m=1\\n,p=0}}^{\infty} 4\left[\cos\left(k_x ma\right)\cos\left(k_y n_{\frac{1}{2}} a\right)\exp\left(ik_z p_{\frac{1}{4}} c\right)\right. \tag{3.37}$$

$$\left. + \cos\left(k_x n_{\frac{1}{2}} a\right)\cos\left(k_y ma\right)\exp\left(-ik_z p_{\frac{1}{4}} c\right)\right] D(m, n_{\frac{1}{2}}, p_{\frac{1}{4}})$$

$$\approx \sum_{\substack{m=1\\n,p=0}}^{\infty}\left[8D(m,n_{\frac{1}{2}},p_{\frac{1}{4}}) - 4k_\perp^2\left[m^2 + n_{\frac{1}{2}}^2\right]a^2 D(m,n_{\frac{1}{2}},p_{\frac{1}{4}}) - 4k_z^2 p_{\frac{1}{4}}^2 c^2 D(m,n_{\frac{1}{2}},p_{\frac{1}{4}})\right].$$

Finally, we consider the atoms at $\vec{r}_l{}^4 = (\pm m_{\frac{1}{2}}, \pm n, p_{\frac{3}{4}})$ and $\vec{r}_l{}^4 = (\pm n, \pm m_{\frac{1}{2}}, -p_{\frac{3}{4}})$. Along the axis, where $n = 0$, we find

$$D_k^4|_{\text{planes}} = \sum_{m,p=0}^{\infty} 2\left[\cos\left(k_x m_{\frac{1}{2}} a\right)\exp\left(ik_z p_{\frac{3}{4}} c\right)\right. \tag{3.38}$$

$$\left. + \cos\left(k_y m_{\frac{1}{2}} a\right)\exp\left(-ik_z p_{\frac{3}{4}} c\right)\right] D(m_{\frac{1}{2}}, 0, p_{\frac{3}{4}})$$

$$\approx \sum_{m,p=0}^{\infty}\left[4D(m_{\frac{1}{2}},0,p_{\frac{3}{4}}) - k_\perp^2 m_{\frac{1}{2}}^2 a^2 D(m_{\frac{1}{2}},0,p_{\frac{3}{4}}) - 2k_z^2 p_{\frac{3}{4}}^2 c^2 D(m_{\frac{1}{2}},0,p_{\frac{3}{4}})\right],$$

and in the bulk we have

$$D_k^4|_{\text{bulk}} = \sum_{\substack{n=1\\m,p=0}}^{\infty} 4\left[\cos\left(k_x m_{\frac{1}{2}} a\right)\cos\left(k_y na\right)\exp\left(ik_z p_{\frac{3}{4}} c\right) + \right. \tag{3.39}$$

$$\left. + \cos\left(k_x na\right)\cos\left(k_y m_{\frac{1}{2}} a\right)\exp\left(-ik_z p_{\frac{3}{4}} c\right)\right] D(m_{\frac{1}{2}}, n, p_{\frac{3}{4}})$$

$$\approx \sum_{\substack{n=1\\m,p=0}}^{\infty}\left[8D(m_{\frac{1}{2}},n,p_{\frac{3}{4}}) - 4k_\perp^2\left[n^2 + m_{\frac{1}{2}}^2\right]a^2 D(m_{\frac{1}{2}},n,p_{\frac{3}{4}}) - 4k_z^2 p_{\frac{3}{4}}^2 c^2 D(m_{\frac{1}{2}},n,p_{\frac{3}{4}})\right].$$

We have divided the dipole wave sum into summations over four sublattices, and then

proceeded to expand the result in the limit $kR \ll 1$. The result may be divided into three parts,

$$D_{\vec{k}}^{zz} = D_0 + \frac{D_{k_\perp}}{R^2}(k_\perp R)^2 + \frac{D_{k_z}}{h^2}(k_z h)^2, \tag{3.40}$$

representing the zero wavevector contribution, the transverse contribution, and the longitudinal contribution, respectively. We introduce the radial system size R, and the longitudinal system size h, to emphasize that the small parameter we are expanding in is kR, or kh. Collecting together like terms in the dipole wave summation we find

$$\begin{aligned}
D_0 = {} & 4\sum_{m=1}^{\infty} D(m,0,0) + 2\sum_{p=1}^{\infty} D(0,0,p) + 4\sum_{m,n=1}^{\infty} D(m,n,0) \\
& + 4\sum_{m,p=0}^{\infty}\left[2D(m_1,0,p_1) + D(0,m_{\frac{1}{2}},p_{\frac{1}{4}}) + D(m_{\frac{1}{2}},0,p_{\frac{3}{4}})\right] \\
& + 8\sum_{m,n,p=0}^{\infty}\left[D(m_1,n_1,p_1) + D(m_{\frac{1}{2}},n_{\frac{1}{2}},p_{\frac{1}{2}}) + D(m_1,n_{\frac{1}{2}},p_{\frac{1}{4}}) + D(m_{\frac{1}{2}},n_1,p_{\frac{3}{4}})\right] \\
-D_{k_\perp} = {} & \sum_{m=1}^{\infty}(ma)^2 D(m,0,0) + 2\sum_{m,n=1}^{\infty}(ma)^2 D(m,n,0) \\
& + 2\sum_{m,p=0}^{\infty}\left[((m+1)a)^2 D(m_1,0,p_1) + \left(m+\frac{1}{2}\right)^2 a^2\left(D(0,m_{\frac{1}{2}},p_{\frac{1}{4}}) + D(m_{\frac{1}{2}},0,p_{\frac{3}{4}})\right)\right] \\
& + 4\sum_{m,n,p=0}^{\infty}\left[((m+1)a)^2 D(m_1,n_1,p_1) + \left(m+\frac{1}{2}\right)^2 a^2 D(m_{\frac{1}{2}},n_{\frac{1}{2}},p_{\frac{1}{2}})\right. \\
& \qquad \left. + \left(\left(m+1\right)^2 + \left(n+\frac{1}{2}\right)^2\right)a^2\left(D(m_1,n_{\frac{1}{2}},p_{\frac{1}{4}}) + D(m_{\frac{1}{2}},n_1,p_{\frac{3}{4}})\right)\right] \\
-D_{k_z} = {} & \sum_{p=1}^{\infty}(pc)^2 D(0,0,p) + 2\sum_{m,p=0}^{\infty}\left[2((p+1)c)^2 D(m_1,0,p_1)\right. \\
& \qquad \left. + \left(\left(p+\frac{1}{4}\right)c\right)^2 D(0,m_{\frac{1}{2}},p_{\frac{1}{4}}) + \left(\left(p+\frac{3}{4}\right)c\right)^2 D(m_{\frac{1}{2}},0,p_{\frac{3}{4}})\right] \\
& + 4\sum_{m,n,p=0}^{\infty}\left[((p+1)c)^2 D(m_1,n_1,p_1) + \left(\left(p+\frac{1}{2}\right)c\right)^2 D(m_{\frac{1}{2}},n_{\frac{1}{2}},p_{\frac{1}{2}}) + \right. \\
& \qquad \left. + \left(\left(p+\frac{1}{4}\right)c\right)^2 D(m_1,n_{\frac{1}{2}},p_{\frac{1}{4}}) + \left(\left(p+\frac{3}{4}\right)c\right)^2 D(m_{\frac{1}{2}},n_1,p_{\frac{3}{4}})\right]
\end{aligned} \tag{3.41}$$

In a spherical sample ($R = h$) we find $D_0 * a^3 = 3.205$, where $a = 5.175$Å is the transverse unit cell length. Recall that in the continuum limit the zero momentum dipole wave sum is zero. The value obtained here is due strictly to the underlying lattice. We find $D_0 * a^3 = \frac{c}{a}\lambda_{dip}$, with $\lambda_{dip} = 1.54$. The transverse and longitudinal components of the dipole sum converge much

slower than the zero frequency contribution. If we take the system size to be $R = 1000$, we find $D_{k_\perp} * \frac{a^3}{R^2} = 32.41$ and $D_z * \frac{a^3}{R^2} = -43.22$. In the continuum limit, the result is $D_{k_\perp} = -\frac{1}{2} D_z$.

In a cylindrical sample, we find $D_0 * a^3 = 11.272$, while $D_{k_\perp}$ and D_z depend on the aspect ratio of the cylinder. This dependence on the aspect ratio is consistent with the result obtained in Section 3.1.2 by treating the dipole sum in the continuum limit (valid for a simple cubic crystal). The demagnetization field for a long thin cylinder is zero; hence, we may write the zero momentum dipole sum as $D_0 * a^3 = \frac{c}{a}\left(\frac{4\pi}{3} + \lambda_{dip}\right)$, with the correction due to the lattice being $\lambda_{dip} = 1.24$.

Ewald Summation in LiHoF4

We now calculate the Fourier transform of the dipolar interaction in $LiHoF_4$ making use of the Ewald summation method. Ewald summation leads to rapid convergence of the dipole wave sum over the entire Brillouin zone. We follow the papers of Aharony and Fisher, and of Bowden and Clark [92, 93]. The paper of Bowden and Clark generalizes the Ewald summation method to systems with more than one atom per unit cell, such as $LiHoF_4$, by summing over a set of sublattices. Here, rather than summing over sublattices, we prefer to introduce a geometric factor to account for each of the atoms in the unit cell. We begin by performing the Ewald summation in a spherical sample. In Section 3.3.1, we go on to perform the Ewald summation in a long thin cylinder, relevant to a system with needle like domains. We have found no such calculation in the literature.

The dipolar interaction may be written as

$$D^{zz}_{\vec{k}} = \frac{1}{N}\sum_{i\neq j}\frac{1}{r^3_{ij}}\left(\frac{3z^2_{ij}}{r^2_{ij}} - 1\right)e^{i\vec{k}\cdot\vec{r}_{ij}} = \frac{\partial^2}{\partial z^2}\sum_{l\neq 0}\frac{e^{i\vec{k}\cdot\vec{r}_l}}{|\vec{r}_l - \vec{r}|}\bigg|_{\vec{r}=0}, \tag{3.42}$$

where, in the last line, we have set $\vec{r}_i - \vec{r}_j = \vec{r}_l$ and the sum runs over all atoms in the lattice excluding the atom at $\vec{r}$. We begin by making use of the Gaussian integral

$$\frac{1}{|\vec{r}_l - \vec{r}|} = \frac{2}{\sqrt{\pi}}\int_0^\infty d\rho e^{-\rho^2|\vec{r}_l - \vec{r}|^2} \tag{3.43}$$

to obtain

$$D^{zz}_{\vec{k}}(\vec{r}) = \frac{\partial^2}{\partial z^2}\sum_{l\neq 0} e^{i\vec{k}\cdot\vec{r}_l}\frac{2}{\sqrt{\pi}}\int_0^\infty d\rho e^{-\rho^2|\vec{r}_l - \vec{r}|^2}. \tag{3.44}$$

Note that we are now treating the dipole wave sum as a function of $\vec{r}$. Rearranging, and adding

and subtracting the $l = 0$ contribution, we find

$$D^{zz}_{\vec{k}}(\vec{r}) = \frac{\partial^2}{\partial z^2}\frac{2}{\sqrt{\pi}}\int_0^\infty d\rho\left[\sum_l e^{-\rho^2|\vec{r}_l-\vec{r}|^2+i\vec{k}\cdot(\vec{r}_l-\vec{r})}\right]e^{i\vec{k}\cdot\vec{r}} - \frac{\partial^2}{\partial z^2}\frac{1}{r}, \tag{3.45}$$

where $r = |\vec{r}|$. The function in square brackets is a periodic function of $\vec{r}$ on the lattice; hence, we may consider its Fourier transform

$$g(\vec{K}) = \frac{1}{V_c}\sum_l \int_{cell} d^3\vec{r}\, e^{-\rho^2|\vec{r}_l-\vec{r}|^2+i(\vec{k}+\vec{K})\cdot(\vec{r}_l-\vec{r})}e^{-i\vec{K}\cdot\vec{r}_l}. \tag{3.46}$$

At this point, we must take the basis of our lattice into consideration. Specializing to the case of $LiHoF_4$, the fractional coordinates of the four holmium ions in the basis are given by $(0,0,0),(1/2,1/2,1/2),(0,1/2,1/4)$ and $(1/2,0,3/4)$. We consider each atom (labeled 1 to 4) separately, breaking the sum up into four terms

$$\begin{aligned}
g_1(\vec{K}) &= \frac{1}{V_c}\sum_{l_0}\int_{cell} d^3\vec{r}\, e^{-\rho^2|\vec{r}_l-\vec{r}|^2+i(\vec{k}+\vec{K})\cdot(\vec{r}_l-\vec{r})} = \frac{1}{V_c}\int d^3\vec{r}\, e^{-\rho^2 r^2+i(\vec{k}+\vec{K})\cdot\vec{r}} \\
g_2(\vec{K}) &= \frac{e^{-i\vec{K}\cdot(\frac{a}{2},\frac{a}{2},\frac{c}{2})}}{V_c}\int d^3\vec{r}\, e^{-\rho^2 r^2+i(\vec{k}+\vec{K})\cdot\vec{r}} \\
g_3(\vec{K}) &= \frac{e^{-i\vec{K}\cdot(0,\frac{a}{2},\frac{c}{4})}}{V_c}\int d^3\vec{r}\, e^{-\rho^2 r^2+i(\vec{k}+\vec{K})\cdot\vec{r}} \\
g_4(\vec{K}) &= \frac{e^{-i\vec{K}\cdot(\frac{a}{2},0,\frac{3c}{4})}}{V_c}\int d^3\vec{r}\, e^{-\rho^2 r^2+i(\vec{k}+\vec{K})\cdot\vec{r}}.
\end{aligned} \tag{3.47}$$

The summation over l_0 includes all Bravais lattice vectors, rather than being over each atom in the crystal. We replace the sum of integrals over unit cells with a single integral over all space. At this point, we specialize to the case of a spherical sample, and perform the integral appearing in the $g_n(\vec{K})$ functions in spherical coordinates

$$I = \int r^2\sin(\theta)dr d\theta d\phi e^{-\rho^2 r^2+i|\vec{k}+\vec{K}|r\cos(\theta)} = 4\pi\int r^2 dr\frac{\sin(|\vec{k}+\vec{K}|r)}{|\vec{k}+\vec{K}|r}e^{-\rho^2 r^2}. \tag{3.48}$$

Taking $y = |\vec{k}+\vec{K}|r$, we may write

$$g_m(\vec{K}) = \frac{\alpha_m}{V_c}\frac{4\pi}{|\vec{k}+\vec{K}|^3}\int y\sin(y)\exp\big(-\frac{\rho^2 y^2}{|\vec{k}+\vec{K}|^2}\big)dy, \tag{3.49}$$

where the α_m are geometric factors from our four atomic sites. Summing over all four contri-

butions yields

$$g(\vec{K}) = \frac{\alpha(\vec{K})}{V_c} \frac{4\pi}{|\vec{k}+\vec{K}|^3} \int y \sin(y) \exp\big(-\frac{\rho^2 y^2}{|\vec{k}+\vec{K}|^2}\big) dy, \tag{3.50}$$

where the geometric factor is

$$\alpha(\vec{K}) = \sum_m \alpha_m = 1 + e^{-i\vec{K}\cdot(\frac{a}{2},\frac{a}{2},\frac{c}{2})} + e^{-i\vec{K}\cdot(0,\frac{a}{2},\frac{c}{4})} + e^{-i\vec{K}\cdot(\frac{a}{2},0,\frac{3c}{4})}. \tag{3.51}$$

Making use of equation (3.50), we return to the dipole wave sum, which is given by $\lim_{\vec{r}\to 0} D^{zz}_{\vec{k}}(\vec{r})$, with $D^{zz}_{\vec{k}}(\vec{r})$ given in equation (3.45). We separate the integral appearing in equation (3.45) into two parts to obtain

$$\begin{aligned} D^{zz}_{\vec{k}}(\vec{r}) &= \frac{\partial^2}{\partial z^2} \frac{2}{\sqrt{\pi}} \left[\int_0^\Lambda d\rho \sum_{\vec{K}} g(\vec{K}) e^{i(\vec{k}+\vec{K})\cdot\vec{r}} + \int_\Lambda^\infty d\rho \sum_l e^{i\vec{k}\cdot\vec{r}_l} e^{-\rho^2|\vec{r}_l-\vec{r}|^2} \right] - \frac{\partial^2}{\partial z^2}\frac{1}{r} \\ &= -\frac{1}{V_c} \sum_{\vec{K}} \frac{(k^z+K^z)^2}{|\vec{k}+\vec{K}|^2} \frac{2\alpha(\vec{K})}{\sqrt{\pi}} e^{i(\vec{k}+\vec{K})\cdot\vec{r}} \int_0^{\frac{\Lambda}{|\vec{k}+\vec{K}|}} dz F_{|\vec{k}+\vec{K}|R}(z) \\ &\qquad + \frac{\partial^2}{\partial z^2}\frac{2}{\sqrt{\pi}} \sum_l e^{i\vec{k}\cdot\vec{r}_l} H(\Lambda|\vec{r}_l-\vec{r}|) - \frac{\partial^2}{\partial z^2}\frac{1}{r}, \end{aligned} \tag{3.52}$$

with

$$F_x(z) = 4\pi \int_0^x y \sin(y) e^{-z^2y^2} dy \qquad\qquad H(s) = \frac{\Lambda}{s} \int_s^\infty dy e^{-y^2}. \tag{3.53}$$

We have introduced a convergence factor Λ. When the integration variable ρ is large, we perform the summation in real space; when ρ is small, we perform the summation in Fourier space. An appropriate choice of Λ ensures the rapid convergence of the dipole wave sum.

Separating the $\vec{K} = 0$ and $\vec{r}_l = 0$ components of the sums from the rest, we find

$$\begin{aligned} D^{zz}_{\vec{k}} = &-\frac{1}{V_c}\left(\frac{k^z}{k}\right)^2 \frac{8}{\sqrt{\pi}} \int_0^{\frac{\Lambda}{k}} dz F_{kR}(z) - \frac{1}{V_c} \sum_{\vec{K}\neq 0} \frac{(k^z+K^z)^2}{|\vec{k}+\vec{K}|^2} \frac{2\alpha(\vec{K})}{\sqrt{\pi}} \int_0^{\frac{\Lambda}{|\vec{k}+\vec{K}|}} dz F_{|\vec{k}+\vec{K}|R}(z) \\ &+ \lim_{r\to 0} \frac{\partial^2}{\partial z^2}\frac{2}{\sqrt{\pi}} \sum_{\vec{r}_l\neq 0} e^{i\vec{k}\cdot\vec{r}_l} H(\Lambda|\vec{r}_l-\vec{r}|) - \lim_{r\to 0}\left(\frac{\partial^2}{\partial z^2}\frac{1}{r} - \frac{\partial^2}{\partial z^2}\frac{2}{\sqrt{\pi}} H(\Lambda r)\right). \end{aligned} \tag{3.54}$$

This expression is an extension of Aharony and Fisher's work in [93] to a lattice with a basis. The above expression matches equation (14) of Bowden and Clark [92], except that in the above expression we have summed over the four atoms in the basis introducing a geometric factor, rather than summing over each sublattice separately. Following Bowden and Clark, we

consider each of the four terms in equation (3.54) separately.

We begin with

$$A = -\frac{1}{V_c}\left(\frac{k^z}{k}\right)^2 \frac{8}{\sqrt{\pi}} \int_0^{\frac{\Lambda}{k}} dz F_{kR}(z) \tag{3.55}$$

In the limit $kR \gg 1$, we may take the range of $y = kr$ in the integral in $F_y(z)$ to be zero to infinity. This neglects boundary effects; however, as discussed in the introduction to this chapter, boundary effects are only significant when $kR < 10$. Making use of the integral

$$\int_0^\infty y \sin(y) e^{-z^2 y^2} dy = \frac{\sqrt{\pi}}{4z^3} \exp\big(-\frac{1}{4z^2}\big) \tag{3.56}$$

we find

$$A = -\frac{1}{V_c}\left(\frac{k^z}{k}\right)^2 8\pi \int_0^{\frac{\Lambda}{k}} \frac{e^{-\frac{1}{4z^2}}}{z^3} dz = -\frac{1}{V_c}\left(\frac{k^z}{k}\right)^2 16\pi \exp\left(-\frac{k^2}{4\Lambda^2}\right). \tag{3.57}$$

We have dropped the boundary term

$$\partial A = \frac{1}{V_c}\left(\frac{k^z}{k}\right)^2 32\sqrt{\pi} \int_0^{\frac{\Lambda}{k}} dz \int_{kR}^\infty dy\, y \sin(y) e^{-z^2 y^2}. \tag{3.58}$$

Similarly, we find

$$\begin{aligned} B &= -\frac{1}{V_c} \sum_{\vec{K}\neq 0} \frac{(k^z + K^z)^2}{|\vec{k}+\vec{K}|^2} \frac{2\alpha(\vec{K})}{\sqrt{\pi}} \int_0^{\frac{\Lambda}{|\vec{k}+\vec{K}|}} dz F_\infty(z) \\ &= -\frac{1}{V_c} \sum_{\vec{K}\neq 0} \frac{(k^z + K^z)^2}{|\vec{k}+\vec{K}|^2} 4\pi\alpha(\vec{K}) \exp\left(-\frac{|\vec{k}+\vec{K}|^2}{4\Lambda^2}\right), \end{aligned} \tag{3.59}$$

with a boundary contribution of

$$\partial B = \frac{1}{V_c} \sum_{\vec{K}\neq 0} \frac{(k^z + K^z)^2}{|\vec{k}+\vec{K}|^2} 8\sqrt{\pi}\alpha(\vec{K}) \int_0^{\frac{\Lambda}{|\vec{k}+\vec{K}|}} dz \int_{|\vec{k}+\vec{K}|R}^\infty dy\, y \sin(y) e^{-z^2 y^2}. \tag{3.60}$$

We may rewrite the third term as

$$C = \lim_{r\to 0} \frac{\partial^2}{\partial z^2} \frac{2}{\sqrt{\pi}} \sum_{\vec{r}_l \neq 0} e^{i\vec{k}\cdot\vec{r}_l} H(\Lambda|\vec{r}_l - \vec{r}|) = \sum_{\vec{r}_l \neq 0} e^{i\vec{k}\cdot\vec{r}_l} \frac{\partial^2}{\partial z_l^2} \left(\frac{\mathrm{erfc}(\Lambda|\vec{r}_l|)}{|\vec{r}_l|}\right), \tag{3.61}$$

where we have used the fact $\lim_{r\to 0} \frac{\partial^2}{\partial z^2} f(|\vec{r}_l - \vec{r}|) = \frac{\partial^2}{\partial z_l^2} f(|\vec{r}_l|)$, and made use of the compli-

mentary error function

$$\mathrm{erfc}(z) = \frac{2}{\sqrt{\pi}} \int_z^\infty e^{-y^2} dy. \tag{3.62}$$

Taking the derivatives, we find $C = \sum_{\vec{r}_l \neq 0} e^{i\vec{k}\cdot\vec{r}_l} E^\Lambda(\vec{r}_l)$ with

$$E^\Lambda(\vec{r}_l) = \left[\frac{2\Lambda}{\sqrt{\pi}} \frac{e^{-(\Lambda r_l)^2}}{r_l^2} \left(2\Lambda^2 z_l^2 + \frac{3z_l^2}{r_l^2} - 1 \right) + \frac{\mathrm{erfc}(\Lambda r_l)}{r_l^3} \left(\frac{3z_l^2}{r_l^2} - 1 \right) \right]. \tag{3.63}$$

Finally, using the error function, we may rewrite the last term as follows

$$\begin{aligned} D &= -\lim_{r\to 0} \left(\frac{\partial^2}{\partial z^2} \frac{1}{r} - \frac{\partial^2}{\partial z^2} \frac{2}{\sqrt{\pi}} H(\Lambda r) \right) \\ &= -\lim_{r\to 0} \left(\frac{\partial^2}{\partial z^2} \left[\frac{1}{r} \left(1 - \frac{2}{\sqrt{\pi}} \int_{\Lambda r}^\infty dy e^{-y^2} \right) \right] \right) = -\lim_{r\to 0} \left(\frac{\partial^2}{\partial z^2} \left[\frac{1}{r} \mathrm{erf}(\Lambda r) \right] \right). \end{aligned} \tag{3.64}$$

Making use of the series expansion

$$\mathrm{erf}(z) = \frac{2}{\sqrt{\pi}} \sum_{n=0}^\infty \frac{(-1)^n z^{2n+1}}{n!(2n+1)} \tag{3.65}$$

we find

$$D = \frac{4\Lambda^3}{3\sqrt{\pi}}. \tag{3.66}$$

Our result for the dipolar sum is then

$$\begin{aligned} D_{\vec{k}}^{zz} = &\frac{4\Lambda^3}{3\sqrt{\pi}} + \sum_{\vec{r}_l \neq 0} e^{i\vec{k}\cdot\vec{r}_l} E^\Lambda(\vec{r}_l) - \frac{1}{V_c} \left(\frac{k^z}{k} \right)^2 16\pi \exp\left(-\frac{k^2}{4\Lambda^2} \right) \\ &- \frac{1}{V_c} \sum_{\vec{K}\neq 0} \frac{(k^z + K^z)^2}{|\vec{k}+\vec{K}|^2} 4\pi\alpha(\vec{K}) \exp\left(-\frac{|\vec{k}+\vec{K}|^2}{4\Lambda^2} \right). \end{aligned} \tag{3.67}$$

Note that in the limit $\Lambda \to 0$ we recover the original dipole sum, as we must. The first two terms in the above expression are generally valid. The remaining pair of terms are valid for a spherical sample in the limit $R \gg \lambda$. When considering the limit $k \to 0$, it is important to remember that we must include contributions from the boundary. In practice, it is easiest to perform the dipole sum directly for small values of k, and use the Ewald summation method otherwise.

Ewald Summation in a Cylindrical Sample

We now consider the Ewald summation method for a cylindrical sample. Long thin cylinders are of particular interest because $LiHoF_4$ forms needle like domains, as discussed in the introduction to this chapter. We perform our analysis using plane waves; however, an expansion in cylindrical waves may prove useful for obtaining analytic results. We leave the cylindrical wave calculation as a subject of future work. We begin by evaluating integral (3.48) in cylindrical coordinates

$$I = \int d^3\vec{r} e^{-\rho^2 r^2 + i(\vec{k}+\vec{K})\cdot\vec{r}} = \int_{-h}^{h}\int_0^{2\pi}\int_0^R e^{-\rho^2(r^2+z^2)+i|\vec{k}_\perp+\vec{K}_\perp|r\cos\theta+i(k^z+K^z)z} r dr d\theta dz. \quad (3.68)$$

Performing the angular integral gives

$$I = 2\pi\int_{-h}^{h}\int_0^R r e^{-\rho^2 r^2} J_0(|\vec{k}_\perp+\vec{K}_\perp|r) e^{-\rho^2 z^2} e^{i(k^z+K^z)z} dr dz. \quad (3.69)$$

The r and z integrals are separable so that $I = I_R I_h$ with

$$I_R = 2\pi\int_0^R r e^{-\rho^2 r^2} J_0(|\vec{k}_\perp+\vec{K}_\perp|r) dr \qquad I_h = \int_{-h}^{h} e^{-\rho^2 z^2} e^{i(k^z+K^z)z} dz \quad (3.70)$$

We begin by evaluating I_h for a long thin cylinder. We find

$$I_h = 2\int_0^{h=\infty} e^{-\rho^2 z^2}\cos((k^z+K^z)z) dz = \frac{\sqrt{\pi}}{\rho}\exp\left(\frac{-(k^z+K^z)^2}{4\rho^2}\right). \quad (3.71)$$

Recall from equation (3.50) that $g(\vec{K}) = \frac{4\pi}{V_c} I$. We find

$$g(\vec{K}) = \frac{\alpha(\vec{K})}{V_c}\frac{2\pi^{\frac{3}{2}}}{|\vec{k}_\perp+\vec{K}_\perp|^2}\frac{e^{-\frac{(k^z+K^z)^2}{4\rho^2}}}{\rho}\int_0^{|\vec{k}_\perp+\vec{K}_\perp|R} y J_0(y)\exp\left(\frac{-\rho^2 y^2}{|\vec{k}_\perp+\vec{K}_\perp|^2}\right) dy, \quad (3.72)$$

and, following the same steps as for the spherical sample, we find the dipole wave sum to be

$$D^{zz}_{\vec{k}}\Big|_{k_\perp\neq 0} = -\frac{4\pi}{V_c}\sum_{\vec{K}\neq 0}\frac{(k^z+K^z)^2}{|\vec{k}_\perp+\vec{K}_\perp|^2}\alpha(\vec{K})\int_0^{\frac{\Lambda}{|\vec{k}_\perp+\vec{K}_\perp|}}\frac{e^{-\frac{(k^z+K^z)^2}{4z^2|\vec{k}_\perp+\vec{K}_\perp|^2}}}{z} G_{|\vec{k}_\perp+\vec{K}_\perp|R}(z) dz \quad (3.73)$$

$$-\frac{16\pi}{V_c}\left(\frac{k^z}{k_\perp}\right)^2\int_0^{\frac{\Lambda}{k_\perp}}\frac{e^{-\frac{(k^z)^2}{4z^2(\vec{k}_\perp)^2}}}{z} G_{k_\perp R}(z) dz + \frac{4\Lambda^3}{3\sqrt{\pi}} + \sum_{\vec{r}_l\neq 0} e^{i\vec{k}\cdot\vec{r}_l} E^\Lambda(\vec{r}_l),$$

where

$$G_x(z) = \int_0^x y J_0(y) e^{-z^2 y^2} dy = \frac{1}{2z^2} e^{-\frac{1}{4z^2}} \Big|_{x=\infty}. \tag{3.74}$$

This result is not valid when $k_\perp = 0$ as the expressions involve a division by zero. In the special case $k_\perp = 0$ and $k^z \neq 0$, the result is

$$\begin{aligned} D^{zz}_{\vec{k}}\Big|_{k_\perp=0} = &-\frac{4\pi}{V_c} \sum_{\vec{K}_\perp \neq 0} \frac{(k^z+K^z)^2}{|\vec{K}_\perp|^2} \alpha(\vec{K}) \int_0^{\frac{\Lambda}{|\vec{K}_\perp|}} \frac{e^{-\frac{(k^z+K^z)^2}{4z^2|\vec{K}_\perp|^2}}}{z} G_{|\vec{K}_\perp|R}(z) dz \\ &-\sum_{K^z} \frac{\alpha(\vec{K})\pi}{V_c} \int_{\frac{(k^z+K^z)^2}{4\Lambda^2}}^{\infty} e^{-z}(1-e^{-\frac{[(k^z+K^z)R]^2}{4z}}) dz + \frac{4\Lambda^3}{3\sqrt{\pi}} + \sum_{\vec{r}_l \neq 0} e^{i\vec{k}\cdot\vec{r}_l} E^\Lambda(\vec{r}_l). \end{aligned} \tag{3.75}$$

The first summation is over all reciprocal lattice vectors with $\vec{K}_\perp \neq 0$, and the second summation is over all reciprocal lattice vectors such that $\vec{K}_\perp = 0$. Note that the summation over K^z includes the $K^z = 0$ term. If $\vec{k} = 0$, the above result is still correct, except for the fact we must now neglect the $\vec{K} = 0$ term from the second summation. The discontinuity between the $\vec{k} = 0$ result and the result at finite $\vec{k}$ is due to the boundary terms neglected in taking the limit $h \to \infty$ in equation (3.71).

We now evaluate the dipole sum in the limit, $k_\perp R \gg 1$. Defining

$$\beta(\vec{K}) = 1 + \gamma(\vec{K}) \qquad\qquad \gamma(\vec{K}) = \frac{(k^z+K^z)^2}{|\vec{k}_\perp + \vec{K}_\perp|^2} \tag{3.76}$$

we find, in the limit $k_\perp R \gg 1$,

$$\begin{aligned} D^{zz}_{\vec{k}} = &-\frac{2\pi}{V_c} \sum_{\vec{K}\neq 0} \gamma(\vec{K})\alpha(\vec{K}) \int_0^{\frac{\Lambda}{|\vec{k}_\perp+\vec{K}_\perp|}} \frac{e^{-\frac{\beta(\vec{K})}{4z^2}}}{z^3} dz \\ &-\frac{8\pi}{V_c}\gamma(0) \int_0^{\frac{\Lambda}{k_\perp}} \frac{e^{-\frac{\beta(0)}{4z^2}}}{z^3} dz + \frac{4\Lambda^3}{3\sqrt{\pi}} + \sum_{\vec{r}_l \neq 0} e^{i\vec{k}\cdot\vec{r}_l} E^\Lambda(\vec{r}_l). \end{aligned} \tag{3.77}$$

Performing the integral over z yields

$$D^{zz}_{\vec{k}} = -\frac{4\pi}{V_c} \sum_{\vec{K}\neq 0} \frac{(k^z+K^z)^2}{(\vec{k}+\vec{K})^2} \alpha(\vec{K}) e^{-\frac{|\vec{k}+\vec{K}|^2}{4\Lambda^2}} - \frac{16\pi}{V_c}\left(\frac{k^z}{k}\right)^2 e^{-\frac{k^2}{4\Lambda^2}} + \frac{4\Lambda^3}{3\sqrt{\pi}} + \sum_{\vec{r}_l \neq 0} e^{i\vec{k}\cdot\vec{r}_l} E^\Lambda(\vec{r}_l). \tag{3.78}$$

This is identical to the result for the spherical sample, which is to be expected as the shape

dependence of the sum is important in the opposite limit $k_\perp R \ll 1$.

In the limit $x = k_\perp R \ll 1$ we find for equation (3.74)

$$G_x(z) = \int_0^x y J_0(y) e^{-z^2 y^2} dy \approx \frac{1}{2z^2}(1 - e^{-z^2 x^2}). \tag{3.79}$$

We may then write the $\vec{K} = 0$ component of the momentum space summation in equation (3.73) as,

$$I_0 = -\frac{16\pi}{V_c}\gamma(0)\int_0^{\frac{\Lambda}{k_\perp}} \frac{e^{-\frac{\gamma(0)}{4z^2}}}{z} G_{k_\perp R}(z) dz = -\frac{4\pi}{V_c}\gamma(0)\int_{\frac{k_\perp^2}{\Lambda^2}}^{\infty} e^{-\frac{\gamma(0)u}{4}}(1 - e^{-\frac{x^2}{u}}) du. \tag{3.80}$$

Assuming Λ is chosen so that $\Lambda R \gg 1$, which is a reasonable assumption because good convergence is usually achieved with Λ chosen to be approximately the inverse lattice spacing, we find

$$I_0 = -\frac{4\pi}{V_c}\int_{\frac{k_z^2}{4\Lambda^2}}^{\infty} e^{-z}\left(1 - \exp\left(-\frac{(k^z R)^2}{4z}\right)\right) dz \approx -\frac{4\pi}{V_c}\int_{\frac{k_z^2}{4\Lambda^2}}^{\infty} e^{-z} dz = -\frac{4\pi}{V_c} e^{-\frac{k_z^2}{4\Lambda^2}}. \tag{3.81}$$

We are left with the task of evaluating terms in equation (3.73) for which $\vec{K} \neq 0$. We separate terms for which $|\vec{K}_\perp| = 0$ (the K_z summation) and treat them in the same fashion as we treated the integral I_0. For $|\vec{K}_\perp| \neq 0$, we have $|\vec{k}_\perp + \vec{K}_\perp| R \gg 1$, and we may make use of equation (3.74). The final result for the dipole sum in a finite sized cylindrical sample in the limit $k_\perp R \ll 1$ is given by

$$D_{\vec{k}}^{zz} = -\frac{4\pi}{V_c}\sum_{|\vec{K}_\perp|\neq 0} \frac{(k^z + K^z)^2}{(\vec{k} + \vec{K})^2}\alpha(\vec{K}) e^{-\frac{|\vec{k}+\vec{K}|^2}{4\Lambda^2}} - \frac{\pi}{V_c}\sum_{K^z}\alpha(\vec{K}) e^{-\frac{(k^z+K^z)^2}{4\Lambda^2}} + \frac{4\Lambda^3}{3\sqrt{\pi}} + \sum_{\vec{r}_l \neq 0} e^{i\vec{k}\cdot\vec{r}_l} E^\Lambda(\vec{r}_l). \tag{3.82}$$

If we take $k_\perp = 0$, we will obtain the same result as will be obtained by performing the integrals in (3.75).

If $\vec{k} = 0$ then the result above is still valid as long as the $K^z = 0$ term is excluded from the second summation. We reiterate the fact that the apparent discontinuity at $\vec{k} = 0$ is due to the boundary term neglected when taking the limit of a long cylinder $h \to \infty$. In reality, there is no discontinuity, but the function varies extremely rapidly in the region near $\vec{k} = 0$. What equation (3.82) gives us is the small momentum behaviour ($k_\perp R \ll 1$) of the dipole wave sum in a long cylinder ($k_z h \gg 1$) of $LiHoF_4$.

In order to perform the dipolar sum in $LiHoF_4$, we take $\Lambda = \frac{2}{a}$, and consider a system with size $R = 10000a$, where $a = 5.175$Å is the transverse lattice spacing. This roughly corresponds

to a domain with radius $5\mu m$. If $k_\perp R \leq 1$ we use (3.82), otherwise, we use (3.78). In the special case $\vec{k} = 0$, we exclude the $K_z = 0$ term from equation (3.82). In real space, we sum over a cylinder with a radius and height of 10 unit cells, and sum over a corresponding number of reciprocal lattice vectors. This is more than enough to ensure convergence of the series $\sum_{\vec{r}_l \neq 0} e^{i\vec{k}\cdot\vec{r}_l} E^\Lambda(\vec{r}_l)$. In Figures 3.1 and 3.2, we plot the dipole summation as a function of the transverse momenta for various values of the longitudinal momenta. We clearly see the rapid variation of the sum near $\vec{k} = 0$.

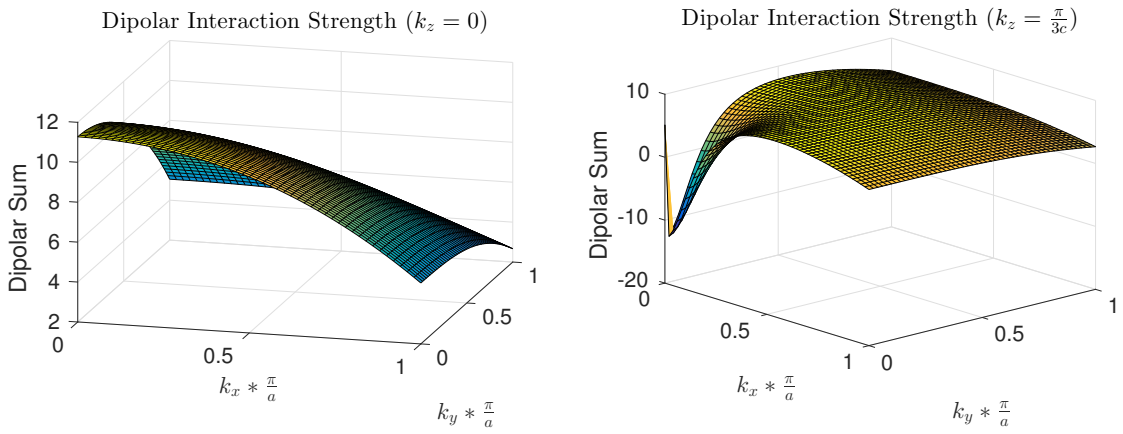

Figure 3.1: In the figure above we see the Fourier transform of the dipolar interaction in a long thin cylindrical sample of $LiHoF_4$ as a function of transverse momenta at $k_z = 0$ (left), and $k_z = \frac{\pi}{3c}$ (right).

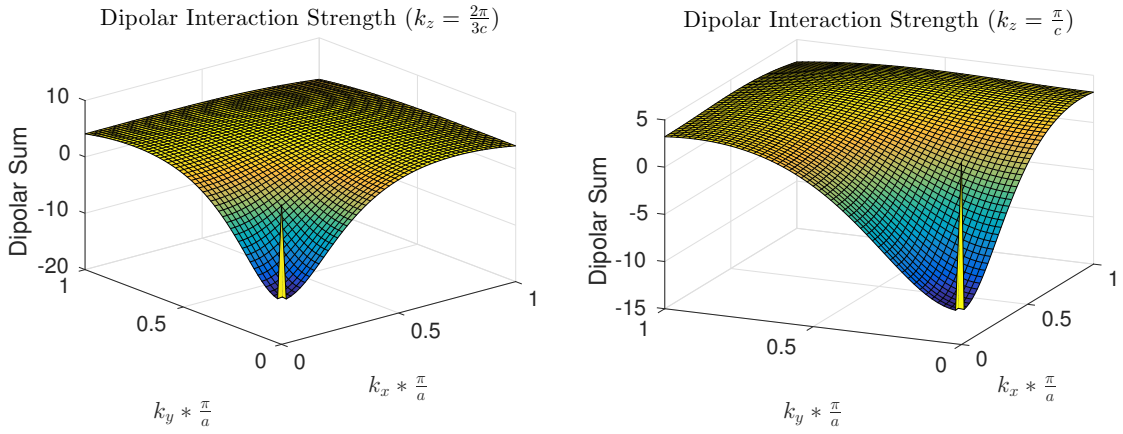

Figure 3.2: In the figure above we see the Fourier transform of the dipolar interaction in a long thin cylindrical sample of $LiHoF_4$ as a function of transverse momenta at $k_z = \frac{2\pi}{3c}$ (left), and $k_z = \frac{\pi}{c}$ (right).

Summary

In this chapter, we considered the Fourier transform of the dipolar interaction, necessary for a momentum space analysis of systems such as $LiHoF_4$. In Section 3.1, we performed the dipole wave sum in the continuum limit. This gave correct results when the underlying lattice of the system being dealt with is simple cubic. In an infinite spherical sample, we found there is an ambiguity in the zero momentum limit of the dipole wave sum. This ambiguity is resolved by considering the effect of the boundary. In Section 3.1.2, we redid the previous calculation for a long thin cylindrical sample, and show that the small momentum behaviour will depend on the aspect ratio of the cylinder.

After performing the dipole wave sum in the continuum limit, we turned to the dipole wave sum for a sample of $LiHoF_4$, where we must account for the underlying lattice. In Section 3.2, we examined the small momentum behaviour of the dipole wave sum in $LiHoF_4$ by direct summation. Direct summation becomes unreasonably slow away from $k = 0$. In order to obtain the dipole wave sum in $LiHoF_4$ over the entire Brillouin zone, we made use of the Ewald summation method. We performed the Ewald summation for a spherical sample, and for a long thin cylindrical sample. The cylindrical sample reflects the dipolar field felt in a sample of $LiHoF_4$ that is divided into needle like domains. The results obtained via Ewald summation in a long thin cylindrical sample are used throughout the rest of this thesis.

Chapter 4

Spin Half Spin Half Model

Consider a spin half Ising system in a transverse field coupled to a spin half nuclear spin bath with Hamiltonian

$$\mathscr{H} = -\frac{J}{2}\sum_{i\neq j} V_{ij} S_i^z S_j^z - \Delta \sum_i S_i^x + A_z \sum_i I_i^z S_i^z + \frac{A_\perp}{2}\sum_i (I_i^+ S_i^- + I_i^- S_i^+). \tag{4.1}$$

The Ss represent electronic spin operators, and the Is represent nuclear spin operators. We assume a longitudinal ferromagnetic interaction between electronic spins, and take Δ, and the hyperfine interaction, to be positive. Our choice of energy units is arbitrary. For simplicity, we choose energy units such that $J = 1$, and it is to be understood that the transverse field and hyperfine interaction are now in units of J. We introduce this relatively simple Hamiltonian as a toy model that illustrates the effects of an anistropic hyperfine interaction on the transverse field Ising model. With the inclusion of a transverse field acting directly on the nuclear spins, $\mathscr{H}_n = -\Delta_n \sum_i I_i^x$, this serves as a toy model for $LiHoF_4$. Many of the qualitative features of $LiHoF_4$ are easily illustrated by this model.

In Section 4.4.1, we will show the spin half spin half (SHSH) model undergoes a ferromagnetic to paramagnetic phase transition at a critical temperature of

$$\Delta_c \approx \frac{V_0}{2} + \frac{1}{2}\left(\frac{A_z^2}{A_\perp} - A_\perp\right). \tag{4.2}$$

For $\Delta > \Delta_c$, there will be no longitudinal mean field (MF) acting on the system. In this case,

the single ion Hamiltonian,

$$\mathscr{H}_{0i} = -\Delta S_i^x + A_z I_i^z S_i^z + \frac{A_\perp}{2}(I_i^+ S_i^- + I_i^- S_i^+) = \begin{pmatrix} \frac{A_z}{4} & -\frac{\Delta}{2} & 0 & 0 \\ -\frac{\Delta}{2} & -\frac{A_z}{4} & \frac{A_\perp}{2} & 0 \\ 0 & \frac{A_\perp}{2} & -\frac{A_z}{4} & -\frac{\Delta}{2} \\ 0 & 0 & -\frac{\Delta}{2} & \frac{A_z}{4} \end{pmatrix}, \tag{4.3}$$

may be diagonalized analytically. We use as our basis $|\vec{\Psi}\rangle = (|\Uparrow\uparrow\rangle, |\Downarrow\uparrow\rangle, |\Uparrow\downarrow\rangle, |\Downarrow\downarrow\rangle)$, where the double arrows denote electronic spins, and the single arrows denote nuclear spins. The eigenvalues of the single ion Hamiltonian are

$$\begin{aligned} E_1 &= -\frac{1}{2}\sqrt{\Delta^2 + \frac{(A_z + A_\perp)^2}{4}} - \frac{A_\perp}{4} & E_2 &= -\frac{1}{2}\sqrt{\Delta^2 + \frac{(A_z - A_\perp)^2}{4}} + \frac{A_\perp}{4} \\ E_3 &= \frac{1}{2}\sqrt{\Delta^2 + \frac{(A_z + A_\perp)^2}{4}} - \frac{A_\perp}{4} & E_4 &= \frac{1}{2}\sqrt{\Delta^2 + \frac{(A_z - A_\perp)^2}{4}} + \frac{A_\perp}{4} \end{aligned} \tag{4.4}$$

and their associated eigenvectors are

$$\begin{aligned} |1\rangle &= \alpha_1 \begin{pmatrix} -\frac{\Delta}{2} \\ E_1 - \frac{A_z}{4} \\ -E_1 + \frac{A_z}{4} \\ \frac{\Delta}{2} \end{pmatrix} & |2\rangle &= \alpha_2 \begin{pmatrix} \frac{\Delta}{2} \\ -E_2 + \frac{A_z}{4} \\ -E_2 + \frac{A_z}{4} \\ \frac{\Delta}{2} \end{pmatrix} \\ |3\rangle &= \alpha_3 \begin{pmatrix} -\frac{\Delta}{2} \\ E_3 - \frac{A_z}{4} \\ -E_3 + \frac{A_z}{4} \\ \frac{\Delta}{2} \end{pmatrix} & |4\rangle &= \alpha_4 \begin{pmatrix} \frac{\Delta}{2} \\ -E_4 + \frac{A_z}{4} \\ -E_4 + \frac{A_z}{4} \\ \frac{\Delta}{2} \end{pmatrix}, \end{aligned} \tag{4.5}$$

where the α's are normalization constants. In the limit $\Delta \gg A_z, A_\perp$, making use of these eigenvalues and eigenvectors, simple analytic expressions for the magnetization, susceptibility, and other physically relevant quantities may be obtained in terms of the parameters of the Hamil-

tonian. We list here, for future reference, the normalization constants expanded in this limit,

$$\begin{aligned}
\alpha_1 &= \frac{1}{\Delta}\left[1-\frac{A_z+A_\perp}{4\Delta}-\frac{(A_z+A_\perp)^2}{8\Delta^2}+\cdots\right] \\
\alpha_2 &= \frac{1}{\Delta}\left[1-\frac{A_z-A_\perp}{4\Delta}-\frac{(A_z-A_\perp)^2}{8\Delta^2}+\cdots\right] \\
\alpha_3 &= \frac{1}{\Delta}\left[1+\frac{A_z+A_\perp}{4\Delta}-\frac{(A_z+A_\perp)^2}{8\Delta^2}+\cdots\right] \\
\alpha_4 &= \frac{1}{\Delta}\left[1+\frac{A_z-A_\perp}{4\Delta}-\frac{(A_z-A_\perp)^2}{8\Delta^2}+\cdots\right].
\end{aligned} \tag{4.6}$$

We also list the difference between energy levels, $E_{ji} = E_j - E_i$, to $O\left(\left(\frac{A_{z,\perp}}{\Delta}\right)^3\right)$

$$\begin{aligned}
E_{21} &= \frac{A_\perp}{2}\left[1+\frac{A_z}{2\Delta}+\cdots\right] & E_{41} &= \Delta\left[1+\frac{A_\perp}{2\Delta}+\frac{A_z^2+A_\perp^2}{8\Delta^2}+\cdots\right] \\
E_{43} &= \frac{A_\perp}{2}\left[1-\frac{A_z}{2\Delta}+\cdots\right] & E_{32} &= \Delta\left[1-\frac{A_\perp}{2\Delta}+\frac{A_z^2+A_\perp^2}{8\Delta^2}+\cdots\right] \\
E_{31} &= \Delta\left[1+\frac{(A_z+A_\perp)^2}{8\Delta^2}+\cdots\right] & E_{42} &= \Delta\left[1+\frac{(A_z-A_\perp)^2}{8\Delta^2}+\cdots\right].
\end{aligned} \tag{4.7}$$

We now introduce the single ion basis operators

$$L_{mn} = |m\rangle\langle n|, \tag{4.8}$$

where $m,n \in \{1,..,4\}$ refer to the eigenstates introduced in (4.5). In this thesis, these operators will also be referred to as mean field (MF) operators. We prefer to use the term single ion here, as we are working in a regime where the MF is zero. Further discussion of these operators is available in Appendix A.

In terms of the single ion operators, the z component of the electronic spin operator may be written as

$$S^z = c_{12}[L_{12}+L_{21}] + c_{34}[L_{34}+L_{43}] + c_{14}[L_{14}+L_{41}] + c_{23}[L_{23}+L_{32}] \tag{4.9}$$

where

$$c_{ij} = \frac{1}{2}\alpha_i\alpha_j\left[\frac{A_z^2}{8}-\frac{\Delta^2}{2}+2E_iE_j-\frac{A_z}{2}(E_i+E_j)\right] \tag{4.10}$$

In the limit $\Delta \gg A_z, A_\perp$, we find the matrix elements to be given by (to $O\big(\big(\frac{A_{z,\perp}}{\Delta}\big)^3\big)$)

$$c_{12} = -c_{34} = \frac{A_z}{4\Delta} \qquad\qquad c_{14} = c_{23} = -\frac{1}{2}\left[1 - \frac{5A_z^2 + 3A_\perp^2}{16\Delta^2}\right]. \tag{4.11}$$

The x component of the electronic spin operator is given by

$$S^x = a_{11}L_{11} + a_{22}L_{22} + a_{33}L_{33} + a_{44}L_{44} + a_{13}[L_{13} + L_{31}] + a_{24}[L_{24} + L_{42}], \tag{4.12}$$

where

$$a_{ii} = -\alpha_i^2 \Delta\left(E_i - \frac{A_z}{4}\right) \tag{4.13}$$

and

$$a_{13} = \frac{\alpha_1\alpha_3}{4}\Delta(A_z + A_\perp) \qquad\qquad a_{24} = \frac{\alpha_2\alpha_4}{4}\Delta(A_z - A_\perp). \tag{4.14}$$

We have listed the z and x components of the electronic spin operator in the paramagnetic phase of the model. We now proceed to do so for the nuclear spin operators as well. The z component of the nuclear spin operator is given by

$$I^z = d_{12}[L_{12} + L_{21}] + d_{34}[L_{34} + L_{43}] + d_{14}[L_{14} + L_{41}] + d_{23}[L_{23} + L_{32}] \tag{4.15}$$

where the matrix elements are

$$d_{ij} = -\frac{1}{2}\alpha_i\alpha_j\left[\frac{A_z^2}{8} + \frac{\Delta^2}{2} - \frac{A_z}{2}(E_i + E_j) + 2E_iE_j\right]. \tag{4.16}$$

In the limit $\Delta \gg A_z, A_\perp$, we find the matrix elements to be given by (to $O\big(\big(\frac{A_{z,\perp}}{\Delta}\big)^3\big)$)

$$d_{12} = d_{34} = -\frac{1}{2}\left[1 - \frac{3A_z^2 + 5A_\perp^2}{16\Delta^2}\right]. \qquad\qquad d_{14} = -d_{23} = \frac{A_\perp}{4\Delta} \tag{4.17}$$

The x component of the nuclear spin operator is given by

$$I^x = b_{11}L_{11} - b_{22}L_{22} + b_{33}L_{33} - b_{44}L_{44} + b_{13}[L_{13} + L_{31}] + b_{24}[L_{24} + L_{42}], \tag{4.18}$$

where

$$b_{ii} = \alpha_i^2 \Delta\left(E_i - \frac{A_z}{4}\right) \tag{4.19}$$

and

$$b_{13} = -\frac{\alpha_1\alpha_3}{4}\Delta(A_z + A_\perp) \qquad\qquad b_{24} = \frac{\alpha_2\alpha_4}{4}\Delta(A_z - A_\perp). \tag{4.20}$$

These analytic expressions are listed here for reference, as they are useful for understanding the behaviour of the electronic and nuclear spins. They will be used throughout the remainder of this chapter to analyze the magnetization, susceptibility, and excitation spectrum of the spin half spin half (SHSH) model .

The SHSH Hamiltonian given in equation (4.1) may be divided into two parts, $\mathscr{H} = \mathscr{H}_0 + \mathscr{H}'$, where, in terms of the single ion operators,

$$\mathscr{H}_0 = \sum_i \sum_n E_n L^i_{nn} \tag{4.21}$$

is the diagonalized single ion Hamiltonian, and

$$\mathscr{H}' = -\frac{1}{2}\sum_{i\neq j} V_{ij} S^z_i S^z_j \tag{4.22}$$

is the interaction, with the S^z operator given in terms of the single ion operators in equation (4.9).

Perturbation Theory in the Ordered Phase

In the presence of a longitudinal field, or in the ordered phase of the system, we are no longer able to diagonalize the single ion Hamiltonian of the spin half spin half (SHSH) model exactly; however, we can treat a longitudinal field that is much weaker than the transverse field perturbatively. This allows us to study properties of the ordered phase of our model analytically in the vicinity of the system's quantum critical point. The Hamiltonian is

$$\mathscr{H} = \mathscr{H}_{MF} - \frac{1}{2}\sum_{i\neq j} V_{ij} \widetilde{S}^z_i \widetilde{S}^z_j, \tag{4.23}$$

where $\widetilde{S}^z_i = S^z_i - \langle S^z \rangle_0$, and the subscript 0 denotes the average is taken with respect to the MF Hamiltonian. The MF Hamiltonian is given by

$$\mathscr{H}_{MF} = -\Delta\sum_i S^x_i - H\sum_i S^z_i + A_z\sum_i I^z_i S^z_i + \frac{A_\perp}{2}\sum_i (I^+_i S^-_i + I^-_i S^+_i), \tag{4.24}$$

with $H = h + V_0\langle S^z\rangle$ and $V_0 = \sum_j V_{ij}$. H includes an applied longitudinal field h as well as the MF of the neighbouring electronic spins, which we obtain by using the MF Hamiltonian to solve for the magnetization self consistently. At each site, we divide the MF Hamiltonian into two parts, $\mathscr{H}_{MFi} = \mathscr{H}_{0i} + \mathscr{H}_i^{\varepsilon}$, where $\mathscr{H}_{0i}$ is the single ion Hamiltonian given in (4.3), and $\mathscr{H}_i^{\varepsilon}$ is the longitudinal component of the MF Hamiltonian, which we assume is small. Working in a basis of eigenstates of $\mathscr{H}_{0i}$ we find,

$$\mathscr{H}_i^{\varepsilon} = \begin{pmatrix} 0 & -Hc_{12} & 0 & -Hc_{14} \\ -Hc_{12} & 0 & -Hc_{23} & 0 \\ 0 & -Hc_{23} & 0 & -Hc_{34} \\ -Hc_{14} & 0 & -Hc_{34} & 0 \end{pmatrix}, \tag{4.25}$$

where the c_{ij} are given in equation (4.10). In what follows, we will drop the subscript i, and it is to be assumed that we are referring to the MF Hamiltonian of a single ion.

We now include the effects of $\mathscr{H}^{\varepsilon}$ perturbatively to second order in the ratio of the longitudinal field to the transverse field, $\frac{H}{\Delta}$. We find the perturbed energies to be

$$\begin{aligned} \tilde{E}_1 &= E_1 - \frac{H^2c_{12}^2}{E_{21}} - \frac{H^2c_{14}^2}{E_{41}} & \tilde{E}_2 &= E_2 + \frac{H^2c_{12}^2}{E_{21}} - \frac{H^2c_{23}^2}{E_{32}} \\ \tilde{E}_3 &= E_3 + \frac{H^2c_{23}^2}{E_{32}} - \frac{H^2c_{34}^2}{E_{43}} & \tilde{E}_4 &= E_4 + \frac{H^2c_{14}^2}{E_{41}} + \frac{H^2c_{34}^2}{E_{43}}, \end{aligned} \tag{4.26}$$

and the normalized (to order $\frac{H^2}{\Delta^2}$) wavefunctions to be

$$\begin{aligned} |\tilde{1}\rangle &= \frac{|1\rangle + \frac{Hc_{12}}{E_{21}}|2\rangle + \frac{Hc_{14}}{E_{41}}|4\rangle + \frac{H^2c_{23}c_{12}}{E_{31}E_{21}}|3\rangle + \frac{H^2c_{34}c_{14}}{E_{31}E_{41}}|3\rangle}{\sqrt{1 + \frac{H^2c_{12}^2}{E_{21}^2} + \frac{H^2c_{14}^2}{E_{41}^2}}} \\ |\tilde{2}\rangle &= \frac{|2\rangle - \frac{Hc_{12}}{E_{21}}|1\rangle + \frac{Hc_{23}}{E_{32}}|3\rangle - \frac{H^2c_{14}c_{12}}{E_{42}E_{21}}|4\rangle + \frac{H^2c_{34}c_{23}}{E_{42}E_{32}}|4\rangle}{\sqrt{1 + \frac{H^2c_{12}^2}{E_{21}^2} + \frac{H^2c_{23}^2}{E_{32}^2}}} \\ |\tilde{3}\rangle &= \frac{|3\rangle - \frac{Hc_{23}}{E_{32}}|2\rangle + \frac{Hc_{34}}{E_{43}}|4\rangle + \frac{H^2c_{12}c_{23}}{E_{31}E_{32}}|1\rangle - \frac{H^2c_{14}c_{34}}{E_{31}E_{43}}|1\rangle}{\sqrt{1 + \frac{H^2c_{23}^2}{E_{32}^2} + \frac{H^2c_{34}^2}{E_{43}^2}}} \\ |\tilde{4}\rangle &= \frac{|4\rangle - \frac{Hc_{14}}{E_{41}}|1\rangle - \frac{Hc_{34}}{E_{43}}|3\rangle + \frac{H^2c_{12}c_{14}}{E_{42}E_{41}}|2\rangle + \frac{H^2c_{23}c_{34}}{E_{42}E_{43}}|2\rangle}{\sqrt{1 + \frac{H^2c_{14}^2}{E_{41}^2} + \frac{H^2c_{34}^2}{E_{43}^2}}}. \end{aligned} \tag{4.27}$$

These expressions are listed here for reference, and will be used subsequently to analyze the

magnetization and susceptibility of the SHSH model in the vicinity of its quantum critical point.

Mean Field Electronic Spin Magnetization

We calculate the electronic spin magnetization of the SHSH model self consistently from the MF Hamiltonian given by

$$\mathscr{H}_{MF} = -\Delta\sum_i S_i^x - H\sum_i S_i^z + A_z\sum_i I_i^z S_i^z + \frac{A_\perp}{2}\sum_i (I_i^+ S_i^- + I_i^- S_i^+), \tag{4.28}$$

where $H = h + V_0\langle S^z\rangle_0$ and $V_0 = \sum_j V_{ij}$. At each atomic site, the Hamiltonian is given by

$$\mathscr{H}_{MFi} = \begin{pmatrix} \frac{A_z}{4} - \frac{H}{2} & -\frac{\Delta}{2} & 0 & 0 \\ -\frac{\Delta}{2} & -\frac{A_z}{4} + \frac{H}{2} & \frac{A_\perp}{2} & 0 \\ 0 & \frac{A_\perp}{2} & -\frac{A_z}{4} - \frac{H}{2} & -\frac{\Delta}{2} \\ 0 & 0 & -\frac{\Delta}{2} & \frac{A_z}{4} + \frac{H}{2} \end{pmatrix}, \tag{4.29}$$

where we are using the same basis as in equation (4.3). In this basis, the electronic spin operators are given by

$$S^z = \begin{pmatrix} \frac{1}{2} & 0 & 0 & 0 \\ 0 & -\frac{1}{2} & 0 & 0 \\ 0 & 0 & \frac{1}{2} & 0 \\ 0 & 0 & 0 & -\frac{1}{2} \end{pmatrix} \qquad S^x = \begin{pmatrix} 0 & \frac{1}{2} & 0 & 0 \\ \frac{1}{2} & 0 & 0 & 0 \\ 0 & 0 & 0 & \frac{1}{2} \\ 0 & 0 & \frac{1}{2} & 0 \end{pmatrix}. \tag{4.30}$$

In Figures 4.1 and 4.2, we show the ground state expectation values of the electronic spin operators in the MF approximation for an isotropic and an anisotropic hyperfine interaction, solved for self consistently, plotted as a function of the transverse magnetic field Δ. For brevity, we will often refer to the expectation value of a spin operator as the magnetization, when, in fact, they are proportional to each other. We consider a simple cubic crystal with a nearest neighbour exchange interaction so that $V_0 = 6J$, with $J = 1$ being the exchange coupling. When the hyperfine interaction is isotropic, we find its only effect on the electronic magnetization is a small overall reduction. The effect of an anisotropic hyperfine interaction is far more dramatic, as can be seen in Figure 4.2. We find that a dominant longitudinal hyperfine interaction tends to increase the longitudinal electronic magnetization, stabilizing it against the effects of the transverse field; whereas a dominant transverse hyperfine interaction has the opposite effect.

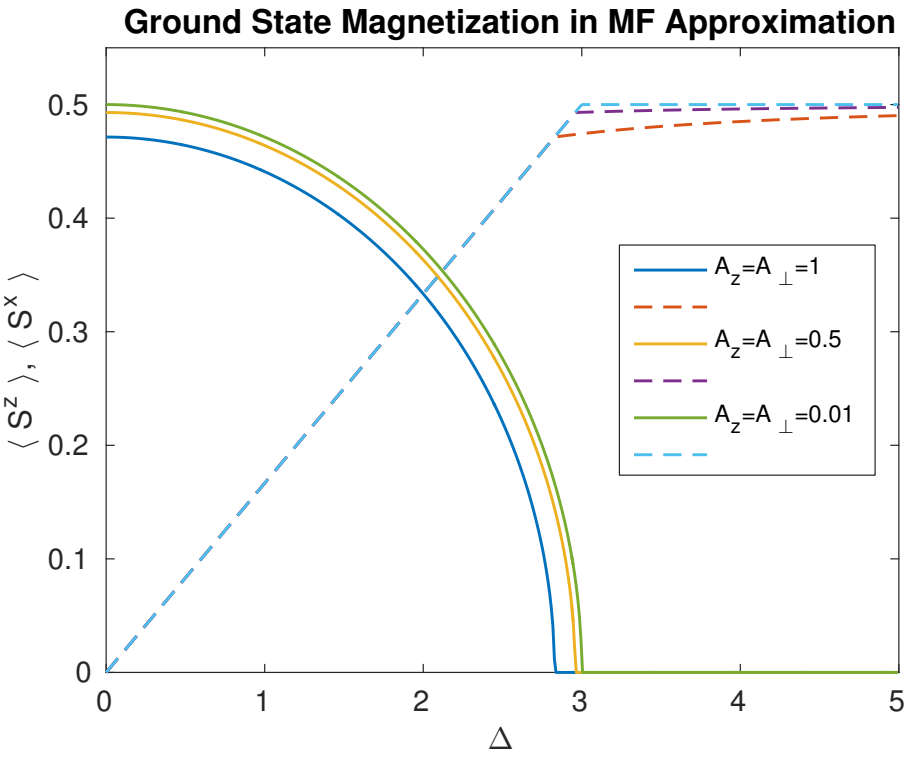

Figure 4.1: The plot above shows z (solid line) and x (dashed line) ground state components of the electronic spin operators (in the MF approximation) of the spin half transverse field Ising model with an isotropic hyperfine interaction, as a function of the applied transverse field Δ. We work in units of the exchange interaction strength J. We find the z component of the magnetization is uniformly reduced with increasing transverse field strength. We obtain these results from the MF Hamiltonian of the spin half spin half model, given in equation (4.28).

In Figures 4.1 and 4.2, we neglect the effect of an applied transverse magnetic field acting on the nuclear spins, $\mathscr{H}_n = \Delta_n \sum_i \frac{I_i^+ + I_i^-}{2}$. When one considers an effective low temperature Hamiltonian for systems such as $LiHoF_4$, such a field is present, and cannot be neglected. This transverse nuclear field is present because when we truncate an electronic spin down to a spin half subspace, the effective operator takes the form

$$J^\mu = C_\mu + \sum_{\nu=x,y,z} C_{\mu\nu}\tau^\nu. \tag{4.31}$$

In the hyperfine interaction, the C_μ terms lead to an effective field acting directly on the nuclear spins. This field may be understood as the effect of a shift in the electron cloud surrounding an ion due to the applied transverse field, that causes a transverse field to act on the nuclear spins via the hyperfine coupling. This transverse field due to an atom's electron cloud may be orders of magnitude larger than the applied field acting directly on the nuclear spins. In

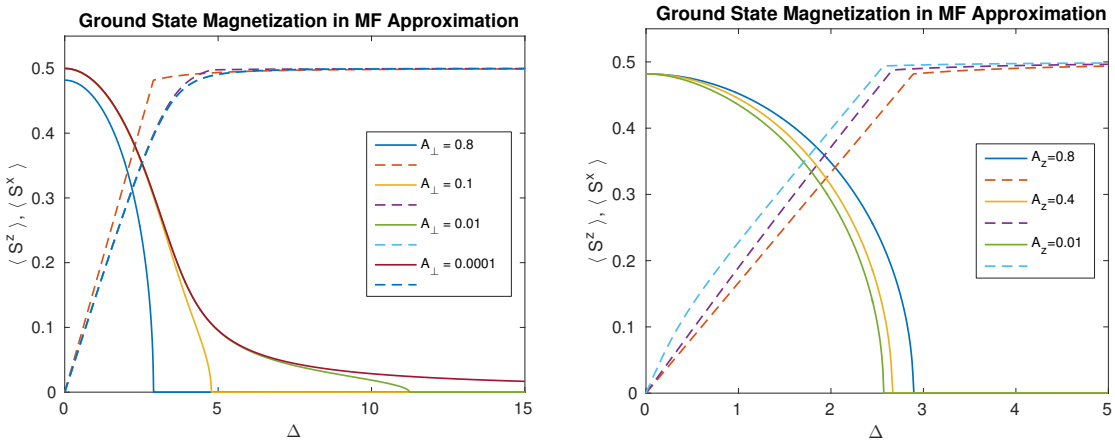

Figure 4.2: The plot above shows z (solid line) and x (dashed line) ground state components of the electronic spin operators (in the MF approximation) of the spin half transverse field Ising model with an anisotropic hyperfine interaction, as a function of the applied transverse field Δ. We work in units of the exchange interaction strength J. The plot on the left shows the magnetization when the longitudinal hyperfine interaction ($A_z = 0.8$) is dominant, whereas the plot on the right is for a dominant transverse hyperfine interaction ($A_\perp = 0.8$). With the longitudinal hyperfine interaction dominant, we see that the critical transverse field is driven to larger values with a decreasing transverse hyperfine interaction $A_\perp$. With $A_\perp$ dominant, decreasing A_z reduces the critical transverse field. We obtain these results from the MF Hamiltonian of the spin half spin half model, given in equation (4.28).

particular, in the Ho^{3+} ion, the field at the nucleus due to the $4f$ electron cloud is close to 800 Tesla [82]. The effect of the the applied field acting directly on the nuclear spins (4.9 Tesla at the zero temperature critical transverse field in $LiHoF_4$) is suppressed by a factor of the nuclear magneton μ_N, which is about 1836 times smaller than the electronic Bohr magneton μ_B.

We see in Figure 4.2, that as $A_\perp \to 0$, with A_z fixed, the critical transverse field is driven to higher values. This is because with $A_\perp = 0$ there is no mechanism for flipping nuclear spins in I^z eigenstates; the nuclear spin up and down subspaces are entirely disjoint, as is apparent in equation (4.2). Within each subspace, the nuclear spins constitute an effective longitudinal field acting on the electronic system. The effect of the transverse field acting on the nuclear spins is a reduction of the critical field values, even when $A_\perp = 0$. This point is illustrated in Figure 4.3 where we have repeated the MF calculation for the anisotropic case with $\Delta_n = \frac{\Delta}{50}$. This roughly corresponds to the ratio of the strength of the effective transverse field acting on the nuclear spins in $LiHoF_4$, to the strength of the effective field acting on the electronic spins, when the system goes critical ($\Delta(B_x^c) \approx 50\Delta_n(B_x^c)$, with B_x^c being the physical critical transverse field of $LiHoF_4$). Even with this modest value of the transverse field acting on the nuclear spins, we see by comparing Figure 4.2 and Figure 4.3 that it has a significant impact

on Δ_c, the point at which Δ drives the longitudinal magnetization to zero.

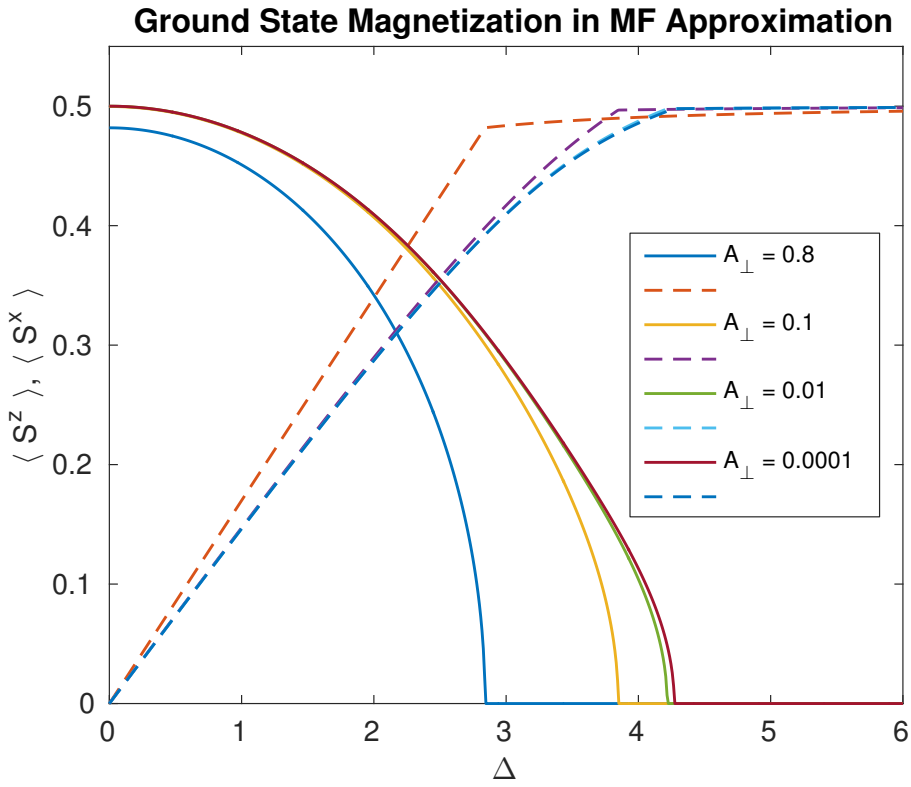

Figure 4.3: The plot above shows z (solid line) and x (dashed line) ground state components of the electronic spin operators (in the MF approximation) of the spin half transverse field Ising model with an anisotropic hyperfine interaction and a transverse field acting directly on the nuclear spins, as a function of transverse field Δ. We work in units of the exchange interaction strength J. The longitudinal hyperfine interaction ($A_z = 0.8$) is dominant, and the applied transverse field acting directly on the nuclear spins is $\Delta_n = \frac{\Delta}{50}$. We obtain these results from the MF Hamiltonian of the spin half spin half model, given in equation (4.28), with an additional term $\mathscr{H}_n = -\frac{\Delta_n}{2}(I^+ + I^-)$ to account for the transverse field acting on the nuclear spins. This additional transverse field leads to a reduction in the critical transverse field of the system.

In the high field limit, with $\Delta > \Delta_c$ so that $\langle S^z \rangle = 0$, and $\Delta \gg A_z, A_\perp$, we find the ground state electronic magnetization in the x direction to be

$$\langle S^x \rangle \approx \frac{1}{2}\left[1 - \frac{5(A_z + A_\perp)^2}{16\Delta^2} + \cdots\right]. \tag{4.32}$$

We see that the effect of the nuclear spins is to suppress the x component of the magnetization in the paramagnetic phase.

In the vicinity of the phase transition, where the longitudinal magnetization is small, we

may use our perturbation theory results given in equation (4.27), and the S^z operator given in equation (4.9), to write down an analytic expression for the longitudinal magnetization. The ground state longitudinal electronic magnetization of the system is given by (to order $\frac{H^2}{\Delta^2}$)

$$\langle\tilde{1}|S^z|\tilde{1}\rangle = \frac{H\left[\frac{2c_{12}^2}{E_{21}} + \frac{2c_{14}^2}{E_{41}} + \frac{2H^2c_{12}^2c_{23}^2}{E_{31}E_{21}^2} + \frac{2H^2c_{34}^2c_{14}^2}{E_{31}E_{41}^2} + \frac{4H^2c_{12}c_{23}c_{34}c_{14}}{E_{31}E_{41}E_{21}}\right]}{\left[1 + \frac{H^2c_{12}^2}{E_{21}^2} + \frac{H^2c_{14}^2}{E_{41}^2}\right]}. \tag{4.33}$$

This expression will be used in Section 4.4 when discussing the susceptibility of the system. For now, we note that $\langle\tilde{1}|S^z|\tilde{1}\rangle = dm$ is the infinitesimal change in the longitudinal electronic magnetization upon application of a small longitudinal field, $H = dH$. To leading order in $\frac{H}{\Delta}$ we have

$$dm = \left[\frac{2c_{12}^2}{E_{21}} + \frac{2c_{14}^2}{E_{41}}\right]dh. \tag{4.34}$$

Recall that $H = h + V_0\langle S^z\rangle_0$. We have used the fact that $dH \approx dh$. Differentiating the MF magnetization with respect to h yields the RPA expression for the susceptibility, as shown in Appendix B. We identify

$$\chi_0^{zz} = \left[\frac{2c_{12}^2}{E_{21}} + \frac{2c_{14}^2}{E_{41}}\right] \approx \frac{1}{2\Delta}\left[1 + \frac{1}{2\Delta}\left(\frac{A_z^2}{A_\perp}\left[1 - \frac{A_z}{2\Delta} + O\left(\frac{A_z^2, A_\perp^2}{\Delta^2}\right)\right] - A_\perp + O\left(\frac{A_z^2, A_\perp^2}{\Delta^2}\right)\right)\right] \tag{4.35}$$

as the single ion longitudinal electronic susceptibility of our SHSH system, at zero temperature. In the final expression, we have expanded in the limit $A_z, A_\perp \ll \Delta$. To leading order we see

$$\chi_0^{zz} \approx \frac{1}{2\Delta} + \frac{1}{4\Delta^2}\left[\frac{A_z^2}{A_\perp} - A_\perp\right], \tag{4.36}$$

which matches the result derived in [64]. This result ceases to be valid when $A_\perp \to 0$ because the lower two energy levels, and the upper two energy levels, of the SHSH system become degenerate; hence E_{21} in equation (4.33) is zero. As previously mentioned in this section, when $A_\perp = 0$, in the absence of a transverse field acting on the nuclear spins, the nuclear spin up and nuclear spin down subspaces are disjoint. When calculating thermodynamic averages in the MF approximation, we may consider the two subspaces separately. Within each subspace, the nuclear spin constitutes a longitudinal field acting on the electronic degree of freedom, and the physics is the same as that of the transverse field Ising model in a longitudinal field, discussed in Appendix B. We will comment further on the degenerate case in Section 4.4, in which we

calculate the single ion susceptibility making use of the MF operator formalism discussed in Appendix A. Degeneracies are easily dealt with using this formalism.

In the non-degenerate case, equation (4.36) shows that an isotropic hyperfine interaction will have little effect on the susceptibility of a magnetic system. However, with an anisotropic hyperfine interaction, where the longitudinal component is dominant, the longitudinal susceptibility is enhanced. Conversely, if the transverse component of the hyperfine interaction is dominant the longitudinal susceptibility is suppressed.

As a final note, we point out that the total magnetization of the system will have a nuclear component, as well as the electronic component discussed above. In the MF Hamiltonian (4.28), we have neglected the effect of the longitudinal field acting directly on the nuclear spins because this term depends on the ratio of the nuclear to the Bohr magneton. The MF Hamiltonian including this term is (including a transverse field acting directly on the nuclear spins)

$$\begin{aligned}\mathscr{H}_{MF} = -\Delta\sum_i S_i^x - H\sum_i S_i^z - \frac{\mu_N}{\mu_B}h\sum_i I_i^z - \frac{\Delta_n}{2}\sum_i (I_i^+ + I_i^-) \\ + A_z\sum_i I_i^z S_i^z + \frac{A_\perp}{2}\sum_i (I_i^+ S_i^- + I_i^- S_i^+).\end{aligned} \tag{4.37}$$

From the free energy we find

$$\frac{-\partial F}{\partial h} = M = \langle S^z\rangle_0 + \frac{\mu_N}{\mu_B}\langle I^z\rangle_0. \tag{4.38}$$

Performing a second derivative yields

$$\frac{-\partial^2 F}{\partial h^2} = \frac{\partial M}{\partial h} = \beta\left[\langle S_z^2\rangle_0 - \langle S_z\rangle_0^2 + 2\frac{\mu_N}{\mu_B}(\langle S_z I_z\rangle_0 - \langle S_z\rangle_0\langle I_z\rangle_0) + \frac{\mu_N^2}{\mu_B^2}(\langle I_z^2\rangle_0 - \langle I_z\rangle_0^2)\right]. \tag{4.39}$$

The result above is the classical result for the relationship between the susceptibility and the electronic and nuclear correlation functions. See the discussion surrounding equation (D.15) for further details. The susceptibility given by χ_0^{zz} in equation (4.36) is the zero temperature Van Vleck contribution to the susceptibility of the system due solely to the electronic spins. For an explanation of the Van Vleck contribution to the susceptibility, see the discussion that follows equation (D.28). For convenience, we note that

$$\chi_0^{zz} = -\mathrm{Re}[g(\omega = 0)], \tag{4.40}$$

where $g(\omega)$ is given in Appendix D. The total Van Vleck contribution to the single ion suscep-

tibility of the system may be written as

$$\frac{-\partial^2 F}{\partial h^2} = \chi^{zz}_{0,\text{total}} = \chi^{zz}_0 + 2\frac{\mu_N}{\mu_B}\chi^{zz}_{0,en} + \frac{\mu_N^2}{\mu_B^2}\chi^{zz}_{0,n}, \tag{4.41}$$

where $\chi^{zz}_{0,en}$ is the mixed electronuclear contribution, and $\chi^{zz}_{0,n}$ is the purely nuclear contribution.

In the following section, we turn our attention to the nuclear spins, and perform a similar MF analysis.

Mean Field Nuclear Spin Magnetization

We now calculate the nuclear spin magnetization of the SHSH model in the MF approximation. For brevity, we will often refer to the expectation value of a spin operator as the magnetization, when, in fact, they are proportional to each other. Using the same basis as for (4.3), the nuclear spin operators are given by

$$I^z = \begin{pmatrix} \frac{1}{2} & 0 & 0 & 0 \\ 0 & \frac{1}{2} & 0 & 0 \\ 0 & 0 & -\frac{1}{2} & 0 \\ 0 & 0 & 0 & -\frac{1}{2} \end{pmatrix} \qquad I^x = \begin{pmatrix} 0 & 0 & \frac{1}{2} & 0 \\ 0 & 0 & 0 & \frac{1}{2} \\ \frac{1}{2} & 0 & 0 & 0 \\ 0 & \frac{1}{2} & 0 & 0 \end{pmatrix}. \tag{4.42}$$

In Figures 4.4 and 4.5, we show the expectation value of the nuclear spin operators as a function of transverse field for an isotropic and an anisotropic hyperfine interaction. We see that the nuclear spins order at the same critical field as the electronic spins.

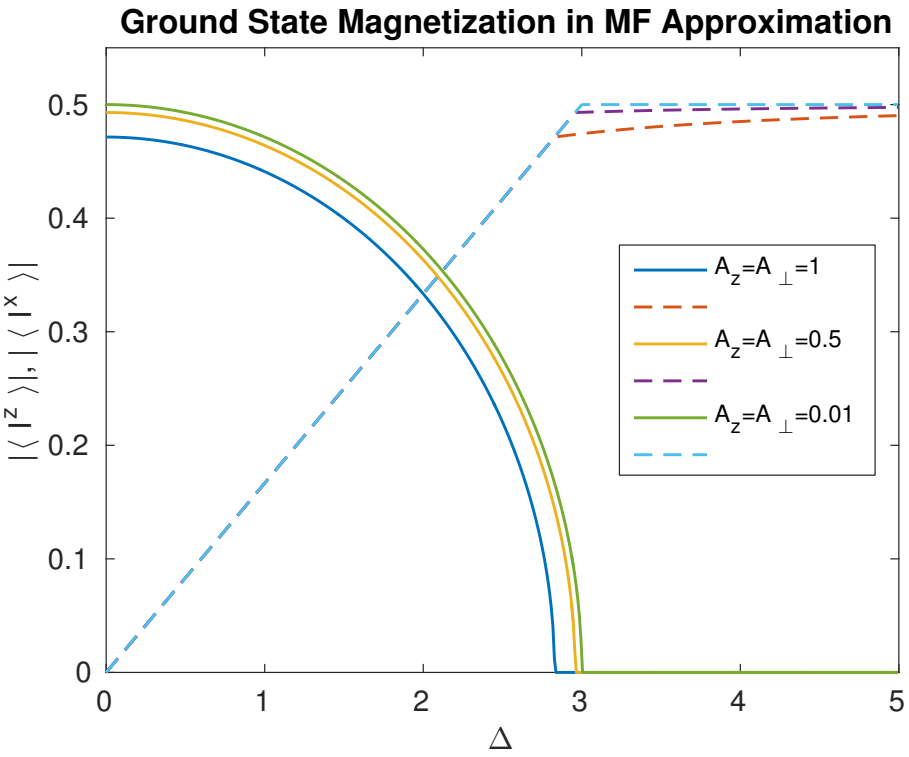

Figure 4.4: The plot above shows the z (solid lines) and x (dashed lines) components of the ground state expectation values of the nuclear spin operators (in the MF approximation) of the spin half transverse field Ising model with an isotropic hyperfine interaction, as a function of transverse field Δ. We work in units of the exchange interaction strength J. We obtain these results from the MF Hamiltonian of the spin half spin half model, given in equation (4.28). We plot the absolute value of the expectation values of the nuclear operators, noting that they are equal and opposite their electronic counterparts.

When the hyperfine interaction is isotropic, the electronic and nuclear magnetizations are similar. However, with an anisotropic hyperfine interaction, we see in Figure 4.5 that the nuclear magnetization is quite different from the electronic magnetization shown in Figure 4.2. When the longitudinal hyperfine interaction is dominant, the longitudinal nuclear spin magnetization is far more resistant to the effects of the transverse field than its electronic counterpart. This can be understood by inspecting equation (4.28). We see that if we set the transverse hyperfine interaction $A_\perp$ to zero, there is no energy benefit associated with aligning the nuclear spins opposite the transverse field. The longitudinal hyperfine interaction holds nuclear spins along the easy axis of the system. When the transverse hyperfine interaction is dominant, we see that the longitudinal nuclear magnetization is more easily reduced by the transverse field than its electronic counterpart. Again, by inspection of equation (4.28), we see that if we take $A_z = 0$, it is energetically favourable for the nuclear spins to lie opposite the transverse field.

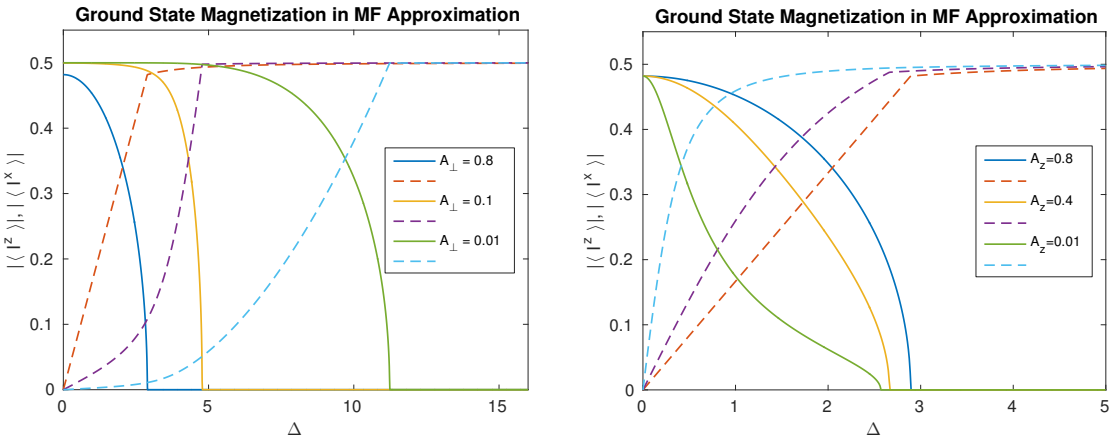

Figure 4.5: The plot above shows the z (solid lines) and x (dashed lines) components of the ground state expectation values of the nuclear spin operators (in the MF approximation) of the spin half transverse field Ising model with an anisotropic hyperfine interaction, as a function of transverse field Δ. We work in units of the exchange interaction strength J. We obtain these results from the MF Hamiltonian of the spin half spin half model, given in equation (4.28). We plot the absolute value of the expectation values of the nuclear operators, noting that they are equal and opposite their electronic counterparts. The plot on the left shows the magnetization while the longitudinal hyperfine interaction ($A_z = 0.8$) is dominant, while the plot on the right is for a dominant transverse hyperfine interaction ($A_\perp = 0.8$)

.

There is no energy benefit associated with spins aligned along the easy axis.

We have ignored the effect of the applied transverse field on the nuclear spins in Figures 4.4 and 4.5. As with the electronic spins, we find the effect of a transverse field acting directly on the nuclear spins is a reduction in Δ_c relative to the critical field when the effect of the transverse field on the nuclear spins is ignored. We also find that if the strength of the transverse field acting on the nuclear spins is comparable to the strength of the hyperfine interaction, there will be qualitative changes in the magnetization of the nuclear spins, as can be seen in Figure 4.6. In this figure we include a transverse field acting directly on the nuclear spins, $H_n = \Delta_n \sum_i \frac{I_i^+ + I_i^-}{2}$, with $\Delta_n = \frac{\Delta}{100}$. We see that with a hyperfine interaction of strength $A_z = A_\perp = 0.01$ the nuclear magnetization is affected by the transverse field.

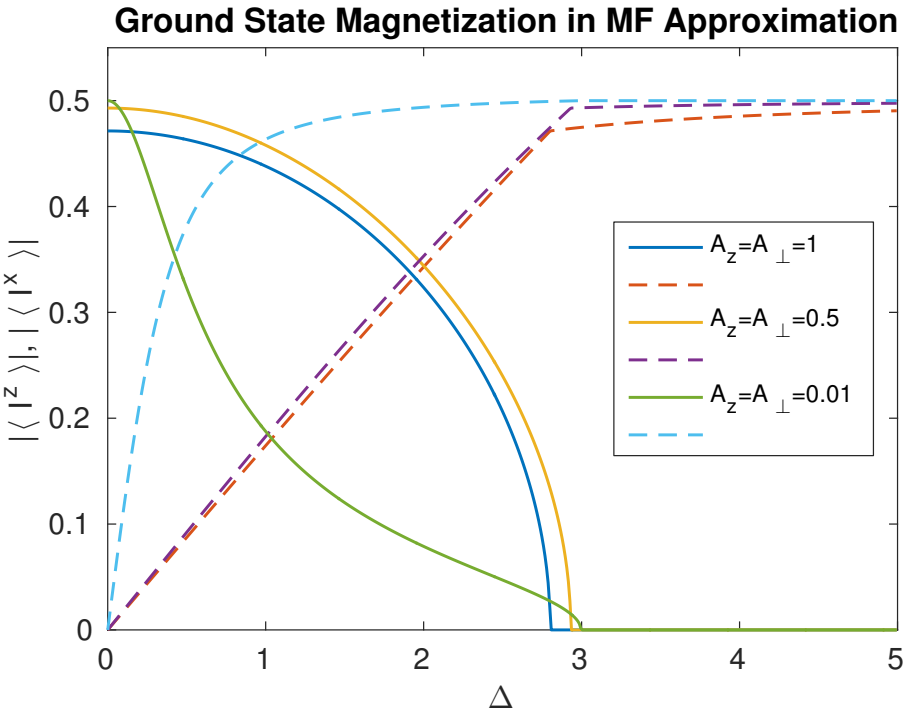

Figure 4.6: The plot above shows the z (solid lines) and x (dashed lines) components of the ground state expectation values of the nuclear spin operators (in the MF approximation) of the spin half transverse field Ising model with an isotropic hyperfine interaction, as a function of transverse field Δ. We work in units of the exchange interaction strength J. We obtain these results from the MF Hamiltonian of the spin half spin half model, given in equation (4.28), with an additional transverse field acting directly on the nuclear spins.. We plot the absolute value of the expectation values of the nuclear operators, noting that they are equal and opposite their electronic counterparts.

In the high field limit, with $\Delta > \Delta_c$ so that $\langle I^z \rangle = 0$, and $\Delta \gg A_z, A_\perp$, we find the ground state magnetization in the x direction to be equal and opposite its electronic counterpart, $\langle I^x \rangle = -\langle \tau^x \rangle$. When the longitudinal magnetization is small, we may use our perturbation theory results (4.27), and the I^z operator (4.15), to write down an analytic expression for the longitudinal component of the nuclear magnetization. The ground state expectation value of the longitudinal nuclear spin operator is given by

$$\langle \tilde{1}|I^z|\tilde{1}\rangle = \frac{H\left[\frac{2c_{12}d_{12}}{E_{21}} + \frac{2c_{14}d_{14}}{E_{41}} + \frac{2H^2c_{12}^2c_{23}d_{23}}{E_{31}E_{21}^2} + \frac{2H^2c_{14}^2c_{34}d_{34}}{E_{31}E_{41}^2} + \frac{2H^2c_{12}c_{34}c_{14}d_{23}}{E_{31}E_{41}E_{21}} + \frac{2H^2c_{12}c_{23}c_{14}d_{34}}{E_{31}E_{41}E_{21}}\right]}{\left[1 + \frac{H^2c_{12}^2}{E_{21}^2} + \frac{H^2c_{14}^2}{E_{41}^2}\right]}. \tag{4.43}$$

To lowest order in $\frac{H}{\Delta}$ we find

$$\langle \tilde{1}|I^z|\tilde{1}\rangle \approx \left[\frac{2c_{12}d_{12}}{E_{21}} + \frac{2c_{14}d_{14}}{E_{41}}\right]H. \tag{4.44}$$

We identify the term in brackets with the Van Vleck contribution to the electronuclear susceptibility given in (4.41). In the limit $A_z, A_\perp \ll \Delta$, we find

$$\chi^{zz}_{o,en} = -\frac{1}{2\Delta}\left[\frac{A_z}{A_\perp}\left(1 - \frac{A_z}{2\Delta} + O\left(\frac{A_z^2, A_\perp^2}{\Delta^2}\right)\right) + \frac{A_\perp}{2\Delta} + O\left(\frac{A_z^2, A_\perp^2}{\Delta^2}\right)\right]. \tag{4.45}$$

Dropping the contribution to the Van Vleck susceptibility coming entirely from the nuclear spins, which is suppressed by a factor of $\frac{\mu_N^2}{\mu_B^2}$, we find from (4.41) that the zero temperature Van Vleck contribution to the susceptibility of our system is given by

$$\chi^{zz}_{0,\text{total}} \approx \chi^{zz}_0 + 2\frac{\mu_N}{\mu_B}\chi^{zz}_{0,en} = \frac{1}{2\Delta}\left(1 + 2\left|\frac{\mu_N}{\mu_B}\right|\frac{A_z}{A_\perp}\right) + \frac{1}{4\Delta^2}\left(\frac{A_z^2}{A_\perp} - A_\perp\right)\left(1 - 2\left|\frac{\mu_N}{\mu_B}\right|\right), \tag{4.46}$$

We note that the overall contribution from the electronuclear term is positive. The minus sign in $\chi^{zz}_{0,en}$ is cancelled by a minus sign in the ratio of the nuclear to the Bohr magneton. As with the electronic component of the susceptibility, we see that a dominant longitudinal hyperfine interaction will lead to an enhancement of the electronuclear susceptibility. We also see that the expressions cease to be valid in the limit $A_\perp \to 0$. This is because degeneracies in the MF Hamiltonian lead to a division by zero in the calculations. We will consider the degenerate case in the following section.

Longitudinal Electronic Correlation Function

We now calculate the cumulant part of the longitudinal electronic spin spin correlation function

$$G(k,\tau) = -\langle T_\tau \widetilde{S^z_k}(\tau)\widetilde{S^z_{-k}}(0)\rangle \tag{4.47}$$

where $\widetilde{S^z} = S^z - \langle S^z\rangle$. This function is of primary importance when it comes to understanding magnetic systems, as explained in Appendix D. It will be used here in the random phase approximation (RPA) to obtain the RPA excitation modes, their spectral weight, and the critical transverse field of the SHSH model. The spectral weights associated with this function are relevant to neutron scattering experiments.

The RPA, or, equivalently, the Gaussian approximation, includes the effect of fluctuations, but treats the fluctuations as non-interacting. This approximation takes the fluctuations to be distributed normally about their mean value. It is essentially the simplest possible correction to MF theory. The RPA breaks down in the vicinity of a phase transition, where the effects of fluctuations become important. Any good textbook, for example Goldenfeld [5], will discuss the validity of the RPA. A common estimate of the error implicit in the RPA involves calculating how sharply peaked the normally distributed fluctuations are around their mean value. This is known as the Ginzburg criterion. In order for the Ginzburg criterion to be satisfied we require

$$E_G = \frac{1}{N}\sum_{ij}\frac{\left|\left\langle (S^z_i - \langle S^z_i\rangle)(S^z_j - \langle S^z_j\rangle)\right\rangle\right|}{\langle S^z_i\rangle\langle S^z_j\rangle} \ll 1 \tag{4.48}$$

The numerator is the zero momentum component of the equal time connected correlation function $S^{zz}_{k=0}(t=0) = \int \frac{d\omega}{2\pi} S^{zz}_{k=0}(\omega)$, which is discussed in Appendix D. This correlation function may be expressed in terms of the spectral density, $S^{zz}_k(\omega) = \frac{\rho^{zz}_k(\omega)}{1-e^{-\beta\omega}}$, where the spectral density is given by

$$\rho^{zz}_k(\omega) = -2\mathrm{Im}\Big[G_k(i\omega \to \omega + i\delta)\Big]. \tag{4.49}$$

In terms of the spectral density, the Ginzburg criterion can be written as

$$E_G = \frac{1}{\langle S^z\rangle_0^2}\int \frac{d\omega}{2\pi}\frac{\rho^{zz}_{k=0}(\omega)}{1-e^{-\beta\omega}} \ll 1, \tag{4.50}$$

where we have assumed a uniform magnetization $\langle S^z_i\rangle = \langle S^z\rangle_0$. In Chapter 6, we develop a field theoretic formalism that allows for simpler estimates of the error involved in the RPA. A rough

estimate of the significance of the effect of fluctuations may be obtained by comparing the prefactors of the effective field theory. In Chapter 7, we will use the field theoretic formalism to make estimates of the significance of fluctuations in various magnetic models.

Written in the Matsubara formalism, the Green's function is given by

$$G(k,\tau) = \frac{-\left\langle T_\tau \widetilde{S^z_k}(\tau) \exp\left(-\int_0^\beta d\tau V(\tau) \right) \widetilde{S^z_{-k}}(0) \right\rangle_0}{\left\langle T_\tau \exp\left(-\int_0^\beta d\tau V(\tau) \right) \right\rangle_0}, \tag{4.51}$$

where

$$V(\tau) = -\frac{1}{2} \sum_k V_k \widetilde{S^z_k}(\tau) \widetilde{S^z_{-k}}(\tau), \tag{4.52}$$

and we define $V_k = \frac{1}{N} \sum_{ij} V_{ij} e^{ik(r_i - r_j)}$.

Making use of the MF basis operator formalism discussed in Appendices A and D, we find the MF, or unperturbed, propagator to be (assuming no degeneracies)

$$\begin{aligned} g(\tau) &= -\left\langle T_\tau \widetilde{S^z}(\tau) \widetilde{S^z}(0) \right\rangle_0 \\ &= -\sum_{j>i} c^2_{ij} D_{ij} \frac{2E_{ji}}{E^2_{ji} - (i\omega_n)^2} - \beta \sum_{j=1}^4 c^2_{jj} D_j \delta_{\omega 0} + \beta \left[\sum_{j=1}^4 c_{jj} D_j \right]^2 \delta_{\omega 0}. \end{aligned} \tag{4.53}$$

Note that the momentum index has been dropped as we are dealing with spins at a single site. All averages are with respect to the MF Hamiltonian. In the case where any of the MF energy levels are degenerate, for example, if we take $A_\perp = 0$ in the SHSH model in which case $E_{21} = E_{43} = 0$, we simply exclude the degenerate terms from the first summation in equation (4.53).

Armed with the unperturbed magnon propagator, we may perform perturbation theory in the fluctuations around the MF. It should be noted that Wick's theorem does not apply to the spin operators in the usual way; hence, the fourth and higher order interactions cannot be factored into simple products of pairs of spin operators. This is because spins do not commute or anticommute. The MF basis operator approach provides a general reduction scheme for spin operators, and has been applied to products of up to four operators in Appendix E. In the RPA, the propagator for the system is

$$G^{RPA}(k, i\omega_n) = \frac{g(i\omega_n)}{1 + g(i\omega_n) V_k}. \tag{4.54}$$

The remainder of this chapter will be devoted to exploring some of the properties of the RPA propagator.

Paramagnetic Phase

We now examine the longitudinal electronic correlation function in the paramagnetic phase of the system, extracting the low frequency spectrum and the critical transverse field. In the $T \to 0$ limit, for low energy excitations, we find

$$-g(i\omega_n) \approx -g_{12}(i\omega_n) - g_{14}(i\omega_n) \approx A + B(i\omega_n)^2, \tag{4.55}$$

where

$$g_{ij}(i\omega_n) = c_{ij}^2 D_{ij} \frac{2E_{ji}}{E_{ji}^2 - (i\omega_n)^2} \tag{4.56}$$

and

$$A = \frac{2c_{12}^2 D_{12}}{E_{21}} + \frac{2c_{14}^2 D_{14}}{E_{41}} \qquad\qquad B = \frac{2c_{12}^2 D_{12}}{E_{21}^3} + \frac{2c_{14}^2 D_{14}}{E_{41}^3}. \tag{4.57}$$

Note that the zero temperature single ion longitudinal electronic susceptibility is given by $\chi_0^{zz} = -g(0) = A$. Recall from (4.36) that expanding in the high field limit, $A_z, A_\perp \ll \Delta$, we have

$$\chi_0^{zz} = \frac{2c_{14}^2}{E_{41}} + \frac{2c_{12}^2}{E_{21}} \approx \frac{1}{2\Delta} + \frac{1}{4\Delta^2}\left[\frac{A_z^2}{A_\perp} - A_\perp\right]. \tag{4.58}$$

We are working in the low temperature limit, so we set the population factors to one, $D_{ij} = 1$. The result (4.58) is consistent with the result derived perturbatively in [64]. This thesis is primarily concerned with the zero temperature limit; however, we note that the formalism used here allows for easy generalization to finite temperatures. In the case $A_\perp \to 0$, where $E_{21} = 0$, the result becomes

$$\chi_0^{zz}\Big|_{A_\perp = 0} = \frac{2c_{14}^2}{E_{41}} \approx \frac{1}{2\Delta}\left[1 - \frac{3A_z^2}{4\Delta^2} + \cdots\right]. \tag{4.59}$$

This is similar to the result for the spin half transverse field Ising model discussed in Appendix B, with the longitudinal hyperfine interaction playing the same role as a longitudinal magnetic field.

In terms of the parameters A and B given in equation (4.57), the RPA Green's function is

given by

$$G(k,i\omega_n) = \frac{1}{\frac{1}{g}+V_k} = \frac{-A^2}{B[\frac{A}{B}-(i\omega_n)^2-\frac{V_kA^2}{B}]}, \tag{4.60}$$

and the spectrum is given by

$$\omega_k = \sqrt{\frac{A}{B}}\sqrt{1-V_kA}. \tag{4.61}$$

Note that this is the spectrum in the low frequency limit. The full RPA spectrum will be discussed in Section 4.5. The spectrum softens to zero, at $k=0$, at a critical field given by $1-V_0\chi_0^{zz}=0$. In the limit $A_z, A_\perp \ll \Delta$, the critical field is given by

$$\Delta_c \approx \frac{V_0}{2}+\frac{1}{2}\left(\frac{A_z^2}{A_\perp}-A_\perp\right). \tag{4.62}$$

The RPA value of the critical field is subject to further corrections due to the nuclear spins. Recall from (4.41) that the total susceptibility contains an electronuclear contribution and a contribution solely from the nuclear spins. The nuclear contribution is suppressed by a factor of $(\frac{\mu_N}{\mu_B})^2$, and may safely be ignored. The leading order correction, due to the electronuclear susceptibility, follows from $1-V_0(\chi_0^{zz}+2\frac{\mu_N}{\mu_B}\chi_{en}^{zz})=0$. We find the following correction to the critical field due to the electronuclear susceptibility

$$\Delta_c \approx \frac{V_0}{2}\left(1+2\left|\frac{\mu_N}{\mu_B}\right|\frac{A_z}{A_\perp}\right)+\frac{1}{2}\left(\frac{A_z^2}{A_\perp}-A_\perp\right)\left(1-2\left|\frac{\mu_N}{\mu_B}\right|\left[1-\frac{A_z}{A_\perp}\right]\right). \tag{4.63}$$

Ferromagnetic Phase

Although we can't diagonalize the MF Hamiltonian of the SHSH model in the ordered phase of the system analytically, we may include the effects of a weak longitudinal field, $H=h+V_0\langle S^z\rangle \ll \Delta$, perturbatively, making use of the expressions derived in Section 4.1. We begin by expressing the MF magnetization (4.33) as

$$\langle\tilde{1}|S^z|\tilde{1}\rangle = m = \chi_0^{zz}H[1-\delta H^2+\gamma H^2], \tag{4.64}$$

where

$$\delta = \frac{c_{12}^2}{E_{21}^2}+\frac{c_{14}^2}{E_{41}^2}, \tag{4.65}$$

and

$$\gamma = \frac{(c_{12}c_{23}E_{41} + c_{14}c_{34}E_{21})^2}{E_{21}E_{31}E_{41}(c_{12}^2E_{41} + c_{14}^2E_{21})}. \tag{4.66}$$

The MF energy levels and matrix elements are given by (4.4) and (4.10) respectively. Differentiating the MF magnetization (4.64) with respect to h, we find the static susceptibility to be

$$\chi^{zz}(H) = \frac{\partial \langle S^z \rangle_0}{\partial h} = \frac{\chi_0^{zz}(H)}{1 - V_0 \chi_0^{zz}(H)}, \tag{4.67}$$

where $\chi_0^{zz}(H)$ is the single ion susceptibility, in the presence of a longitudinal field H. This result may also be obtained by taking the zero momentum and zero frequency component of (4.54). We choose here to differentiate the magnetism to show the equivalence of the two approaches. The single ion susceptibility, keeping terms up to quadratic order in H, is given by

$$\chi_0^{zz}(H) = \chi_0^{zz}\Big[1 - 3\delta H^2 - 3\gamma H^2\Big]. \tag{4.68}$$

Expanding in the limit $A_z, A_\perp \ll \Delta$ we find that

$$\begin{aligned} \delta &= \frac{1}{4\Delta^2}\left[1 - \frac{A_\perp}{\Delta} + O\left(\frac{A_{z,\perp}^2}{\Delta^2}\right) + \frac{A_z^2}{A_\perp^2}\left(1 - \frac{A_z}{\Delta} + O\left(\frac{A_{z,\perp}^2}{\Delta^2}\right)\right)\right] \\ &\approx \frac{1}{4\Delta^2}\left[1 + \frac{A_z^2}{A_\perp^2}\right], \end{aligned} \tag{4.69}$$

and

$$\begin{aligned} \gamma &= \frac{1}{4\Delta^2}\frac{A_z^2}{A_\perp^2}\left[1 + O\left(\frac{A_{z,\perp}}{\Delta}\right)\right]\left[1 + O\left(\frac{A_{z,\perp}}{\Delta}\right) + \frac{A_z}{A_\perp}\frac{A_z}{2\Delta}\left(1 + O\left(\frac{A_{z,\perp}}{\Delta}\right)\right)\right]^{-1} \\ &\approx \frac{1}{4\Delta^2}\frac{A_z^2}{A_\perp^2}\left[1 + \frac{A_z}{A_\perp}\frac{A_z}{2\Delta}\right]^{-1} \end{aligned} \tag{4.70}$$

We include γ here for the sake of completeness; however, we note that it stems from the second order perturbative correction to the wavefunctions in (4.27). This correction is unreliable, and will be dropped from subsequent analysis. Taking only the leading order perturbative correction to the energies and wavefunctions, we find, in the limit $A_z, A_\perp \ll 1$,

$$\chi_0^{zz}(H) = \chi_0^{zz}\left[1 - \frac{3H^2}{4\Delta^2}\left(1 + \frac{A_z^2}{A_\perp^2}\right)\right]. \tag{4.71}$$

If the hyperfine interaction is isotropic this reduces to the result for the transverse Ising model given in equation (B.11) of Appendix B.

We note that the effects of an anisotropic hyperfine interaction ($A_z > A_\perp$) on the susceptibility are twofold. First, the single ion susceptibility is enhanced by an additive factor of $\frac{1}{4\Delta^2}[\frac{A_z^2}{A_\perp} - A_\perp]$, causing the system to magnetize more rapidly upon the application of a longitudinal field. Second, the effect of the longitudinal field is enhanced by a multiplicative factor of $\sqrt{\frac{1}{2}\left(1+\frac{A_z^2}{A_\perp^2}\right)}$. We define the enhanced field to be

$$H_+ = H\sqrt{\frac{1}{2}\left(1+\frac{A_z^2}{A_\perp^2}\right)}, \tag{4.72}$$

which gives

$$\chi_0^{zz}(H) = \chi_0^{zz}\left[1-\frac{3H_+^2}{2\Delta^2}\right]. \tag{4.73}$$

Electronic Spectrum

In Section 4.4.1, we analyzed the low frequency spectrum of the SHSH model in the paramagnetic phase of the system. In this section we use the full RPA longitudinal electronic Green's function to find all the RPA modes of the system, and their associated spectral weights. We will then examine the low frequency spectrum in the ferromagnetic phase, and find how the spectral gap varies with the longitudinal field.

We consider the full zero temperature RPA spectrum, which follows from the poles of

$$G(k,z) = \frac{g(i\omega_n)}{1+g(i\omega_n)V_k} = \frac{\sum_{j=2}^4 |c_{1j}|^2 2E_{j1}\prod_{s\neq j}(E_{s1}^2-z^2)}{V_k\sum_{j=2}^4 |c_{1j}|^2 2E_{j1}\prod_{s\neq j}(E_{s1}^2-z^2) - \prod_{j=2}^4(E_{j1}^2-z^2)}. \tag{4.74}$$

We assume a simple cubic crystal with nearest neighbour exchange interactions between the electronic spins, and calculate the zero wavevector gap in the modes as a function of transverse field, and the associated spectral weights as discussed in Appendix B. We see the upper bands, corresponding to a spin opposed to the MF, and the lower bands, corresponding to a spin in line with the MF, are split by the hyperfine interaction. In the absence of the hyperfine interaction, the upper band would soften to zero at a critical value of the transverse field. We see in the plots that this band is now gapped; however, the spectral weight is transferred down to a lower electronuclear level which fully softens to zero at the quantum critical point.

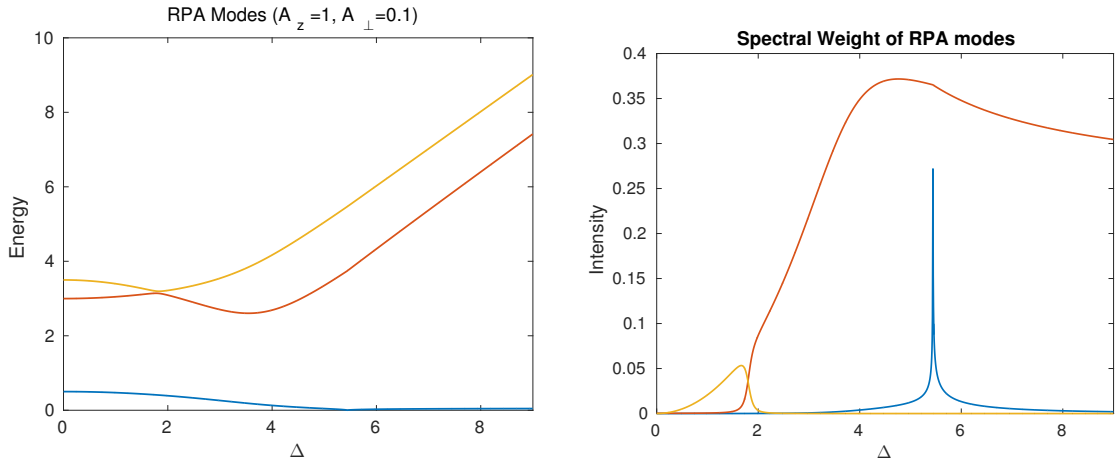

Figure 4.7: The plots above show the RPA modes (left), and their associated spectral weight (right), of the spin half spin half model with an anisotropic hyperfine interaction, calculated from the Green's function, equation (4.74), at zero wavevector $\vec{k} = 0$. We work in units of J, the strength of the exchange coupling between spins. Here, the longitudinal hypefine interaction has the same strength as the exchange interaction, and the transverse hyperfine interaction is a factor of ten smaller. We see the lower mode softens to zero in a quantum phase transition and the associated spectral weight diverges. The middle mode carries most of the spectral weight throughout the rest of the diagram, except in weak transverse fields where the upper mode may carry some of the spectral weight.

In general, the RPA modes of the system are obtained by factoring the denominator of (4.74) numerically. However, in the paramagnetic phase of the system the matrix element $c_{13} = \langle 1|\tau^z|3\rangle$ is zero; hence, there is a common factor of $E_{31}^2 - (i\omega_n)^2$ in the numerator and denominator. This MF mode carries no spectral weight. The remaining equation is quadratic and may be solved analytically. After removing the common factor, the RPA Green's function (4.74) becomes

$$\begin{aligned} G(k,z) &= \frac{|c_{12}|^2 2E_{21}(E_{41}^2 - z^2) + |c_{14}|^2 2E_{41}(E_{21}^2 - z^2)}{V_k[|c_{12}|^2 2E_{21}(E_{41}^2 - z^2) + |c_{14}|^2 2E_{41}(E_{21}^2 - z^2)] - (E_{21}^2 - z^2)(E_{41}^2 - z^2)} \\ &= \frac{az^2 - \chi_0^{zz}}{bz^4 + cz^2 + (1 - V_k\chi_0^{zz})}, \end{aligned} \tag{4.75}$$

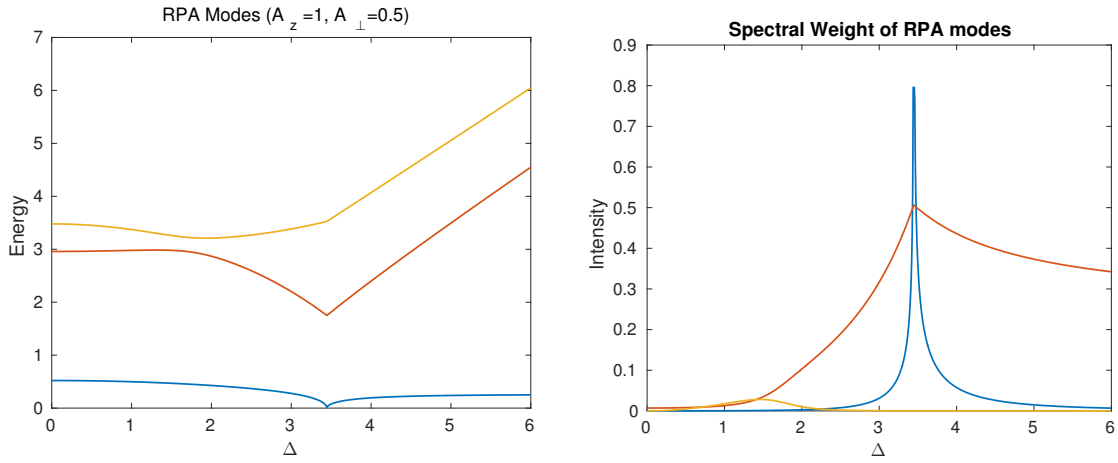

Figure 4.8: The plots above show the RPA modes (left), and their associated spectral weight (right), of the spin half spin half model with an anisotropic hyperfine interaction, calculated from the Green's function, equation (4.74), at zero wavevector $\vec{k} = 0$. We work in units of J, the strength of the exchange coupling between spins. Here, the longitudinal hypefine interaction has the same strength as the exchange interaction, and the transverse hyperfine interaction is a factor of two smaller. We see the lower mode softens to zero in a quantum phase transition and the associated spectral weight diverges. The middle mode carries most of the spectral weight throughout the rest of the diagram, except in weak transverse fields where the upper mode may carry some of the spectral weight.

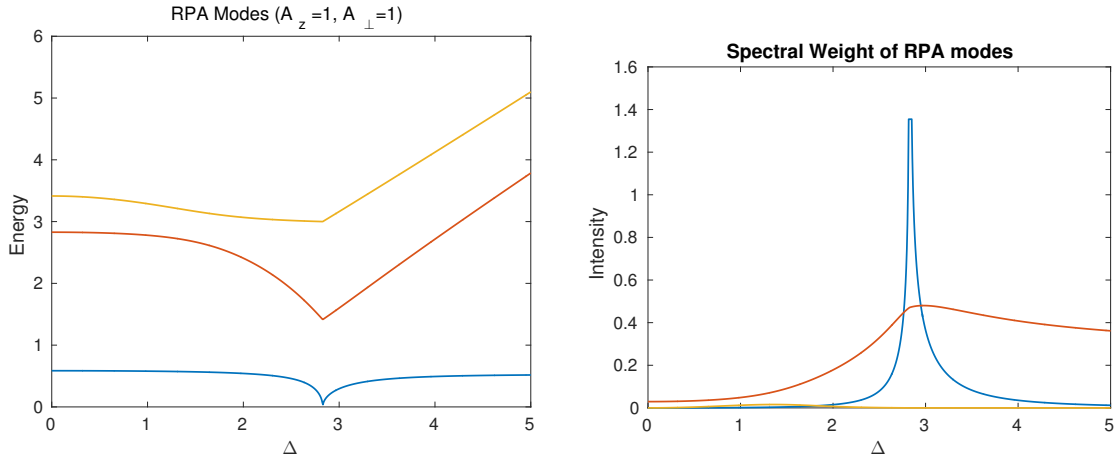

Figure 4.9: The plots above show the RPA modes (left), and their associated spectral weight (right), of the spin half spin spin half model with an anisotropic hyperfine interaction, calculated from the Green's function, equation (4.74), at zero wavevector $\vec{k} = 0$. We work in units of J, the strength of the exchange coupling between spins. We take the strength of the hyperfine interaction to be the same as the strength of the exchange interaction. We see the lower mode softens to zero in a quantum phase transition and the associated spectral weight diverges. The middle mode carries most of the spectral weight throughout the rest of the diagram.

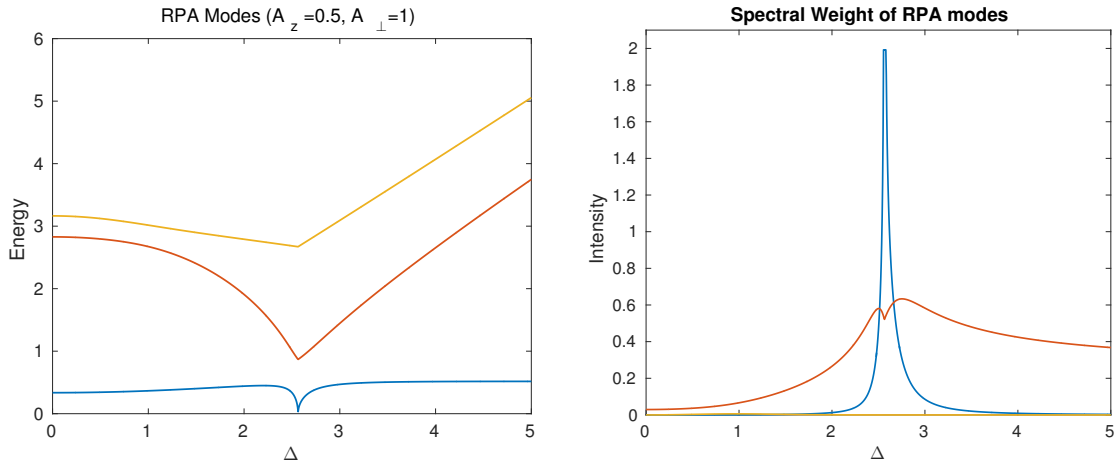

Figure 4.10: The plots above show the RPA modes (left), and their associated spectral weight (right), of the spin half spin spin half model with an anisotropic hyperfine interaction, calculated from the Green's function, equation (4.74), at zero wavevector $\vec{k} = 0$. We work in units of J, the strength of the exchange coupling between spins. Here, the transverse hypefine interaction has the same strength as the exchange interaction, and the longitudinal hyperfine interaction is a factor of two smaller. We see the lower mode softens to zero in a quantum phase transition and the associated spectral weight diverges. The middle mode carries most of the spectral weight throughout the rest of the diagram.

where χ_0^{zz} is given in equation (4.58), and

$$a = \frac{2|c_{12}|^2}{E_{21}E_{41}^2} + \frac{2|c_{14}|^2}{E_{21}^2E_{41}} \approx \frac{2}{A_\perp^2\Delta}\left[1 - \frac{2A_z + A_\perp}{2\Delta} + \frac{A_zA_\perp}{2\Delta^2} - \frac{2A_z^2 + A_\perp^2}{2\Delta^2} + O\left(\frac{A_{z,\perp}^3}{\Delta^3}\right)\right] \tag{4.76}$$

$$b = \frac{1}{E_{21}^2E_{41}^2} \approx \frac{4}{A_\perp^2\Delta^2}\left[1 - \frac{A_z + A_\perp}{\Delta} + \frac{A_zA_\perp}{\Delta^2} - \frac{3(A_z^2 + A_\perp^2)}{8\Delta^2} + O\left(\frac{A_{z,\perp}^3}{\Delta^3}\right)\right]$$

$$c = V_k\alpha - \frac{1}{E_{21}^2} - \frac{1}{E_{41}^2}$$

$$\approx -\frac{4}{A_\perp^2}\left[1 - \frac{A_z}{\Delta} - \frac{A_z^2 - A_\perp^2}{4\Delta^2} - \frac{V_k}{2\Delta}\left(1 - \frac{2A_z + A_\perp}{2\Delta} + \frac{A_zA_\perp}{2\Delta^2} - \frac{2A_z^2 + A_\perp^2}{2\Delta^2}\right) + O\left(\frac{A_{z,\perp}^3}{\Delta^3}\right)\right].$$

Solving the quadratic equation obtained by setting the denominator of equation (4.75) to zero, we find the lowest energy RPA mode in Figures 4.7 - 4.13, in the paramagnetic phase of the system, to be given by

$$E_k^1 = \frac{A_\perp}{2}\sqrt{\frac{1 - V_k\chi_0^{zz}}{1 - \frac{V_k}{2\Delta}}} + O\left(\frac{A_{z,\perp}}{\Delta}\right). \tag{4.77}$$

We see that this mode softens to zero at the critical field given by equation (4.62), and vanishes

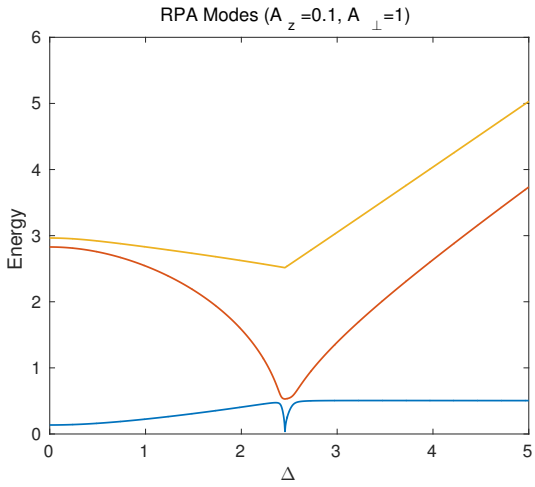

Figure 4.11: RPA Modes

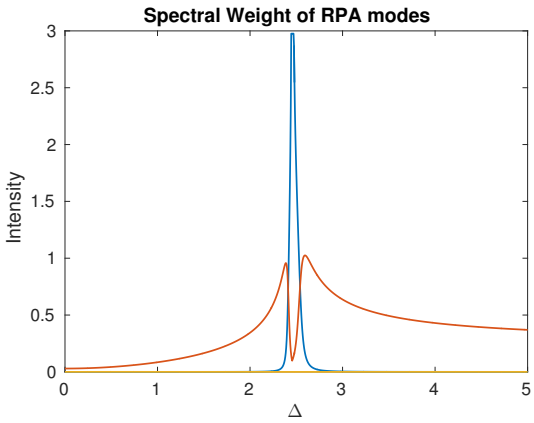

Figure 4.12: Spectral Weight

Figure 4.13: The plots above show the RPA modes (left), and their associated spectral weight (right), of the spin half spin spin half model with an anisotropic hyperfine interaction, calculated from the Green's function, equation (4.74), at zero wavevector $\vec{k} = 0$. We work in units of J, the strength of the exchange coupling between spins. Here, the transverse hypefine interaction has the same strength as the exchange interaction, and the longitudinal hyperfine interaction is a factor of ten smaller. The RPA modes and their spectral weight are colour coordinated. We see the lower mode softens to zero in a quantum phase transition and the associated spectral weight diverges. The middle mode carries most of the spectral weight throughout the rest of the diagram.

altogether in the absence of the transverse hyperfine interaction. The second RPA mode is given by

$$E_k^2 = \Delta\left[1 + \frac{A_\perp}{\Delta} - \frac{V_k}{2\Delta}\left(1 + \frac{A_\perp}{\Delta}\right) + O\left(\frac{A_{z,\perp}^2}{\Delta^2}\right)\right]^{\frac{1}{2}}. \tag{4.78}$$

In the absence of the hyperfine interaction, we recover the RPA mode of the spin half transverse Ising model, given in equation (B.20) of Appendix B, in which case this mode will soften to zero at $\Delta = \frac{V_0}{2}$. With the nuclear spins present, this mode remains gapped at the critical field given by equation (4.62).

We now make use of our perturbation theory results in Section 4.1 to analyze the low energy excitation of the system, in the ferromagnetic phase, near the quantum phase transition. We

expand $-g(i\omega_n) = A + B(i\omega_n)^2$ in the low frequency, low temperature, limit to obtain

$$\begin{aligned} A &= \frac{2c_{12}^2}{E_{21}} + \frac{2c_{13}^2}{E_{31}} + \frac{2c_{14}^2}{E_{41}} \\ B &= \frac{2c_{12}^2}{E_{21}^3} + \frac{2c_{13}^2}{E_{31}^3} + \frac{2c_{14}^2}{E_{41}^3}. \end{aligned} \tag{4.79}$$

Note these expressions contain matrix elements between the first and third MF eigenstates, absent in the paramagnetic phase of the system. The matrix elements, and the differences between the low energy eigenstates, are given by (to leading order in $\frac{H,A_z,A_\perp}{\Delta}$)

$$\begin{aligned} c_{12} &\approx c_{12}^0\left[1 - \frac{H^2}{4\Delta^2}\left(1 + 2\frac{A_z^2}{A_\perp^2}\right)\right] & E_{21} &\approx E_{21}^0\left[1 + \frac{H^2}{2\Delta^2}\frac{A_z^2}{A_\perp^2}\right] \\ c_{13} &\approx \frac{HA_z}{4\Delta^2} & E_{31} &\approx E_{31}^0\left[1 + \frac{H^2}{2\Delta^2}\right] \\ c_{14} &\approx c_{14}^0\left[1 - \frac{H^2}{4\Delta^2}\left(1 - \frac{A_z^2}{A_\perp^2}\right)\right] & E_{41} &\approx E_{41}^0\left[1 + \frac{H^2}{2\Delta^2}\left(1 + \frac{A_z^2}{4A_\perp\Delta}\right)\right] \end{aligned} \tag{4.80}$$

The superscript zero is to indicate that these are the energy differences and the matrix elements of the system in the absence of any longitudinal field. The E_{ji}^0s and c_{ij}^0s are given in equations (4.7) and (4.11), respectively. The corrections above are calculated using the first order perturbative corrections to the wave functions.

As in the paramagnetic phase, the low frequency spectrum of the system is given by

$$\omega_k = \sqrt{\frac{A}{B}}\sqrt{1 - V_k A}. \tag{4.81}$$

However, A and B are now given by equation (4.79), and we have $A = \chi_0^{zz}(H)$ given in equation (4.71). We now consider the gap in the spectrum at zero wavevector. At the critical field, defined by $V_{k=0}\chi_0^{zz}(H=0) = 1$, the expression above reduces to

$$\omega_0 = \sqrt{\frac{3}{2V_0 B|_{H=0}}}\frac{H_+}{\Delta_c}, \tag{4.82}$$

where we keep only terms linear in H. Recall from equation (4.72) that H_+ is the longitudinal field enhanced by an anisotropic hyperfine interaction. In the absence of the nuclear spins, the gap in the spectrum due to an applied longitudinal field at Δ_c is given by $\omega_0 = \sqrt{\frac{3}{2}}H$. This mode in the transverse field Ising model corresponds to the middle mode in Figures 4.7 - 4.13 of the SHSH model. When we include the hyperfine interaction there is a lower energy

electronuclear mode that softens to zero. It is the gap in this mode due to a longitudinal field that is given in equation (4.82). Expanding in the limit $A_z, A_\perp \ll 1$, we find

$$B|_{H=0} = \frac{A_z^2}{\Delta^2 A_\perp^3}\left[1 + \frac{1}{2\Delta}\frac{A_\perp^3}{A_z^2}\right] + O\left(\frac{A_{z,\perp}}{\Delta}\right). \tag{4.83}$$

In the limit $A_z, A_\perp \ll \Delta$, we find the gap in the spectrum at the critical field to be given by

$$\omega_0 \approx H_+ \sqrt{\frac{3A_\perp^3}{2A_z^2 V_0}\left[1 - \frac{A_\perp^3}{2\Delta_c A_z^2}\right]} + O\left(\frac{H^2}{\Delta_c^2}\right). \tag{4.84}$$

We see that the gap in the spectrum between the ground state and the lowest electronuclear level varies linearly with our enhanced field H_+, and the rate at which the gap opens depends on the nuclear spins. In the limit $A_z, A_\perp \to 0$, this mode vanishes and it is the middle mode in Figures 4.7 - 4.13 that will soften to zero at the quantum critical point.

Summary

In this chapter, we introduced the spin half spin half model (SHSH)

$$\mathscr{H} = -\frac{J}{2}\sum_{i\neq j} V_{ij} S_i^z S_j^z - \Delta \sum_i S_i^x + A_z \sum_i I_i^z S_i^z + \frac{A_\perp}{2}\sum_i (I_i^+ S_i^- + I_i^- S_i^+). \tag{4.85}$$

This relatively simple model demonstrates the effects of the hyperfine interaction on the transverse field Ising model, and, with the inclusion of a transverse field acting on the nuclear spins, may be used to illustrate many of the qualitative features of the magnetic material $LiHoF_4$. The single ion Hamiltonian of the SHSH model can be diagonalized exactly in the paramagnetic phase of the system. We began by doing so, and gave the electronic and nuclear spin operators in this basis. In Section 4.1, we introduced a longitudinal field to the system and gave second order perturbation theory results suitable for analyzing the system in the vicinity of its quantum critical point.

In Sections 4.2 and 4.3, we illustrated the electronic and nuclear magnetizations of the system in the MF approximation. We proceeded to use our perturbation theory results to give analytic expressions for the magnetizations in the presence of a longitudinal field, and showed the longitudinal susceptibility of the system is enhanced or suppressed by an anisotropic hyperfine interaction.

After exploring the MF results, we turned to the longitudinal electronic Green's function of the SHSH model in Section 4.4. Treating the Green's function in the RPA, we derived the low energy paramagnetic spectrum and the critical value of the transverse field. We then used perturbation theory to analyze the susceptibility of the system, and we found that both the single ion susceptibility, and the longitudinal field itself, are enhanced by an anisotropic hyperfine interaction with a dominant longitudinal component.

Finally, in Section 4.5, we calculated all the RPA modes of the SHSH model, and their associated spectral weight, by factoring the RPA Green's function numerically. We saw that what would have been the soft mode in the absence of the nuclear spins is now gapped. This mode carries most of the spectral weight except near the transition, where the spectral weight is transferred to a lower energy mode that softens completely at the critical transverse field. This is the primary result of this chapter. We closed the chapter by making use of the basis of paramagnetic eigenstates to derive analytic expressions for the RPA modes.

Chapter 5

LiHoF4 in the Random Phase Approximation

In this chapter, we analyze the longitudinal electronic correlation function of $LiHoF_4$ in the random phase approximation (RPA), making use of the effective low temperature Hamiltonian derived in Section 2.2. The techniques developed in this thesis, and presented in Chapter 4 for the simpler spin half spin half model, make such an analysis straightforward. The low energy excitations in $LiHoF_4$ have been measured via neutron scattering experiments by Rønnow *et al.* in [36]. Their data shows that the expected soft mode at the system's critical point is gapped. This result was subsequently analyzed using a numerical approximation that includes the leading order corrections to the RPA in a high density approximation, that is, an expansion in the inverse coordination number of the system, in [67]. The numerical calculation shows the gap in the crystal field spectrum caused by the hyperfine interaction, but their is no discussion of the other excitation modes of the system and their associated spectral weight. Most importantly, although there is a brief mention of a lower energy electronuclear mode that softens to zero at the quantum critical point, there is no discussion of this mode. In this chapter, we calculate the low energy mode that softens to zero, and we calculate the transfer of spectral weight from the gapped mode to the low energy mode that occurs near the phase transition. A previous RPA analysis has been carried out on a toy model for $LiHoF_4$ in a transverse field by Banerjee and Dattagupta in [94]. Their work includes only a longitudinal hyperfine interaction, and fails to capture the full complexity $LiHoF_4$. Most importantly, they neglect the effect of the transverse field acting directly on the nuclear spins due to a shift in the electronic cloud of each holmium ion's $4f$ electronic cloud caused by an applied transverse magnetic field, and the mixing of the nuclear spins by the transverse component of the hyperfine interaction. These effects are crucial in the vicinity of the quantum critical point, as the phase transition is dependent on the mobility of the nuclear spins. The low temperature effective Hamiltonian used here does not

suffer from these shortcomings.

We begin by self consistently solving for the expectation value of the τ^z operator in the mean field (MF) Hamiltonian, $H_{MF} = \sum_i H^i_{MF}$, where

$$H^i_{MF} = -\frac{\Delta}{2}\tau^x_i - V_0\langle\tau^z\rangle\tau^z_i + \vec{\Delta}_n \cdot \vec{I}_i + A_z\tau^z_i I^z_i + \\ + A_\perp \tau^+_i I^-_i + A^\dagger_\perp \tau^-_i I^+_i + A_{++}\tau^+_i I^+_i + A^\dagger_{++}\tau^-_i I^-_i, \tag{5.1}$$

with

$$V_0 = C^2_{zz}\left[J_D \sum_j D^{zz}_{ij} - 4J_{nn}\right]. \tag{5.2}$$

Recall, that the exchange interaction involves a sum over each holmium ion's four nearest neighbours, and in the two by two low energy subspace $J^z = C_{zz}\tau_z$. We assume a long thin cylindrical sample, consistent with the domain structure of $LiHoF_4$ near its phase transition as discussed in Section 2.1.3, in which case $a^3 D^{zz}_0 = a^3 \sum_j D^{zz}_{ij} = 11.272$, where $a = 5.175$Å is the transverse lattice spacing. The strength of the dipolar interaction is $\frac{J_D}{a^3} = 7mK$, and the strength of the antiferromagnetic exchange interaction is $J_{nn} = 1.2mK$. We see from this that at zero wave vector the strength of the dipolar interaction is more than 16 times that of the exchange interaction. The transverse fields, Δ and Δ_n, and the hyperfine couplings, A_z, $A_\perp$ and A_{++}, are functions of the physical transverse field B_x. All these energies are given in Section 2.2.

In Figure 5.1, we plot the energy levels of the MF Hamiltonian as a function of the physical transverse magnetic field B_x. The upper and lower sets of energy levels correspond to an electronic spin in line with the MF of the system, and an electronic spin opposed to the MF of the system, respectively. The two clusters of energy levels in Figure 5.1 stem from the lower two electronic crystal field excitations plotted in Figure 2.3 of Chapter 2. Each of these electronic energy levels is split into eight electronuclear levels by the hyperfine interaction, separated by $A_z \approx 200mK$. In Figure 5.2, we plot the transverse and longitudinal electronic magnetization, $\langle J^z\rangle = C_{zz}\langle\tau^z\rangle$ and $\langle J^x\rangle = C_x + \sum_{\nu=x,y,z} C_{x\nu}\langle\tau^\nu\rangle$, along with the transverse and longitudinal nuclear spin magnetization. Note that at the phase transition, the transverse nuclear magnetization nearly saturates at $\langle I^x\rangle = \frac{7}{2}$, whereas the transverse electronic magnetization, strongly effected by the crystal field, is far from its saturation value of $\langle J^x\rangle = 8$.

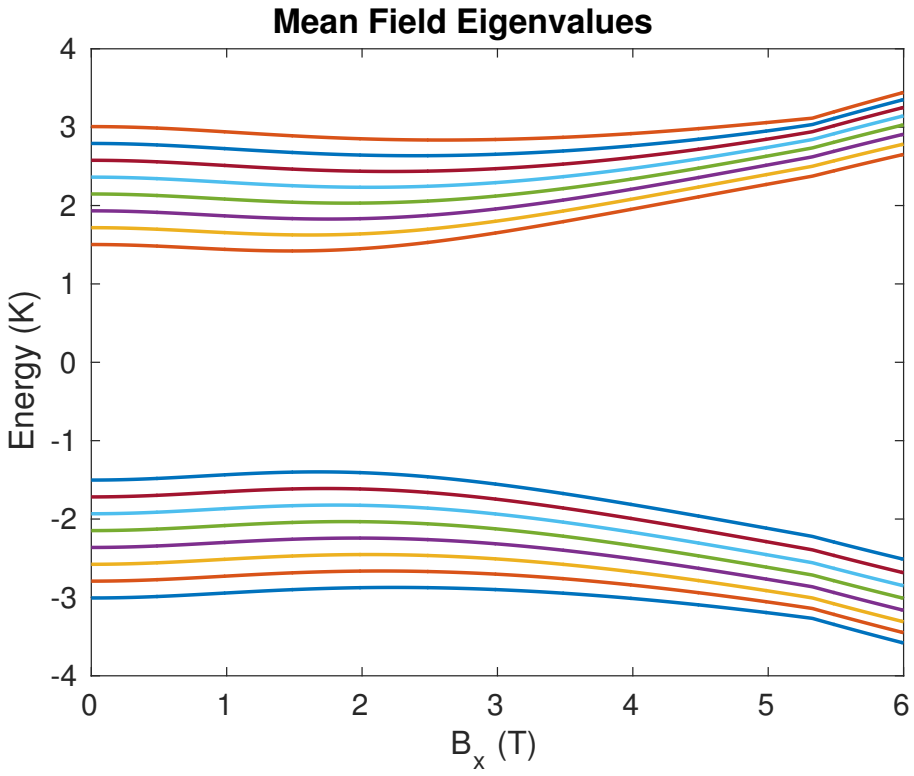

Figure 5.1: The plot above shows the energy levels of the effective low temperature mean field Hamiltonian of $LiHoF_4$, given in equation (5.1), as a function of the physical transverse magnetic field, B_x. We consider a long thin cylindrical, or needle shaped, sample.

Electronic Spectrum

In this section, we calculate the connected imaginary time ordered longitudinal electronic spin correlation function (Green's function for short)

$$G_k(\tau) = -\langle T_\tau \widetilde{J}^z_k(\tau)\widetilde{J}^z_{-k}(0)\rangle = -C^2_{zz}(B_x)\langle T_\tau \widetilde{\tau}^z_k(\tau)\widetilde{\tau}^z_{-k}(0)\rangle, \tag{5.3}$$

where $\widetilde{J}^z = J^z - \langle J^z\rangle = C_{zz}(\tau^z - \langle\tau^z\rangle)$, in order to determine the excitation spectrum of the $LiHoF_4$ system. This function is relevant to the neutron scattering experiments of Rønnow *et al.* [36], with the spectral weight of each excitation mode corresponding to the intensity of scattered neutrons. The electronic spin operator τ^z is given by

$$\tau^z = \begin{bmatrix} 1 & 0 \\ 0 & -1 \end{bmatrix} \otimes I_8, \tag{5.4}$$

where I_8 is the eight by eight identity matrix corresponding to the nuclear subspace. We mention this to remind the reader we are dealing with the sixteen lowest electronuclear levels of

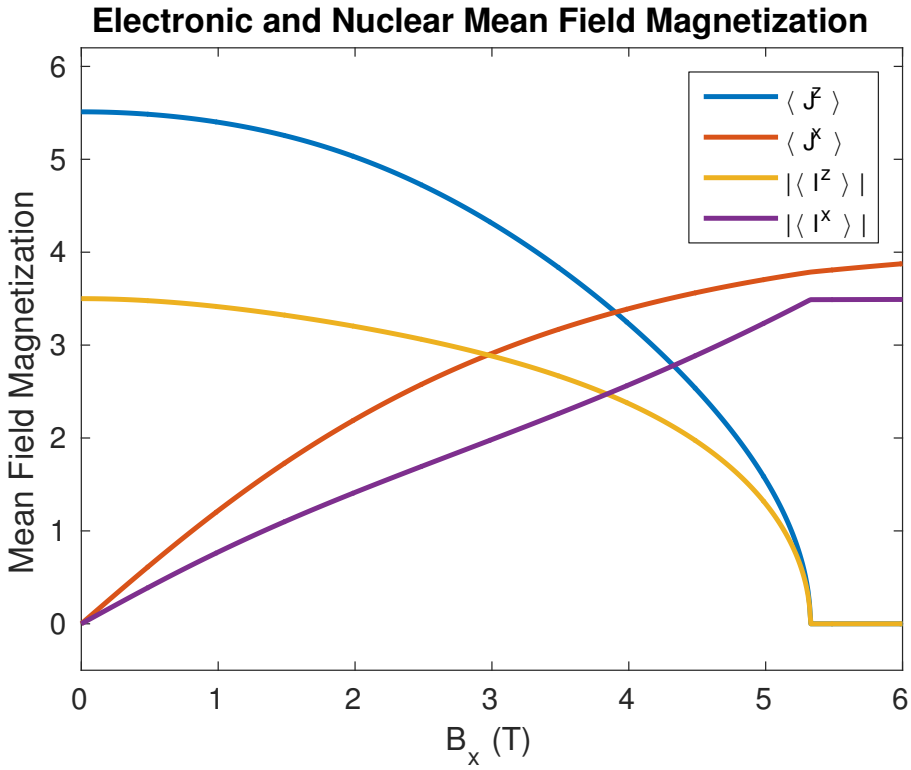

Figure 5.2: The plot above shows the transverse and longitudinal electronic ($\langle J^x \rangle$ and $\langle J^z \rangle$), and nuclear ($|\langle I^x \rangle|$ and $|\langle I^z \rangle|$), magnetizations of $LiHoF_4$. The magnetizations are calculated self consistently from the mean field Hamiltonian given in equation (5.1). We consider a long thin cylindrical, or needle shaped, sample. We see the nuclear magnetizations, $|\langle I^x \rangle|$ and $|\langle I^z \rangle|$, saturate near the quantum phase transition and in the zero field limit, respectively. The electronic magnetizations, $\langle J^x \rangle$ and $\langle J^z \rangle$, fail to saturate due to the disordering effect of the crystal field.

the Hamiltonian. Transforming to frequency space, in the random phase approximation (RPA), the Green's function is given by

$$G_k^{RPA}(i\omega_n) = \frac{C_{zz}^2 g(i\omega_n)}{1 + V_k g(i\omega_n)}, \tag{5.5}$$

where the unperturbed propagator is given by

$$g(\tau) = -\langle T_\tau \widetilde{\tau}^z(\tau)\widetilde{\tau}^z(0)\rangle_0, \tag{5.6}$$

and the subscript 0 denotes the average is to be taken with respect to the MF Hamiltonian. In what follows, we will drop the superscript RPA from the Green's function, as it is to be understood that we are working in the RPA throughout this chapter.

The interaction is given by $V_k = C_{zz}^2[J_D D_k^{zz} - J_{nn}\gamma_k]$. Note that D_k^{zz} is the Fourier transform

of the dipolar interaction, discussed in Chapter 3, and

$$\gamma_k = 2\mathrm{Re}\left[\cos\left(\frac{k_x a}{2}\right)e^{-\frac{ik_z c}{4}} + \cos\left(\frac{k_y a}{2}\right)e^{\frac{ik_z c}{4}}\right] = 2\cos\left(\frac{k_z c}{4}\right)\left[\cos\left(\frac{k_x a}{2}\right) + \cos\left(\frac{k_y a}{2}\right)\right] \tag{5.7}$$

is the Fourier transform of the exchange interaction taking into account the four nearest neighbour atoms at $(\pm\frac{a}{2}, 0, -\frac{c}{4})$ and $(0, \pm\frac{a}{2}, \frac{c}{4})$. We take only the real part of V_k, as the imaginary part vanishes from the Hamiltonian upon summation.

In terms of the MF eigenstates, we define $c_{ij} = \langle i|\tau^z|j\rangle_0$ to be the MF matrix elements of the τ^z operator, $E_{ji} = E_j - E_i$ to be the difference between the ith and jth energy levels, and the population factor to be $D_{ij} = D_i - D_j$, where $D_i = \frac{e^{-\beta E_i}}{Z_0}$ and Z_0 is the MF partition function. In terms of these parameters, the unperturbed propagator is given by $g(i\omega_n) = \sum_{i<j} g_{ij}(i\omega_n) + g_{el}\delta_{i\omega_n,0}$, where

$$g_{ij}(i\omega_n \neq 0) = -|c_{ij}|^2 D_{ij}\frac{2E_{ji}}{E_{ji}^2 - (i\omega_n)^2}. \tag{5.8}$$

We will drop the elastic contribution to the unperturbed propagator g_{el} that arises in the ordered phase of the system ($\langle\tau^z\rangle \neq 0$) at finite temperatures. This term is discussed in Appendix D. It vanishes in the limit $T \to 0$, and will not effect the calculation of the inelastic spectrum. In the limit $T \to 0$, we find only the lowest eigenstate is populated, hence our unperturbed propagator becomes

$$-g(i\omega_n)\Big|_{T=0} = \sum_{j>1}|c_{1j}|^2\frac{2E_{j1}}{E_{j1}^2 - (i\omega_n)^2} \approx \chi_0^{zz} + \chi_2^{zz}(i\omega_n)^2, \tag{5.9}$$

where

$$\chi_0^{zz} = \sum_{j>1}\frac{2|c_{1j}|^2}{E_{j1}} \qquad\qquad \chi_2^{zz} = \sum_{j>1}\frac{2|c_{1j}|^2}{E_{j1}^3}. \tag{5.10}$$

We expect this expansion to be valid for frequencies much less than the minimum gap in the MF spectrum, $|\omega| \ll min\{E_{21}(\Delta)\} = E_{21}(\Delta_c) \approx 80mK$. Note that χ_0^{zz} is simply the electronic component of the static single ion longitudinal susceptibility of the effective low temperature Hamiltonian given in equation (5.1) in the MF approximation. For $LiHoF_4$, we have $\chi_0^{zz}|_{liho} = C_{zz}^2\chi_0^{zz}$.

Using the identity

$$\lim_{\varepsilon\to 0^+}\frac{1}{x\pm i\varepsilon}=\mathscr{P}\big(\frac{1}{x}\big)\mp i\pi\delta(x) \tag{5.11}$$

we may rewrite the unperturbed propagator as

$$-g(i\omega_n\to\omega+i0^+)\Big|_{T=0}=\sum_{j>1}|c_{1j}|^2\left(2\mathscr{P}\big(\frac{1}{E_{j1}}\big)+i\pi\Big[\delta(E_{j1}-\omega)-\delta(E_{j1}+\omega)\Big]\right). \tag{5.12}$$

The spectral weight carried by each MF excitation is proportional to the square of the associated matrix element.

In Figure 5.3, we plot the matrix elements of the electronic spin operator $c_{1j}=\langle 1|\tau^z|j\rangle$ between the ground state and the excited states. We see that the mixing of the lower MF eigenstates is orders of magnitude smaller than the mixing of the upper eigenstates, with the exception of the mixing of the ground state with the first excited state. This matrix element is included as a dashed line with the upper matrix elements. A rough argument can be made explaining why matrix elements between the lower eigenstates are small. As the transverse magnetic field is increased, the electronic spin rolls over in the magnetic field, that is, $\langle\vec{\tau}\rangle=\langle\tau^z\rangle\to\langle\vec{\tau}\rangle=\langle\tau^z\rangle+\langle\tau^x\rangle$, with the τ^x component of the ground state becoming increasingly large with the applied transverse field B_x. Application of the τ^z operator to the ground state flips the x component of the electronic spin. When this is projected onto one of the lower MF eigenstates there is little overlap, leading to a small matrix element, whereas when it is projected onto one of the upper eigenstates, which have a τ^x component predominantly opposite the applied field, there will be significant overlap.

Plugging the expression for the unperturbed propagator back into the RPA Green's function, we find

$$G(k,i\omega_n)=\frac{1}{\frac{1}{g}+V_k}=\frac{-C_{zz}^2(\chi_0^{zz})^2}{\chi_2^{zz}[\frac{\chi_0^{zz}}{\chi_2^{zz}}-(i\omega_n)^2-\frac{V_k(\chi_0^{zz})^2}{\chi_2^{zz}}]}, \tag{5.13}$$

and the lowest energy mode of the longitudinal electronic spectrum is given by

$$\omega_k=\sqrt{\frac{\chi_0^{zz}}{\chi_2^{zz}}}\sqrt{1-V_k\chi_0^{zz}}. \tag{5.14}$$

The spectrum softens to zero at a critical field defined implicitly by $1=V_k\chi_0^{zz}$. In Figure 5.4, we plot the static ($k=0$) longitudinal RPA susceptibility of $LiHoF_4$, along with the minimum energy gap in the excitation spectrum at zero wavevector, in the vicinity of the quantum critical

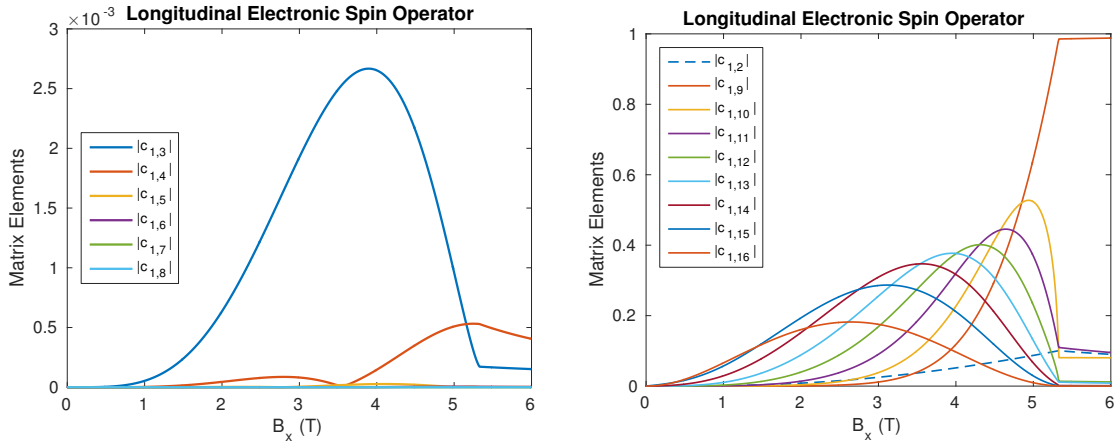

Figure 5.3: The plots above show the matrix elements of the electronic spin operator τ^z, with $c_{ij} = \langle i|\tau^z|j\rangle$, for the low temperature effective Hamiltonian for $LiHoF_4$, given in equation (5.1), in the MF basis. We plot the matrix elements as a function of the physical transverse field B_x (in Tesla). Note the scale of the vertical axis in the plot to the left is three orders of magnitude smaller than that of the plot to the right.

point. We see that the susceptibility diverges, and the gap softens all the way to zero, at the quantum critical point. Note that the susceptibility shown in Figure 5.4 is the susceptibility in a long thin cylindrical sample consisting of a single domain. As discussed in Section 2.1.3, in a sample consisting of multiple domains the susceptibility in the ferromagnetic phase is constant, and is dominated by the motion of the highly mobile domain walls.

The excitation mode given in equation (5.14) is the lowest energy mode of the RPA spectrum in the vicinity of the quantum critical point. The other modes of the spectrum may be found numerically by looking at the zeros of $C_{zz}^2 G^{-1} = \frac{1}{g} + V_k$, where g is the unperturbed propagator given in equation (5.9). At $T = 0$ the unperturbed propagator has poles located at the energy difference between the ground state and each excited state of the MF Hamiltonian. The effect of the interaction is to shift the location of these poles. Explicitly, we find

$$C_{zz}^{-2} G(k, i\omega_n) = \frac{\sum_{j=2}^{16} |c_{1j}|^2 2E_{j1} \prod_{s\neq j}(E_{s1}^2 - (i\omega_n)^2)}{V_k \sum_{j=2}^{16} |c_{1j}|^2 2E_{j1} \prod_{s\neq j}(E_{s1}^2 - (i\omega_n)^2) - \prod_{j=2}^{16}(E_{j1}^2 - (i\omega_n)^2)}. \tag{5.15}$$

The poles of the Green's function are given by the zeros of the polynomial in the denominator of (5.15). Numerically, finding the poles can be quite time consuming because near a pole $g \sim \frac{\alpha_i}{E_{i1}^2 - \omega^2}$, and, if $\alpha_i = 2|c_{1i}|^2 E_{i1}$ is small, a very fine frequency scan must be made in order to see the divergence. It is much faster to consider the denominator of equation (5.15) as a continuous function of frequency ($i\omega_n \to z$) and find the zeros of the polynomial. Points where $|c_{1j}|^2$ vanish correspond to points where a pole in the RPA Green's function carries no spectral weight. We see this by noting that if a factor of $|c_{1j}|^2$ is zero then there is a common factor

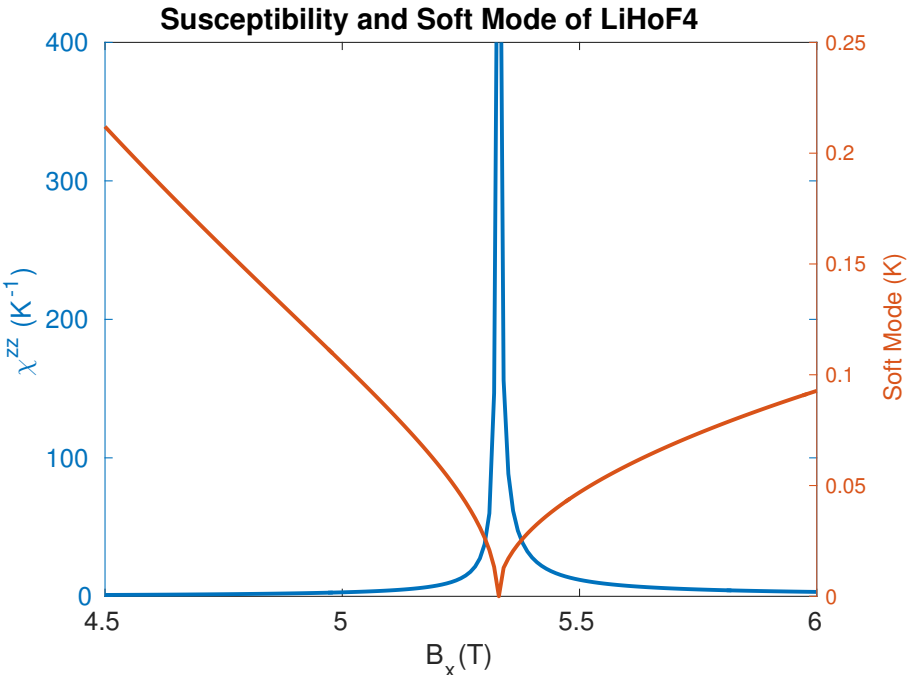

Figure 5.4: The plot above shows the zero wavevector longitudinal susceptibility of $LiHoF_4$ in the random phase approximation, along with the lowest energy mode (at zero wavevector, $k = 0$) in the electronic (RPA) spectrum, as a function of the applied transverse magnetic field B_x (in Tesla). We consider a long thin cylindrical sample. We see that the susceptibility diverges, and the lowest energy mode softens all the way to zero, at the quantum critical point.

of $E_{j1}^2 - (i\omega_n)^2$ in both the numerator and denominator that cancels reducing the degree of the polynomial. Setting $t = z^2 = (i\omega_n)^2$, we find the zeros of the polynomial

$$Q(t) = V_k \sum_{j=2}^{16} |c_{1j}|^2 2E_{j1} \prod_{s\neq j} (E_{s1}^2 - t) - \prod_{j=2}^{16} (E_{j1}^2 - t). \tag{5.16}$$

In Figure 5.5, we plot the full RPA spectrum at zero wavevector ($k = 0$) as a function of transverse magnetic field. At zero field, we see the upper and lower bands, corresponding to electronic spin up and electronic spin down, respectively, split into clusters of eight by the inclusion of the nuclear degrees of freedom. These states are then mixed by the transverse field. In the absence of the nuclear spins, the middle mode that splits off from the group would soften to zero in a quantum phase transition. We see that the mode is gapped by the nuclear spins; however, the lowest energy electronuclear mode softens to zero.

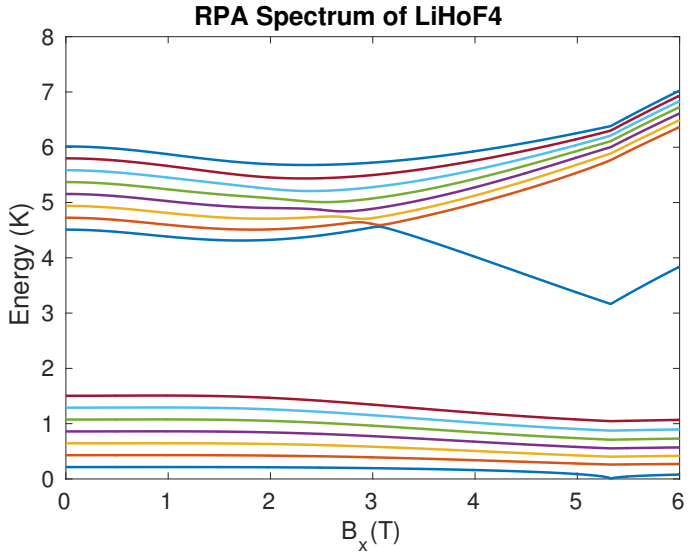

Figure 5.5: The plot above shows the RPA spectrum (in Kelvin) of the low temperature effective Hamiltonian for $LiHoF_4$ given in (5.1), at zero wavevector, as a function of the transverse magnetic field B_x (in Tesla).

We now consider the spectral weight of the RPA modes. We may rewrite the Green's function as

$$C_{zz}^{-2} G_k(z) = \frac{\sum_{j=2}^{16} |c_{1j}|^2 2E_{j1} \prod_{s\neq j}(E_{s1}^2 - z^2)}{\prod_{p=1}^{15}\left[(z-E_k^p)(z+E_k^p)\right]}, \tag{5.17}$$

where E_k^p denotes the p^{th} RPA mode. Note that the Green's function has the form $C_{zz}^{-2} G_k(z) = \frac{P(z)}{Q(z)}$, where $P(z)$ and $Q(z)$ are polynomials. Performing a partial fraction decomposition (assuming no degenerate modes) yields

$$C_{zz}^{-2} G_k(z) = \sum_{p=1}^{15}\left[\frac{P(E_k^p)}{Q'(E_k^p)}\frac{1}{(z-E_k^p)} + \frac{P(-E_k^p)}{Q'(-E_k^p)}\frac{1}{(z+E_k^p)}\right], \tag{5.18}$$

where

$$\begin{aligned} P(E_k^p) = P(-E_k^p) &= \sum_{j=2}^{16} |c_{1j}|^2 2E_{j1} \prod_{s\neq j}\left[E_{s1}^2 - (E_k^p)^2\right] \\ Q'(E_k^p) = -Q'(-E_k^p) &= 2E_k^p \prod_{s\neq p}\left[(E_k^p)^2 - (E_k^s)^2\right]. \end{aligned} \tag{5.19}$$

The spectral density is given by (at $T = 0$)

$$\rho_k(\omega) = -2Im[G_k(\omega + i0^+)] = \frac{2\pi}{N} C_{zz}^2 \sum_p |\langle 0|\tau_k^z|p\rangle|^2 \left[\delta(\omega - E_k^p) - \delta(\omega + E_k^p)\right], \quad (5.20)$$

where $|p\rangle$ denotes a many body RPA eigenstate of the Hamiltonian. Taking the imaginary part of the RPA Green's function, we find that

$$\rho_k(\omega) = 2\pi C_{zz}^2 \sum_{p=1}^{15} \frac{P(E_k^p)}{Q'(E_k^p)} \left[\delta(\omega - E_k^p) - \delta(\omega + E_k^p)\right]. \quad (5.21)$$

In Figures 5.6 and 5.7, we plot the intensities of the RPA modes of the longitudinal Green's function. Figure 5.6 shows the soft mode E_1, along with the upper set of modes E_8 to E_{15}. The modes not shown carry no spectral weight. We see that away from the phase transition, the spectral weight is carried by the upper electronuclear levels, which are plotted in Figure 5.7. In the vicinity of the quantum critical point, the spectral weight is transferred to the lowest electronuclear level. The spectral weight of this mode diverges at the quantum critical point, where the mode softens to zero.

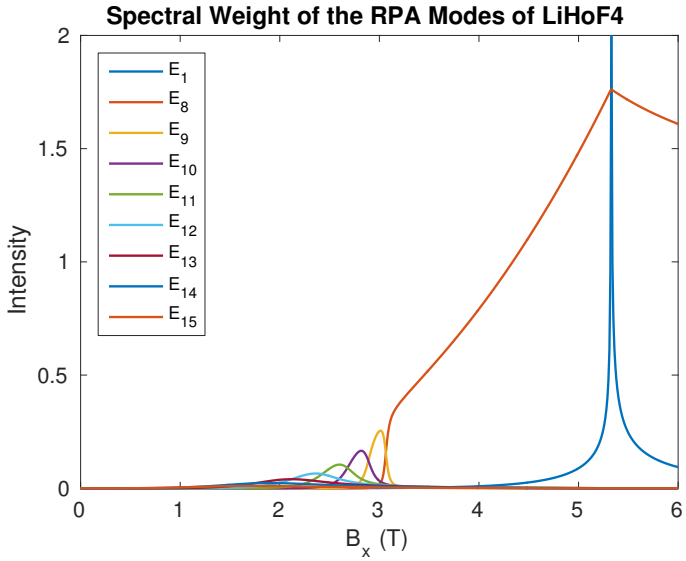

Figure 5.6: The plot above shows the spectral weight of the RPA modes (E_1 and E_8 to E_{15}) of $LiHoF_4$, calculated from the longitudinal Green's function (5.15), at zero momentum $\vec{k} = 0$, as a function of the physical transverse magnetic field field B_x (in Tesla). We see the spectral weight of the lowest energy mode diverges at the quantum critical point. Above $B_x \approx 3T$, most of the spectral weight is carried by E_8, except near the phase transition. The modes not shown in the figure carry no spectral weight.

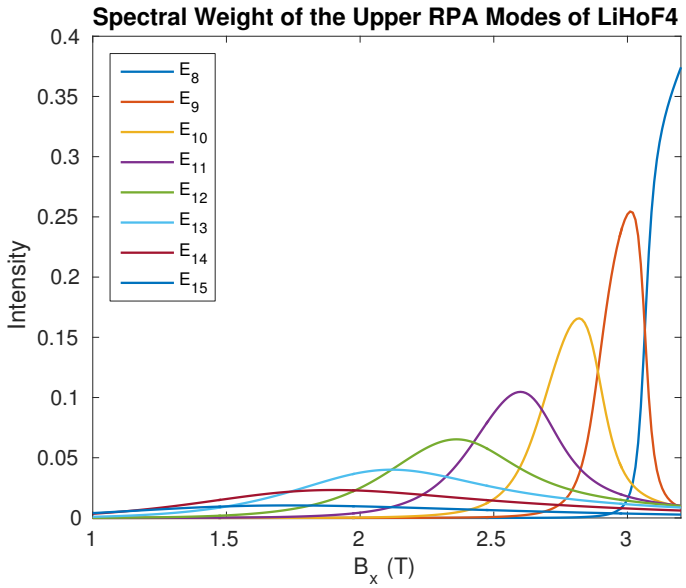

Figure 5.7: The plot above shows the spectral weight of the upper RPA modes (E_8 to E_{15}) of $LiHoF_4$, calculated from the longitudinal Green's function (5.15), at zero momentum $\vec{k} = 0$, as a function of the physical transverse field B_x between $1T$ and $3.5T$. Above $B_x \approx 3T$, E_8 is the dominant mode. The peaks in the intensities, in order of decreasing amplitudes, correspond to E_9, E_{10}, ..., E_{15}.

In addition to considering the RPA modes as a function of transverse field, we may examine how they vary in momentum space. We do so by tracing out the triangle $[0,0,0] \rightarrow [\frac{\pi}{a},0,0] \rightarrow [\frac{\pi}{a},0,\frac{\pi}{c}] \rightarrow [0,0,0]$, at the critical MF, $\Delta_c^0 = 5.33T$. At zero momentum, the spectral weight of the lowest mode diverges. As we vary the momentum, the weight carried by this mode decays, and it is the upper electronic mode that carries the spectral weight. Note that the eighth RPA mode, which carries the spectral weight away from $k = 0$, varies extremely rapidly as $|\vec{k}| \rightarrow 0$. This is a result of the shape dependence of the dipole-wave sum near $|\vec{k}| = 0$.

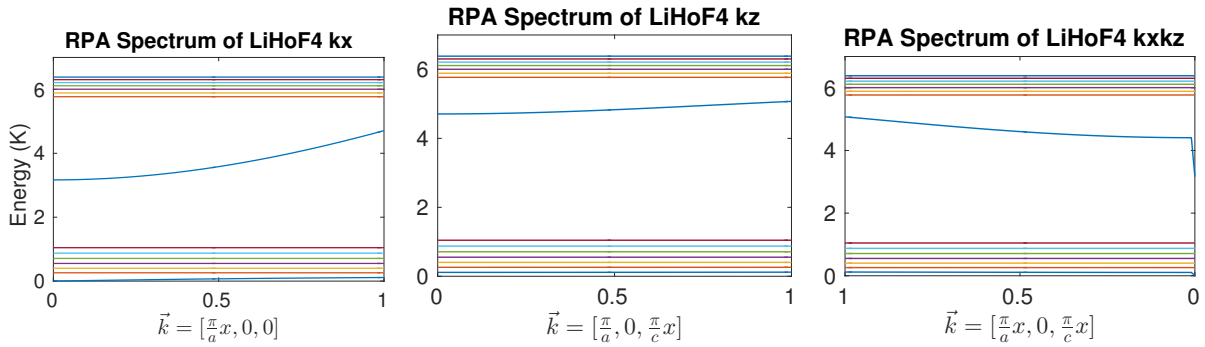

Figure 5.8: The plot above shows the RPA spectrum of $LiHoF_4$ in momentum space, at the critical mean field $\Delta_c^0 = 5.33T$, calculated from the longitudinal Green's function given in equation (5.15). The central mode, separated from the rest, carries the spectral weight away from $k = 0$. Near $k = 0$, spectral weight is transferred to the lowest energy mode.

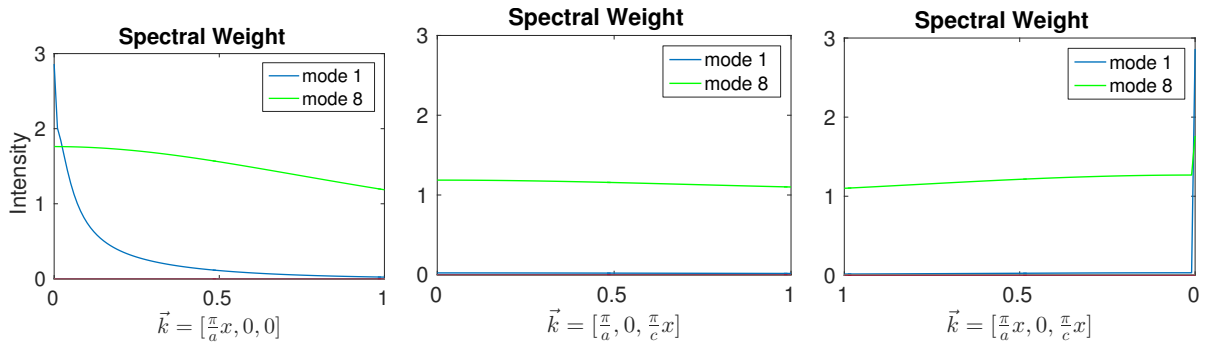

Figure 5.9: The plot above shows the spectral weight of the RPA modes of $LiHoF_4$ in momentum space, calculated from the longitudinal Green's function given in equation (5.15), at the critical mean field, $\Delta_c^0 = 5.33T$.

Summary

In this chapter, we examined some of the properties of the longitudinal Green's function (relevant to neutron scattering experiments) for electronic spins in $LiHoF_4$, using the random phase approximation (RPA). To begin, we solved the mean field (MF) Hamiltonian self consistently, and illustrated the MF energy levels, as well as the electronic and nuclear magnetizations.

In Section 5.1, we considered the longitudinal electronic Green's function in the low energy limit, as a function of the transverse magnetic field. We extracted the static (zero wave vector) longitudinal RPA susceptibility, and calculated the energy of the lowest energy excitation in the vicinity of the quantum critical point. We then considered the full RPA Green's function, and extracted the full RPA spectrum, along with the spectral weight of each mode. In the absence of the hyperfine interaction the dominant electronic mode softens to zero in a quantum phase transition. We found that the hyperfine interaction gaps this mode, with spectral weight being

transferred down to the lowest electronuclear level, which softens to zero. A calculation of this low energy soft mode and its associated spectral weight does not exist in the literature. In addition, we examined the RPA modes in momentum space near the quantum critical point. We found that in momentum space the spectral weight carried by the lowest electronuclear level decays, and the spectral weight is transferred back to the upper gapped mode.

Chapter 6

Field Theoretic Treatment of Quantum Ising Systems

In this chapter, we develop a field theoretic treatment of quantum Ising systems with an arbitrary single ion Hamiltonian. This formalism is suitable for a renormalization group treatment of such systems. Furthermore, the formalism allows for diagrammatic techniques to be used to incorporate the effects of fluctuations in quantum Ising systems perturbatively throughout a system's phase diagram, where the perturbation parameter is the inverse coordination number. This approximation is referred to as the high density approximation by Brout, who introduced it in a 1959 paper on random ferromagnetic systems [60, 61]. The formalism is well suited for dealing with systems such as $LiHoF_4$ because we are able to easily include the nuclear degrees of freedom of the holmium ions, and, due to the dominant dipolar coupling between electronic spins, the effective coordination number is large.

We obtain a field theory for a quantum Ising system by making use of the well known Hubbard-Stratonovich (HS) transformation. Mühlschlegel and Zittartz (MZ), in 1963, were the first to apply the HS transformation to an Ising system [95]. They considered a spin half Ising system in a longitudinal applied field, and, after applying the the HS transformation, they used a variational approach to analyze the resulting free energy. MZ were only concerned with the static properties of the system. They did not consider the time dependence of the quantum spin operators. In this thesis, we consider the dynamic properties of a quantum Ising system with an arbitrary single ion Hamiltonian, and develop a diagrammatic method for calculating corrections due to spatial and temporal fluctuations, rather than employing the variational approach of MZ. We will say more on this subject after a more general discussion of diagrammatic perturbation theory in the following paragraphs. In 1975, the HS transformation was applied by Young to the spin half transverse field Ising model to illustrate quantum effects in the renormalization group approach to phase transitions [58]. We fully develop Young's ap-

proach, generalizing to systems with an arbitrary single ion Hamiltonian, and thereby derive a field theory suitable for both renormalization group calculations, and for calculating the effect of fluctuations away from a system's critical region. We note that Young's work was carried out independently of the more thorough work of Hertz on quantum phase transitions [31].

Diagrammatic perturbation theory has proven to be an invaluable tool in the study of many body systems. The book of Mattuck is a good introduction to the use of diagrams in Bose and Fermi systems [96]. Spin systems are complicated by the fact that the spin operators do not commute or anticommute, so the Wick reduction theorem does not apply in the usual way. Building on work on random ferromagnetic systems, Brout introduced a diagrammatic perturbation theory for ferromagnetic spin systems in 1960 [60, 61]. The theory was subsequently developed by Brout, Englert, Stinchcombe, and others, and is presented in two 1963 papers [97, 98]. The diagrammatic perturbation theory is analogous to that used in Bose and Fermi systems, with an important difference - each vertex corresponds to a spin cumulant, the analogue of a propagator in Bose and Fermi systems, and each line corresponds to an interaction between sites. Englert refers to the diagrams as the dual of Feynman diagrams [97]. Brout's diagrammatic perturbation theory is outlined in Appendix C.

A theory similar to Brout's, corresponding to a rearrangement of the terms in Brout's theory, was introduced by Horwitz and Callen [99, 100]. Brout's theory, treated in the random phase approximation (RPA), suffers from unphysical behaviour in the ordered phase of the system. Brout accounts for this by enforcing a constraint on the total number of spins in the system [61], thereby introducing a chemical potential into the equations. The essential difference between the Horwitz and Callen theory, and the theory of Brout, is that Horwitz and Callen renormalize the vertices of their theory (the spin cumulants) by summing over all tree level diagrams, thereby working around the mean field (MF) ground state and avoiding any unphysical behaviour. Horwitz and Callen do not introduce a chemical potential in their work. We note that a diagrammatic perturbation theory equivalent to that of Brout was developed independently by Vaks, Larkin, and Pikin, and published in a 1968 paper [101].

In this thesis, we avoid the unphysical behaviour in the theory of Brout by taking the interaction to be $V = -\frac{1}{2}\sum_{i\neq j} V_{ij}(S_i^z - \langle S^z\rangle_0)(S_j^z - \langle S^z\rangle_0)$, rather than $V = -\frac{1}{2}\sum_{i\neq j} V_{ij}S_i^z S_j^z$, where the subscript zero indicates the average is to be taken with respect to the MF Hamiltonian. This is equivalent to following the renormalization procedure of Horwitz and Callen. We apply the HS transformation to the interaction, and trace over all spin variables to obtain an effective field theory. This scalar field theory is then treated using the usual Feynman diagram methods. We find the results to be equivalent to those of the Brout theory, which has been applied to the transverse field Ising model in a series of 1973 papers by Stinchcombe [26, 62, 63]. We find the formalism presented here to be conceptually simpler than the formalism of Brout. Further-

more, the field theoretic formalism presented here allows for a renormalization group treatment of a system's critical region. In Brout's theory, the behaviour of a system in its critical region is plagued by unphysical divergences.

Brout's formalism has only been applied to systems with simple single ion Hamiltonians. This is because the spin cumulants, which correspond to the vertices of the diagrammatic theory, become increasingly difficult to calculate as the complexity of the single ion Hamiltonian is increased. We overcome this difficulty by working in a basis of MF eigenstates. By doing so, we are able to deal with systems having arbitrarily complicated single ion Hamiltonians, and systems having additional degrees of freedom at each atomic site, such as the nuclear spins in $LiHoF_4$. The MF basis is discussed in Appendix A. In order to calculate the spin cumulants in the MF basis, we make use of a general reduction scheme of Yang and Wang [102]. The same reduction scheme is presented for spin operators in the appendix of the earlier paper by Vaks, Larkin and Pikin [101]; however, except for simple spin systems such as the Ising model in a longitudinal field, the reduction of spin operators is of little practical utility. The reduction of spin operators working in the MF basis can be done quite generally, and we have carried out the reduction for cumulants of up to four spin operators in Appendix E.

The reduction of MF basis operators has been developed into a general formalism for the analysis of magnetic systems with complicated single ion Hamiltonians by Wang and collaborators, and is reviewed in a 1987 paper by Wentworth and Wang [103]. The result of the formalism is a high temperature series expansion that reduces to MF theory in the zero temperature limit. High temperature series expansions are of little use in the examination of quantum critical behaviour. We note that the formalism of Wang *et al.* is complicated by the multiple site indices appearing in the spin cumulants associated with each vertex in the diagrammatic version of the theory [102, 103]. In Section 6.3.1, we show that it is only necessary to consider cumulants of spins at a single site. Furthermore, in the formalism presented by Wentworth and Wang, MF operators are grouped according to their dependence on imaginary time τ. The field theoretic formalism presented in this thesis avoids this complication by decoupling the interaction between spins with a HS transformation, which leads to spin cumulants with no repeated τ indices.

Series expansion techniques for the zero temperature behaviour of spin half transverse field Ising systems are investigated in a 1971 paper by Pfeuty and Elliott [104]. The authors make use of perturbation theory to calculate the static properties of the model, with the perturbation parameter being the ratio of the strength of the exchange interaction to the strength of the transverse field, $\frac{J}{\Delta}$, or its inverse. These techniques break down near the quantum critical point, where the value of the perturbation parameter is one. The diagrammatic techniques used in this thesis go beyond the series expansion techniques of Pfeuty and Elliot [104] by

allowing for the calculation of the dynamic, rather than static, properties of a quantum Ising system. Furthermore, the field theory allows for a renormalization group treatment of the critical behaviour.

We have discussed the series techniques of Wang and collaborators, and of Pfeuty and Elliot, and have explained why, for the analysis of quantum critical behaviour, they are inferior to the work carried out in this thesis. We now return to the work of Mühlschlegel and Zittartz (MZ) [95], and elaborate on the differences between their work, related approaches, and the work carried out in this chapter. In the field theoretic treatment of MZ, the free energy of the spin half quantum Ising model was evaluated by assuming a quadratic form for the variational function determining the energy of the fluctuating HS field [95]. This approach allows for the effect of fluctuations to be incorporated through the variational parameters in the quadratic function; however, because the theory is Gaussian in nature, interactions between the fluctuations are ignored. In principle, it is an improvement over the standard Gaussian approximation because the parameters in the theory are renormalized. However, in practice, the variational parameters turn out to be exactly what you would find by calculating the parameters from the microscopic Hamiltonian. MZ also consider the leading order correction to the Gaussian result; however, this is only possible due to the simple nature of the spin half Ising model in a longitudinal field that they base their work on.

Mühlschlegel and Zittartz make contact with the work of Brout by introducing a Lagrange multiplier to enforce a constraint on the total number of spins in the system, $\mu[N-\sum_i(S_i^z)^2]=0$. We note this constraint is only appropriate for spin half systems. Adding this constraint to the Hamiltonian corresponds to shifting the interaction between spins, $V_{ij} \rightarrow V_{ij}+2\mu\delta_{ij}$, or, in momentum space, $V_k \rightarrow V_k+2\mu$. The renormalized interaction, which we will discuss in Section 6.4 of this thesis, is then assumed to have the form

$$\sum_k T_k(i\omega_r=0)=\sum_k \frac{V_k+2\mu}{1-(V_k+2\mu)\chi_0^{zz}}=0, \tag{6.1}$$

where χ_0^{zz} is the longitudinal single ion susceptibility of the system. The assumption (6.1), which determines the Lagrange multiplier μ, is somewhat mysterious in the work of MZ. They simply state that it leads to the solution of Brout. We will have more to say about the nature of this assumption in the following paragraphs. The resulting expression for the free energy obtained by MZ is similar to the result to be given in equation (6.61) with the following caveats. First, in equation (6.61), the time dependence of the quantum operators will be taken into consideration. In a quantum system, time and space are intrinsically linked, and the time dependence of operators cannot be ignored. To obtain the expression for the free energy given in equation (24) of Section V of the MZ paper [95], the summation over Matsubara frequencies

in equation (6.61) must be dropped, and $g(i\omega_r)$ must be replaced with $g(i\omega_r = 0) = \chi_0^{zz}$ (the longitudinal component of the MF susceptibility). Second, the Lagrange multiplier should be set to zero because, in this thesis, we work with the unconstrained theory. With $\mu = 0$, the result is equivalent to the results of Horwitz and Callen [99]. MZ have compared the results of Horwitz and Callen, and those of Brout, in the high temperature limit ($\beta V_0 \ll 1$), and found that differences due to the presence of the Lagrange multiplier μ appear at sixth order in perturbation theory. The results of the theory, with or without the constraint μ, would be the same if the calculation was done exactly (to infinite order in perturbation theory). Constraining the total number of spins in the system by introducing μ will improve the results of the theory obtained perturbatively; however, the work of MZ demonstrates that the improvement only occurs at high orders of the perturbation parameter.

We now return to assumption (6.1), and discuss its significance. Making use of the identity

$$\frac{1}{N}\sum_k \chi_k^{zz} = \frac{1}{N}\sum_k \frac{\chi_0^{zz}}{1-(V_k+2\mu)\chi_0^{zz}} = \chi_0^{zz}, \tag{6.2}$$

where χ_k^{zz} is the longitudinal susceptibility in the random phase approximation, and χ_0^{zz} is the single ion susceptibility, we may rewrite assumption (6.1) as

$$\frac{1}{N}\sum_k \frac{V_k}{1-(V_k-\alpha)\chi_0^{zz}} = \alpha, \tag{6.3}$$

with $\alpha = -2\mu$. As discussed in [105], equation (6.3) is one of the defining equations of the correlated effective field (CEF) approximation, which was introduced by Lines in 1972 [106–108]. Note that our definition of α differs from that of Lines by a factor of V_0, that is, $\alpha = V_0\alpha_{Lines}$. Following [105, 107], we now proceed to outline the CEF approximation.

To begin, we write the Ising Hamiltonian as

$$\mathscr{H} = -\frac{1}{2}\sum_i S_i^z\left[\sum_{j\neq i} V_{ij}\left(\langle S_j^z\rangle + S_j^z - \langle S_j^z\rangle\right)\right]. \tag{6.4}$$

The fundamental assumption of the CEF approximation is that, because spins on different sites are correlated, $S_j^z - \langle S_j^z\rangle = A_{ij}(S_i^z - \langle S_i^z\rangle)$. Making use of this approximation, we find the effective field acting at each site to be

$$H_i^z = \sum_{j\neq i} V_{ij}\left(\langle S_j^z\rangle + A_{ij}[S_i^z - \langle S_i^z\rangle]\right). \tag{6.5}$$

In a spin half system, where $(S_i^z)^2 = 1$, we may drop the term involving S_i^z from equation (6.5)

because it simply contributes a constant shift to the ground state energy of the Hamiltonian. The effective field may be divided into its static and fluctuating parts by taking $\langle S_i^z \rangle = \langle S^z \rangle_0 + \phi_i$, where $\langle S^z \rangle_0$ is determined from the static field Hamiltonian

$$\mathscr{H}_0 = S^z(V_0 - \alpha)\langle S^z \rangle_0, \tag{6.6}$$

with

$$\alpha = \sum_j V_{ij} A_{ij} \tag{6.7}$$

being an unknown parameter representing the correlations with neighbouring spins, or, equivalently, a constraint on the total number of spins in the system. To leading order in the fluctuations, consideration of the RPA susceptibility leads to the condition

$$\frac{1}{N}\sum_k \frac{V_k}{1-(V_k-\alpha)\chi_0^{zz}} = \alpha. \tag{6.8}$$

Equations (6.6) and (6.8) may be used to solve self consistently for α and $\langle S^z \rangle_0$. These equations are identical to the RPA equations of the Ising model treated in standard MF theory augmented with a constraint on the total number of spins. This correspondence is noted by Lines in [107]. Lines also notes the equivalence of the CEF approximation and the Onsager reaction field approach. As noted in [105], the CEF approximation may be viewed as a renormalization of the single site susceptibility. That is, we define the renormalized single ion susceptibility to be

$$\chi_r^{zz} = \frac{\chi_0^{zz}}{1+\chi_0^{zz} V_0 \alpha}, \tag{6.9}$$

and the RPA susceptibility then follows from the usual equation

$$\chi_k^{zz} = \frac{\chi_r^{zz}}{1-\chi_r^{zz} V_k}. \tag{6.10}$$

Thus far, we have only considered static properties of spin systems. Spin dynamics within the CEF approximation are discussed in a 1975 paper of Lines [109]. Corrections to the dynamic susceptibility are obtained by replacing χ_0^{zz} with its dynamic counterpart, that is, $\chi_0^{zz} \to \chi_0^{zz}(\omega) = -g(\omega)$. The dynamic susceptibility in the correlated field approximation is

simply given by (in the Matsubara formalism)

$$\chi_k^{zz}(i\omega_n) = -G_k^{zz}(i\omega_n) = \frac{-g(i\omega_n)}{1+g(i\omega_n)(V_k-\alpha)}. \tag{6.11}$$

Correlations between spins lead to a static renormalization of the interaction between spins in the RPA expression for the susceptibility.

We have briefly outlined the CEF approximation, or, equivalently, an improvement of standard MF/RPA theory via the introduction of a constraint on the number of spins in the system. We will now discuss its application to the dipolar ferromagnetic insulator $LiHoF_4$, and the improvements offered by the techniques developed in this chapter. The CEF approximation has been used to study the static transverse susceptibility of $LiHoF_4$, in the absence of a transverse magnetic field, by Page *et al.* in a 1984 paper [110]. Page *et al.* find that CEF theory offers a significant improvement over standard MF theory in their calculation of the transverse susceptibility near the system's critical temperature; however, the correlation parameter goes to zero in the zero temperature limit, thus reducing the theory to the standard RPA. It would be interesting to see the CEF approximation applied to the $LiHoF_4$ system in a transverse field at zero temperature where the fluctuations are more significant. The main advantage of the high density approximation is that it allows, in principle, for systematic improvements in the calculation by carrying the perturbation theory calculation to higher orders. Admittedly, this comes at the cost of a considerable amount of straightforward but tedious algebra. The CEF approximation allows for the effect of interactions between fluctuations to be accounted for to leading order in a simpler manner, particularly at finite temperatures. Another advantage of the formalism developed in this chapter is that it provides a rigorous method for obtaining an effective field theory from the underlying Hamiltonian, thus allowing for a renormalization group treatment of a system's critical behaviour. We mention, for the sake of completeness, that Stinchcombe's work on the high density approximation in spin half transverse field Ising systems has been applied to $LiHoF_4$ in a paper of Page *et al.*, separate from their CEF work [111]; however, in this paper, the approximations used in the calculations are very rough, meaning that this application of the high density approximation should not be taken seriously.

The CEF approximation does not take into consideration any time dependence of the correlation parameter α. An approximation, similar to the CEF theory, that makes use of the high density approximation of interest in this chapter, has been developed by Jensen [68, 112]. In Jensen's formalism, α becomes a time dependent parameter. In accord with the work of Jensen, our discussion will be given in terms of the imaginary time Green's function $G_k^{zz}(i\omega_n)$ discussed in Appendix D. Jensen introduces an effective medium coupling $K(i\omega_n)$ that renormalizes the

interaction between spins. The effective medium coupling is defined by

$$K(i\omega_n) = \frac{1}{N}\sum_k V_k \frac{G_k(i\omega_n)}{G(i\omega_n)} = \frac{1}{N}\sum_k \frac{V_k}{1+\left[V_k - K(i\omega_n)\right]G(i\omega_n)}, \tag{6.12}$$

where

$$G(i\omega_n) = \frac{1}{N}\sum_k G_k(i\omega_n) \tag{6.13}$$

is the single site Green's function of the interacting theory. Equation (6.12) is a dynamic version of equation (6.8) of the CEF approximation, with the single ion Green's function $\chi_0^{zz} = -g(0)$ in the MF approximation being replaced with the exact single site Green's function of the interacting theory given by equation (6.13). Note that $G(i\omega_n)$ is exact, and contains all corrections to the MF Green's function $g(i\omega_n)$. Jensen proceeds by expanding the single sight Green's function in powers of the inverse coordination number (the high density approximation), and solving the resulting equations self consistently. Jensen refers to the high density approximation without introducing the effective medium as the unconditional cumulant expansion. In both the unconditional cumulant expansion, and the effective medium theory of Jensen [68, 112], terms involving the fourth order cumulant contribute corrections of order $\frac{1}{z}$, terms involving the sixth order cumulant contribute corrections of order $\frac{1}{z^2}$, and so on. In Section 2 of his 1994 paper on HoF_3 [112], Jensen states: "The unconditional cumulant expansion accounts correctly for the fourth-order cumulant term in the [single site Green's function], but an analysis of the sixth and higher-order terms shows that this procedure does not lead to a good estimate of the higher order contributions in the single-site series." We take this to mean that to order $\frac{1}{z}$ the considerably more complicated effective medium theory does not offer any advantage over the formalism developed in this chapter. For further discussion of Jensen's effective medium theory, and its comparison with alternative formalisms, see Section 7.2 of the book by Jensen and Mackintosh [65].

The effective medium theory, to order $\frac{1}{z}$, has been applied to $LiHoF_4$ by Jensen in the 2007 paper of Rønnow *et al.* [67]. Rønnow *et al.* use a set of crystal field parameters, and choose a value of exchange interaction that provide a good fit to the low temperature phase diagram. We use the same set of crystal field parameters throughout this thesis. Rønnow *et al.* proceed to calculate the dominant mode in the low energy excitation spectrum at $T = 0.31K$ and show that, after scaling the calculated energies by a factor of 1.15, it agrees with the spectrum measured via neutron scattering experiments. They note this crystal field mode is gapped by the presence of the hyperfine interaction, with critical fluctuations deriving from a lower energy pole of the MF Hamiltonian, although this is not shown in their work.

In Chapter 5, we have provided an analysis of all the RPA modes of $LiHoF_4$, and their associated spectral weights, which is not currently present in the literature. The formalism developed in the current chapter is suitable for obtaining corrections to the RPA results, and, at order $\frac{1}{z}$, it should be equivalent to the more complicated effective medium theory. In Chapter 7, we use the formalism developed in the current chapter to calculate the zero temperature magnetization of $LiHoF_4$, this being the simplest application of the theory. A calculation of the spectrum and the phase diagram, and its comparison to the effective medium theory, would be of interest.

We begin the current chapter by using a heuristic model to illustrate the effect of exchange anisotropy in a Heisenberg magnet in Section 6.1. We clearly show how the Goldstone modes gain mass when anisotropy breaks the rotational invariance of the system. Then, in Section 6.2, we discuss first order phase transitions using a Landau energy function. This is relevant since, as will be shown in Section 6.3, additional degrees of freedom beyond spin half may, in principle, lead to a cubic term in the energy function, resulting in a first order phase transition. Finally, in Section 6.3, we treat a quantum Ising system with an arbitrary single ion Hamiltonian more rigorously using the HS transformation, deriving a diagrammatic perturbation theory suitable for incorporating the effects of fluctuations.

Field Theory: From Heisenberg to Ising Systems

Consider the classical Heisenberg model with uniaxial anisotropy in a magnetic field transverse to the easy axis of the system

$$\begin{aligned} H = &-\frac{1}{2}\sum_{r,r'} J_z(r-r')S^z(r)S^z(r') - \frac{1}{2}\sum_{r,r'} J_\perp(r-r')(S^x(r)S^x(r') + S^y(r)S^y(r')) \\ &- B_x\sum_r S^x(r) + \mu\sum_r (\vec{S}(r)^2 - 1)^2. \end{aligned} \tag{6.14}$$

We consider a continuous spin variable $\vec{S}$, with the final term enforcing a constraint on the size of the spin, that is, it ensures that the maximum magnetization of the system is bounded. Taylor expanding $\vec{S}(r')$ around the point r, and an integration by parts, leads to a soft spin model

$$\beta H = \int d^3\vec{r}\left[\frac{1}{2}r_z(\nabla S^z)^2 + \frac{1}{2}r_0^z S_z^2 + \frac{1}{2}r_\perp((\nabla S^x)^2 + (\nabla S^y)^2) + \frac{1}{2}r_0^\perp(S_x^2 + S_y^2) + \frac{1}{4}u_0 S^4 - \Delta S^x\right] \tag{6.15}$$

where $S^4 = ((\vec{S})^2)^2$. Here the size of the spin, or the maximum magnetization, is unbounded, but there is an energy penalty for unphysically large values of the magnetization. Our goal

starting with equation (6.14) is to motivate the origin of the soft spin model. In what follows, we ignore the physical parameters in (6.14), and work with the parameters in the soft spin model instead. We may assume, with out loss of generality, that $r_z = 1$. This corresponds to a re-scaling of the spins ($S^z \to \frac{1}{\sqrt{r^z}} S^z$). This model is meant to illustrate the effects of anisotropic exchange in a Heisenberg ferromagnet. In particular, we will consider the limit $J_\perp(r-r') \to 0$, in which case we have an Ising system. It is a simple matter to include nuclear spins in such a theory; however, the resulting equations become quite cumbersome, and are not of interest to us here. The effect of the hyperfine interaction will be included when we treat quantum Ising systems in Section 6.3.

Minimizing the homogenous part of the Hamiltonian density with respect to the spins,

$$\beta h = \frac{1}{2} r_0^z S_z^2 + \frac{1}{2} r_0^\perp (S_x^2 + S_y^2) + \frac{1}{4} u_0 S^4 - \Delta S^x, \tag{6.16}$$

gives the MF magnetization, $\langle \vec{S} \rangle_{MF} = (m_x, m_y, m_z)$. We assume the system is anisotropic ($r_0^z \neq r_0^\perp$) and take $u_0 > 0$. The two relevant parameter regimes are the paramagnetic regime, where $r_0^z, r_0^\perp > 0$, and the ferromagnetic regime, where $r_0^z, r_0^\perp < 0$. We ignore all other parameter regimes as they are not physically relevant to the systems of interest in this thesis. In the paramagnetic regime, $m_z = m_y = 0$, and the transverse magnetization satisfies $\Delta = m_x(r_0^\perp + u_0 m_x^2)$. In the ferromagnetic regime, $m_y = 0$, $m_x = \frac{\Delta}{r_0^\perp - r_0^z}$, and the total magnetization is given by $m^2 = \frac{-r_0^z}{u_0}$.

Paramagnetic Regime

We expand our spins around the MF, $\vec{S} = \vec{m} + \vec{\phi}$, where $\vec{\phi} = (\phi_x, \phi_y, \phi_z)$ are the fluctuations, and $\vec{m} = (m_x, 0, 0)$ is the MF magnetization. This leads to an effective Hamiltonian for the fluctuations in the magnetization,

$$\begin{aligned} \beta H = \beta H_{MF} + \int d^3\vec{r} \Bigg[& \frac{1}{2}(r_0^\perp + 3u_0 m_x^2)\phi_x^2 + \frac{1}{2}(r_0^\perp + u_0 m_x^2)\phi_y^2 + \frac{1}{2}(r_0^z + u_0 m_x^2)\phi_z^2 \\ & + \frac{r_\perp}{2}\Big((\nabla\phi_x)^2 + (\nabla\phi_y)^2 \Big) + \frac{1}{2}(\nabla\phi_z)^2 + u_0 m_x \phi_x (\phi_x^2 + \phi_y^2 + \phi_z^2) + \frac{u_0}{4}(\vec{\phi}^2)^2 \Bigg] \end{aligned} \tag{6.17}$$

where constant terms are included in H_{MF}. Note that terms linear in the fluctuations vanish, as is to be expected as we're looking at fluctuations around the MF (expanding about a minimum). The presence of the cubic term is a reflection of the fact that the transverse field breaks the rotational symmetry in the x direction. The Hamiltonian remains symmetric under $\phi_z \to -\phi_z$ and $\phi_y \to -\phi_y$, hence any non zero minimum in these fields will be degenerate. The MF

Hamiltonian $\beta H_{MF}(\Delta) = \int d^3\vec{r}[\frac{r_0^\perp}{2}m_x^2 + \frac{u_0}{4}m_x^4 - \Delta m_x]$ doesn't contain fluctuations; however, it is still a function of temperature and the transverse field, and is important for calculating thermodynamic quantities.

The effect of the transverse field is apparent in equation (6.17). We see that as the transverse field is increased, and hence the transverse magnetization, the energy cost of the fluctuations increases. Assuming we are in the Ising universality class, with $|r_0^z| > |r_0^\perp|$, in the absence of the transverse field, the system would go critical (in the Gaussian approximation) at $r_0^z(T_c^0) = 0$. The transverse field suppresses the critical temperature. The system now goes critical when $|r_0^z(T_c^\Delta)| = u_0 m^2$, with $T_c^\Delta < T_c^0$.

In Fourier space, the Gaussian component of the function is given by

$$\beta H_0 = \frac{1}{2}\frac{1}{V}\sum_k \Big[(r_0^\perp + 3u_0 m_x^2 + r_\perp k^2)\phi_x^2 + (r_0^\perp + u_0 m_x^2 + r_\perp k^2)\phi_y^2 + (r_0^z + u_0 m_x^2 + k^2)\phi_z^2\Big]. \tag{6.18}$$

We identify the coefficients of the fields with the inverse of the connected two point correlation functions $S^{\mu\nu}(k) \approx \frac{1}{\beta}\chi^{\mu\nu}(k)$, χ being the susceptibility (see Appendix D for a discussion of the susceptibilities and correlation functions). We find

$$\begin{aligned} S^{xx}(k) &= \frac{1}{r_0^\perp + 3u_0 m_x^2 + r_\perp k^2} \\ S^{yy}(k) &= \frac{1}{r_0^\perp + u_0 m_x^2 + r_\perp k^2} \\ S^{zz}(k) &= \frac{1}{r_0^z + u_0 m_x^2 + k^2}. \end{aligned} \tag{6.19}$$

Alternatively, the transverse susceptibility,

$$\chi^{xx}(k=0) = \frac{\partial m_x}{\partial B_x} = \frac{\beta}{(r_0^\perp + 3u_0 m_x^2)}, \tag{6.20}$$

is easily obtained by differentiating the equation for the magnetization, $\Delta = \beta B_x = m_x(r_0^\perp + u_0 m_x^2)$. Note that when the longitudinal susceptibility goes critical at $r_0^z = -u_0 m^2$ the transverse susceptibilities remain finite.

Ferromagnetic Regime

We now expand our spin about the MF magnetization in the ferromagnetic regime, $\vec{S} = \vec{m} + m\vec{\phi}$, with $\vec{m} = (m_x, 0, m_z)$, and $m = |\vec{m}|$. We find

$$\begin{aligned}\beta H = \beta H_{MF} + \int d^3\vec{r}\Bigg[&2u_0 m_x m_z m^2 \phi_x \phi_z + \frac{m^2}{2}\left(u_0 m_x^2 + 3u_0 m_z^2 + r_0^z\right)\phi_z^2 + \frac{m^2}{2}(\nabla\phi^z)^2 \\ &+ \frac{m^2}{2}\left(u_0 m_z^2 + 3u_0 m_x^2 + r_0^\perp\right)\phi_x^2 + \frac{m^2}{2} r_\perp (\nabla\phi^x)^2 + \frac{m^2}{2}\left(r_0^\perp - r_0^z\right)\phi_y^2 + \frac{m^2}{2} r_\perp (\nabla\phi^y)^2 \\ &+ u_0 m_z m^3 \phi_z(\phi_x^2 + \phi_y^2) + u_0 m_x m^3 \phi_x(\phi_z^2 + \phi_y^2) + u_0 m_x m^3 \phi_x^3 + u_0 m_z m^3 \phi_z^3 + \frac{u_0}{4} m^4 (\vec{\phi}^2)^2\Bigg]\end{aligned} \tag{6.21}$$

where H_{MF} contains constant (homogenous in space) terms. Again, there are no linear terms as we are looking at fluctuations around the ground state. The inclusion of a factor of m in our definition of the fluctuation means that the $\vec{\phi}$ field represents only the direction of the fluctuation. We see that the symmetry of the system is broken in both the x and z directions; however, the Hamiltonian remains invariant under the transformation $\phi_y \to -\phi_y$.

In the Gaussian approximation, transforming to momentum space and dropping the constant MF component, the Hamiltonian is given by

$$\begin{aligned}\beta H_0 = \frac{m^2}{2}\frac{1}{V}\sum_k \Bigg[&\left(2u_0 m_z^2 + k^2\right)\phi_z^2 + \left(r_0^\perp - r_0^z + 2u_0 m_x^2 + r_\perp k^2\right)\phi_x^2 \\ &+ \left(r_0^\perp - r_0^z + r_\perp k^2\right)\phi_y^2 + 4u_0 m_x m_z \phi_x \phi_z\Bigg].\end{aligned} \tag{6.22}$$

In zero transverse field this reduces to

$$\beta H_0 = \frac{m^2}{2}\frac{1}{V}\sum_k \left[\left(2|r_0^z| + k^2\right)\phi_z^2 + \left(r_0^\perp - r_0^z + r_\perp k^2\right)\phi_\perp^2\right] \tag{6.23}$$

where $\phi_\perp^2 = \phi_x^2 + \phi_y^2$. The two point correlation functions are,

$$S^{zz}(k) = \frac{m^{-2}}{2|r_0^z| + k^2} \qquad\qquad S^\perp(k) = \frac{m^{-2}}{r_0^\perp - r_0^z + r_\perp k^2}. \tag{6.24}$$

In the absence of anisotropy, the transverse correlation functions would have poles at $k = 0$, corresponding to the Goldstone modes of the system. The effect of anisotropy is to give mass to what were the Goldstone modes.

First Order Phase Transitions in an Ising System

In the Landau theory of phase transitions, the standard approach is to write down an energy function for the order parameter consistent with the symmetries of the system. In an Ising system, this is typically taken to mean that the cubic term in the theory should be neglected. However, a cubic term may be included by defining the function piecewise

$$\beta H = \begin{cases} \frac{1}{2}\sum_k (r_0 + k^2)S^2 + \frac{g_0}{3}S^3 + \frac{u_0}{4}S^4 & S \leq 0 \\ \frac{1}{2}\sum_k (r_0 + k^2)S^2 - \frac{g_0}{3}S^3 + \frac{u_0}{4}S^4 & S > 0 \end{cases}. \tag{6.25}$$

A linear term is excluded because for $r_0 > 0$ we want the function to have a minimum at $S = 0$. Equation (6.25) is a valid function, and is symmetric under the transformation $S \to -S$ despite the cubic term. In Section 6.3.3 we will see that in a quantum system with more than two energy levels at each site, a cubic term may be present. In the formalism developed in Section 6.3, there will be either a plus or a minus sign associated with the cubic term that arises from a sign ambiguity in the Hubbard-Stratonovich transformation. If the cubic term is present, choosing to work with one sign or the other amounts to specifying in which direction the system will order. In what follows, we will choose the minus sign.

We consider a scalar field theory of the form

$$\beta H = \frac{1}{2}\sum_k (r_0 + k^2)S^2 - \frac{g_0}{3}S^3 + \frac{u_0}{4}S^4. \tag{6.26}$$

Minimizing the homogenous ($k = 0$) part of the Hamiltonian yields the MF equation,

$$m(r_0 - g_0 m + u_0 m^2) = 0, \tag{6.27}$$

where $m = \langle S \rangle_{MF}$.

Consider $r_0 > 0$. If $g_0^2 < 4u_0 r_0$, the potential has a single minimum at $m = 0$. As r_0 is reduced, the potential develops an inflection point at $m = \frac{g_0}{2u_0}$ when $g_0^2 = 4u_0 r_0$. Reducing r_0 further causes a secondary minimum at $m = \frac{g_0 + \sqrt{g_0^2 - 4u_0 r_0}}{2u_0}$ to be lowered and shifted to the right (assuming $g_0 > 0$). As r_0 is reduced, the secondary minimum will become degenerate with the minimum at $m = 0$, at which point the system undergoes a first order phase transition. When $r_0 = 0$, $m = 0$ becomes an inflection point and $m = \frac{g_0}{u_0}$ becomes the unique global minimum. The point where the two minima are degenerate occurs with $m \in (\frac{g_0}{2u_0}, \frac{g_0}{u_0})$; hence, the discontinuity in the magnetization can be at most $\Delta m|_{max} = \frac{g_0}{u_0}$. When $r_0 < 0$, $m = 0$ becomes a maximum, and there will be minima to either side at $m = \frac{g_0 \pm \sqrt{g_0^2 - 4r_0 u_0}}{2u_0}$.

If we expand about the MF, $S = m + \phi$, we may write the homogenous part of the Hamiltonian as

$$\beta H = \beta H_{MF} + \int d^3\vec{r}\left[\frac{1}{2}\left(r_0 + 2g_0 m + 3u_0 m^2\right)\phi^2 - \frac{1}{3}\left(g_0 - 3u_0 m\right)\phi^3 + \frac{u_0}{4}\phi^4\right]. \quad (6.28)$$

In the following section, we derive an expression analogous to the one above beginning with a microscopic model for a quantum Ising system. Unlike equation (6.28), the resulting theory fully incorporates the spatial dependence and time dependence of the interactions between the fluctuations.

Quantum Ising Systems

Consider a quantum spin system of the form $H = H_0 + H'$, where H_0 is the MF Hamiltonian, and may include any number of single ion terms such as a transverse field, single ion anisotropy, or hyperfine interactions. For example H_0 could be the MF Hamiltonian of $LiHoF_4$, $H_0 = \sum_i H^i_{MF}$, with

$$\begin{aligned} H^i_{MF} = &-\frac{\Delta}{2}S^x_i - V_0\langle S^z\rangle_0 S^z_i + \vec{\Delta}_n \cdot \vec{I}_i + A_z S^z_i I^z_i \\ &+ A_\perp S^+_i I^-_i + A^\dagger_\perp S^-_i I^+_i + A_{++} S^+_i I^+_i + A^\dagger_{++} S^-_i I^-_i . \end{aligned} \quad (6.29)$$

We take H' to be a longitudinal coupling between spin fluctuations,

$$H' = -\frac{1}{2}\sum_{i\neq j} V_{ij}\widetilde{S}^z_i \widetilde{S}^z_j, \quad (6.30)$$

where $\widetilde{S}^z = S^z - \langle S^z\rangle_0$. The subscript 0 indicates the average is to be taken with respect to the MF Hamiltonian, and $\langle S^z\rangle_0$ is determined self consistently. In Fourier space, the interaction becomes

$$H' = -\frac{1}{2}\sum_k V_k \widetilde{S}^z_k \widetilde{S}^z_{-k} = -\frac{1}{2}\sum_k V^R_k \widetilde{S}^z_k \widetilde{S}^z_{-k}, \quad (6.31)$$

where, in the final expression, we note that in, for example, an exchange coupled crystal that lacks inversion symmetry, $V_k = V^R_k + iV^I_k$ may have an imaginary component; however, since $V_k = V^*_{-k}$ the imaginary component vanishes upon summation. In what follows, we simply write V_k and it is to be understood we are talking about the real component. We assume the interaction is ferromagnetic.

In this section, we apply the Hubbard-Stratonovich transformation to H' in order to derive

an effective field theory for a quantum Ising system. We then proceed to use the field theory to develop a diagrammatic perturbation theory for systematically including the effects of fluctuations in quantum Ising systems. We show that the diagrammatic form of the theory is equivalent to that of Brout [60], which was introduced in 1959, and applied to the spin half transverse field Ising model in a series of 1973 papers by Stinchcombe [26, 62, 63]. The field theoretic formalism presented here generalizes Stinchcombe's results to systems having an arbitrary single ion Hamiltonian, as well as offering a great deal of simplicity and clarity when compared to previous work. Furthermore, the effective field theory is suitable for a renormalization group treatment of a system's critical behaviour.

Partition Function

Statistical mechanics requires knowledge of the partition function,

$$Z = Z_0 \left\langle T_\tau \exp\left[-\frac{1}{\beta} \int_0^\beta d\tau \beta H'(\tau) \right] \right\rangle_0 . \tag{6.32}$$

We now apply the Hubbard-Stratonovich (HS) transformation,

$$e^{\frac{x^2}{2}} = \int_{-\infty}^{\infty} \frac{dy}{\sqrt{2\pi}} e^{-\frac{y^2}{2} \pm xy}, \tag{6.33}$$

to the exponential, following the procedure in [58, 95]. Here we generalize Young's work [58] to systems with more than two degrees of freedom, and we carefully work out coefficients of the resultant field theory to all orders. Note that there is a sign ambiguity in the HS transformation. As discussed in Section 6.2, the choice of sign may determine in what direction the field will order in the resulting theory. In what follows, we choose the minus sign. We let $x_i = (BJ)_i = \sum_{j \neq i} B_{ij} \widetilde{S}^z_j$ be components of a vector, and note that $\frac{1}{2}\vec{x}^2 = \frac{1}{2}\sum_{i \neq j} \beta V_{ij} \widetilde{S}^z_i \widetilde{S}^z_j$, with $(B^2)_{ij} = \beta V_{ij}$. We apply the HS transform to each component of the vector $\vec{x}$, at each imaginary time step τ. The partition function is then

$$Z = Z_0 \int \frac{\mathscr{D}Q}{\sqrt{2\pi}} \exp\left(-\frac{1}{2\beta} \int_0^\beta d\tau \sum_i Q_i^2(\tau) \right) \times \left\langle T_\tau \exp\left(-\frac{1}{\beta} \int_0^\beta d\tau \sum_{i \neq j} Q_i(\tau) B_{ij} \widetilde{S}^z_j \right) \right\rangle_0 . \tag{6.34}$$

What we have done here is replace the interactions between spins with interactions of a single spin with a site dependent Gaussian random field. This is an analytic procedure for obtaining a functional integral representation of the theory. We will now proceed to integrate out the microscopic degrees of freedom from our Hamiltonian by completing the trace over the single ion Hamiltonian, thus obtaining an effective field theory from our microscopic quantum

model. Keep in mind that the single ion Hamiltonian may contain the hyperfine interaction. By performing this trace, the nuclear degrees of freedom are incorporated into the coefficients of the resulting field theory. We have arranged the factors of β to make our field dimensionless.

The spatial Fourier transforms of the exchange interaction and the fields are given by

$$B_{ij} = \frac{1}{N}\sum_k B_k e^{-ik(r_i-r_j)} \qquad B_k = \frac{1}{N}\sum_{ij} B_{ij} e^{ik(r_i-r_j)} = \sum_j B_{ij} e^{ik(r_i-r_j)} \tag{6.35}$$
$$Q_i = \frac{1}{\sqrt{N}}\sum_k Q_k e^{-ikr_i} \qquad Q_k = \frac{1}{\sqrt{N}}\sum_i Q_i e^{ikr_i}.$$

After Fourier transforming, we find the partition function to be

$$\frac{Z}{Z_0} = \int \frac{\mathscr{D}Q}{\sqrt{2\pi}} \exp\Big(-\frac{1}{2\beta}\int_0^\beta d\tau \sum_k |Q_k(\tau)|^2 \Big) \times \Big\langle T_\tau \exp\Big(-\frac{1}{\beta}\int_0^\beta d\tau \widehat{V}(\tau) \Big) \Big\rangle_0, \tag{6.36}$$

where

$$\widehat{V}(\tau) = \sum_k Q_{-k}(\tau) B_k \widetilde{S}^z_k(\tau), \tag{6.37}$$

where we integrate over the real and imaginary parts of the HS field separately. However, noting $Q_k = Q^*_{-k}$, we see that this double counts each degree of freedom. This may be dealt with by restricting momentum space summations to half the Brillouin zone, or introducing factors of one half.

It is advantageous at this point to establish a relationship between the HS field, and the imaginary time connected longitudinal correlation function, $G_k(\tau-\tau') = -\langle T_\tau \widetilde{S}^z_k(\tau)\widetilde{S}^z_{-k}(\tau')\rangle$, as was done for the Hubbard model in [113]. We add a fictitious site and time dependent magnetic field, $H'' = \sum_i h_i(\tau)\widetilde{S}^z_i$ to our Hamiltonian so that our interaction becomes

$$\widehat{V}(\tau) = \sum_k \Big[h_{-k}(\tau) + Q_{-k}(\tau) B_k \Big] \widetilde{S}^z_k(\tau). \tag{6.38}$$

A factor of β has been absorbed into the applied field in order to make it dimensionless. Now, by shifting the field, $Q_{-k}(\tau) = Q'_{-k}(\tau) - \frac{h_{-k}(\tau)}{B_k}$, we may transfer all the dependence of the partition function on the applied field to the Gaussian prefactor,

$$\frac{Z}{Z_0} = \int \frac{\mathscr{D}Q}{\sqrt{2\pi}} \exp\Big(-\frac{1}{2}\int_0^1 d\tau \sum_k \Big| Q_k(\tau) - \frac{h_k(\tau)}{B_{-k}} \Big|^2 \Big) \tag{6.39}$$
$$\times \Big\langle T_\tau \exp\Big(-\int_0^1 d\tau \sum_k Q_{-k}(\tau) B_k \widetilde{S}^z_k(\tau) \Big) \Big\rangle_0,$$

where we take $\tau \to \frac{\tau}{\beta}$ in order to make the integrals dimensionless. The correlation function is

then given by

$$G_k(\tau-\tau') = -\frac{\delta \ln Z}{\delta h_{-k}(\tau)\delta h_k(\tau')}\bigg|_{h=0}. \tag{6.40}$$

By performing the derivatives we find

$$G_k(\tau-\tau') = -\frac{1}{\beta V_k}\left[\left\langle Q_k(\tau)Q_{-k}(\tau')\right\rangle_Q - 1\right], \tag{6.41}$$

where the subscript Q on the average is a reminder the average is now being taken using the partition function of the HS field given in equation (6.36). In Fourier space, this becomes

$$G_k(i\omega_n) = \beta\int_0^1 d\tau e^{i\omega_n\tau}G_k(\tau) = -\frac{1}{V_k}\left[\langle|Q_k(i\omega_n)|^2\rangle_Q - 1\right]. \tag{6.42}$$

This establishes a general result between the spin correlation function and the field. Typically, the HS field is governed by a much simpler equation of motion than the original spins, so working with the field is advantageous. Also, note that

$$\langle\widetilde{S}_k^z(\tau)\rangle = \langle S_k^z(\tau)\rangle - \langle S_k^z(\tau)\rangle_0 = \frac{1}{\sqrt{\beta V_k}}\left\langle Q_k(\tau)\right\rangle_Q, \tag{6.43}$$

where, as before we take $\tau \to \frac{\tau}{\beta}$ so that our dimensionless $\tau \in [0,1]$.

We now return to the partition function given in equation (6.36), and perform a cumulant expansion leading to,

$$\begin{aligned}\frac{Z}{Z_0} = \int\frac{\mathscr{D}Q}{\sqrt{2\pi}}\exp\bigg(-\frac{1}{2\beta}\int_0^\beta d\tau\sum_k|Q_k(\tau)|^2\bigg) \\ \times T_\tau\bigg[\exp\bigg(\sum_{n=1}^\infty\frac{(-1)^n}{n!\beta^n}\prod_{i=1}^n\int_0^\beta d\tau_i\langle M_n\big(\widehat{V}(\tau)\big)\rangle_0\bigg)\bigg],\end{aligned} \tag{6.44}$$

where M_n is the nth cumulant of the interaction.

Consider the second order cumulant

$$\langle M_2(V(\tau))\rangle_0 = T_\tau\bigg[\sum_k\sum_{k'}Q_{-k}(\tau_1)Q_{-k'}(\tau_2)B_kB_{k'}\langle M_2(\widetilde{S}_k^z(\tau_1)\widetilde{S}_{k'}^z(\tau_2))\rangle_0\bigg]. \tag{6.45}$$

Now,

$$T_\tau\Big\langle M_2(\widetilde{S}^z_k(\tau_1)\widetilde{S}^z_{k'}(\tau_2))\Big\rangle_0 = T_\tau\frac{1}{N}\sum_{ij}e^{-ikr_i}e^{-ik'r_j}\Big\langle M_2(\widetilde{S}^z_i(\tau_1)\widetilde{S}^z_j(\tau_2))\Big\rangle_0 \tag{6.46}$$
$$= T_\tau\Big\langle M_2(S^z(\tau_1)S^z(\tau_2))\Big\rangle_0\delta_{k,-k'}.$$

The average in the second expression is with respect to a single site Hamiltonian; hence, all the terms in the sum vanish except those with $i=j$. We are left with the expression on the right, in which the site index has been dropped as we are always dealing with averages of spins at a single site. Note that we have used the fact that $\Big\langle M_2(\widetilde{S}^z(\tau_1)\widetilde{S}^z(\tau_2))\Big\rangle_0 = \Big\langle M_2(S^z(\tau_1)S^z(\tau_2))\Big\rangle_0$

At third order a quick calculation shows that

$$T_\tau\Big\langle M_3(\widetilde{S}^z_{k_1}(\tau_1)\widetilde{S}^z_{k_2}(\tau_2)\widetilde{S}^z_{k_3}(\tau_3))\Big\rangle_0 = T_\tau\frac{1}{\sqrt{N}}\Big\langle M_3(S^z(\tau_1)S^z(\tau_2)S^z(\tau_3))\Big\rangle_0\delta_{k_1+k_2+k_3,0}. \tag{6.47}$$

We wish to establish the general result

$$T_\tau\Big\langle M_n(\widetilde{S}^z_{k_1}(\tau_1)\widetilde{S}^z_{k_2}(\tau_2)\dots\widetilde{S}^z_{k_n}(\tau_n))\Big\rangle_0 = T_\tau\frac{1}{N^{\frac{n-2}{2}}}\Big\langle M_n(S^z(\tau_1)S^z(\tau_2)\dots S^z(\tau_n))\Big\rangle_0\delta_{\sum_{i=1}^n k_i,0}. \tag{6.48}$$

We begin by writing the cumulant as

$$T_\tau\Big\langle M_n(\widetilde{S}^z_{k_1}(\tau_1)\widetilde{S}^z_{k_2}(\tau_2)\dots\widetilde{S}^z_{k_n}(\tau_n))\Big\rangle_0 = \frac{T_\tau}{N^{\frac{n}{2}}}\Big[\prod_n\sum_{i_n}e^{-ikr_{i_n}}\Big]\Big\langle M_n(\widetilde{S}^z_{i_1}(\tau_1)\widetilde{S}^z_{i_2}(\tau_2)\dots\widetilde{S}^z_{i_n}(\tau_n))\Big\rangle_0 \tag{6.49}$$
$$= T_\tau\frac{1}{N^{\frac{n-2}{2}}}\Big\langle M_n(\widetilde{S}^z(\tau_1)\widetilde{S}^z(\tau_2)\dots\widetilde{S}^z(\tau_n))\Big\rangle_0\delta_{\sum_{i=1}^n k_i,0}.$$

The final line follows from the fact that spins belonging to different lattice sites are independent because the average is taken with respect to the single ion (MF) Hamiltonian; hence, cumulants of spins belonging to different lattice sites are equal to zero, as discussed in Section C.1 of Appendix C.

We are left with the task of establishing $M_n(\prod_{i=1}^n\widetilde{S}^z(\tau_i)) = M_n(\prod_{i=1}^n S^z(\tau_i))$. This follows almost directly from the definition of the cumulants; here we give a brief proof by induction.

We assume the result is true for M_n, and then consider

$$M_{n+1}\left(\prod_{i=1}^{n+1}\widetilde{S}_i^z\right)=\left\langle\prod_{i=1}^{n+1}\widetilde{S}_i^z\right\rangle_0-\sum_{\substack{n_1+\ldots+n_i=n+1\\ n_i\neq 1}}M_{n_1}\ldots M_{n_i}, \tag{6.50}$$

where the lower order cumulants all satisify our desired result by the induction hypothesis, and we exclude any terms containing $M_1(\widetilde{S^z})$ as this term equals zero. The first term on the right hand side of the equation is the $(n+1)$st central moment of the spins, which may be expressed as the $(n+1)$st cumulant plus terms that cancel with the lower order cumulants on the far right hand side of the equation. This proves our result. The τ ordered averages of the spin cumulants are dealt with in Appendix E.

In frequency space we have

$$M_n(\{\omega_{r_i}\})=\prod_{i=1}^{n}\left[\int_0^\beta d\tau_i e^{i\omega_{r_i}\tau_i}\right]M_n(\{\tau_i\})\qquad M_n(\{\tau_i\})=\frac{1}{\beta^n}\sum_{\{r_i\}}\prod_{i=1}^{n}\left[e^{-i\omega_{r_i}\tau_i}\right]M_n(\{\omega_{r_i}\})$$

$$Q(i\omega_r)=\frac{1}{\beta}\int_0^\beta e^{i\omega_r\tau}Q(\tau)\qquad\qquad Q(\tau)=\sum_r e^{-i\omega_r\tau}Q(i\omega_r), \tag{6.51}$$

which gives

$$\prod_{i=1}^{n}\int_0^\beta d\tau_i\langle M_n(V(\tau))\rangle_0=\sum_{\{k_i\}}\sum_{\{r_i\}}\prod_{i=1}^{n}\left[Q_{k_i}(\{i\omega_{r_i}\})B_{-k_i}\right]M_n(\{-i\omega_{r_i}\})\delta_{k_1+\ldots+k_n,0} \tag{6.52}$$

We may now write the partition function as

$$\frac{Z}{Z_0}=\int\frac{\mathscr{D}Q}{\sqrt{2\pi}}e^{-H[Q]} \tag{6.53}$$

where the Hamiltonian is understood to be dimensionless. The integration is over all complex fields $Q_k(i\omega_r)$; however, $Q_k(i\omega_{r_i})=Q_{-k}(-i\omega_{r_i})^*$. Recall, this double counts all the degrees of freedom, and we must restrict our k summation, or introduce factors of one half. The Hamiltonian is given by

$$H[Q]=\sum_{n=1}^{\infty}\left[\sum_{\{r_i\}}\sum_{\{k_i\}}\frac{u_n(\{k_i\},\{i\omega_{r_i}\})}{n!}\prod_{i=1}^{n}Q_{k_i}(i\omega_{r_i})\right], \tag{6.54}$$

with

$$\frac{u_2}{2!} = \frac{1}{2}\left[\delta_{i\omega_{r_1},-i\omega_{r_2}} - \frac{1}{\beta}(V_{k_1}V_{k_2})^{\frac{1}{2}}M_2(-i\omega_{r_1},-i\omega_{r_2})\right]\delta_{k_1,-k_2}, \tag{6.55}$$

where we have used $B_k = \sqrt{\beta V_k}$. Note that M_2, and the higher order spin cumulants, contain additional zero frequency contributions that vanish in the zero temperature limit, and in the paramagnetic phase of the system. The higher order coefficients are given by

$$u_n = \frac{(-1)^{n+1}}{N^{\frac{n}{2}-1}}\left[\prod_{i=1}^{n}(\beta V_{-k_i})^{\frac{1}{2}}\right]\frac{1}{\beta^n}M_n(\{-i\omega_{r_i}\})\delta_{\sum k_i,0}. \tag{6.56}$$

Gaussian Approximation

We now analyze our quantum Ising system in the Gaussian approximation. We begin by performing a momentum and frequency summation on u_2, given in equation (6.55), to get

$$\sum_{r_2,k_2} u_2 = [1 + V_k g(i\omega_r)], \tag{6.57}$$

where we have used

$$\sum_{r_2} M_2(-i\omega_{r_1},-i\omega_{r_2}) = -\beta g(i\omega_{r_1}), \tag{6.58}$$

and the MF Green's function,

$$g(i\omega_r) = -\sum_{n>m} c_{mn}^2 D_{mn}\frac{2E_{nm}}{E_{nm}^2-(i\omega_r)^2} - \beta\left(\sum_m c_{mm}^2 D_m - \left[\sum_m c_{mm}D_m\right]^2\right)\delta_{\omega_{r_1},0}, \tag{6.59}$$

is derived in Appendix E. The MF Green's function contains poles at the differences between each of the systems MF eigenstates, $E_{nm} = E_n - E_m$, as well as an additional zero frequency contribution that vanishes in the paramagnetic phase, and in the limit $T \to 0$. The c_{mn} are the MF matrix elements of the S^z operator, and the population factors are $D_{mn} = D_m - D_n$, where $D_m = Z_0^{-1}e^{-\beta E_m}$.

The partition function in the Gaussian approximation is given by

$$\frac{Z}{Z_0} = \int \frac{\mathscr{D}Q}{\sqrt{2\pi}}\exp\left(-\frac{1}{2}\sum_{r,k}\left[1 + V_k g(i\omega_r)\right]|Q_k(i\omega_r)|^2\right) = \prod_{r,k}\frac{1}{1+V_k g(i\omega_r)}, \tag{6.60}$$

and the corresponding (Gibb's) free energy, $F = U - TS - HM$, $dF = -SdT - MdH$, where H

is the externally applied field, is

$$F = F_0 + \frac{1}{\beta}\sum_{r,k}\frac{1}{2}\ln\left[1 + V_k g(i\omega_r)\right]. \tag{6.61}$$

The path integral double counts all the degrees of freedom, hence, there is an additional factor of $\frac{1}{2}$ in the summations. The momentum space summations are over the entire Brillouin zone.

Differentiating the free energy with respect to V_k we obtain

$$\frac{\partial F}{\partial V_k} = -\langle\widetilde{\tau}_k\widetilde{\tau}_{-k}\rangle = \frac{1}{\beta}\sum_r \frac{g(i\omega_r)}{1 + V_k g(i\omega_r)}. \tag{6.62}$$

We identify the term after the summation with the imaginary time connected Green's function in the Gaussian approximation. Alternatively, taking the derivative before performing the path integral yields

$$-\langle\widetilde{\tau}_k\widetilde{\tau}_{-k}\rangle = \frac{1}{\beta}\sum_r g(i\omega_r)\left\langle |Q_k(i\omega_r)|^2\right\rangle_Q, \tag{6.63}$$

where the average is now taken with respect to the partition function

$$Z_Q^0 = \int\frac{\mathscr{D}Q}{\sqrt{2\pi}}\exp\left(-\frac{1}{2}\sum_{r,k}\mathscr{D}_k^{-1}(i\omega_r)|Q_k(i\omega_r)|^2\right), \tag{6.64}$$

and the free field propagator is defined to be

$$\mathscr{D}_k(i\omega_r) = \frac{1}{1 + V_k g(i\omega_r)}. \tag{6.65}$$

We find that

$$\left\langle |Q_k(i\omega_r)|^2\right\rangle_Q = \frac{\int\mathscr{D}|Q|\exp\left(-\sum_{r,k>0}\mathscr{D}_k^{-1}(i\omega_r)|Q_k(i\omega_r)|^2\right)|Q_k(i\omega_r)|^3}{\int\mathscr{D}|Q|\exp\left(-\sum_{r,k>0}\mathscr{D}_k^{-1}(i\omega_r)|Q_k(i\omega_r)|^2\right)|Q_k(i\omega_r)|} = \mathscr{D}_k(i\omega_r), \tag{6.66}$$

where the integral has been performed in polar coordinates, and the momentum summations have been restricted to $k > 0$ to avoid factors of two. From this, we can relate the imaginary time connected two point correlation function to the auxiliary field Q; we find, at the Gaussian

level,

$$G_k(i\omega_r) = g(i\omega_r)\left\langle |Q_k(i\omega_r)|^2 \right\rangle_Q = \frac{g(i\omega_r)}{1+V_k g(i\omega_r)}. \tag{6.67}$$

This result can also be derived directly from equation (6.42).

Higher order correlations between the HS fields may be generated from

$$Z_Q^h = \int \frac{\mathscr{D}Q}{\sqrt{2\pi}} \exp\left(-\frac{1}{2}\sum_{r,k} \mathscr{D}_k^{-1}(i\omega_r)|Q_k(i\omega_r)|^2 + \frac{1}{2}\sum_{r,k}\left[h_k^*(i\omega_r)Q_k(i\omega_r) + h_k(i\omega_r)Q_k^*(i\omega_r)\right]\right). \tag{6.68}$$

Integrating, we find $Z_Q^h = Z_Q^0 e^{W(h)}$, where

$$W(h) = \frac{1}{2}\sum_{k,r} h_k(i\omega_r)\mathscr{D}_k(i\omega_r)h_k^*(i\omega_r). \tag{6.69}$$

The connected field correlation functions are then given by

$$\left\langle \prod_i Q_{k_i}(i\omega_{r_i}) \right\rangle = \frac{\delta}{\delta h_i} W(h)\bigg|_{h=0}. \tag{6.70}$$

In the low temperature limit, the additional zero frequency contribution to $g(i\omega_r)$ vanishes, and we find

$$\begin{aligned} \mathscr{D}_k(i\omega_r)\Big|_{T=0} = D_k(i\omega_r) &= \frac{\prod_{n>1}[E_{n1}^2 - (i\omega_r)^2]}{\prod_{n>1}[E_{n1}^2-(i\omega_r)^2] - V_k\sum_{n>1}|c_{1n}|^2 2E_{n1}\prod_{p\neq n,1}[E_{p1}^2-(i\omega_r)^2]} \\ &= \frac{\prod_{n>1}[E_{n1}^2-(i\omega_r)^2]}{\prod_p[(E_k^p)^2-(i\omega_r)^2]}, \end{aligned} \tag{6.71}$$

where, in the final expression, we have factored the numerator into the RPA modes of the system. The spectral weight of each RPA mode follows from

$$A_k(\omega) = -\frac{1}{\pi}\mathrm{Im}[D_k(i\omega_r \to \omega + i0^+)] = \sum_p A_k^p\left[\delta(\omega - E_k^p) - \delta(\omega + E_k^p)\right], \tag{6.72}$$

where

$$A_k^p = \frac{\prod_{n>1}\left[(E_k^p)^2 - E_{n1}^2\right]}{2E_k^p \prod_{s\neq p}\left[(E_k^p)^2 - (E_k^s)^2\right]}. \tag{6.73}$$

The free energy is given by

$$\lim_{T\to 0} F = F_0 - \frac{1}{2\beta}\sum_{r,k}\sum_{p}\left[\ln\left[E_{p1}^2 - (i\omega_r)^2\right] - \ln\left[(E_k^p)^2 - (i\omega_r)^2\right]\right]. \tag{6.74}$$

Terms not included in the expression above decay exponentially with temperature. We may perform the frequency summation by making use of the following trick

$$\frac{-1}{\beta}\frac{\partial}{\partial a}\sum_r \ln(a^2 - z_r^2) = \frac{-1}{\beta}\sum_r\left[\frac{1}{z_r + a} - \frac{1}{z_r - a}\right] = n_B(-a) - n_B(a) = -\coth\left(\frac{\beta a}{2}\right), \tag{6.75}$$

where n_B is the Bose-Einstein distribution function. Integrating the result with respect to a yields

$$\frac{-1}{\beta}\sum_r \ln(a^2 - z_r^2) = -\frac{2}{\beta}\ln\left[\sinh\left(\frac{\beta a}{2}\right)\right] + C. \tag{6.76}$$

Subsequent analysis will show that the integration constant is zero. Applying this to the free energy we find

$$\lim_{T\to 0} F = F_0 + \frac{1}{\beta}\sum_k\sum_p\left[\ln\left[\sinh\left(\frac{\beta E_k^p}{2}\right)\right] - \ln\left[\sinh\left(\frac{\beta E_{p1}}{2}\right)\right]\right]. \tag{6.77}$$

Note that in the limit $V_k \to 0$ we have $F \to F_0$ and $E_k^p \to E_{p1}$. All the terms under the summation in the above equation vanish, giving the correct free energy. This justifies setting the integration constant discussed above to zero.

The thermodynamics of the transverse field Ising model has been dealt with in some detail by Stinchcombe in [63]. Here we review some of the basics using the field theoretic formalism. The energy levels of the transverse field Ising model in the MF approximation are given by $E^{\pm} = \pm E = \pm\frac{1}{2}\sqrt{\Delta^2 + H^2}$, where Δ is the applied transverse field, and the longitudinal field $H = h + V_0\langle S^z\rangle_0$ includes an applied component h, and a contribution from the MF of the rest

of the crystal. The MF magnetization is defined implicity by

$$\langle S^z \rangle_0 = \tanh(\beta E) \frac{H}{2\sqrt{\Delta^2 + H^2}} \tag{6.78}$$

The lowest order term in the free energy per spin is then

$$f_0 = \frac{F_0}{N} = E_g - \frac{1}{\beta} \ln \left[2 \cosh (\beta E) \right], \tag{6.79}$$

where the ground state energy per spin is $E_g = \frac{V_0}{2} \langle S^z \rangle_0^2$. From this we find the MF magnetizations to be

$$-\frac{\partial f_0}{\partial h} = \langle S^z \rangle_0 \qquad\qquad -\frac{\partial f_0}{\partial \Delta} = \langle S^x \rangle_0 = \frac{\Delta}{H} \langle S^z \rangle_0. \tag{6.80}$$

In the paramagnetic phase of the system, the entropy in a fixed transverse field is given by

$$s_0 = -\frac{\partial f_0}{\partial T} = \ln \left[2 \cosh (\beta E) \right] - \beta E \tanh (\beta E). \tag{6.81}$$

For the transverse field Ising model we have $E_{21} = 2E$, and the RPA spectrum is given by $E_k^2 = E_{21}^2 - \frac{2|V_k|\Delta^2}{E_{21}}$. In the zero temperature limit we find

$$F_1 \big|_{T=0} = \frac{1}{2} \sum_k \left[E_k - E_{21} \right]. \tag{6.82}$$

This term yields corrections due to quantum fluctuations around the MF ground state.

The Interacting Field Theory

We now systematically include corrections to the Gaussian results for a quantum Ising system due to the interactions between the fluctuating fields. We begin with a brief look at the cubic term in the theory in Section 6.3.3. We find that this cubic term may be non-zero in the paramagnetic phase of a quantum Ising system with more than two degrees of freedom. If such is the case, the system will undergo a first order phase transition. Unfortunately, in all systems studied by the author to date, the cubic term vanishes. After our look at the cubic term, we outline how to derive corrections to thermodynamic qua due to all powers of the HS field, and calculate the leading order corrections to the Green's function in Section 6.3.3.

Cubic Term

At third order in our Hubbard-Stratonovich field we find the coefficient to be

$$u^{(3)} = \frac{1}{\sqrt{N}} \beta^{\frac{3}{2}} V_{-k_1}^{\frac{1}{2}} V_{-k_2}^{\frac{1}{2}} V_{-k_3}^{\frac{1}{2}} \frac{1}{\beta^3} M_3(\{\omega_{r_i}\}) \delta_{k_1+k_2+k_3,0}. \tag{6.83}$$

We restrict our attention to the low temperature limit of a system in its paramagnetic phase (above some quantum critical point), in which case

$$\lim_{T\to 0} M_3(\{\omega_{r_i}\}) = 2\beta \sum_{p>n\neq 1} \mathrm{Re}[c_{1n}c_{np}c_{p1}] \sum_{P\{\omega_{r_i}\}} \frac{E_{p1}E_{n1} - (i\omega_{r_1})(i\omega_{r_2})}{(E_{p1}^2 - (i\omega_{r_1})^2)(E_{n1}^2 - (i\omega_{r_2})^2)} \delta_{\omega_{r_1}+\omega_{r_2}+\omega_{r_3},0}. \tag{6.84}$$

In a two level system, no such term exists because it involves matrix elements c_{ij} between at least three MF energy levels. The leading order correction to the Gaussian results will be quartic in the Hubbard-Stratonovich field. With three or more levels, the cubic term may be non-zero in the paramagnetic phase of the system. This indicates the phase transition will be first order. This is a surprising result - additional degrees of freedom, beyond spin one half, may lead to a first order phase transition in a quantum Ising system. This leads to the question: In what systems, if any, will this term be significant?

First of all, we note that if the single ion Hamiltonian is diagonal in the S^z basis, there will be no off-diagonal terms in the matrix elements of the S^z operator because $c_{i\neq j} = 0$. So, for example, in a spin one Ising system with longitudinal single ion anisotropy (an $(S_i^z)^2$ term) we don't expect the physics discovered here to be relevant. Secondly, if the S^z operator only causes transitions between neighbouring single ion eigenstates, for example, a large spin in an applied transverse magnetic field, the phase transition will not be first order. The cubic term of the effective field theory will be non-zero in the paramagnetic phase of the system when there are non-zero matrix elements, c_{ij}, such that $c_{1n}c_{np}c_{p1}$ is non-zero. It would be of interest to determine if any such systems exist, or if they are forbidden by a general principle.

Systematic Corrections to the Gaussian Results

The calculation of spin correlation functions has been reduced to the calculation of correlation functions of an interacting field with generating functional

$$Z_Q^h = \int \frac{\mathscr{D}Q}{\sqrt{2\pi}} \exp\Bigg(-\frac{1}{2}\sum_{r,k} \mathscr{D}_k^{-1}(i\omega_r)|Q_k(i\omega_r)|^2 + \frac{1}{2}\sum_{r,k}\Big[h_k^*(i\omega_r)Q_k(i\omega_r) + h_k(i\omega_r)Q_k^*(i\omega_r)\Big] - V(Q)\Bigg), \tag{6.85}$$

where,

$$V(Q) = \frac{1}{n!}\sum_{n=3}^{\infty}\Bigg[\sum_{\{r_i\}}\sum_{\{k_i\}} u^{(n)}(\{k_i\},\{i\omega_{r_i}\})\prod_{i=1}^{n} Q_{k_i}(i\omega_{r_i})\Bigg], \tag{6.86}$$

contains all the higher interactions between the fields. In what follows, we will consider the third and fourth order terms dropping all higher order interactions. For notational convenience, we define $g \equiv u^{(3)}(\{k_i\},\{i\omega_{r_i}\})$ and $u \equiv u^{(4)}(\{k_i\},\{i\omega_{r_i}\})$, suppressing all momentum and frequency dependence. Note that these functions are symmetric under permutations of the frequencies and momenta. Our partition functional is then

$$Z_Q = \int \frac{\mathscr{D}Q}{\sqrt{2\pi}} \exp\Bigg(-\frac{1}{2}\sum_{r,k} \mathscr{D}_k^{-1}(i\omega_r)|Q_k(i\omega_r)|^2 - \frac{1}{3!}\Bigg[\sum_{\{r_i\}}\sum_{\{k_i\}} g\prod_{i=1}^{3} Q_{k_i}(i\omega_{r_i})\Bigg] - \frac{1}{4!}\Bigg[\sum_{\{r_i\}}\sum_{\{k_i\}} u\prod_{i=1}^{4} Q_{k_i}(i\omega_{r_i})\Bigg]\Bigg). \tag{6.87}$$

We begin by calculating the leading order correction to the magnetization

$$\langle S_k^z(\tau)\rangle = \langle S_k^z(\tau)\rangle_0 + \frac{1}{\beta}\sum_r e^{-i\omega_r\tau}\frac{1}{\sqrt{\beta V_k}}\Big\langle Q_k(i\omega_r)\Big\rangle, \tag{6.88}$$

with

$$\Big\langle Q_k(i\omega_r)\Big\rangle = \frac{\delta}{\delta h_k^*}\ln Z_Q^h\Big|_{h=0}. \tag{6.89}$$

We treat the interaction perturbatively. The leading order correction involves one power of g,

and is given by

$$\langle S_k^z(\tau)\rangle_1 = \frac{-1}{\sqrt{\beta V_k}}\frac{1}{\beta}\sum_r e^{-i\omega_r\tau}\frac{1}{3!}\sum_{\{r_i\}}\sum_{\{k_i\}} g(\{r_i\}\{k_i\})\Big\langle Q_k(i\omega_r)Q_{k_1}(i\omega_{r_1})Q_{k_2}(i\omega_{r_2})Q_{k_3}(i\omega_{r_3})\Big\rangle_0 . \tag{6.90}$$

Note that because g is symmetric in the momenta and frequencies, the coefficient for the various Wick contractions of the field will be the same. Recall that the path integral double counts each degree of freedom; therefore, we must restrict the momentum summations to half the Brillouin zone, or introduce a factor of one half. In the following, we introduce an additional factor of one half and leave the momentum space summations unrestricted. As we are considering unrestricted momentum summations, we must consider, for example, contractions of $k_2 = -k_3$ and $k_3 = -k_2$ separately. Hence, all combinatoric factors cancel. Contracting the fields, we find

$$\langle S_k^z(\tau)\rangle_1 = -\frac{1}{2\sqrt{N}}\sum_r e^{-i\omega_r\tau}\mathscr{D}_k(i\omega_r)\sum_{r',k'} T_{k'}(i\omega_{r'})\frac{1}{\beta^3}M_3(i\omega_r, i\omega_{r'}, -i\omega_{r'}), \tag{6.91}$$

where we define the renormalized interaction, or T matrix, to be

$$T_k(i\omega_r) = V_k\mathscr{D}_k(i\omega_r) = \frac{V_k}{1+g(i\omega_r)V_k}. \tag{6.92}$$

The role of the HS field is to renormalize the bare interaction between spins. Integrating over the imaginary time we find

$$\langle S_k^z\rangle_1 = \int_0^\beta d\tau\langle S_k^z(\tau)\rangle_1 = -\frac{\mathscr{D}_k(0)}{\sqrt{N}}\sum_{r',k'}\beta T_{k'}(i\omega_{r'})\frac{1}{\beta^3}M_3(0, i\omega_{r'}, -i\omega_{r'}). \tag{6.93}$$

This is the leading order correction to the magnetization of the system.

We now turn to $\langle|Q_k(i\omega_r)|^2\rangle$, and calculate the leading order corrections to the spin correlation function. Expanding the interaction, the leading order corrections will come from a single power of u, and from two powers of g. We write

$$\langle|Q_k(i\omega_r)|^2\rangle = \langle|Q_k(i\omega_r)|^2\rangle_0 + \langle|Q_k(i\omega_r)|^2\rangle_u + \langle|Q_k(i\omega_r)|^2\rangle_{g^2} + \cdots \tag{6.94}$$

Wick contracting the auxiliary fields, we find the leading order correction due to the quartic

coupling to be

$$\langle |Q_k(i\omega_r)|^2\rangle_u = \frac{1}{2N}\beta V_k \mathscr{D}_k^2(i\omega_r)\sum_{k',r'}\beta T_{k'}(i\omega_{r'})\frac{1}{\beta^4}M_4(i\omega_r,-i\omega_r,i\omega_{r'},-i\omega_{r'}), \tag{6.95}$$

where, as with the magnetization calculation, all combinatoric factors cancel. We have introduced an additional factor of one half to compensate for double counting the degrees of freedom in the path integral. Equation (6.95) is conveniently written as

$$\langle |Q_k(i\omega_r)|^2\rangle_u = -\frac{g_u(i\omega_r)V_k}{[1+g_0(i\omega_r)V_k]^2}, \tag{6.96}$$

with

$$g_u(i\omega_r) = -\frac{\beta}{2N}\sum_{k',r'}\beta T_{k'}(i\omega_{r'})\frac{1}{\beta^4}M_4(i\omega_r,-i\omega_r,i\omega_{r'},-i\omega_{r'}). \tag{6.97}$$

We find the field correlation function to approximately be given by

$$\langle |Q_k(i\omega_r)|^2\rangle_0 + \langle |Q_k(i\omega_r)|^2\rangle_u = \frac{1}{1+g_0V_k}\left[1-\frac{g_uV_k}{1+g_0V_k}\right] \approx \frac{1}{1+(g_0+g_u)V_k} \tag{6.98}$$

We now consider the contribution from two powers of g. There are two different diagrams corresponding to this contribution, $\langle |Q_k(i\omega_r)|^2\rangle_{g^2} = \langle |Q_k(i\omega_r)|^2\rangle_L + \langle |Q_k(i\omega_r)|^2\rangle_B$, which we consider separately. The first, $\langle |Q_k(i\omega_r)|^2\rangle_L$, comes from a loop diagram where the external fields are each coupled to a separate vertex. The second, $\langle |Q_k(i\omega_r)|^2\rangle_B$, comes from a "balloon" diagram where the external fields are coupled to the same vertex. As before, all combinatoric factors cancel. The loop diagram is given by

$$\langle |Q_k(i\omega_r)|^2\rangle_L = -\frac{g_L(k,i\omega_r)V_k}{[1+g_0(i\omega_r)V_k]^2}, \tag{6.99}$$

with

$$g_L(k,i\omega_r) = -\frac{\beta}{2N}\sum_{k_1}\sum_{r_1,r_2}\beta^2 T_{k_1}(i\omega_{r_1})T_{k-k_1}(i\omega_{r_2}) \times \frac{1}{\beta^6}M_3(i\omega_r,i\omega_{r_1},i\omega_{r_2})M_3(-i\omega_r,-i\omega_{r_1},-i\omega_{r_2}). \tag{6.100}$$

In the low temperature limit, where we need only consider overall momentum conservation,

$\delta_{i\omega_r+i\omega_{r_1}+i\omega_{r_2},0}$, equation (6.100) reduces to

$$g_L(k,i\omega_r) = -\frac{\beta}{2N}\sum_{k',r'}\beta^2 T_{k'}(i\omega_{r'})T_{k-k'}(-i\omega_r - i\omega_{r'}) \times \frac{1}{\beta^6}M_3(i\omega_r, i\omega_{r'}, -i\omega_r - i\omega_{r'})M_3(-i\omega_r, -i\omega_{r'}, i\omega_r + i\omega_{r'}). \tag{6.101}$$

As with g_u, we have introduced an additional factor of one half to compensate for double counting the degrees of freedom in the path integral.

The balloon diagram is given by

$$\langle |Q_k(i\omega_r)|^2\rangle_B = -\frac{g_B(i\omega_r)V_k}{[1+g_0(i\omega_r)V_k]^2}, \tag{6.102}$$

where

$$g_B(i\omega_r) = -\frac{\beta}{2N}\sum_{k'}\sum_{r_1,r_2}\beta^2 T_0(i\omega_{r_1})T_{k'}(i\omega_{r_2})\frac{1}{\beta^6}M_3(i\omega_r, -i\omega_r, i\omega_{r_1})M_3(-i\omega_{r_1}, i\omega_{r_2}, -i\omega_{r_2}). \tag{6.103}$$

In the low temperature limit, where we need only consider overall momentum conservation, we have

$$g_B(i\omega_r) = \beta^2 V_0 \frac{1}{\beta^3}M_3(i\omega_r, -i\omega_r, 0)\langle S^z\rangle_1, \tag{6.104}$$

where

$$\langle S^z\rangle_1 = \frac{1}{\sqrt{N}}\langle S^z_{k=0}\rangle_1 = -\frac{R_0}{2N}\sum_{r',k'}\beta T_{k'}(i\omega_{r'})\frac{1}{\beta^3}M_3(0, i\omega_{r'}, -i\omega_{r'}), \tag{6.105}$$

and $R_0 = D_0(0)$ is the ratio of MF to RPA energy levels at zero wavevector as discussed in Appendix D.

Combining these corrections, we find

$$\langle |Q_k(i\omega_r)|^2\rangle \approx \frac{1}{1+(g_0+g_u+g_L+g_B)V_k}, \tag{6.106}$$

which, using equation (6.42), leads to

$$G_k(i\omega_r) \approx \left[\frac{g_0+g_u+g_L+g_B}{1+(g_0+g_u+g_L+g_B)V_k}\right]. \tag{6.107}$$

The diagrams corresponding to the corrections g_u, g_L, and g_B are given in Figure 6.1. Expressing the correlation function in the form given in equation (6.107) allows for easy comparison to the work of Stinchcombe [26, 62, 63]. We find the function $\mathscr{G} \approx g_0 + g_u + g_L + g_B$ to be equivalent to equation (2.7) of [62]. The approach presented here is simpler than Stinchcombe's approach, and it clearly illustrates how the fluctuations screen the bare interaction between spins. We have also generalized Stinchcombe's work to systems with an arbitrary single ion Hamiltonian.

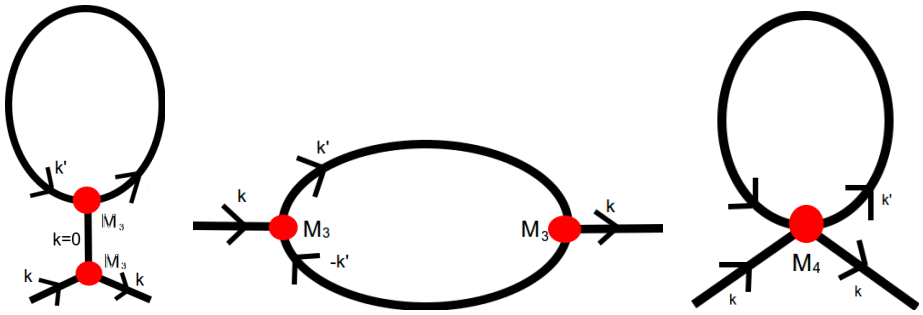

Figure 6.1: The figure above shows the one loop diagrams that contribute to the leading order correction (order $\frac{1}{z}$, z being the coordination number) to the connected two point longitudinal correlation function of a quantum Ising system given in equation (6.107). The left most diagram is the balloon contribution g_B, the center diagram is the loop contribution g_L, and the rightmost diagram corresponds to g_u.

We close this section with a statement of the momentum space Feynman rules for calculating corrections to the Gaussian results for the Hubbard Stratonovich field to all orders.

1. We associate an external leg of our diagram with momentum k and frequency $i\omega_r$ with each of the Hubbard-Stratonovich fields in our correlation function. Each external leg carries a factor of $\sqrt{\beta V_k}\mathscr{D}_k(i\omega_r)$.

2. We consider vertices of all orders. A vertex of order n has a factor of order $\frac{1}{\beta^n}M_n$ associated with it. We join the vertices to each other, and to all the external legs, in all possible ways that leave the diagram connected. The order of each diagram is determined by the number of free momentum summations it contains as discussed in Appendix C.

3. Each internal line has a momentum k and frequency $i\omega_r$ associated with it and contributes a factor of $\beta V_k \mathscr{D}_k(i\omega_r)$. Energy and momentum conservation at each vertex is determined by the associated spin cumulant.

4. Sum over each internal frequency, and for each internal momenta, add a summation $\frac{1}{N}\sum_k$.

The Renormalized Interaction

As noted following equation (6.92), the role of the Hubbard-Stratonovich field is to renormalize the bare interaction between spins. As the renormalized interaction (The T matrix),

$$T_k(i\omega_r) = V_k \mathscr{D}_k(i\omega_r) = \frac{V_k}{1 + g(i\omega_r)V_k} \tag{6.108}$$

plays a central role in calculating corrections to the RPA results, we present it here in some detail. A similar analysis is carried out by Stinchcombe in [62] for the case of a spin half system. The expressions below generalize Stinchcombe's result to systems with an arbitrary single ion Hamiltonian.

We begin by writing the renormalized interaction as

$$T_k(i\omega_r) = V_k D_k(i\omega_r) + T_k^0 \delta_{i\omega_r,0}. \tag{6.109}$$

In terms of the MF energy levels of our system, and MF matrix elements of the longitudinal spin operator, we find

$$\begin{aligned} D_k(i\omega_r) &= \frac{\prod_{n>m}(E_{nm}^2 - (i\omega_r)^2)}{\prod_{n>m}(E_{nm}^2 - (i\omega_r)^2) - V_k \sum_{p>q} c_{qp}^2 D_{qp} 2E_{pq} \prod_{\substack{n>m \\ n,m\neq p,q}} (E_{nm}^2 - (i\omega_r)^2)} \\ &= \frac{\prod_{n>m}(E_{nm}^2 - (i\omega_r)^2)}{\prod_p ((E_k^p)^2 - (i\omega_r)^2)} \end{aligned} \tag{6.110}$$

and

$$\begin{aligned} T_k^0 &= \frac{V_k}{\frac{\prod_p (E_k^p)^2}{\prod_{n>m} E_{nm}^2} - \beta V_k \left[\sum_m c_{mm}^2 D_m - \left(\sum_m c_{mm} D_m \right)^2 \right]} - \frac{V_k \prod_{n>m} E_{nm}^2}{\prod_p (E_k^p)^2} = \\ &= \frac{\beta V_k^2 \left[\sum_m c_{mm}^2 D_m - \left(\sum_m c_{mm} D_m \right)^2 \right] \prod_{n>m} E_{nm}^4}{\prod_p (E_k^p)^2 \left[\prod_p (E_k^p)^2 - \beta V_k \left[\sum_m c_{mm}^2 D_m - \left(\sum_m c_{mm} D_m \right)^2 \right] \prod_{n>m} E_{nm}^2 \right]} \end{aligned} \tag{6.111}$$

where in the final expression for $D_k(i\omega_r)$ we have written the denominator in terms of the RPA modes E_k^p. Note that T_k^0 vanishes in the limit $T \to 0$ and in the paramagnetic phase of the system.

We see that $D_k(i\omega_r)$ has zeros at the MF energy levels of our system. This fact proves useful when performing frequency summations in the fluctuation analysis because when $D_k(i\omega_r)$ is multiplied by a function with poles at the MF energy levels, we may ignore those poles.

Summary

We introduced this chapter with a general discussion of the problem of including the effects of fluctuations in quantum Ising systems, and have emphasized the simplicity and utility of the field theoretic approach developed here. After the general discussion, in Section 6.1, we introduced a classical heuristic model of an anisotropic Heisenberg spin system. We showed that a field transverse to the easy axis in this model leads to a reduction in the critical temperature of the system, and derived expressions showing how the energy cost of fluctuations is affected by anisotropy. Finally, we showed that the effect of anisotropy is to give mass to what were the Goldstone modes. In Section 6.2, we briefly discussed how a cubic term in an effective free energy function for a system leads to a first order phase transition. This may be relevant to quantum Ising systems with more than a spin half degree of freedom.

In Section 6.3, we developed a field theoretic formalism for treating quantum Ising systems with an arbitrary single ion Hamiltonian. We then proceeded to analyze the resulting theory in the Gaussian approximation in Section 6.3.2. In section 6.3.3, we discussed systematic corrections to the Gaussian result, beginning with a look at the cubic term. We found that, in principle, the cubic term may be present in the paramagnetic phase of a system with more than a spin half degree of freedom at each site. If such a term exists, this would lead to a first order phase transition. We proceeded to use the field theoretic formalism to calculate the leading order corrections to the magnetization, and the longitudinal Green's function, then we stated the Feynman rules for systematically obtaining higher order corrections.

Chapter 7

Corrections to Mean Field Magnetization

In this chapter, we calculate the leading order correction to the mean field (MF) magnetization of quantum Ising systems. Recall, the magnetization is given by $\langle S^z \rangle \approx \langle S^z \rangle_0 + \langle S^z \rangle_1$, where $\langle S^z \rangle_0$ is the MF magnetization, and the leading order correction is given by equation (6.105)

$$\langle S^z \rangle_1 = -\frac{R_0}{2N} \sum_{r,k} \beta T_k(i\omega_r) \frac{1}{\beta^3} M_3(0, i\omega_r, -i\omega_r). \tag{7.1}$$

This result is the $\frac{1}{z}$ term, z being the coordination number, in the high density approximation developed in Chapter 6. The diagram corresponding to equation (7.1) is shown in Figure 7.1. We may compare this result to equation (2.10) of Stinchcombe [62]. The result of Stinchcombe is missing the prefactor R_0 because Stinchcombe does not screen the interaction corresponding to the zero momentum and frequency line in Fig. 1d of his paper (the vertical line in Figure 7.1 of this thesis). In Section 7.2, we will deal explicitly with the spin half transverse field Ising model, and demonstrate the prefactor is necessary in order to obtain the correct leading order correction to the magnetization.

We restrict our attention to the zero temperature limit, in which case the renormalized interaction (the T matrix) is given by

$$T_k(i\omega_r)\Big|_{T=0} = V_k \frac{\prod_{n>1}(E_{n1}^2 - (i\omega_r)^2)}{\prod_p((E_k^p)^2 - (i\omega_r)^2)}, \tag{7.2}$$

and the prefactor R_0 is the zero wave vector and zero frequency component of the free field propagator $\mathscr{D}_k(i\omega_r)$ given by

$$R_0 = \frac{1}{1 + g(0)V_{k=0}}\Big|_{T=0} = \frac{\prod_{n>1} E_{n1}^2}{\prod_p (E_{k=0}^p)^2}, \tag{7.3}$$

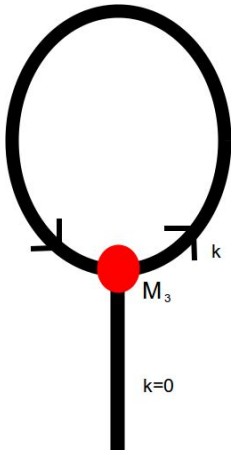

Figure 7.1: The diagram above corresponds to the leading order correction to the magnetization of a quantum Ising system in the high density approximation (an expansion in the inverse coordination number).

The third order spin cumulant, derived in Appendix E, is given by

$$M_3(0,i\omega_r,-i\omega_r)\Big|_{T=0} = \sum_{n>1}(c_{11}-c_{nn})|c_{1n}|^2 A_1^0(0,i\omega_r,-i\omega_r) + \sum_{\substack{n>1\\p>n}} \mathrm{Re}[c_{1n}c_{np}c_{p1}]A_2^0(0,i\omega_r,-i\omega_r), \tag{7.4}$$

where

$$A_1^0(0,i\omega_r,-i\omega_r) = -2\beta\frac{3E_{n1}^2-(i\omega_r)^2}{[E_{n1}^2-(i\omega_r)^2]^2} \tag{7.5}$$

$$A_2^0(0,i\omega_r,-i\omega_r) = 4\beta\left[\frac{E_{n1}}{E_{p1}(E_{n1}^2-(i\omega_r)^2)}+\frac{E_{p1}}{E_{n1}(E_{p1}^2-(i\omega_r)^2)} + \frac{E_{p1}E_{n1}+(i\omega_r)^2}{(E_{n1}^2-(i\omega_r)^2)(E_{p1}^2-(i\omega_r)^2)}\right].$$

Note that A_1^0 and A_2^0 are functions of the summation indices, n and p, as well. We suppress these indices for the sake of compactness. Combining terms, we may write the zero temperature

correction to the magnetization as

$$\langle S^z\rangle_1 = \frac{R_0}{2N}\sum_k V_k\left[\sum_{n>1}(c_{11}-c_{nn})|c_{1n}|^2 A_3^n + \sum_{p>n\neq 1}\mathrm{Re}[c_{1n}c_{np}c_{p1}]A_4^{np}\right], \tag{7.6}$$

where

$$A_3^n = -\frac{2}{\beta}\sum_r \frac{3E_{n1}^2-(i\omega_r)^2}{E_{n1}^2-(i\omega_r)^2}\frac{\prod_{m\neq n,1}(E_{m1}^2-(i\omega_r)^2)}{\prod_p((E_k^p)^2-(i\omega_r)^2)} \tag{7.7}$$

$$A_4^{np} = \frac{4}{\beta}\sum_r \frac{1}{\prod_l (E_k^l)^2-(i\omega_r)^2}\left[\frac{E_{n1}}{E_{p1}}\prod_{m\neq n,1}(E_{m1}^2-(i\omega_r)^2) + \frac{E_{p1}}{E_{n1}}\prod_{m\neq p,1}(E_{m1}^2-(i\omega_r)^2) + (E_{p1}E_{n1}+(i\omega_r)^2)\prod_{m\neq n,p,1}(E_{m1}^2-(i\omega_r)^2)\right].$$

We see that all the poles at the MF energy levels vanish from A_4^{np} due to the zeros of the screened interaction; however, we still must deal with MF poles in A_3^n. Furthermore, we must treat points at which the MF energy levels and the RPA energy levels are degenerate carefully because the order of the associated poles in A_3^n and A_4^{np} will change. There is also the possibility that a pair of the RPA modes are degenerate. In such cases, we simply shift one of the RPA modes by a small amount to avoid the degeneracy.

Our next task is to perform the frequency summations. We do so in the usual way, viz., we write

$$A_j = -\frac{1}{\beta}\sum_r f_j(z=i\omega_r) = \sum_p r_p n_B(z_p) \tag{7.8}$$

where r_p is the residue of f_j at the p^{th} pole z_p, and $n_B(z_p)$ is the Bose-Einstein distribution function

$$n_B(z) = \frac{1}{e^{\beta z}-1}. \tag{7.9}$$

Note that $f_j(z) = f_j(-z)$; hence, $\mathrm{Res}[f_j(z_0)] = -\mathrm{Res}[f_j(-z_0)]$. This simplifies our task somewhat because it means we only need to consider positive poles. The A_4^{np} function has simple poles at each of the RPA energy levels. Making use of the fact $n_B(z)-n_B(-z) = \coth(\frac{\beta z}{2})$, and

using $\mathrm{Res}[f(z);c] = lim_{z\to c}(z-c)f(z)$ to find the residue of f at c, we find that

$$A_4^{np} = \sum_l \frac{2}{E_k^l \prod_{q\neq l}(E_k^q)^2 - (E_k^l)^2}\left[\frac{E_{n1}}{E_{p1}}\prod_{m\neq n,1}(E_{m1}^2 - (E_k^l)^2) + \frac{E_{p1}}{E_{n1}}\prod_{m\neq p,1}(E_{m1}^2 - (E_k^l)^2)\right. \quad (7.10)$$
$$\left. + (E_{p1}E_{n1} - (E_k^l)^2)\prod_{m\neq n,p,1}(E_{m1}^2 - (E_k^l)^2)\right]\coth(\frac{\beta E_k^l}{2}).$$

In the zero temperature limit, $\coth(\frac{\beta E_k^l}{2})$ is simply equal to one. Analysis of the A_3^n function requires more care than analysis of the A_4^{np} function because we must consider the possibility that the RPA modes and the MF energy levels are degenerate. If there are no degeneracies, there are simple poles at each RPA mode and the n^{th} MF energy level, and the result of the frequency summation is

$$A_3^n|_{E_n\neq E_k^p} = -2\left[E_{n1}\frac{\prod_{m\neq n,1}(E_{m1}^2 - E_{n1}^2)}{\prod_p((E_k^p)^2 - E_{n1}^2)}\coth(\frac{\beta E_{n1}}{2})\right. \quad (7.11)$$
$$\left. + \sum_p \frac{3E_{n1}^2 - (E_k^p)^2}{E_{n1}^2 - (E_k^p)^2}\frac{\prod_{m\neq n,1}E_{m1}^2 - (E_k^p)^2}{2E_k^p\prod_{q\neq p}(E_k^q)^2 - (E_k^p)^2}\coth(\frac{\beta E_k^p}{2})\right].$$

In order to deal with the case where the n^{th} MF energy level is degenerate with one of the RPA modes, $E_{n1} = E_k^q$, we begin by rewriting A_3^n as

$$A_3^n = -\frac{1}{\beta}\sum_r \frac{P(z = i\omega_r)}{(E_k^q - i\omega_r)^2 Q(z = i\omega_r)}, \quad (7.12)$$

where

$$P(z) = 2[3(E_k^q)^2 - z^2]\prod_{m\neq n,1}[E_{m1}^2 - z^2] \quad (7.13)$$
$$Q(z) = [E_k^q + z]^2\prod_{p\neq q}[(E_k^p)^2 - z^2].$$

We now have a second order pole at the E_k^q, and simple poles at all the other RPA modes. The residue at the second order pole is given by

$$\mathrm{Res}|_{E_k^q} = \lim_{z\to E_k^q}\frac{d}{dz}\frac{P(z)}{Q(z)} = \frac{P'(E_k^q)Q(E_k^q) - P(E_k^q)Q'(E_k^q)}{Q(E_k^q)^2}, \quad (7.14)$$

where

$$P'(E_k^q) = -4E_k^q \prod_{m\neq n,1} [E_{m1}^2 - (E_k^q)^2] - 8(E_k^q)^3 \sum_{m\neq n,1} \prod_{r\neq m,n,1} [E_{r1}^2 - (E_k^q)^2] \tag{7.15}$$
$$Q'(E_k^q) = 4E_k^q \prod_{p\neq q} [(E_k^p)^2 - (E_k^q)^2] - 8(E_k^q)^3 \sum_{p\neq q} \prod_{r\neq p,q} [(E_k^r)^2 - (E_k^q)^2].$$

This gives the following result for the frequency summation

$$A_3^n|_{E_n=E_k^q} = \frac{P'(E_k^q)Q(E_k^q) - P(E_k^q)Q'(E_k^q)}{Q(E_k^q)^2} \coth(\frac{\beta E_k^q}{2}) \tag{7.16}$$
$$- \sum_{p\neq q} \frac{3(E_k^q)^2 - (E_k^p)^2}{[(E_k^q)^2 - (E_k^p)^2]^2} \frac{\prod_{m\neq n,1}(E_{m1}^2 - (E_k^p)^2)}{E_k^p \prod_{r\neq p,q}((E_k^r)^2 - (E_k^p)^2)} \coth(\frac{\beta E_k^p}{2})$$

To summarize, we have found the leading order correction to the magnetization at zero temperature to be

$$\langle S^z \rangle_1 = \frac{R_0}{2N} \sum_k V_k \Big[\sum_{n>1} (c_{11} - c_{nn}) |c_{1n}|^2 A_3^n + \sum_{p>n\neq 1} \mathrm{Re}[c_{1n} c_{np} c_{p1}] A_4^{np} \Big], \tag{7.17}$$

with A_3^n given by equation (7.11) if there are no degeneracies between the RPA modes of the system and the MF eigenstates, and A_3^n given by equation (7.16) if such degeneracies do exist. In the paramagnetic phase of the system, the contribution from A_3^n vanishes, and we are left with only the contribution from A_4^{np}, given in equation (7.10). In the event that two of the RPA modes of the system are degenerate, we simply shift one of the modes by a small amount, rather than deal with a higher order pole in the associated frequency summation.

Landau Theory

Recall from Section 6.3.3 that the partition function governing the Hubbard-Stratonovich field corresponding to fluctuations in a quantum Ising system is given by (to fourth order in the field)

$$Z_Q = \int \frac{\mathscr{D}Q}{\sqrt{2\pi}} \exp\Big(-\frac{1}{2} \sum_{r,k} \mathscr{D}_k^{-1}(i\omega_r) |Q_k(i\omega_r)|^2 \tag{7.18}$$
$$- \frac{1}{3!} \Big[\sum_{\{r_i\}} \sum_{\{k_i\}} g \prod_{i=1}^{3} Q_{k_i}(i\omega_{r_i}) \Big] - \frac{1}{4!} \Big[\sum_{\{r_i\}} \sum_{\{k_i\}} u \prod_{i=1}^{4} Q_{k_i}(i\omega_{r_i}) \Big] \Big),$$

where, in the low temperature limit,

$$\mathscr{D}_k(i\omega_r)\Big|_{T\to 0} = D_k(i\omega_r) = \frac{\prod_{n>1}[E_{n1}^2 - (i\omega_r)^2]}{\prod_p[(E_k^p)^2 - (i\omega_r)^2]}, \tag{7.19}$$

and the higher order coefficients are functions of the fluctuating Matsubara frequencies and momenta, $g = g(\{k_i\},\{i\omega_{r_i}\})$ and $u = u(\{k_i\},\{i\omega_{r_i}\})$. In a renormalization group treatment of the system, the frequency and momentum dependence of g and u is irrelevant, and we may simply write

$$Z_Q = \int \left[\sqrt{\frac{\beta V_0 N}{2\pi}}\mathscr{D}Q\right] e^{-\beta V_0 N L[Q]}, \tag{7.20}$$

with the Landau energy function being

$$\begin{aligned} L[Q] = \frac{1}{2}\sum_{r,k} D_k^{-1}(i\omega_r)|Q_k(i\omega_r)|^2 \\ - \frac{\widetilde{g_0}}{3}\left[\sum_{\{r_i\}}\sum_{\{k_i\}}\prod_{i=1}^{3} Q_{k_i}(i\omega_{r_i})\right] + \frac{\widetilde{u_0}}{4}\left[\sum_{\{r_i\}}\sum_{\{k_i\}}\prod_{i=1}^{4} Q_{k_i}(i\omega_{r_i})\right], \end{aligned} \tag{7.21}$$

The fields have been rescaled ($Q \to \sqrt{\beta V_0 N}Q$). This eliminates any explicit dependence on β or N from the resulting Landau energy function, although, the function still has implicit temperature dependence because the prefactors are functions of the temperature dependent spin cumulants. The prefactors in the Landau theory, $\widetilde{g_0}$ and $\widetilde{u_0}$, are obtained by setting the frequency and momentum dependence of g and u to zero, and rescaling them as follows

$$\begin{aligned} \widetilde{g_0} &= \frac{g(\{k_i = 0\},\{i\omega_{r_i} = 0\})}{2\sqrt{\beta V_0 N}} \\ \widetilde{u_0} &= \frac{u(\{k_i = 0\},\{i\omega_{r_i} = 0\})}{6\beta V_0 N}. \end{aligned} \tag{7.22}$$

In Landau MF theory, we assume the system is uniformly magnetized, and ignore the frequency and momentum dependence of the quadratic term, taking

$$D_k^{-1}(i\omega_r) \to \widetilde{r_0} = R_0^{-1} = \frac{\prod_p (E_{k=0}^p)^2}{\prod_{n>1} E_{n1}^2}. \tag{7.23}$$

Using the results of E we find, in the low temperature limit,

$$\widetilde{g_0}\Big|_{T\to 0} = 3V_0^2\Bigg[\sum_{n>1}(c_{11}-c_{nn})|c_{1n}|^2\frac{1}{E_{n1}^2} - \sum_{p>n\neq 1}\mathrm{Re}[2c_{1n}c_{np}c_{p1}]\frac{1}{E_{p1}E_{n1}}\Bigg] \tag{7.24}$$

$$\begin{aligned}\widetilde{u_0}\Big|_{T\to 0} = -4V_0^3\Bigg[&\sum_{n>1}\frac{|c_{1n}|^2}{E_{n1}^3}[(c_{11}-c_{nn})^2-|c_{1n}|^2] \\ &+\sum_{n\neq p>1}c_{11}c_{1n}c_{np}c_{p1}\frac{1}{E_{np}}\left(\frac{1}{E_{n1}^2}-\frac{1}{E_{p1}^2}\right)+\sum_{m\neq p>1}\mathrm{Re}[c_{mm}c_{m1}c_{1p}c_{pm}]\frac{1}{E_{m1}^2E_{p1}} \\ &-\sum_{p>n>1}\frac{|c_{1n}|^2|c_{1p}|^2}{E_{n1}E_{p1}}\left(\frac{1}{E_{p1}}+\frac{1}{E_{n1}}\right)-\sum_{n>1}\sum_{\substack{p>1\\p\neq n}}\sum_{\substack{q>1\\q\neq n,p}}c_{1n}c_{np}c_{pq}c_{q1}\frac{1}{E_{n1}E_{np}E_{q1}}\Bigg].\end{aligned}$$

It follows from equation (6.88) that the magnetization in terms of the rescaled field is

$$\langle S^z\rangle = \langle S^z\rangle_0 + \langle Q\rangle_Q, \tag{7.25}$$

with the subscript 0 indicating an average with respect to the MF Hamiltonian, and the subscript Q indicating an average with respect the Landau free energy function given in equation (7.21), which ignores the frequency and momentum dependence of the fluctuations, and their interactions. We use the tilde on the coefficients of the effective field theory because they represent the energy cost of the fluctuation field Q. As shown in equation 6.28, these parameters are related to the parameters of the field theory for $\langle S^z\rangle$ by

$$\begin{aligned} r_0 &= \widetilde{r_0} + 2\widetilde{g_0}\langle S^z\rangle_0 + 9\widetilde{u_0}\langle S^z\rangle_0^2 \\ g_0 &= \widetilde{g_0} + 3\widetilde{u_0}\langle S^z\rangle_0 \\ u_0 &= \widetilde{u_0}. \end{aligned} \tag{7.26}$$

The Landau energy function given in equation (7.21), which is derived from a microscopic model, is amenable to treatment via the renormalization group. The methods used here are more rigorous then obtaining an effective field theory based solely on symmetry considerations.

The Landau coefficients, $\widetilde{r_0}$, $\widetilde{g_0}$ and $\widetilde{u_0}$, may be used to estimate the size of the region in which fluctuations of the order parameter will play a significant role in a quantum Ising system. In order for the Gaussian approximation to be valid, we require $\widetilde{r_0} \gg \widetilde{g_0}, \widetilde{u_0}$. In Figure 7.2, we plot the Landau coefficients for the spin half transverse field Ising model (TFIM) as a function of the transverse magnetic field. The left hand plot shows the coefficients in the absence of a longitudinal magnetic field, and the right hand plot shows the coefficients in the presence of a longitudinal field having the same strength as the nearest neighbour exchange interaction

between spins. The TFIM is discussed in Section 7.2. We find that, in the absence of a longitudinal field, the point at which $\widetilde{r_0}$ and $\widetilde{g_0}$ cross corresponds to the point at which corrections due to fluctuations begin to have significant impact on the longitudinal magnetization (the order parameter) of the system, shown in Figure 7.4. When a longitudinal field is applied, we see that $\widetilde{r_0} > \widetilde{g_0}, \widetilde{u_0}$ for any value of the transverse field, hence the system is stabilized against order parameter fluctuations, in line with our expectations.

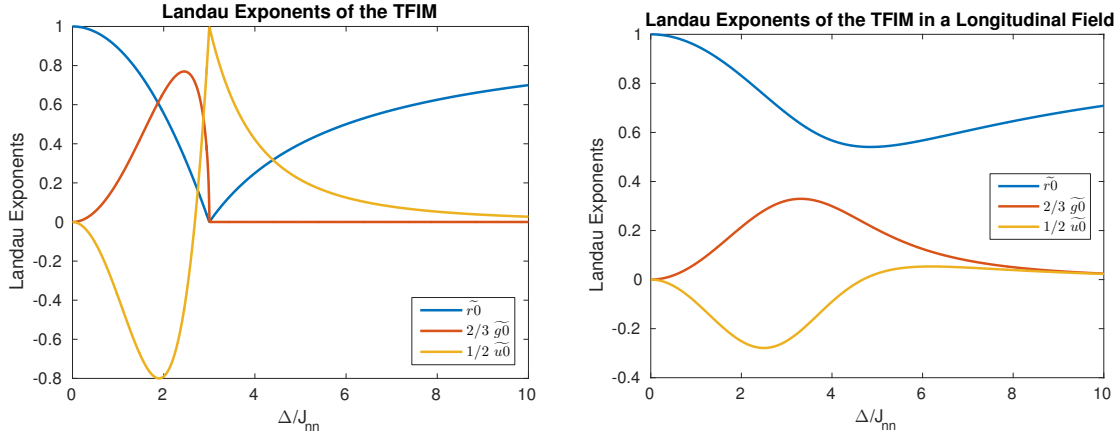

Figure 7.2: In this figure, we plot the Landau exponents, $\widetilde{r_0}, \widetilde{g_0}, \widetilde{u_0}$ given in equations 7.23 and 7.24, of the effective field theory for the transverse field Ising model at zero temperature, as a function of the transverse field Δ. The figure on the left shows the system in the absence of a longitudinal field, whereas the figure on the right shows the exponents in the presence of a longitudinal field of $h = J_{nn}$, where J_{nn} is the nearest neighbour exchange interaction between the spins.

In Figure 7.3, we plot the Landau coefficients of the spin half spin half model (SHSH) in the left hand plot, and for $LiHoF_4$ in the right hand plot. The SHSH model is given in equation (7.37). We take $\varepsilon = 0$, so that there is no transverse field acting directly on the nuclear spins, and consider a weak isotropic hyperfine interaction, $A_z = A_\perp = 0.01 J_{nn}$, where J_{nn} is the strength of the exchange interaction. In this limit, one might expect the Landau coefficients to reduce to those of the TFIM; however, comparing the $\widetilde{u_0}$ function of the SHSH model with that obtained from the TFIM, we find this is not the case. The discrepancy between the two plots persists even when the hyperfine interaction is further reduced. The reason for this is that, at the MF level, when the hyperfine interaction is taken to zero in the SHSH model the Hamiltonian consists of two disjoint copies of the TFIM, with each copy corresponding to a different nuclear spin state. The interaction term in the Hamiltonian couples these two subspaces. That is, a fluctuation in one nuclear subspace may have an effect on the other nuclear subspace. These additional degrees of freedom are not present in the TFIM. In the plot of the Landau coefficients of $LiHoF_4$ on the right hand side of Figure 7.3, it appears that

the fluctuations will only play a role in a narrow region around the quantum critical point. A glance at the plot of the longitudinal magnetization of $LiHoF_4$ shown in Figure 7.6 indicates this is not the case. The problem is that the Landau MF field theory fails to take into account the frustrated long range nature of the dipolar interaction, which causes the $LiHoF_4$ system to be significantly more susceptible to the effect of fluctuations than is indicated by the Landau MF theory. The condition $\widetilde{r_0} \gg \widetilde{g_0}, \widetilde{u_0}$ is necessary for the effect of fluctuations to be small; however, as the $LiHoF_4$ system demonstrates, it is not sufficient.

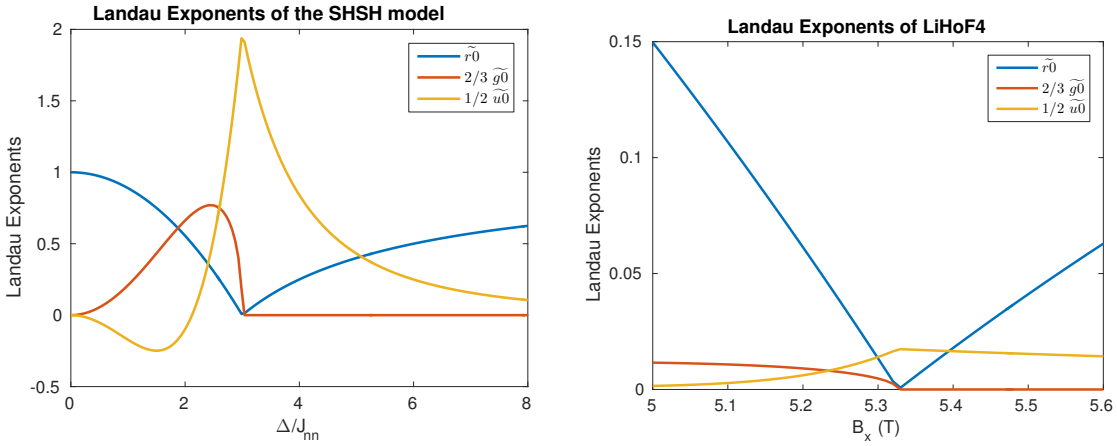

Figure 7.3: In this figure, we plot the zero temperature Landau exponents, $\widetilde{r_0}, \widetilde{g_0}, \widetilde{u_0}$ given in equations 7.23 and 7.24, of the effective field theory for the spin half spin half model (left) and $LiHoF_4$ (right), as a function of the transverse magnetic field. For the spin half spin half model, given in equation (7.37), we assume a nearest neighbour exchange interaction J_{nn} between spins, and we assume there is no effective field acting directly on the nuclear spins ($\varepsilon = 0$). We assume a weak isotropic hyperfine interaction $A_z = A_\perp = 0.01 J_{nn}$. The $LiHoF_4$ Hamiltonian is given in equation (7.39).

Spin Half Transverse Field Ising Model

We now apply the theory developed for including the effects of fluctuations in quantum Ising systems to find the leading order zero temperature correction to the magnetization of the spin half transverse field Ising model. This may be compared to the result of Stinchcombe given in equation (2.43) of [63]. We note that Stinchcombe's result is obtained by differentiating the free energy given in equation (6.82), rather than evaluating equation (7.1), so the following calculation is an independent consistency check of the theory.

For a spin half system, the leading order zero temperature correction to the magnetization is given by

$$\langle S^z \rangle_1 = \frac{R_0}{2N} \sum_k V_k (c_{11} - c_{22}) |c_{12}|^2 A_3, \tag{7.27}$$

where

$$R_0 = \frac{E_{21}^2}{E_{k=0}^2}, \tag{7.28}$$

and, assuming the RPA mode and mean field energy level are not degenerate,

$$A_3 = \frac{-2E_{21}}{E_k^2 - E_{21}^2} - \frac{3E_{21}^2 - E_k^2}{E_{21}^2 - E_k^2} \frac{1}{E_k}. \tag{7.29}$$

The MF matrix elements, energy levels, and RPA mode are derived in Appendix B.

The correction to the MF magnetization vanishes in the paramagnetic phase of the system, so we will focus on the ferromagnetic phase. Following Stinchcombe [63], we make the following definitions

$$x = \frac{2\Delta}{V_0} \qquad\qquad \gamma(k) = \frac{V_k}{V_0}, \tag{7.30}$$

where Δ is the transverse field acting on the system. In terms of these parameters, in the ferromagnetic phase of the system, we find

$$E_{21} = \frac{\Delta}{x} \qquad\qquad E_k = \frac{\Delta}{x} \sqrt{1 - x^2 \gamma(k)}. \tag{7.31}$$

Plugging these values into A_3 yields

$$A_3 = -\frac{2}{x\Delta\gamma(k)} \left[\frac{1 + \frac{1}{2} x^2 \gamma(k)}{\sqrt{1 - x^2 \gamma(k)}} - 1 \right] \tag{7.32}$$

For the prefactor and matrix elements we find

$$R_0(c_{11}-c_{22})|c_{12}|^2 = \frac{x^2}{4}\frac{1}{\sqrt{1-x^2}} \tag{7.33}$$

Putting everything together yields

$$\langle S^z\rangle_1 = \begin{cases} -\frac{1}{2N\sqrt{1-x^2}}\sum_k\left[\frac{1+\frac{1}{2}x^2\gamma(k)}{\sqrt{1-x^2\gamma(k)}}-1\right] & \Delta<\Delta_c \\ 0 & \Delta\geq\Delta_c \end{cases} \tag{7.34}$$

which is in agreement with equation (2.43) of Stinchcombe [63]. We see that the prefactor R_0, which is missing from equation (2.10) of Stinchcombe [62], is required to obtain the correct result. We see that the approximation breaks down as $x\to 1$, or, equivalently, as $\Delta\to\Delta_c$. This is to be expected because in the critical region fluctuations contribute at all orders, and cannot be neglected. The Landau function discussed in Section 7.1 is suitable for a renormalization group treatment of a system's critical behaviour.

We now specialize to the case of a simple cubic crystal, with lattice spacing a, and a nearest neighbour exchange interaction. In this case, we have $V_k = 2J[\cos(k_x a)+\cos(k_y a)+\cos(k_z a)]$, and $\gamma_k = \frac{V_k}{6J}$. The MF magnetization in the ferromagnetic phase of the system is

$$\langle S^z\rangle_0 = \frac{1}{2}\sqrt{1-x^2}, \tag{7.35}$$

with $x=\frac{\Delta}{3J}$, and the leading order correction to the longitudinal magnetization in the ferromagnetic phase is

$$\langle S^z\rangle_1 = -\frac{1}{4N\langle S^z\rangle_0}\sum_k\left[\frac{1+\frac{1}{2}x^2\gamma(k)}{\sqrt{1-x^2\gamma(k)}}-1\right]. \tag{7.36}$$

In Figure 7.4, we plot the MF magnetization of the transverse field Ising model, along with the leading order correction calculated from equation (7.36). We see that the correction becomes unreliable, and, in fact, diverges near the quantum critical point, where fluctuations become important. The leading order correction to the critical value of the transverse field follows from the point at which the corrected magnetization reaches zero. As discussed by Stinchcombe in [63], the correction to the transverse field is consistent with the result obtained by considering the transverse magnetization, or the longitudinal static susceptibility, neither of which suffer from the divergence seen in the corrected magnetization. We find for the transverse Ising model the critical transverse field is about 95% of its MF value.

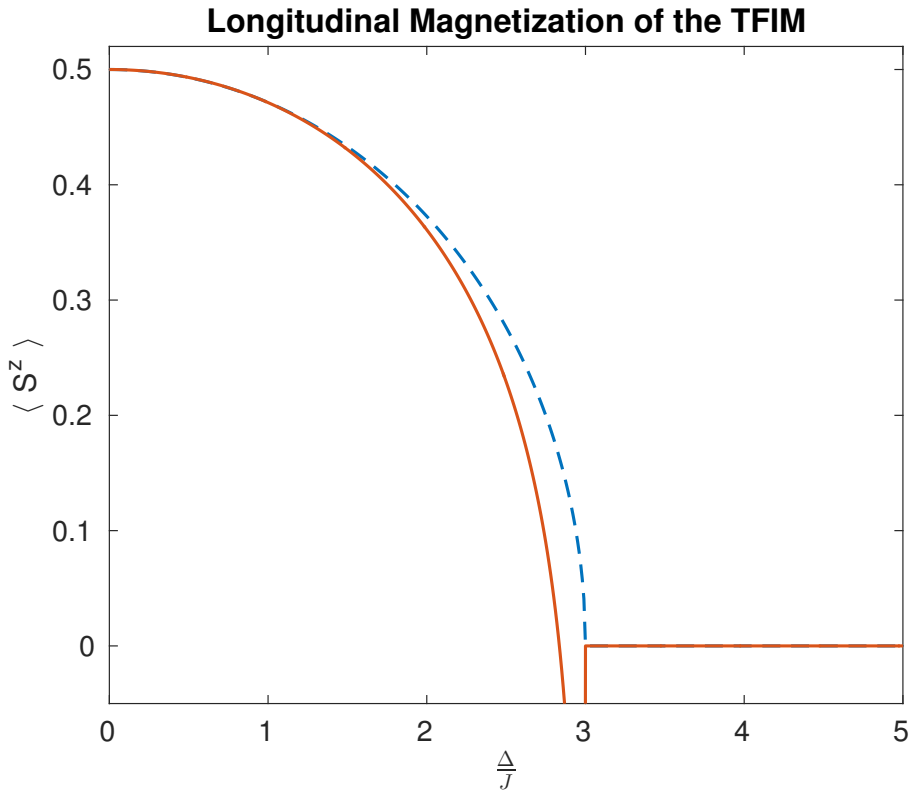

Figure 7.4: In this figure, we plot the mean field longitudinal magnetization of the transverse field Ising model (dashed line), along with the leading order correction in the high density approximation calculated from equation (7.36), as a function of the transverse field Δ. We consider a simple cubic crystal with exchange interaction strength J. We see the theory breaks down in the vicinity of the critical transverse field where fluctuations become more important. The point at which the corrected magnetization reaches zero gives the leading order correction to the critical transverse field. We find $\Delta_c \approx 2.84J$.

Spin Half Spin Half Model

In this section, we calculate the leading order correction to the MF magnetization of the spin half spin half model

$$H = -\frac{1}{2}\sum_{i\neq j} V_{ij} S_i^z S_j^z - \Delta \sum_i \left(S_i^x - \varepsilon I_i^x \right) + A_z \sum_i I_i^z S_i^z + \frac{A_\perp}{2} \sum_i (I_i^+ S_i^- + I_i^- S_i^+). \tag{7.37}$$

We include a transverse field $\Delta_n = \varepsilon\Delta$ acting directly on the nuclear spins because in systems such as $LiHoF_4$, the effective transverse field acting on the nuclear spins can be a significant fraction of the effective field splitting the electronic levels. We take our interaction to be

$$V_{ij} = J_D D_{ij}^{zz} - J_{nn}\delta_{ij}, \tag{7.38}$$

with D_{ij}^{zz} being the longitudinal dipolar interaction, and J_{nn} being a nearest neighbour exchange interaction. We assume a long thin cylindrical sample, or needle like domain, in a material with a simple cubic Bravais lattice. In this case, as discussed in Chapter 3, the dipolar interaction is given by (in momentum space)

$$a^3 D_k = \begin{cases} \frac{4\pi}{3} & : k = 0 \\ \frac{4\pi}{3} + \frac{4\pi}{3}\left(1 - 3\frac{k_z^2}{k^2}\right) & : k \neq 0 \end{cases}$$

with a being the unit cell length. At $k = 0$, we have the Lorentz local field, and no contribution from the demagnetization field, which is zero in a long cylinder. Away from $k = 0$, we use the result for a spherical sample, which is valid provided $kR >> 1$, with R being the system size. In momentum space, our total interaction will be $V_k = J_D D_k^{zz} - 2J_{nn}[\cos(k_x a) + \cos(k_y a) + \cos(k_z a)]$. In this toy model, we allow both J_D and J_{nn} to be tunable parameters. This allows us to investigate how the competition between dipolar and exchange energies (ferromagnetic for $J_{nn} < 0$, or antiferromagnetic for $J_{nn} > 0$) affects the magnitude of the corrections to MF theory. We may also reduce the overall strength of the interaction, $V_k \to pV_k$, with $p < 1$, in accordance with what is expected if some of the magnetic ions in the crystal are doped with non-magnetic impurities.

We take $J_D = 0$ and $\varepsilon = 0$, and we set $A_z = A_\perp$. This corresponds to an exchange coupled transverse field Ising model with an isotropic hyperfine interaction. The calculation of the leading order correction to the magnetization, given in equation (7.17), involves summations of complicated functions over the MF energy levels and the Brillouin zone. We do the summations numerically. In order to test that the numerical summations are correct, we consider the SHSH model with $A_z = A_\perp = 0.01 J_{nn}$. With this small value of the isotropic hyperfine interaction, we expect that the results will be similar to the result for the transverse field Ising model with no hyperfine interaction, which is illustrated in Figure 7.4, and indeed, this is the case. The program used to calculate the summations in the SHSH model is easily adapted to systems with Hamiltonians containing more MF eigenstates, such as $LiHoF_4$. In Figure 7.5, we plot the MF magnetization and corrected magnetization of the SHSH model with $A_z = A_\perp = 0.01 J_{nn}$. We leave further investigation of the effects of fluctuations in the SHSH model as the subject of future work.

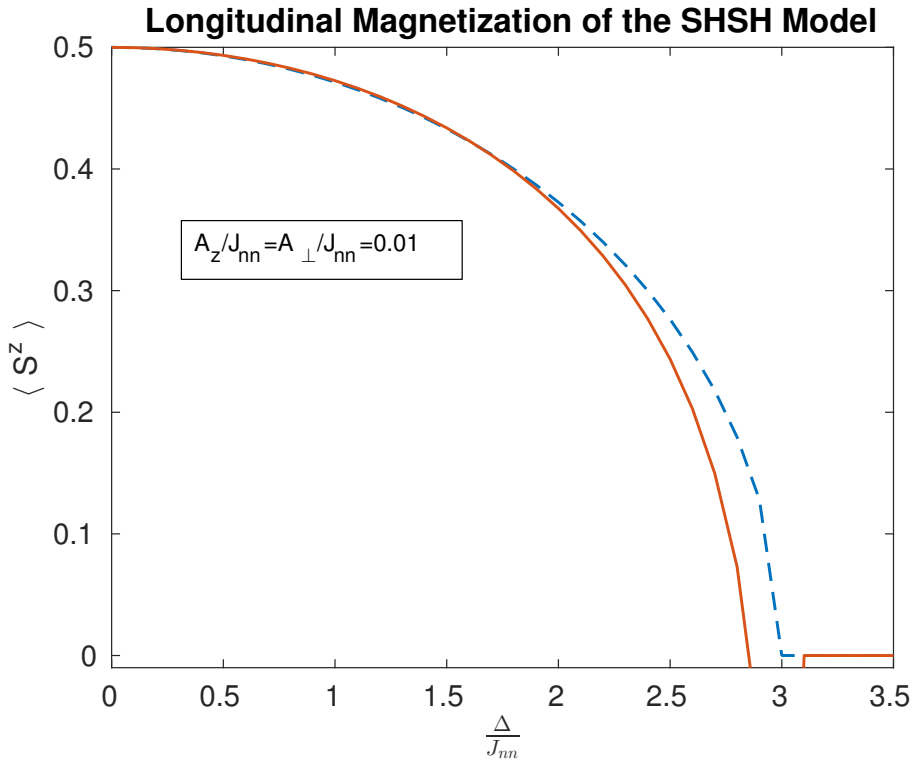

Figure 7.5: In this figure, we plot the MF magnetization of the spin half spin half model given in equation (7.37), along with its leading order correction in the high density approximation calculated from equation (7.17). We set the dipolar interaction to zero, and assume no transverse field acting directly on the nuclear spins. We assume an isotropic hyperfine interaction, with $A_z = A_\perp = 0.01 J_{nn}$.

LiHoF4

In this section, we obtain the leading order correction to the longitudinal magnetization of $LiHoF_4$, using the effective low temperature Hamiltonian

$$\begin{aligned} H = &-\frac{\Delta}{2}\sum_i \tau_i^x - \frac{1}{2}J_D C_{zz}^2 \sum_{i\neq j} D_{ij}^{zz}\tau_i^z\tau_j^z + \frac{1}{2}J_{nn}C_{zz}^2 \sum_{<ij>} \tau_i^z\tau_j^z + \\ &+ \sum_i \vec{\Delta}_n \cdot \vec{I}_i + A_z \sum_i \tau_i^z I_i^z + A_\perp \sum_i \tau_i^+ I_i^- + A_\perp^\dagger \sum_i \tau_i^- I_i^+ + \\ &+ A_{++}\sum_i \tau_i^+ I_i^+ + A_{++}^\dagger \sum_i \tau_i^- I_i^- . \end{aligned} \tag{7.39}$$

All the parameters in the model are given in Chapter 2. The longitudinal magnetization is given by $J^z \approx C_{zz}\langle\tau^z\rangle_0 + C_{zz}\langle\tau^z\rangle_1$, where $\langle\tau^z\rangle_0$ is the MF expectation value of the Pauli operator τ^z, and $\langle\tau^z\rangle_1$ is given by equation (7.17). The interaction in equation (7.17) is given by $V_k = C_{zz}^2[J_D D_k^{zz} - J_{nn}\gamma_k]$, and all the relevant matrix elements, MF energy levels, and RPA modes are calculated in Chapter 5.

B_x	4.0T	4.9T	5.4T	6.0T
$\langle J^z\rangle_0$	3.2293	1.7784	$2.8 * 10^{-7}$	$3.0 * 10^{-8}$
N=20 $\langle J^z\rangle_0 + \langle J^z\rangle_1$	1.5102	-2.8062	$-1.0 * 10^{-5}$	$-8.2 * 10^{-8}$
N=30 $\langle J^z\rangle_0 + \langle J^z\rangle_1$	1.4951	-2.8502	$-1.0 * 10^{-5}$	$-8.3 * 10^{-8}$
N=40 $\langle J^z\rangle_0 + \langle J^z\rangle_1$	1.4873	-2.873	$-1.0 * 10^{-5}$	$-8.4 * 10^{-8}$
N=50 $\langle J^z\rangle_0 + \langle J^z\rangle_1$	1.4825	-2.8869	$-1.0 * 10^{-5}$	$-8.4 * 10^{-8}$

Table 7.1: In this table, we show corrections to the mean field magnetization of $LiHoF_4$ calculated using the high density approximation. Each column corresponds to a different value of the applied transverse magnetic field B_x, and each row corresponds to a finer division of the Brillouin zone (a larger value of N in equation (7.40)).

This calculation is complicated by the Brillouin zone summations. We perform the summations by brute force, summing over finer and finer divisions of the Brillouin zone until suitable convergence is achieved. We carve up the positive quadrant of the Brillouin zone as follows,

$$k_x, k_y \in \left[0, \frac{k_x, k_y}{N}, \frac{\pi}{a}\right] \qquad\qquad k_z \in \left[0, \frac{k_z}{N}, \frac{\pi}{c}\right], \tag{7.40}$$

where $a = 5.175$Å, and $c = 10.75$Å, are the transverse, and longitudinal, lattice spacings of $LiHoF_4$. All other Brillouin zone points may be included via symmetry considerations. We illustrate the convergence by looking at four values of transverse magnetic field, $4.0T, 4.9T, 5.4T$ and $6.0T$. These represent points in the ferromagnetic phase of the system, at the experimental value of the critical transverse field, at the MF value of the critical transverse field, and in the paramagnetic phase of the sytem, respectively. In Table 7.1, we list the corrected magnetization for $N = 20, 30, 40,$ and 50. The point to take from the table is that, even for our most coarse division of the Brillouin zone (N=20), the sums are converging to within two significant figures, with the least reliable correction being near the experimental critical point where the correction diverges.

In Figure 7.6, we plot the longitudinal MF magnetization of $LiHoF_4$, along with the leading order correction in the high density approximation calculated from equation (7.17). Due to the frustrated long range nature of the dipolar interactions in $LiHoF_4$, we expect the effect of fluctuations to be significant, and indeed, we find this to be the case. We also expect, due to the long range nature of the interaction, that the leading order correction in a high density approximation will be accurate, except in the vicinity of the critical point where the

formalism breaks down. The experimental value of the critical transverse field is $B_x^c = 4.9\text{T}$. The leading order correction to the magnetization gives a critical value of the transverse field of about $B_x^c = 4.4\text{T}$, significantly underestimating the experimental value. It is not clear whether this discrepancy is due to the choice of crystal field parameters, and the magnitude of the exchange interaction, or whether it is a shortcoming of the approximation. The reduced critical temperature in this approximation is about 81% of its MF value.

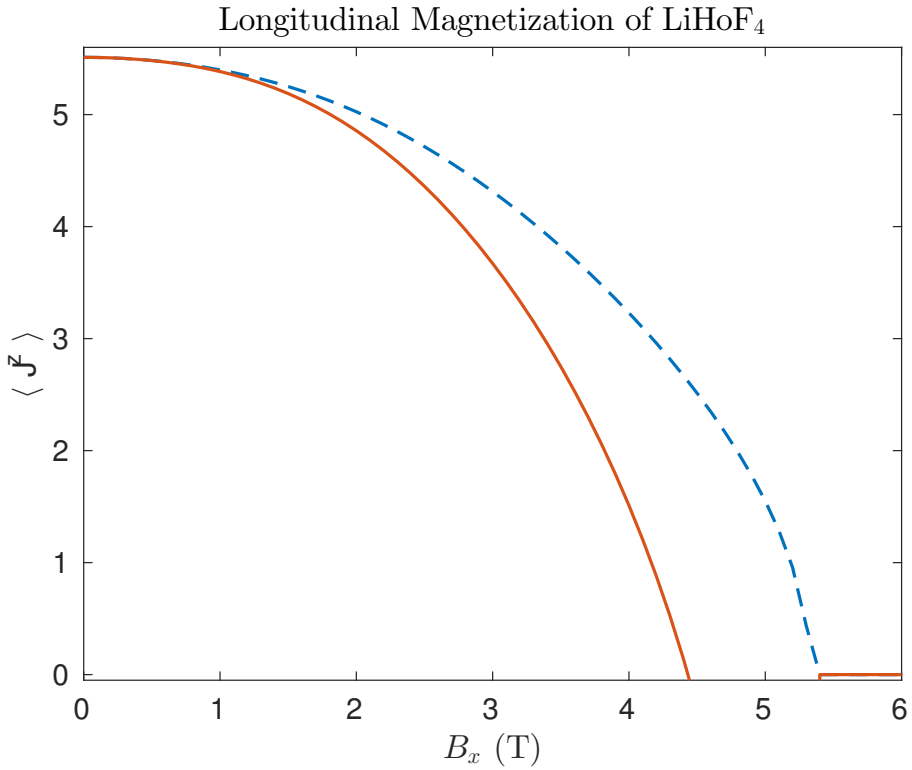

Figure 7.6: The figure above shows the MF longitudinal magnetization of $LiHoF_4$ (dashed line), along with the leading order correction calculated from equation (7.17), as a function of the transverse field B_x. The point at which the corrected magnetization reaches zero gives the leading order correction to the critical transverse field. We find $B_x^c \approx 4.4\text{T}$. The experimental value of the critical transverse field is $B_x^c = 4.9\text{T}$; hence, with our choice of crystal field parameters, and nearest neighbour exchange interaction, the leading order correction underestimates the critical transverse field by about as much as it is overestimated by MF theory.

Summary

In this chapter, we have the high density approximation developed in Chapter 6 to find the leading order correction to the magnetization of several quantum Ising systems. We began by discussing the form of the correction to the magnetization for a general quantum Ising system, and then, in Section 7.1, we discussed how to derive a Landau free energy function from our more general formalism. The coefficients of the Landau theory may be used to estimate when fluctuations will have a significant impact on a quantum Ising system.

In Section 7.2, we applied the theory to the spin half transverse field Ising model (TFIM), making contact with the results derived by Stinchcombe in [63]. In Section 7.37, we applied the formalism to the spin half spin half (SHSH) model. The calculation of the corrections to the MF magnetization involves Brillouin zone summations over complicated functions. By considering the SHSH model with a small hyperfine interaction, we reproduced the results obtained for the TFIM, which verifies the program used to calculate the numerical summations is correct. Section 7.4 is concerned with the application of the theory to the magnetic insulator $LiHoF_4$. We found the corrections to MF theory to be quite large, which is to be expected in a dipolar coupled system.

Chapter 8

Conclusions and Future Work

The work in this thesis can be divided into two main parts: (1) the properties of the magnetic insulating crystal $LiHoF_4$, and (2) the development of a formalism for incorporating the effect of fluctuations in general quantum Ising systems, of which $LiHoF_4$ is a particular example.

Regarding (1), we have introduced a new effective low temperature Hamiltonian for $LiHoF_4$ that fully incorporates the nuclear degrees of freedom in Chapter 2. We find that the dominant mixing of the hyperfine states is due to an effective transverse field acting directly on the nuclear spins. This field is an order of magnitude larger than the effective transverse component of the hyperfine interaction. The origin of this effective field is a shift in the $4f$ electron cloud of each Ho^{3+} ion due to an applied transverse magnetic field. Chapter 3 contains an analysis of the dipole-dipole interaction that is the dominant coupling between the electronic degrees of freedom in $LiHoF_4$. The Fourier analysis of the long range dipolar interaction, taking into consideration the underlying lattice of the $LiHoF_4$ crystal, is an important aspect of the theoretical investigation of the material.

In Chapter 4, we present the spin half spin half (SHSH) model

$$H = -\frac{1}{2}\sum_{i\neq j} V_{ij} S_i^z S_j^z - \Delta \sum_i S_i^x + A_z \sum_i S_i^z I_i^z + \frac{A_\perp}{2}\sum_i (S_i^+ I_i^- + S_i^- I_i^+), \tag{8.1}$$

a toy model meant to illustrate the effects of an anisotropic hyperfine interaction in a transverse field Ising system. We find that $A_z > A_\perp$ leads to an enhancement of the single ion susceptibility, an increase in the critical transverse field, as well as an enhancement of an applied longitudinal field. The enhancement of a longitudinal field has not been previously noted. With the addition of a transverse field acting directly on the nuclear spins, equation (8.1) serves as a toy model for $LiHoF_4$. We go on to analyze the zero temperature spectrum of the SHSH model in the random phase approximation (RPA). We find that what would have been the electronic soft mode is gapped by the hyperfine interaction, with spectral weight being transferred to a lower

energy electronuclear mode that fully softens at the quantum critical point. In Chapter 5, we perform an RPA analysis of the $LiHoF_4$ system, observing behaviour of the low energy modes similar to that of the toy model.

Regarding (2), we have made use of the well known Hubbard-Stratonovich transformation to derive an effective field theory for quantum Ising systems with an arbitrary single ion Hamiltonian in Chapter 6. This formalism is used to derive a diagrammatic perturbation theory for incorporating the effects of fluctuations in quantum Ising systems beyond the RPA. We find the formalism to be equivalent to the high density approximation of Brout [60, 61], which has been applied to the spin half transverse field Ising model by Stinchcombe [26, 62, 63]; however, the field theoretic derivation offers significant simplicity and clarity when compared to previous approaches. Basically, in this thesis, we have taken a ground up approach. We have used the Hubbard-Stratonovich transformation to obtain an effective field theory suitable for renormalization group analysis of a system's critical behaviour, and we have worked in a basis of mean field eigenstates (Hubbard operators) in order to rigorously obtain the theory. We find that a regular nuclear spin bath, or any other regular modification to the single ion Hamiltonian, will not fundamentally alter the nature of the quantum phase transition in a transverse field Ising system. The strength of the field theoretic formalism developed in this thesis is its versatility. It is easily applied to real quantum Ising ferromagnets such as $LiHoF_4$, and the formalism may be generalized to study antiferromagnetic materials and spin glass, as well as offering the possibility of studying quantum Ising systems in time dependent potentials. We have demonstrated the validity of the formalism by applying it to the calculation of corrections to the zero temperature magnetization of $LiHoF_4$ in Chapter 7.

Future Work

The work presented in this thesis, in particular the field theoretic formalism presented in Chapter 6, has many interesting applications beyond the scope of what is presented in this thesis. Furthermore, there remain many fascinating possibilities for further research on $LiHoF_4$. We conclude this thesis with a discussion of this future work. To begin, we discuss some easy applications of the random phase approximation (RPA) to $LiHoF_4$ that we have left undeveloped. We proceed to consider a fluctuation analysis of $LiHoF_4$ that goes beyond the magnetization corrections presented in Chapter 7, and some interesting modifications of the Hamiltonian for future deliberation. We move on from $LiHoF_4$ by discussing some possible improvements of the field theoretic formalism presented in Chapter 6, and outlining a few of its most significant applications.

Our primary focus in this thesis has been on the behaviour of quantum Ising systems in

the zero temperature limit. The RPA results for the spin half spin half (SHSH) model, and for $LiHoF_4$, presented in Chapters 4 and 5 respectively, are easily generalized to finite temperatures. The SHSH model will yield analytic expressions for the temperature dependence of experimentally relevant quantities, such as the paramagnetic susceptibility. Furthermore, our analysis of the SHSH model and $LiHoF_4$ has been focused on the dynamic longitudinal electronic susceptibility, which is relevant to, for example, neutron scattering experiments. A calculation of the transverse electronic susceptibility, and the specific heat, is straightforward, and would be of experimental interest, as would a calculation of the nuclear susceptibilities. The dynamic nuclear susceptibilities, or equivalently, the nuclear correlation functions, are of particular interest as they are relevant to magnetic resonance experiments that may be used to probe the low energy properties of the $LiHoF_4$ system. See the paper of Schechter and Stamp for further details [38].

Our fluctuation analysis of quantum Ising systems in Chapter 7 is limited to the zero temperature magnetization, this being the simplest application of the field theoretic formalism. We would like to see these calculations generalized to finite temperatures, and we would like to see the field theoretic formalism applied to the calculation of dynamic correlation functions, which yield the energies and lifetimes of excited states. The groundwork for such calculations has been laid out in Chapter 6 and Appendix E. In particular, it would be interesting to use the field theoretic formalism to see if the longitudinal hyperfine interaction in $LiHoF_4$ stabilizes the system against the disordering effects of thermal fluctuations, or a transverse magnetic field. In low transverse fields, this may account for the discrepancy between the experimental phase diagram and the phase diagram that has been obtained from Monte Carlo simulations [69]. Using the effective low temperature Hamiltonian for $LiHoF_4$, derived in Chapter 2, it would also be of interest to compare results obtained from the field theoretic formalism of Chapter 6 to results obtained using the effective medium theory of Jensen, results obtained using the correlated effective field approximation of Lines, and results obtained via Monte Carlo simulations. The formalisms of Jensen and Lines are discussed in the introduction to Chapter 6. The role of fluctuations when there is competition between dipolar and exchange interactions, such as in $LiHoF_4$, is another interesting avenue for future work. The SHSH model, as presented in Section 7.3, is amenable to such an investigation.

Regarding the $LiHoF_4$ Hamiltonian derived in Chapter 2, we would like to see it analyzed with modifications to account for doping of the system with non-magnetic yttrium ions, and the inclusion of an oscillator bath environment. A preliminary theoretical investigation of the effect of doping has been carried out by Schechter and Stamp [37, 38], and of the effects of an oscillator bath environment by Banerjee and Dattagupta [94]; however, none of this work takes full account of the complexity of the low temperature $LiHoF_4$ Hamiltonian. In the work of

Banerjee and Dattagupta, only a longitudinal hyperfine interaction is considered. Schechter and Stamp consider transverse hyperfine interactions; however, the effective transverse field acting directly on the nuclear spins upon application of a physical transverse field is not apparent in their work. Furthermore, we would like to see the model used to calculate the dynamics of the system with time dependent parameters, thus going beyond the thermodynamics that has been the primary focus of this thesis. In particular, we would like to see the model used to calculate Landau-Zener transitions, and the effects of an AC magnetic field.

We have discussed some possibilities for future research on $LiHoF_4$ relevant to the work done in this thesis. We now consider the field theoretic formalism of Chapter 6, and some of its potential applications apart from the $LiHoF_4$ system. The primary drawback of the field theoretic formalism is the algebraic complexity of the resulting equations, and the need to perform Brillouin zone summations over complicated functions. The algebraic difficulties stem from the calculation of the spin cumulants that make up the coefficients of the field theory. Simplifications, or approximations, of the spin cumulants would be of considerable use. In order to utilize the field theoretic formalism, it would be useful to optimize the time required to perform the Brillouin zone summations necessary for acquiring results. In this thesis, the Brillouin zone summations have been performed by brute force. Consideration of the symmetry of the underlying crystal lattice will lead to improvements over the brute force approach.

A simple application of the field theoretic formalism, to a system with more complexity than the spin half transverse field Ising model, is to the Blume-Capel model

$$H = -D\sum_i (1-(S_i^z)^2) + \vec{H}\sum_i \vec{S}_i + J\sum_{\langle ij\rangle} S_i^z S_j^z, \tag{8.2}$$

where we take $\vec{S}$ to be spin one. In a spin one system, the spin cumulants, and hence the coefficients of the effective field theory, will be more complicated than in the spin half case; however, they will be much simpler than in a system with four or more single ion energy levels. The parameter D may be used to control the number of $S^z = 0$ states occuring in the system. With $D = -\infty$ the model reduces to the spin half case, and with $D = 0$ we have a standard spin one Ising system. This model was introduced in 1966 by Blume in an attempt to model the antiferromagnetic insulator UO_2 [114], and more generally in a series of papers by Capel to account for the behaviour of triplet ($S = 1$) spin systems [115–117]. A variant of the model was introduced by Blume, Emery, and Griffiths in an attempt to model $He^3 - He^4$ mixtures [118]. As discussed in the book of Cardy, the Blume-Capel model may also be used to study a spin half system with mobile vacancies corresponding to the $S^z = 0$ states [119]. This model is of interest in the study of phase transitions because the order of the phase transition depends on the parameter D. We would like to see the field theoretic formalism of Chapter 6 applied to

the interesting and versatile Blume-Capel model.

In the development of the field theoretic formalism of Chapter 6, we have limited ourselves to the consideration of ferromagnetic interactions between spins. We may equally well consider antiferromagnetic interactions; however, the field in the resulting theory is no longer a valid order parameter. Instead, if the system has a bipartite lattice, we must consider the staggered magnetization which corresponds to making the field transformation $Q \to (-1)^{\|\vec{r}\|}Q$, where $\|\vec{r}\|$ is even or odd depending on which subsytem the vector $\vec{r}$ points to. For example, in the antiferromagnetic Ising system $DyPO_4$, discussed by Wright *et al.* in reference [120], $\|\vec{r}\|$ is the minimum number of lattice steps between the origin and the lattice point at $\vec{r}$. With a suitable modification of $\|\vec{r}\|$ it is possible to study layered antiferromagnetic materials such as $FeCl_2$, the properties of which are discussed in a chapter of the book by Barbara *et al.* [71]. This material is of particular interest because the Fe ions may be replaced with non-magnetic Mg ions in $Fe_xMg_{1-x}Cl_2$. This leads to random field effects in the presence of a longitudinal magnetic field, as discussed by, for example, Fishman and Aharony, and Cardy [121, 122]. These random field effects are reminiscent of the random field effects in $LiHo_xY_{1-x}F_4$, in which dilution leads to a random field via the off diagonal components of the dipolar interaction [37].

The quenched nature of the disorder in dilute quantum Ising systems, such as $Fe_xMg_{1-x}Cl_2$ and $LiHo_xY_{1-x}F_4$, may be accounted for using the formalism of Chapter 6 by making use of Anderson's replica trick [43]. As discussed by Stephen and Aharony [123], by considering a set of n replicas of the system, and first averaging over the disorder, then expanding and resumming the resulting equation, the partition function may be written $Z(n) = Z_0\langle \exp(-\beta\mathscr{H})\rangle$, with

$$\mathscr{H} = \sum_{ij}\sum_{l} K_l(ij) f_l(ij). \tag{8.3}$$

The coefficients $K_l(ij)$ are functions of the interaction and the concentration of dopents, and

$$\begin{aligned} f_1(ij) &= \sum_{\alpha=1}^{n} S^z_{i\alpha}S^z_{j\alpha} \qquad\qquad f_2(ij) = \sum_{\alpha<\beta} S^z_{i\alpha}S^z_{j\alpha}S^z_{i\beta}S^z_{j\beta} \\ f_l(ij) &= \sum_{\alpha_1<\alpha_2\cdots\alpha_l} S^z_{i\alpha_1}S^z_{j\alpha_1}S^z_{i\alpha_2}S^z_{j\alpha_2}\cdots S^z_{i\alpha_l}S^z_{j\alpha_l}, \end{aligned} \tag{8.4}$$

where the summations are over the n replicas of the system. A Hubbard-Stratonovich transformation may now be applied to each of the l terms in equation (8.3), which yields a set of competing order parameters for the system. The work in this thesis provides a way to carry out the procedure for real magnetic systems such as $LiHo_xY_{1-x}F_4$.

In the work presented in this thesis, we have not considered Hamiltonians with time de-

pendent parameters. A time dependent longitudinal magnetic field is easily included in the field theoretic formalism Chapter of 6, with the assumption being that the system remains in thermodynamic equilibrium so that at each moment in time $Z(t) = \langle \exp(-\beta H(t)) \rangle$ yields the distribution of the system. Note that in the Matsubara formalism we have

$$Z = Z_0 \left\langle T_\tau \exp\left[\int_0^\beta d\tau V(\tau) \right] \right\rangle_0 . \tag{8.5}$$

This encodes corrections to the free energy, $F = -\frac{1}{\beta} \ln Z$, due to both spatial and temporal fluctuations. With the time dependent part of the Hamiltonian included in $V(\tau)$, our basis of eigenstates is time independent. However, the formalism contains memory effects through the time dependence of $V(\tau)$. A preliminary investigations shows that the time dependence yields a shifted free energy with a complex part corresponding to the decay rate of the collective spin wave excitations. We see this as an interesting and fruitful avenue for future research.

We have discussed further research to be done on the magnetic insulator $LiHoF_4$, as well as some of the future applications of the field theoretic formalism developed in this thesis, which is suitable for treating general quantum Ising systems. This includes applications to disordered systems, and systems with time dependent parameters. We think these topics will be among the most important physics of the 21st century, and would welcome the opportunity to pursue this research further.

Bibliography

[1] Bertrand Russell. *The History of Western Philosophy*. Simon and Schuster, 1st edition, 1945. → pages 1

[2] Stephen Blundell. *Magnetism: A Very Short Introduction*. Oxford University Press, 1st edition, 2012. → pages 1

[3] W Heisenberg. Mehrkörperproblem und Resonanz in der Quantenmechanik. *Zeitschrift für Physik*, 38:411–426, 1926. → pages 2

[4] PAM Dirac. On the Theory of Quantum Mechanics. *Proc. of the Royal Society of London*, 112:661–677, 1926. → pages 2

[5] Nigel Goldenfeld. *Lectures on Phase Transitions and the Renormalization Group*. Westview Press, 1st edition, 1992. → pages 2, 4, 80, 186

[6] R Peierls. On Ising's Model of Ferromagnetism. *Mathematical Proceedings of the Cambridge Philosophical Society*, 32:477–481, 1936. → pages 3

[7] L Onsager. Crystal Statistics. 1. A Two-Dimensional Model with an Order-Disorder Transition. *Phys. Rev.*, 65:117–149, 1944. → pages 3

[8] JE Battison, A Kasten, MJM Leask, JB Lowry, and BM Wanklyn. Ferromagnetism in Lithium Holmium Fluoride: 2. Optical and Spectroscopic Measurements. *J. Phys. C: Solid State Physics*, 8:4089–4095, 1975. → pages 3, 32, 34

[9] J Magariño, J Tuchendler, JP D'Haenens, and A Linz. Submillimeter Resonance Spectroscopy of Ho^{3+} in Lithium Yttrium Fluoride. *Phys. Rev. B*, 13:2805–2808, 1976. → pages 30

[10] PE Hansen, T Johansson, and R Nevald. Magnetic properties of lithium rare-earth fluorides: Ferromagnetism in $LiErF_4$ and $LiHoF_4$ and crystal-field parameters at the rare-earth and Li sites. *Phys. Rev. B*, 12:5315–5324, 1975. → pages vii, 3, 24, 25

[11] AH Cooke, DA Jones, JFA Silva, and MR Wells. Ferromagnetism in $LiHoF_4$ 1: Magnetic Measurements. *J. Phys. C*, 8:4083–4088, 1975. → pages 3, 17, 33, 34

[12] PJ Walker. Melt Growth of $LiHoF_4$. *Journal of Crystal Growth*, 49:77–80, 1980. → pages 4

[13] J Magariño, J Tuchendler, P Beauvillain, and I Laursen. EPR Experiments in $LiTbF_4$, $LiHoF_4$, and $LiErF_4$ at Submillimeter Frequencies. *Phys. Rev. B*, 21:18–28, 1980. → pages 4, 30

[14] LM Holmes, T Johansson, and HJ Guggenheim. Ferromagnetism in $LiTbF_4$. *Solid State Communications*, 12:993–997, 1973. → pages 4

[15] C Kraemer, N Nikseresht, JO Piatek, N Tsyrulin, B Dalla Piazza, K Kiefer, B Klemke, TF Rosenbaum, G Aeppli, C Gannarelli, K Prokes, A Podlesnyak, T Strssle, L Keller, O Zaharko, KW Krmer, and HM Rønnow. Dipolar Ferromagnetism and Quantum Criticality in $LiErF_4$. *Science*, 336:1416–1419, 2012. → pages 4

[16] Conradin Kraemar. *Quantum Phase Transition in a Magnetic Model System*. PhD thesis, ETH Zürich, 2009. → pages viii, 4, 20, 22

[17] AI Larkin and DE Khmel'nitskii. Phase Transitions in Uniaxial Ferroelectrics. *Soviet Physics JETP*, 29:1123–1128, 1969. → pages 4

[18] A Aharony. Critical Behaviour of Magnets with Dipolar Interactions: V. Uniaxial Magnets in d Dimensions. *Phys. Rev. B*, 8:3363–3946, 1973. → pages 4

[19] A Aharony and BI Halperin. Exact Relations among Amplitudes at Critical Points of Marginal Dimensionality. *Phys. Rev. Lett*, 35:1308–1310, 1975. → pages

[20] E Brézin and J Zinn-Justin. Critical behaviour of uniaxial systems with strong dipolar interactions. *Phys. Rev. B*, 13:251–254, 1976. → pages 4

[21] J Nikkel and B Ellman. Testing renormalization group theory at the critical dimension in $LiHoF_4$. *Phys. Rev. B*, 64:214420–1–214420–3, 2001. → pages 5

[22] P Beauvillain, JP Renard I Laursen, and PJ Walker. Critical behaviour of the magnetic susceptibility of the uniaxial ferromagnet $LiHoF_4$. *Phys. Rev. B*, 18:3360–3368, 1978. → pages 5

[23] JA Griffin, M Huster, and RJ Folweiler. Critical behaviour of the spontaneous magnetization at marginal dimensionality in $LiHoF_4$. *Phys. Rev. B*, 22:4370–4378, 1980. → pages 5

[24] PG de Gennes. Collective Motions of Hydrogen Bonds. *Solid State Communications*, 1:132–137, 1963. → pages 5

[25] R Brout, KA Müller, and H Thomas. Tunnelling and Collective Excitations in a Microscopic Model of Ferroelectricity. *Solid State Communications*, 4:507–510, 1966. → pages 5

[26] RB Stinchcombe. Ising model in a transverse field: 1. Basic theory. *J. Phys. C.*, 6:2459–2483, 1973. → pages 5, 14, 15, 107, 120, 135, 156, 180, 189

[27] D Bitko, TF Rosenbaum, and G Aeppli. Quantum Critical Behaviour for a Model Magnet. *Phys. Rev. Lett.*, 77:940–943, 1996. → pages 5, 7, 17

[28] Subir Sachdev. *Quantum Phase Transitions*. Cambridge University Press, 1st edition, 1999. → pages 6, 7, 15, 195

[29] M Vojta. Quantum phase transitions. *Rep. Prog. Phys.*, 66:2069–2110, 2003. → pages 7

[30] SL Sondhi, SM Girvin, JP Carini, and D Shahar. Continious quantum phase transitions. *Reviews of Modern Physics*, 69:315–333, 1997. → pages 6, 195

[31] JA Hertz. Quantum Critical Phenomena. *Phys. Rev. B*, 14:1165–1185, 1976. → pages 6, 14, 107

[32] M Suzuki. Relationship between d-Dimensional Quantal Spin Systems, and (d+1)-Dimensional Ising Systems. *Progress in Theoretical Physics*, 56:1454–1469, 1976. → pages 7

[33] D Belitz and TR Kirkpatrick. Why Quantum Phase Transitions are Interesting. *Journal of Low Temperature Physics*, 126:1107–1121, 2002. → pages 7

[34] D Belitz, TR Kirkpatrick, and T Vojta. How generic scale invariance influences quantum and classical phase transitions. *Rev. Mod. Phys.*, 77:579–632, 2005. → pages 7

[35] G Mennenga, LJ de Jongh, and WJ Huiskamp. Field Dependent Specific Heat Study of the Dipolar Ising Ferromagnet $LiHoF_4$. *J. Magn. Magn. Mat.*, 44:59–76, 1984. → pages 8, 27, 31, 32, 33, 37

[36] HM Rønnow, R. Parthasarathy, J Jensen, G Aeppli, TF Rosenbaum, and DF McMorrow. Quantum Phase Transition of a Magnet in a Spin Bath. *Science*, 308:389–392, 2005. → pages 8, 15, 93, 95

[37] M Schechter and PCE Stamp. Significance of the Hyperfine Interactions in the Phase Diagram of $LiHo_xY_{1-x}F_4$. *Phys. Rev. Lett.*, 95:267208–1–267208–4, 2005. → pages 8, 13, 157, 159

[38] M Schechter and PCE Stamp. Derivation of the low-T phase diagram of $LiHo_xY_{1-x}F_4$: A dipolar quantum Ising magnet. *Phys. Rev. B*, 78:054438–1–054438–17, 2008. → pages 8, 13, 30, 157

[39] NV Prokof'ev and PCE Stamp. Theory of the Spin Bath. *Rep. Prog. Phys.*, 63:669–726, 2000. → pages 10, 11

[40] RP Feynman and FL Vernon. The Theory of a General Quantum System Interacting with a Linear Dissipative System. *Annals of Physics*, 24:118–173, 1963. → pages 10

[41] AO Caldeira and AJ Leggett. Quantum Tunnelling in a Dissipative System. *Annals of Physics*, 149:374–456, 1983. → pages 10

[42] M Dube and PCE Stamp. Dynamics of a pair of interacting spins coupled to an environmental sea. *Int. Jour. of Mod. Phys.*, 12:1191–1245, 1998. → pages 10

[43] M Mezard, G Parisi, and M Virasoro. *Spin Glass Theory and Beyond: An Introduction to the Replica Method and Its Applications*. World Scientific Publishing Co., 1st edition, 1987. → pages 12, 13, 159

[44] VS Denchev, S Boixo, SV Isakov, N Ding, R Babbush, V Smelyanskiy, J Martinis, and H Neven. What is the Computational Value of Finite-Range Tunneling? *Phys. Rev. X*, 6:031015–1–031015–19, 2016. → pages 12

[45] T Simonite. Google's Quantum Dream Machine. *MIT Technology Review*, 2015. → pages 12

[46] D Porras and JI Cirac. Effective quantum spin systems with trapped ions. *Phys Rev Lett*, 92:207901–1–207901–4, 2004. → pages 13

[47] JW Britton, BC Sawyer AC Keith, CC Joseph Wang, JK Freericks, H Uys, MJ Biercuk, and JJ Bollinger. Engineered two-dimensional Ising interaction in a trapped-ion quantum simulator with hundreds of spins. *Nature*, 484:489–492, 2012. → pages 13

[48] T Graß, D Raventós, B Juliá-Diaz, C Gogolin, and M Lewenstein. Quantum annealing for the number-partitioning problem using a tunable spin glass of ions. *Nature Communications*, 7:11524:1–9, 2016. → pages 13

[49] J Brooke, D Bitko, TF Rosenbaum, and G Aeppli. Quantum Annealing of a Disordered Magnet. *Science*, 284:779–781, 1999. → pages 13

[50] M Schechter. $LiHo_xY_{1-x}F_4$ as a random-field Ising ferromagnet. *Phys. Rev. B*, 77:020401–1–020401–4, 2008. → pages 13

[51] AJ Millis, AD Kent, MP Sarachik, and Y Yeshurun. Pure and random-field quantum criticality in the dipolar Ising model: Theory of Mn_12 acetates. *Phys Rev B*, 81:024423–1–024423–11, 2010. → pages 13

[52] DH Reich, TF Rosenbaum, and G Aeppli. Glassy Relaxation without Freezing in a Random Dipolar-Coupled Ising Magnet. *Phys. Rev. Lett.*, 59:1969–1972, 1987. → pages 13

[53] DH Reich, B Ellman, J Yang, TF Rosenbaum, G Aeppli, and DP Belanger. Dipolar magnets and glasses: Neutron-scattering, dynamical, and calorimetric studies of randomly distributed Ising spins. *Phys. Rev. B*, 42:4631–4644, 1990. → pages 13

[54] M Suzuki. Phenomenlogical Theory of Spin-Glasses and some Rigorous Results. *Progress in Theoretical Physics*, 58:1151–1165, 1977. → pages 13

[55] S Ghosh, R Parthasarathy, TF Rosenbaum, and G Aeppli. Coherent Spin Oscillations in a Disordered Magnet. *Science*, 296:2195–2198, 2002. → pages 13

[56] JA Quilliam, S Meng, and JB Kycia. Experimental phase diagram and dynamics of a dilute dipolar-coupled Ising system. *Phys Rev B*, 85:184415–1–184415–16, 2012. → pages 13

[57] MJP Gingras and P Henelius. Collective Phenomena in the $LiHo_xY_{1-x}F_4$ Quantum Ising Magnet: Recent Progress and Open Questions. *Journal of Physics: Conference Series*, 320:1–12, 2011. → pages 13

[58] AP Young. Quantum Effects in the Renormalization Group Approach to Phase Transitions. *J. Phys. C.*, 8:L309–L313, 1975. → pages 14, 106, 120

[59] M. Brando, D Belitz, FM Grosche, and TR Kirkpatrick. Metallic quantum ferromagnets. *Rev. of Modern Physics*, 88:025006–1–025006–71, 2016. → pages 14

[60] R Brout. Statistical Mechanical Theory of a Random Ferromagnet System. *Phys Rev*, 115:824–835, 1959. → pages 14, 15, 106, 107, 120, 156, 180, 182

[61] R Brout. Statistical Mechanical Theory of Ferromagnetism. High Density Behaviour. *Phys Rev*, 118:1009–1019, 1960. → pages 14, 15, 106, 107, 156, 180, 182

[62] RB Stinchcombe. Ising model in a transverse field: 2. Spectral functions and damping. *J. Phys. C.*, 6:2484–2506, 1973. → pages 14, 15, 107, 120, 135, 136, 138, 148, 156, 189

[63] RB Stinchcombe. Thermal and magnetic properties of the transverse Ising model. *J. Phys. C.*, 6:2507–2524, 1973. → pages 14, 15, 107, 120, 128, 135, 147, 148, 154, 156, 189

[64] PB Chakraborty, P Henelius, H Kjønsberg, AW Sandvik, and S.M. Girvin. Theory of the magnetic phase diagram of $LiHoF_4$. *Phys. Rev. B*, 70:144411–1–144411–13, 2004. → pages 17, 21, 25, 34, 35, 37, 72, 82

[65] J Jensen and AR Mackintosh. *Rare Earth Magnetism Structures and Excitations*. Clarendon Press - Oxford, 1st edition, 1991. → pages 19, 113, 191

[66] C Keller and H Schmutz. Die Reaktion yon Lithiumfluorid mit den Trifluoriden der Lanthaniden und einiger Actiniden. *J. Inorg. Nucl. Chem*, 27:900–901, 1965. → pages 20

[67] HM Rønnow, J Jensen, R. Parthasarathy, G Aeppli, TF Rosenbaum, DF McMorrow, and C Kraemer. Magnetic Excitations Near the Quantum Phase Transition in the Ising Ferromagnet $LiHoF_4$. *Phys. Rev. B*, 75:055426–1–055426–8, 2007. → pages vii, 20, 21, 22, 25, 26, 93, 113

[68] J Jensen. The coherent potential approximation and the diagrammatic 1/Z expansion for an anisotropic spin-1 paramagnet. *J. Phys. C: Solid State Phys.*, 17:5367–5384, 1984. → pages 20, 22, 112, 113

[69] SMA Tabei, MJP Gingras, YJ Kao, and T Yavors'kii. Perturbative Quantum Monte Carlo Study of $LiHoF_4$ in a Transverse Magnetic Field. *Phys. Rev. B*, 78:184408–1–184408–20, 2008. → pages 21, 25, 26, 33, 35, 157

[70] KHJ Buschow and FR de Boer. *Physics of Magnetism and Magnetic Materials*. Kluwer Academic/Plenum Publishers New York, 1st edition, 2003. → pages 23

[71] B Barbara, D Gignoux, and C Vettier. *Lectures on Modern Magnetism*. Science Press Beijing, 1st edition, 1988. → pages 23, 159

[72] KWH Stevens. Matrix Elements and Operator Equivalents Connected with the Magnetic Properties of Rare Earth Ions. *Proc. Phys. Soc., Sect. A*, 65:209–215, 1952. → pages 23

[73] B Bleaney and KWH Stevens. Paramagnetic Resonance. *Rep. Prog. Phys.*, 16:108–159, 1953. → pages 29

[74] MT Hutchings. Point Charge Calculations of Energy Levels of Magnetic Ions in Crystalline Electric Fields. *Solid State Phys.*, 16:227–273, 1964. → pages 23

[75] C Görller-Walrand and Koen Binnemans. Rationalization of Crystal-Field Parameterization. In KA Gschneidner and J Eyring, editors, *Handbook on the Physics and Chemistry of Rare Earths Vol 23*, chapter 155, pages 121–283. Elsevier Science B.V., 1996. → pages 23

[76] P Beauvillain, JP Renard, and J Magariño. Determination of Crystal Field Parameters of $LiRF_4$ (R = Tb, Ho, Er) by High Temperature Susceptibility Measurements. *JJ. Magn. Magn. Mater.*, 15-18:31–32, 1980. → pages vii, 24, 25

[77] HP Christensen. Spectroscopic analysis of $LiHoF_4$ and $LiErF_4$. *Phys. Rev. B*, 19:6564–6572, 1979. → pages vii, 24, 25

[78] SN Gifeisman, AM Tkachuk, , and VV Prizmak. Optical Spectra of a Ho^{3+} ion in $LiYF_4$ crystals. *Opt. Spectrosc.*, 44:68–71, 1978. → pages vii, 24, 25

[79] GS Shakurov, MV Vanyunin, BZ Malkin, B Barbara, R Yu Abdulsabirov, and SL Korableva. Direct Measurements of Anticrossings of the Electron-Nuclear Energy Levels in LiYF4:Ho^3+ with Submillimeter EPR Spectroscopy. *Appl. Mag. Res.*, 28:251–265, 2007. → pages vii, 24, 25

[80] P Babkevich, A Finco, M Jeong, B Dalla Piazza, I Kovacevic, G Klughertz, KW Krämer, C Kraemer, DT Adroja, E Goremychkin, T Unruh, T Strässle, A Di Lieto, J Jensen, and HM Rønnow. Neutron spectroscopic study of crystal-field excitations and the effect of the crystal field on dipolar magnetism in $LiRF_4$ (R= Gd, Ho, Tm, and Yb). *Phys. Rev. B*, 92:144422–1–144422–15, 2015. → pages vii, 25

[81] NJ Stone. Table of nuclear magnetic dipole and electronic quadrupole moments. *Atomic Data and Nuclear Data Tables*, 90:75–176, 2005. → pages 28

[82] B Bleaney. Hyperfine Interactions. In RJ Elliot, editor, *Magnetic Properties of Rare Earth Metals*, chapter 8, pages 383–420. Plenum Publishing Company Ltd, 1972. → pages 28, 30, 70

[83] PE Hansen and R Nevald. Transferred hyperfine interaction at 295k between the rare-earth ions and the fluorine and lithium rare-earth fluorides. *Phys. Rev. B*, 16:146–153, 1977. → pages 30

[84] John David Jackson. *Classical Electrodynamics*. John Wiley and Sons Inc., 3rd edition, 1998. → pages 31

[85] Amikam Aharoni. *Introduction to the Theory of Ferromagnetism*. Oxford University Press, 2nd edition, 1996. → pages 32, 43, 46

[86] RB Griffiths. Free Energy of Interacting Magnetic Dipoles. *Phys. Rev.*, 176:655–659, 1968. → pages 33

[87] H Kjønsberg and SM Girvin. The Classical Phase Transition in $LiHoF_4$: Results from Mean Field Theory and Monte Carlo Simulations. In RE Cohen, editor, *Fundamental Physics of Ferroelectrics 2000: Aspen Center for Physics Winter Wkshp.*, pages 323–331. American Institute of Physics, 2000. → pages 34

[88] A Biltmo and P Henelius. The ferromagnetic transition and domain structure in $LiHoF_4$. *EPL*, 87:27002–2–27002–6, 2009. → pages 34

[89] R Skomski. On the Ising character of the quantum-phase transition in $LiHoF_4$. *AIP Advances*, 6:055704–1–055704–5, 2016. → pages 35

[90] T Holstein and H Primakoff. Field Dependence of the Intrinsic Domain Magnetization of a Ferromagnet. *Phys. Rev.*, 58:1098–1113, 1940. → pages 40, 41

[91] MH Cohen and F Keffer. Dipole Sums in the Primitive Cubic Lattices. *Phys. Rev.*, 99:1128–1134, 1955. → pages 41, 42, 44, 46

[92] GJ Bowden and RG Clark. Fourier Transforms of Dipole-Dipole Interactions using Ewald's Method. *J. Phys. C*, 14:L827–L834, 1981. → pages 41, 52, 54

[93] A Aharony and M Fisher. Critical Behaviour of Magnets with Dipolar Interactions. *Phys. Rev. B*, 8:3323–3341, 1973. → pages 52, 54

[94] V Banerjee and S Dattagupta. Model quantum magnet: The effect of hyperfine interactions on the phase diagram and dynamic susceptibility. *Phys. Rev. B*, 64:024427–1–024427–11, 2001. → pages 93, 157

[95] B Muhlschlegel and H Zittartz. Gaussian Average Method in the Statistical Theory of the Ising Model. *Z. Phys.*, 175:553–573, 1963. → pages 106, 109, 120

[96] RD Mattuck. *A Guide to Feynman Diagrams in the Many-Body Problem*. Dover, New York, 2nd edition, 1976. → pages 107

[97] F Englert. Linked Cluster Expansion in the Statistical Theory of Ferromagnetism. *Phys. Rev.*, 129:567–577, 1963. → pages 107, 180

[98] RB Stinchcombe, G Horwitz, F Englert, and R Brout. Thermodynamic Behaviour of the Heisenberg Ferromagnet. *Phys. Rev.*, 130:155–176, 1963. → pages 107, 181, 183

[99] G Horwitz and H Callen. Diagrammatic Expansion for the Ising Model with Arbitrary Spin and Range of Interaction. *Phys. Rev.*, 124:1757–1785, 1961. → pages 107, 110

[100] B Strieb, H Callen, and G Horwitz. Cluster Expansion for the Heisenberg Ferromagnet. *Phys. Rev.*, 130:1798–1808, 1963. → pages 107

[101] VG Vaks, AI Larkin, and SA Pikin. Thermodynamics of an Ideal Ferromagnetic Substance. *Soviet Physics JETP*, 26:188–199, 1968. → pages 107, 108

[102] D Yang and Y Wang. Green's function diagrammatic technique for complicated level systems. *Phys. Rev. B.*, 10:4714–4723, 1974. → pages 108, 170, 171, 173

[103] C Wentworth and YL Wang. Linked-cluster series-expansion technique for quantum spin systems. *Phys. Rev. B*, 36:8687–8706, 1987. → pages 108

[104] P Pfeuty and RJ Elliott. The Ising model with a transverse field: 2 ground state properties. *J. Phys. C: Solid St. Phys.,*, 4:2370–2385, 1971. → pages 108

[105] SRP Smith. Application of the correlated-effective-field approximation to phase transitions in Ising systems with strain interactions. *J. Phys. C: Solid State Phys.*, 17:41–50, 1984. → pages 110, 111

[106] ME Lines. Polarization Fluctuations Near a Ferroelectric Phase Transition. *Phys. Rev. B*, 5:3690–3702, 1972. → pages 110

[107] ME Lines. Correlated-effective-field theory: A statistical approach for grossly anharmonic lattice vibrations. *Phys. Rev. B*, 9:950–957, 1974. → pages 110, 111

[108] ME Lines. Many-body theory of magnetism for ions with complicated level structure. *Phys. Rev. B*, 9:3927–3931, 1974. → pages 110

[109] ME Lines. Spin dynamics in multilevel magnetic systems. *Phys. Rev. B*, 11:1134–1143, 1975. → pages 111

[110] JH Page, SRP Smith, and DR Taylor. Analysis of electric susceptibility data and critical behaviour in the uniaxial ferromagnet $LiHoF_4$ using correlated-effective-field theory. *J. Phys. C: Solid State Phys.*, 17:73–84, 1984. → pages 112

[111] JH Page JT Follinsbee, DR Taylor, and D Zobin. Transverse Susceptibility of the Uniaxial Ferromagnets $LiHoF_4$ and $LiTbF_4$ by Dielectric Measurements. *Physica B*, 107:85–86, 1981. → pages 112

[112] J Jensen. 1/z renormalization behaviour of the mean-field behaviour of the dipole-coupled singlet-singlet system HoF_3. *Phys. Rev. B*, 48:11833–11841, 1994. → pages 112, 113

[113] SQ Wang, WE Evenson, and JR Schrieffer. Theory of Itinerant Ferromagnets Exhibiting Localized-Moment Behaviour Above the Curie Point. *Phys. Rev. Lett.*, 23:92–95, 1969. → pages 121

[114] M Blume. Theory of the First Order Magnetic Phase Change in UO_2. *Phys. Rev.*, 141:517–524, 1966. → pages 158

[115] HW Capel. On the Possibility of First-Order Phase Transtions in Ising Systems of Triplet Ions with Zero-Field Splitting. *Physica*, 32:966–988, 1966. → pages 158

[116] HW Capel. On the Possibility of First-Order Phase Transtions in Ising Systems of Triplet Ions with Zero-Field Splitting 2. *Physica*, 33:295–331, 1967. → pages

[117] HW Capel. On the Possibility of First-Order Phase Transtions in Ising Systems of Triplet Ions with Zero-Field Splitting 3. *Physica*, 37:423–441, 1967. → pages 158

[118] M Blume and VJ Emery RB Griffiths. Ising Model for the λ Transition and Phase Seperation in He^3-He^4 Mixtures. *Phys. Rev. A*, 4:1071–1077, 1971. → pages 158

[119] J Cardy. *Scaling and Renormalization in Statistical Physics*. Cambridge University Press, 1st edition, 1996. → pages 158

[120] JC Wright, HW Moos, JH Colwell, BW Mangum, and DD Thornton. $DYPO_4$: A Three-Dimensional Ising Antiferromagnet. *Phys. Rev. B*, 3:843–858, 1971. → pages 159

[121] S Fishman and Amnon Aharony. Random field effects in disordered anisotropic antiferromagnets. *J. Phys. C: Solid State Phys.*, 12:L729–L733, 1979. → pages 159

[122] J Cardy. Random-field effects in site-disordered Ising antiferromagnets. *Phys. Rev. B*, 29:505–507, 1984. → pages 159

[123] MJ Stephen and A Aharony. Percolation with long-range interactions. *J. Phys. C: Solid State Phys.*, 14:1665–1670, 1981. → pages 159

[124] J Hubbard. Electron Correlations in Narrow Energy Bands iv: The Atomic Representation. *Proceedings of the Royal Society of London, Series A: Mathematical and Physical Sciences*, 285:542–560, 1965. → pages 170

[125] SB Haley and P Erdös. Standard-Basis Method in the Green's-Function Technique of Many-Body Systems with an Application to Ferromagnetism. *Phys. Rev. B*, 5:1106–1119, 1972. → pages 170

[126] R Kubo. Generalized Cumulant Expansion Method. *J. Phys. Soc. Jap.*, 17:1100–1120, 1962. → pages 182

[127] MG Cottam and RB Stinchcombe. Thermodynamic properties of a Heisenberg antiferromagnet. *J. Phys. C*, 3:2283–2304, 1970. → pages 185

[128] Assa Auerbach. *Interacting Electrons and Quantum Magnetism*. Springer-Verlag, 1st edition, 1994. → pages 186

Appendix A

Mean Field Basis Operators

In this appendix, we explore some of the properties of the mean field (MF) operators, often referred to as standard basis operators, or Hubbard operators, in the literature. These operators can be traced back to the 1965 work of Hubbard, in which operators acting between a discrete set of energy levels at each atomic site were used to analyze correlated electron systems [124]. In 1972, Haley and Erdös reintroduced these operators, and presented a formalism that was subsequently developed by Yang and Wang in 1974 [102, 125]. Here, we give some of the basic properties of the MF operators, and present Yang and Wang's general reduction scheme for time ordered products of the MF operators. Further discussion of the MF basis operator formalism is provided in the introduction to Chapter 6. We only consider products of MF basis operators belonging to a single site because, as is shown in Section 6.3.1, considering MF basis operators belonging to different sites is unnecessary in the formalism developed in this thesis. We use the reduction scheme to calculate general expressions for the correlation function of products of up to four MF operators. These are necessary for deriving the spin cumulants of up to four spin operators in Appendix E.

Consider a Hamiltonian of the form

$$H_0 = \sum_i \sum_n E_n L^i_{nn}, \tag{A.1}$$

where we define the MF operators to be

$$L_{mn} = |m\rangle\langle n|, \tag{A.2}$$

where $|m\rangle$ and $|n\rangle$ are MF eigenstates of the system. The superscript i is a site index, and the summation in n is over all MF eigenstates of the system. Note that any single site operator may

be expressed in this basis; for example, we may write

$$S^z = \sum_{mn} c_{mn} L_{mn}. \tag{A.3}$$

In the Heisenberg picture, the MF operators will be time (or imaginary time τ) dependent

$$L_{mn}(\tau) = e^{H_0 \tau} L_{mn} e^{-H_0 \tau}. \tag{A.4}$$

Following reference [102], we note the following identities

$$L_{mn}(\tau) = e^{(E_m - E_n)\tau} L_{mn} \qquad e^{-\beta H_0} L_{mn}(\tau) = e^{-\beta (E_m - E_n)} L_{mn}(\tau) e^{-\beta H_0} \tag{A.5}$$

and

$$[L_{pq}(\tau'), L_{mn}(\tau)] = e^{(E_m - E_n)(\tau - \tau')} [L_{pq}(\tau'), L_{mn}(\tau')]. \tag{A.6}$$

We now define the imaginary time ordered correlation function of the MF operators to be

$$-\langle T_\tau L_{nm}(\tau') L_{mn}(\tau) \rangle = D_{mn} K^0_{mn}(\tau' - \tau). \tag{A.7}$$

Noting that $\langle L_{nm}(\tau') L_{mn}(\tau) \rangle = \langle L_{mn}(\tau) L_{nm}(\tau') + [L_{nm}(\tau'), L_{mn}(\tau)] \rangle$, and using the identities (A.5) and (A.6), we find

$$K^0_{mn}(\tau' - \tau) = \begin{cases} e^{-(E_m - E_n)(\tau' - \tau)} [1 + n(E_m - E_n)], & \tau' > \tau \\ e^{-(E_m - E_n)(\tau' - \tau)} n(E_m - E_n), & \tau' < \tau \end{cases} \tag{A.8}$$

where $n(E) = (e^{\beta E} - 1)^{-1}$ is the Bose distribution function. We will refer to $K^0_{mn}(\tau' - \tau)$ as the MF Green's function. The coefficient D_{mn} is a population factor, with $D_{mn} = D_m - D_n$, where

$$D_m = \langle L_{mm} \rangle_0 = \frac{e^{-\beta E_m}}{Z_0}, \tag{A.9}$$

and the MF partition function is

$$Z_0 = \mathrm{Tr}[e^{-\beta H_0}] = \mathrm{Tr}[e^{-\beta \sum_n E_n L_{nn}}] = \sum_n e^{-\beta E_n}. \tag{A.10}$$

Note that all the above is valid provided we are not dealing with degenerate energy levels. If

$E_n = E_m$, we find

$$-\langle T_\tau L_{nm}(\tau')L_{mn}(\tau)\rangle = -D_n. \tag{A.11}$$

Accounting for degenerate levels, we may write

$$-\langle T_\tau L_{nm}(\tau')L_{mn}(\tau)\rangle = D_{mn}K^0_{mn}(\tau'-\tau) - D_m\delta_{mn}. \tag{A.12}$$

Note that $D_{mn} = 0$ when the energy levels are degenerate. In this thesis we are primarily concerned with systems with a discrete set of non-degenerate single ion energy levels; hence, the degenerate case is ignored in subsequent discussion.

In frequency space, the MF Green's function K^0_{mn} is given by

$$K^0_{mn}(i\omega_r) = \frac{1}{2}\int_{-\beta}^{\beta} d\tau K^0_{mn}(\tau)e^{i\omega_r\tau} = \int_0^{\beta} d\tau K^0_{mn}(\tau)e^{i\omega_r\tau} = \frac{1}{E_m - E_n - i\omega_r} \tag{A.13}$$

where $\omega_r = \frac{2r\pi}{\beta}$ are the usual Bose-Matsubara frequencies. Note that $K^0_{mn}(i\omega_r) = -K^0_{nm}(-i\omega_r)$. The inverse Fourier transform of the MF Green's function is given by

$$K^0_{mn}(\tau) = \frac{1}{\beta}\sum_r \frac{e^{-i\omega_r\tau}}{E_m - E_n - i\omega_r} \tag{A.14}$$

Furthermore, we define the MF propagator for transitions between energy levels m and n to be

$$K_{mn}(\tau) = [K^0_{mn}(\tau) + K^0_{mn}(-\tau)] \qquad K_{mn}(i\omega_r) = \frac{2E_{mn}}{E^2_{nm} - (i\omega_r)^2}. \tag{A.15}$$

This function will be frequently encountered in our analysis of magnetic systems.

Finally, for completeness, we consider the case $K_{mn}(\tau = \tau')$. We find $K^0_{mn}(0) = \frac{1}{2} + n(E_m - E_n)$ and

$$-\langle T_\tau L_{nm}(\tau)L_{mn}(\tau)\rangle = \frac{D_{mn}}{2} + D_{mn}n(E_m - E_n) = -\frac{1}{2}(D_m + D_n). \tag{A.16}$$

The expressions above are sufficient for calculating properties of spin systems within the random phase approximation (RPA). In order to include the effects of fluctuations beyond the RPA, it is necessary to consider higher order correlation functions of the MF operators. We begin by stating Yang and Wang's general reduction theorem for time ordered averages of the

MF operators [102]. Let $O(\tau) = L_{mn}(\tau)$ be an arbitrary MF operator. Then

$$\begin{aligned}\langle T_\tau O(\tau_1)\cdots L_{mn}(\tau)\cdots O(\tau_i)\rangle_0 \\ = K^0_{mn}(\tau_1-\tau)\langle T_\tau[O(\tau_1),L_{mn}(\tau_1)]\cdots O(\tau_i)\rangle_0 \\ + K^0_{mn}(\tau_2-\tau)\langle T_\tau O(\tau_1)[O(\tau_2),L_{mn}(\tau_2)]\cdots O(\tau_i)\rangle_0 \\ \cdots + K^0_{mn}(\tau_i-\tau)\langle T_\tau O(\tau_1)\cdots[O(\tau_i),L_{mn}(\tau_i)]\rangle_0.\end{aligned} \tag{A.17}$$

In the above expression, we have reduced an average over a set of $i+1$ MF operators to a sum of averages over i MF operators. This process can be repeated until we are left with only averages of diagonal operators $L_{mm}(\tau)$, which simply contribute population factors. Note that the reduction is not unique because we may start the process with whichever MF operator we choose, leading to different, but equivalent, algebraic expressions for the relevant correlation function. Subsequent calculations in the zero temperature limit are often simplified by starting the reduction with L_{mn} such that m is minimal, which is the convention we will adopt here unless otherwise noted. We now use the reduction scheme to calculate correlation functions of three and four MF operators.

At third order we must consider the following terms:

$$\langle T_\tau L_{mm}(\tau_1)L_{mm}(\tau_2)L_{mm}(\tau_3)\rangle_0 \qquad \langle T_\tau L_{mm}(\tau_1)L_{mn}(\tau_2)L_{nm}(\tau_3)\rangle_0$$
$$\langle T_\tau L_{mn}(\tau_1)L_{np}(\tau_2)L_{pm}(\tau_3)\rangle_0.$$

Of course, under the time ordering operator, any permutation of the operators is also allowed. The first term simply gives a factor of D_m. In the following, we set $\tau_i - \tau_j = \tau_{ij}$ for brevity. The second term yields (assume $n > m$)

$$\langle T_\tau L_{mm}(\tau_1)L_{mn}(\tau_2)L_{nm}(\tau_3)\rangle_0 = -D_{mn}K^0_{mn}(\tau_{12})K^0_{mn}(\tau_{31}) - D_m K^0_{mn}(\tau_{32}), \tag{A.18}$$

and, for the third term, we find

$$\begin{aligned}\langle T_\tau L_{mn}(\tau_1)L_{np}(\tau_2)L_{pm}(\tau_3)\rangle_0 \\ = -D_{pn}K^0_{mn}(\tau_{31})K^0_{pn}(\tau_{23}) + D_{pm}K^0_{mn}(\tau_{21})K^0_{pm}(\tau_{23}).\end{aligned} \tag{A.19}$$

At fourth order we must consider:

$$\langle T_\tau L_{mm}(\tau_1)L_{mm}(\tau_2)L_{mm}(\tau_3)L_{mm}(\tau_4)\rangle_0 \tag{A.20}$$
$$\langle T_\tau L_{mm}(\tau_1)L_{nn}(\tau_2)L_{mn}(\tau_3)L_{nm}(\tau_4)\rangle_0 \qquad \langle T_\tau L_{mm}(\tau_1)L_{mm}(\tau_2)L_{mn}(\tau_3)L_{nm}(\tau_4)\rangle_0$$
$$\langle T_\tau L_{mm}(\tau_1)L_{mn}(\tau_2)L_{np}(\tau_3)L_{pm}(\tau_4)\rangle_0 \qquad \langle T_\tau L_{mn}(\tau_1)L_{nm}(\tau_2)L_{mn}(\tau_3)L_{nm}(\tau_4)\rangle_0$$
$$\langle T_\tau L_{mn}(\tau_1)L_{nm}(\tau_2)L_{mp}(\tau_3)L_{pm}(\tau_4)\rangle_0 \qquad \langle T_\tau L_{mn}(\tau_1)L_{np}(\tau_2)L_{pq}(\tau_3)L_{qm}(\tau_4)\rangle_0.$$

Under the time ordering operator all permutations of these operators are also allowed. The first term simply gives a factor of D_m. The second and third terms are given by

$$\begin{aligned}
&\langle T_\tau L_{mm}(\tau_1)L_{mm}(\tau_2)L_{mn}(\tau_3)L_{nm}(\tau_4)\rangle_0 \qquad (A.21)\\
&\qquad = K^0_{mn}(\tau_{13})\langle T_\tau L_{mn}(\tau_1)L_{mm}(\tau_2)L_{nm}(\tau_4)\rangle_0\\
&\qquad\quad + K^0_{mn}(\tau_{23})\langle T_\tau L_{mm}(\tau_1)L_{mn}(\tau_2)L_{nm}(\tau_4)\rangle_0 - D_m K^0_{mn}(\tau_{43})\\
&\langle T_\tau L_{mm}(\tau_1)L_{nn}(\tau_2)L_{mn}(\tau_3)L_{nm}(\tau_4)\rangle_0\\
&\qquad = K^0_{mn}(\tau_{13})\langle T_\tau L_{mn}(\tau_1)L_{nn}(\tau_2)L_{nm}(\tau_4)\rangle_0\\
&\qquad\quad - K^0_{mn}(\tau_{23})\langle T_\tau L_{mm}(\tau_1)L_{mn}(\tau_2)L_{nm}(\tau_4)\rangle_0,
\end{aligned}$$

where the contractions of three operators may be read from equations (A.18) and (A.19). The remaining fourth order contractions are given as follows

$$\begin{aligned}
&\langle T_\tau L_{mm}(\tau_1)L_{mn}(\tau_2)L_{np}(\tau_3)L_{pm}(\tau_4)\rangle_0 \qquad (A.22)\\
&\qquad = K^0_{mn}(\tau_{12})\langle T_\tau L_{mn}(\tau_1)L_{np}(\tau_3)L_{pm}(\tau_4)\rangle_0\\
&\qquad\quad - K^0_{mn}(\tau_{32})\langle T_\tau L_{mm}(\tau_1)L_{mp}(\tau_3)L_{pm}(\tau_4)\rangle_0\\
&\langle T_\tau L_{mn}(\tau_1)L_{nm}(\tau_2)L_{mn}(\tau_3)L_{nm}(\tau_4)\rangle_0\\
&\qquad = K^0_{mn}(\tau_{23})\langle T_\tau L_{mn}(\tau_1)[L_{nn}(\tau_2) - L_{mm}(\tau_2)]L_{nm}(\tau_4)\rangle_0\\
&\qquad\quad + K^0_{mn}(\tau_{43})\langle T_\tau L_{mn}(\tau_1)L_{nm}(\tau_2)[L_{nn}(\tau_4) - L_{mm}(\tau_4)]\rangle_0\\
&\langle T_\tau L_{mn}(\tau_1)L_{nm}(\tau_2)L_{mp}(\tau_3)L_{pm}(\tau_4)\rangle_0\\
&\qquad = -K^0_{mn}(\tau_{21})\langle T_\tau L_{mm}(\tau_2)L_{mp}(\tau_3)L_{pm}(\tau_4)\rangle_0\\
&\qquad\quad + K^0_{mn}(\tau_{41})\langle T_\tau L_{nm}(\tau_2)L_{mp}(\tau_3)L_{pn}(\tau_4)\rangle_0\\
&\langle T_\tau L_{mn}(\tau_1)L_{np}(\tau_2)L_{pq}(\tau_3)L_{qm}(\tau_4)\rangle_0\\
&\qquad = -K^0_{mn}(\tau_{21})\langle T_\tau L_{mp}(\tau_2)L_{pq}(\tau_3)L_{qm}(\tau_4)\rangle_0\\
&\qquad\quad + K^0_{mn}(\tau_{41})\langle T_\tau L_{np}(\tau_2)L_{pq}(\tau_3)L_{qn}(\tau_4)\rangle_0.
\end{aligned}$$

By starting the reduction with L_{np} in the first equation in expression (A.22), expressions for

spin correlations and cumulants simplify in the low temperature limit. Starting with L_{np} we find

$$\begin{aligned}\langle T_\tau L_{mm}(\tau_1)L_{mn}(\tau_2)L_{np}(\tau_3)L_{pm}(\tau_4)\rangle_0 \\ = K^0_{np}(\tau_{23})\langle T_\tau L_{mm}(\tau_1)L_{mp}(\tau_2)L_{pm}(\tau_4)\rangle_0 \\ - K^0_{np}(\tau_{43})\langle T_\tau L_{mm}(\tau_1)L_{mn}(\tau_2)L_{nm}(\tau_4)\rangle_0.\end{aligned} \tag{A.23}$$

The expressions derived here for contractions of three and four MF operators will be used in Appendix E to derive spin cumulants. It is the spin cumulants that play a central role in the analysis of fluctuations in magnetic systems, as was shown in Chapter 6 of this thesis.

Appendix B

Transverse Ising Model

Here we consider the spin half transverse Ising model in the absence of any coupling to nuclear spins

$$\mathscr{H} = -\frac{1}{2}\sum_{i\neq j} V_{ij} S_i^z S_j^z - \Delta \sum_i S_i^x - h\sum_i S_i^z, \tag{B.1}$$

where $\vec{S} = \frac{1}{2}\vec{\tau}$ are spin half operators, and $\vec{\tau}$ are the Pauli matrices. We analyze the model using the mean field (MF) operators presented in Appendix A. The results here are well known; however, we present them to illustrate the use of the MF operators, and so that the resulting equations are available for reference in this thesis.

The Hamiltonian may be divided into the MF part and the fluctuating part, $\mathscr{H} = \mathscr{H}_{MF} + \mathscr{H}'$. The MF part of the Hamiltonian is given by

$$\mathscr{H}_{MF} = -\Delta \sum_i S_i^x - H\sum_i S_i^z, \tag{B.2}$$

where $H = h + V_0\langle S^z\rangle$. If we consider a simple cubic crystal with nearest neighbour interactions, the interaction strength is $V_0 = \sum_j V_{ij} = 6J$. The fluctuations are given by

$$\mathscr{H}' = -\frac{1}{2}\sum_{i\neq j} V_{ij} \widetilde{S}_i^z \widetilde{S}_j^z, \tag{B.3}$$

where $\widetilde{S}_i^z = S_i^z - \langle S^z\rangle_0$, where the subscript zero denotes the average is to be taken with respect to the MF Hamiltonian. Note that a constant contribution to the ground state energy has been dropped.

Mean Field Operator Approach

We work in a basis consisting of eigenstates of the MF Hamiltonian

$$\mathscr{H}_{MF_i} = \begin{pmatrix} -\frac{H}{2} & -\frac{\Delta}{2} \\ -\frac{\Delta}{2} & \frac{H}{2} \end{pmatrix}. \tag{B.4}$$

The eigenvalues of this matrix are $E_\pm = \pm E = \pm\sqrt{\frac{\Delta^2}{4} + \frac{H^2}{4}}$ and the associated eigenvalues are

$$|\Psi_1\rangle = \alpha_1 \begin{pmatrix} \frac{H}{2} + \frac{\Delta}{2} + E \\ -\frac{H}{2} + \frac{\Delta}{2} + E \end{pmatrix} \qquad |\Psi_2\rangle = \alpha_2 \begin{pmatrix} -\frac{H}{2} + \frac{\Delta}{2} + E \\ -\frac{H}{2} - \frac{\Delta}{2} - E \end{pmatrix}, \tag{B.5}$$

where 1 corresponds to the E_- state and 2 corresponds to the E_+ state. If we define the MF operators to be $L_{ij} = |\Psi_i\rangle\langle\Psi_j|$, then the z component of the electronic spin operator is given by

$$S^z = c_{11}[L_{11} - L_{22}] + c_{12}[L_{12} + L_{21}], \tag{B.6}$$

where

$$c_{11} = \frac{H}{4E} \qquad c_{12} = \frac{\Delta}{4E}. \tag{B.7}$$

Magnetization

The ground state MF magnetization is given by

$$\langle\Psi_1|S^z|\Psi_1\rangle = \langle S^z\rangle_0 = \frac{h + V_0\langle S^z\rangle_0}{2\sqrt{\Delta^2 + (h + V_0\langle S^z\rangle_0)^2}}. \tag{B.8}$$

Inspection of this equation immediately reveals that in order to have $\langle S^z\rangle_0 = 0$, we require $h = 0$. With $h = 0$, we see that $\langle S^z\rangle_0 = 0$ is a possible solution. Another possible solution is

$$\langle S^z\rangle_0 = \frac{1}{2}\sqrt{1 - \left(\frac{2\Delta}{V_0}\right)^2} \tag{B.9}$$

provided that $\Delta < \frac{V_0}{2}$. This solution corresponds to the ferromagnetic phase of the system.

Susceptibility and Correlation Functions

The longitudinal component of the static susceptibility is given by $\chi^{zz} = \frac{\partial \langle S^z \rangle_0}{\partial h}$. Differentiating the ground state MF magnetization with respect to h, we find the zero temperature static susceptibility to be

$$\chi^{zz} = \frac{\chi_0^{zz}(H)}{1 - V_0 \chi_0^{zz}(H)}, \tag{B.10}$$

where the single ion susceptibility is

$$\chi_0^{zz}(H) = \frac{\Delta^2}{2(\Delta^2 + H^2)^{\frac{3}{2}}} \approx \frac{1}{2\Delta}\left[1 - \frac{3H^2}{2\Delta^2} + O\big(\frac{H^4}{\Delta^4}\big)\right]. \tag{B.11}$$

As will be shown, the static susceptibility may also be obtained from the imaginary time connected two point correlation function.

Using the Matsubara formalism, the cumulant part of the two point correlation function, or connected Green's function, for the system is given by

$$G(k,\tau) = -\left\langle T_\tau \widetilde{S}_k^z(\tau) \widetilde{S_{-k}^z}(0) \right\rangle = \frac{-\left\langle T_\tau \widetilde{S}_k^z(\tau) \exp\left(-\int_0^\beta d\tau V(\tau)\right) \widetilde{S_{-k}^z}(0) \right\rangle_0}{\left\langle T_\tau \exp\left(-\int_0^\beta d\tau V(\tau)\right) \right\rangle_0} \tag{B.12}$$

where in the final expression the averages are taken with respect to $\mathscr{H}_{MF}$. We define the unperturbed propagator to be

$$\begin{aligned} g(\tau) &= -\left\langle T_\tau \widetilde{S}^z(\tau) \widetilde{S}^z(0) \right\rangle_0 \\ &= -c_{12}^2 \left\langle L_{12}L_{21} + L_{21}L_{12} \right\rangle_0 - c_{11}^2 \left\langle L_{11}L_{11} + L_{22}L_{22} \right\rangle_0 + \langle S^z \rangle_0^2, \end{aligned} \tag{B.13}$$

where the τ dependence of the operators has been suppressed. Note that the cross terms between the L_{ij} and L_{ii} operators, as well as the terms between the L_{ii} and L_{jj} operators with $i \neq j$, are identically zero. Contracting the operators and transforming to frequency space we find

$$-g(i\omega_n) = c_{12}^2 D_{12} \frac{2E_{21}}{E_{21}^2 - (i\omega_r)^2} + \beta c_{11}^2 (D_1 + D_2 - D_{12}^2)\delta_{\omega_r,0}, \tag{B.14}$$

with $E_{21} = 2E = \sqrt{\Delta^2 + H^2}$. Note that at $T = 0$, we have $-g(0) = \chi_0^{zz}$, where χ_0^{zz} is the static

single ion susceptibility given in (B.11). We find that when $\langle S^z \rangle \neq 0$, at finite temperatures, the spectrum develops a purely elastic zero frequency component.

In the random phase approximation, the Green's function is given by

$$G^{RPA}(k, i\omega_n) = \frac{g(i\omega_n)}{1 + g(i\omega_n)V_k}. \tag{B.15}$$

We see that in the zero temperature limit the static susceptibility given in equation (B.10) follows from the RPA Green's function

$$\chi^{zz} = -G^{RPA}(0,0)\Big|_{T=0} = \frac{-g(0)}{1 + g(0)V_0}\Big|_{T=0}. \tag{B.16}$$

For low energies, in the limit $T \to 0$, we find

$$-g(i\omega_n) \approx A + B(i\omega_n)^2, \tag{B.17}$$

with

$$A = \frac{2c_{12}^2 D_{12}}{E_{21}} \qquad\qquad B = \frac{2c_{12}^2 D_{12}}{E_{21}^3}. \tag{B.18}$$

The Green's function is given by

$$G(k, i\omega_n) = \frac{1}{\frac{1}{g} + V_k} = \frac{-A^2}{B[\frac{A}{B} - (i\omega_n)^2 - \frac{V_k A^2}{B}]}, \tag{B.19}$$

and the spectrum is given by

$$\omega_k = \sqrt{\frac{A}{B} - \frac{V_k A^2}{B}} = E_{21}\sqrt{1 - V_k \chi_0^{zz}(H)}. \tag{B.20}$$

In the absence of a longitudinal field, the spectrum softens to zero at a critical transverse field Δ_c defined implicitly by $1 = V_0 \chi_0^{zz}|_{H=0}$. To leading order in $\frac{H}{\Delta}$, the gap in the spectrum at Δ_c due to a longitudinal field will be

$$\omega_0 \approx H\sqrt{\frac{3V_0}{4\Delta_c}} = \sqrt{\frac{3}{2}}H. \tag{B.21}$$

These expressions prove useful for comparison with the results of the spin half spin half model dealt with in Chapter 4.

Appendix C

A Diagramatic Expansion for Spin Systems

We begin this appendix with a general discussion of spin cumulants and their associated generating functions. Spin cumulants play a central role in the treatment of interacting systems of spins using diagrammatic perturbation theory. The development of a diagrammatic method for treating quantum Ising systems is a primary accomplishment of this thesis; hence, spin cumulants are discussed for reference in Section C.1.

A diagrammatic expansion for spin systems was introduced by Brout in 1959 [60, 61]. The history of this formalism, its application by Stinchcombe to the spin half transverse field Ising model [26], and related approaches, are discussed in Chapter 6, where we develop a field theoretic formalism for quantum Ising systems, and a corresponding set of rules to perform diagrammatic perturbation theory, and show that the resultant theory is equivalent to that of Brout. We present an overview of Brout's theory for easy reference in Section C.2.

Cumulants and the Generating Function

Following a 1963 paper of Englert [97], we consider the expression

$$\ln\langle e^{tx}\rangle = \sum_{n=1}^{\infty} \frac{t^n}{n!} M_n(x). \tag{C.1}$$

The function $Z = \langle e^{tx}\rangle$ is the generating function for x since its derivatives $\frac{\partial^n}{\partial t^n}|_{t=0} Z = \langle x^n\rangle$ generate the moments of x, and $M_n(x)$ are the associated cumulants. A moment can be expressed

in terms of cumulants by considering all possible subdivisions of the moment in question,

$$M_n(x) = \langle x^n \rangle - \sum_{n_1+n_2+\ldots+n_k=n} M_{n_1} M_{n_2} \ldots M_{n_k}. \tag{C.2}$$

The first four cumulants of x are given in terms of the moments by

$$\begin{aligned} M_1(x) &= \langle x \rangle \\ M_2(x) &= \langle x^2 \rangle - \langle x \rangle^2 \\ M_3(x) &= \langle x^3 \rangle - 3\langle x^2 \rangle \langle x \rangle + 2\langle x \rangle^3 \\ M_4(x) &= \langle x^4 \rangle - 4\langle x^3 \rangle \langle x \rangle - 3\langle x^2 \rangle^2 + 12\langle x^2 \rangle \langle x \rangle^2 - 6\langle x \rangle^4. \end{aligned} \tag{C.3}$$

For a spin system, we generalize to the joint cumulant generating function

$$\ln Z = \ln \left\langle T_\tau \exp(\sum_i h_i^\mu(\tau_j) S_i^\mu(\tau_j)) \right\rangle_0, \tag{C.4}$$

where we have given each imaginary time τ a label j. This is to indicate we are dealing with a discrete set of imaginary times; summation over the set is implicit. That is

$$h_i^\mu(\tau_j) S_i^\mu(\tau_j) = \sum_{j=1}^{n} h_i^\mu(\tau_j) S_i^\mu(\tau_j). \tag{C.5}$$

The superscript $\mu = (x, y, z)$ or $(+, -, z)$, and again, summation over the repeated index is implicit. Joint cumulants for spin systems are discussed in a 1963 paper of Stinchcombe *et al.* [98]. The cumulants are given by

$$\prod_{j=1}^{n} \frac{\partial}{\partial h^\mu(\tau_j)} \bigg|_{h=0} \ln Z = M_n \left(T_\tau \prod_{j=1}^{n} S^\mu(\tau_j) \right). \tag{C.6}$$

Note that in the definition of the cumulant, we have left off the site index of the spin. This is because cumulants of spins belonging to different sites are equal to zero due to their statistical independence (averages are with respect to the single ion Hamiltonian H_0). Indeed, the statistical independence of spins at different sites leads to

$$\ln \left\langle T_\tau \exp\left[\sum_i h_i^\mu(\tau_j) S_i^\mu(\tau_j) \right] \right\rangle_0 = \sum_i \ln \left\langle T_\tau \exp\left[h_i^\mu(\tau_j) S_i^\mu(\tau_j) \right] \right\rangle_0, \tag{C.7}$$

because spins on different sites commute. We see that any mixed partial derivatives of our cumulant generating function involving spins at different sites yields zero. Hence, any joint

cumulant of spins at different sites is equal to zero.

We may generalize our discussion of spin cumulants to a continous formulation by defining the generating functional to be $Z = \left\langle T_\tau \exp(\int_0^\beta d\tau f(\tau)) \right\rangle_0$. The cumulant generating functional is then given by

$$\ln Z = \sum_n \frac{1}{n!} \int_0^\beta d\tau_1 \ldots \int_0^\beta d\tau_n M_n \Big(T_\tau f(\tau_1) \ldots f(\tau_n) \Big). \tag{C.8}$$

This is known as Kubo's generalized cumulant expansion, and is reviewed in a clear 1962 paper of Kubo [126]. If we take $f(\tau) = h^\mu(\tau) S^\mu(\tau)$ then the moment of a time ordered product of spins and the associated cumulants are obtained by taking functional derivatives with respect to $h^\mu(\tau)$, rather than taking ordinary derivatives as in equation (C.6).

The Diagramatic Expansion

Averages of spin operators are of primary importance in magnetic systems. The two point correlation function yields the excitation spectrum of the system and is intimately related with the magnetic susceptibility, as will be discussed in Appendix D. Brout, building on his work on random ferromagnets, has introduced a diagrammatic perturbation theory for calculating averages of spin operators where the perturbation parameter is $\frac{1}{z}$, z being the effective number of neighbours felt by each spin [60, 61]. This is known as the high density approximation. We briefly outline Brout's formalism here.

Taking $Q_n(\tau_1, \ldots, \tau_n) = T_\tau \prod_i S_{n_i}^{\mu_i}(\tau_i)$, with n_i being a site index, and $\mu_i \in (+, -, z)$, we're interested in calculating averages of the form

$$\langle Q \rangle = \frac{\left\langle T_\tau \exp\Big(- \int_0^\beta d\tau V'(\tau) \Big) Q \right\rangle_0}{\left\langle T_\tau \exp\Big(- \int_0^\beta d\tau V'(\tau) \Big) \right\rangle_0}, \tag{C.9}$$

where, suppressing the imaginary time dependence, $V' = -\frac{1}{2} \sum_{i \neq j} V_{ij}^{\mu\nu} S_i^\mu S_j^\nu$. The prime on the interaction is meant to indicate $i = j$ is excluded from the summation. We now introduce a factor of ξ into the average, $V'(\tau) \to \xi V'(\tau)$ and $Q \to \xi Q$, to keep track of the order of terms in a series expansion, and we bring the denominator of the above expression into the numerator

as follows

$$\begin{aligned}\xi\langle Q\rangle &= \frac{\sum_{n=0}^{\infty}\frac{(-1)^n}{n!}\xi^{n+1}\int_0^\beta\ldots\int_0^\beta d\tau_1\ldots d\tau_n\left\langle T_\tau V'(\tau_1)\ldots V'(\tau_n)Q\right\rangle_0}{\sum_{n=0}^{\infty}\frac{(-1)^n}{n!}\xi^{n}\int_0^\beta\ldots\int_0^\beta d\tau_1\ldots d\tau_n\left\langle T_\tau V'(\tau_1)\ldots V'(\tau_n)\right\rangle_0} \\ &= \sum_{n=1}^{\infty}\frac{(-\xi)^{n-1}}{(n-1)!}\int_0^\beta\ldots\int_0^\beta d\tau_1\ldots d\tau_{n-1}M_n(V(\tau_1)\ldots V(\tau_{n-1})Q),\end{aligned} \tag{C.10}$$

where $V=-\frac{1}{2}\sum_{ij}V_{ij}^{\mu\nu}S_i^\mu S_j^\nu$ now includes terms where $i=j$. In the first line, the spatial sums in the interaction V' exclude terms with $i=j$. In order to obtain the cumulants in our diagrammatic theory, we add and subtract the missing terms, which leads to the unrestricted sum in the interaction V in the final line. Now that ξ has served its purpose, we set it to one. Note that each power of the interaction V carries a factor of -1 which cancels with the overall factor of $(-1)^{n-1}$; hence, for a ferromagnet, the overall sign of each diagram is positive. M_n in the above expression is to be taken as the cumulants of the interaction V and Q_n, i.e.,

$$M_1(Q)=\langle Q\rangle_0 \qquad\qquad M_2(V_{\tau_1}Q)=\langle V_{\tau_1}Q\rangle_0-\langle V_{\tau_1}\rangle_0\langle Q\rangle_0, \tag{C.11}$$

and so on. Recall that the interaction V involves a double sum over crystal sites, and, when the average is taken with respect to H_0, spins at different sites are statistically independent. By expanding the above expressions in terms of cumulants at single sites, we are led to the following graphical representation of the series in equation (C.10) [98]:

1. There are primary and secondary vertices. The primary vertices are labelled by the spins in Q, and the secondary vertices are labelled by spins from the interaction. Draw a circle around each primary vertex.

2. Each bond carries a factor of i, j, τ_i, and makes a contribution of $\frac{1}{2}V_{ij}^{\mu\nu}$ from the interaction. The bonds representing an interaction between the z components of two spins are given by a wavy line. The bonds representing an S^+ or S^- interaction are given by straight lines with an arrow.

3. Join the bonds to the primary vertices and each other in all possible ways. Neglect any diagrams in which the bonds are completely independent of the primary vertices. Each vertex represents a cumulant of the spin operators. The cumulant is determined by the number of bonds flowing into it; each wavy line is a factor of S^z, each straight line flowing into the vertex is a factor of S^-, and each straight line flowing out of a vertex is a factor of S^+. The spin from the primary vertex should be included in the cumulant from

the primary vertex.

4. Each graph carries a symmetry factor. We get a factor of $(n-1)!$ from permutations of the interaction V_τ, that cancels with the factor of $\frac{1}{(n-1)!}$ in the perturbation expansion. We also get a factor of 2^{n_l}, where n_l is the number of longitudinal bonds, from swapping the spins in each longitudinal interaction. Finally, since not all permutations lead to distinct diagrams, we must divide by a factor of g, the symmetry factor for each diagram.

5. Last of all, we integrate over all imaginary times, and sum over all spatial indices, from the secondary vertices. The sum over the spatial indices is unrestricted.

Fourier transforming each spin into frequency space, and each interaction into momentum space, leads to the same set of rules, only now we label each bond with momentum q and Matsubara frequency $i\omega_n$. We conserve momentum and frequency at each vertex and sum over momenta and frequencies from each secondary vertex. Each momentum summation carries a factor of $\frac{1}{N}$, where N is the total number of sites in the sample. Note that in each diagram, all of the momentum dependence comes from the interaction, which is associated with the lines in the diagram. The vertices, which are associated with the spin cumulants, carry no momentum dependence. The spatial index on the spins is no longer relevant, as we are now dealing with cumulants of spins at a single site.

We have calculated the moment of a time ordered product of n spins $\langle Q_n \rangle$. In our diagrammatic rules for $\langle Q_n \rangle$, we allow the diagrams to have disjoint parts provided that each disjoint part contains at least one primary vertex, viz., we must sum over every possible subdivision of the primary vertices. Recall that a moment can be expressed in terms of cumulants by considering all possible subdivisions of the moment in question. That is,

$$\langle Q_n \rangle = M_n + \sum_{n_1+n_2+\ldots+n_k=n} M_{n_1} M_{n_2} \ldots M_{n_k}, \tag{C.12}$$

where the second term represents the sum over the product of all possible cumulants of lower order. From this it follows that the n^{th} order cumulant M_n is given by all totally connected diagrams, where each primary vertex is connected to every other primary vertex.

In Chapter 6 of this thesis, we derive an effective field theory for quantum Ising systems. By performing a perturbation expansion of the field theory in the standard way, we are able to derive a set of diagrammatic rules equivalent to those listed above. The field theory is conceptually much simpler than the approach of Brout, and offers the advantage of a renormalization group treatment of a system's critical behaviour.

Recall that the perturbative parameter in our treatment of spin systems is $\frac{1}{z}$, z being the effective number of neighbouring spins. In momentum space, the order of each diagram is

determined by the number of free momentum summations it contains. Indeed, following reference [127], if r_0 is the effective range of the interaction, and a is the density of spins, then $z \sim r_0^3 a$, and the range in reciprocal space will be $q_0 \sim \frac{1}{r_0} \sim (\frac{a}{z})^{\frac{1}{3}}$. In one dimension, the fraction of terms in the first Brillouin zone for which $q < q_0$ is $\frac{n_0}{n} = \frac{q_0}{2\pi a}$. Similarly, the fraction of terms $\frac{N_0}{N}$ for which $q < q_0$ in a momentum summation over the first Brillouin zone in three dimensions is

$$\frac{N_0}{N} = \frac{\frac{4}{3}\pi q_0^3}{(2\pi)^3 a} \sim \frac{1}{z}. \tag{C.13}$$

Now, if $g(q)$ is some function with range q_0 we find

$$\frac{1}{N}\sum_q g(q) \sim \frac{N_0}{N}\bar{g} = \bar{g}\frac{1}{z}, \tag{C.14}$$

where $\bar{g}$ is the average of $g(q)$ with $q \leq q_0$.

Appendix D

Susceptibilities and Correlation Functions

Consider a Hamiltonian for a spin system of the form $H = H_0 + V$, where $H_0 = \sum_i H_{0i}^{\mu}$ is a sum of single ion Hamiltonians, and $V = -\frac{1}{2}\sum_{i\neq j} V_{ij}^{\mu\nu} S_i^{\mu} S_j^{\nu}$ is an interaction between spins at different sites. The indices are $\mu, \nu = x, y, z$, or $\mu, \nu = z, +, -$, depending on what proves more convenient, and we sum over repeated indices. In the Matsubara formalism, the cumulant part of the imaginary time spin spin correlation functions, or Green's functions, are given by

$$G_{ij}^{\mu\nu}(\tau_1 - \tau_2) = -\left\langle T_\tau \widetilde{S_i^{\mu}}(\tau_1)\widetilde{S_j^{\nu}}(\tau_2)\right\rangle = \frac{-\left\langle T_\tau \widetilde{S_i^{\mu}}(\tau_1)\exp\left(-\int_0^\beta d\tau V(\tau)\right)\widetilde{S_j^{\nu}}(\tau_2)\right\rangle_0}{\left\langle T_\tau \exp\left(-\int_0^\beta d\tau V(\tau)\right)\right\rangle_0}, \quad \text{(D.1)}$$

where $\widetilde{S_i^{\mu}} = S_i^{\mu} - \langle S_i^{\mu}\rangle$. The averages in the final expression are taken with respect to H_0. As is conventional, we define the Green's function with an overall minus sign. In the absence of the minus sign in our definition of G, we use the symbol $\chi = -G$ because, upon analytic continuation to real times, χ will yield the dynamic susceptibility of the spin system. The poles of the Green's functions yield the resonance peaks seen in, for example, neutron scattering experiments. A goal of condensed matter physics, and a primary accomplishment of this thesis, is to develop ways of evaluating expressions like equation (D.1). In the following, we will explore some of its properties, and define other relevant, related, functions. The discussion in the introduction to this appendix can be found in many textbooks. We reproduce the material here to establish notation and conventions, primarily following references [5, 128].

Transforming to Fourier space we have

$$S_i^\mu(\tau) = \frac{1}{\sqrt{N}}\sum_k e^{-ikr_i} S_k^\mu(\tau) \qquad S_k^\mu(\tau) = \frac{1}{\sqrt{N}}\sum_i e^{ikr_i} S_i^\mu(\tau) \tag{D.2}$$
$$S_k^\mu(\tau) = \frac{1}{\beta}\sum_n e^{i\omega_n\tau} S_k^\mu(i\omega_n) \qquad S_k^\mu(i\omega_n) = \int_0^\beta d\tau e^{-i\omega_n\tau} S_k^\mu(\tau)$$

for the spins, and

$$G_{ij}^{\mu\nu}(\tau) = \frac{1}{N}\sum_k e^{-ik(r_i-r_j)} G_k^{\mu\nu}(\tau) \qquad G_k^{\mu\nu}(\tau) = \frac{1}{N}\sum_{ij} e^{ik(r_i-r_j)} G_{ij}^{\mu\nu}(\tau) \tag{D.3}$$
$$G_k^{\mu\nu}(\tau_1-\tau_2) = \frac{1}{\beta}\sum_n e^{-i\omega_n(\tau_1-\tau_2)} G_k^{\mu\nu}(i\omega_n) \qquad G_k^{\mu\nu}(i\omega_n) = \int_0^\beta d\tau e^{i\omega_n\tau} G_k^{\mu\nu}(\tau)$$

for the correlation function. The interaction, in Fourier space, is given by

$$V_{ij}^{\mu\nu} = \frac{1}{N}\sum_q V_q^{\mu\nu} e^{-iq(r_i-r_j)} \qquad V_q^{\mu\nu} = \frac{1}{N}\sum_{ij} V_{ij}^{\mu\nu} e^{iq(r_i-r_j)}, \tag{D.4}$$

and

$$\int_0^\beta d\tau V(\tau) = -\frac{1}{2}\int_0^\beta d\tau \sum_{i\neq j} V_{ij}^{\mu\nu} \widetilde{S_i^\mu}(\tau)\widetilde{S_j^\nu}(\tau) \tag{D.5}$$
$$= -\frac{1}{2\beta}\sum_q\sum_n V_q^{\mu\nu} \widetilde{S_q^\mu}(i\omega_n)\widetilde{S_{-q}^\nu}(-i\omega_n).$$

As previously mentioned, the dynamic susceptibility (response function) of the system follows from the imaginary time correlation function. The relation is

$$\chi_k^{\mu\nu}(\omega) = -G_k^{\mu\nu}(i\omega_n \to \omega + i0^+), \tag{D.6}$$

where, in real space,

$$\chi_{ij}^{\mu\nu}(t-t') = -G_{ij}^{\mu\nu}(t-t') = i\theta(t-t')\langle[\widetilde{S_i^\mu}(t), \widetilde{S_j^\nu}(t')]\rangle. \tag{D.7}$$

The spectral density is given by

$$\rho_k^{\mu\nu}(\omega) = 2\mathrm{Im}\left[\chi_k^{\mu\nu}(\omega)\right] \tag{D.8}$$
$$= \frac{2\pi}{NZ}\sum_{m,n}\delta(\omega + E_n - E_m)\langle n|S_k^\mu|m\rangle\langle m|S_{-k}^\nu|n\rangle\left(e^{-\beta E_n} - e^{-\beta E_m}\right),$$

or, in terms of the Green's functions,

$$\rho_k^{\mu\nu}(\omega) = i\Big[G_k^{\mu\nu}(i\omega_n \to \omega + i0^+) - G_k^{\mu\nu}(i\omega_n \to \omega - i0^+)\Big]. \tag{D.9}$$

Note that the spectral density is often written in terms of $A_k^{\mu\nu}(\omega) = \frac{1}{2\pi}\rho_k^{\mu\nu}(\omega)$ in which case

$$\chi_k^{\mu\nu}(\omega) = -\int_{-\infty}^{\infty} d\omega' \frac{A_k^{\mu\nu}(\omega')}{\omega - \omega' + i0^+}. \tag{D.10}$$

The real and imaginary parts of of the dynamic susceptibility are related by a Kramers-Kronig transform

$$\mathrm{Re}[\chi_k^{\mu\nu}(\omega)] = \mathscr{P}\int_{-\infty}^{\infty} \frac{d\Omega}{\pi} \frac{\mathrm{Im}[\chi_k^{\mu\nu}(\Omega)]}{\Omega - \omega}. \tag{D.11}$$

The connected real time correlation function is given by

$$S_{ij}^{\mu\nu}(t - t') = \langle \widetilde{S_i^{\mu}}(t) \widetilde{S_j^{\nu}}(t') \rangle. \tag{D.12}$$

This function is related to the spectral density by the fluctuation dissipation theorem

$$S_k^{\mu\nu}(\omega) = \frac{\rho_k^{\mu\nu}(\omega)}{1 - e^{-\beta\omega}}. \tag{D.13}$$

Finally, we consider the static susceptibility, $\chi^{\mu\nu}(k) = \mathrm{Re}[\chi_k^{\mu\nu}(\omega = 0)]$. In the high temperature limit ($\omega \ll T$), we find it to be related to the equal time correlation function as follows,

$$\beta S_k^{\mu\nu}(t = 0) \approx \int \frac{d\omega}{\pi} \frac{\mathrm{Im}[\chi_k^{\mu\nu}(\omega)]}{\omega} = \chi^{\mu\nu}(k), \tag{D.14}$$

where the Kramers-Kronig relation is used to obtain the final expression. The classical expression for the static susceptibility may also be obtained by differentiating the free energy

$$\chi_{ij}^{\mu\nu} = -\frac{\partial^2 F}{\partial h_i^{\mu} \partial h_j^{\nu}}, \tag{D.15}$$

where h_i^{μ} is a field conjugate to spin S_i^{μ}. We differentiate between static and dynamic expressions for the susceptibility by the absence of a time (or frequency) argument in the static case.

Ising Model: Structure of the Green's Function

In this section, we specialize to the case of the Ising model, that is, we only consider a longitudinal interaction between spins on different sites. The formalism discussed in Appendix C, was applied to the Ising model in a transverse field in a series of 1973 papers by Stinchcombe [26, 62, 63]. Here, we review the structure of the connected longitudinal correlation function, as presented in reference [26].

Recall from Appendix C that the connected two point longitudinal correlation function, or, equivalently, the second order cumulant, may be expressed as a sum of totally connected diagrams. If we define an irreducible diagram as a diagram that cannot be seperated into two parts by severing a single bond, then the correlation function may be written as

$$\begin{aligned} G_k^{\mu\nu}(i\omega_n) &= \mathscr{G}_k^{\mu\nu}(i\omega_n) - \mathscr{G}_k^{\mu z}(i\omega_n) V_k G_k^{z\nu}(i\omega_n) \\ &= \mathscr{G}_k^{\mu\nu}(i\omega_n) - \frac{\mathscr{G}_k^{\mu z}(i\omega_n) V_k \mathscr{G}_k^{z\nu}(i\omega_n)}{1 + V_k \mathscr{G}_k^{zz}(i\omega_n)}, \end{aligned} \tag{D.16}$$

where $\mathscr{G}^{\mu\nu}$ is the sum over all irreducible diagrams. This is an exact result; all the complexity of the problem is contained in the calculation of $\mathscr{G}^{\mu\nu}$. Note that μ and ν may refer electronic spin components, or they may equally well refer to nuclear spin components. The z index refers strictly to an electronic spin, and comes from the longitudinal interspin interaction. Our definition of G differs from that of Stinchcombe by a minus sign. What Stinchcombe refers to as G, we refer to as χ. Furthermore, our $\mathscr{G}^{\mu\nu}$ is equivalent to Stinchcombe's $-\mathscr{M}^{\mu\nu}$, and Stinchcombe uses a different Fourier transform convention than what is used in this thesis. This accounts for the factors of β appearing in Stinchcombe's work that aren't present here. The conventions adopted in this thesis are meant to eliminate numerical factors from subsequent calculations.

The longitudinal component of our Green's function reduces to

$$G_k^{zz}(i\omega_n) = \frac{\mathscr{G}_k^{zz}(i\omega_n)}{1 + V_k \mathscr{G}_k^{zz}(i\omega_n)}. \tag{D.17}$$

To lowest order we have $\mathscr{G}_k^{zz}(i\omega_n) \to g(i\omega_n) = -\langle S^z(i\omega_n) S^z(-i\omega_n)\rangle_0$, where the average is taken with respect to the single ion Hamiltonian. Making this substitution yields the longitudinal Green's function in the random phase approximation (RPA),

$$G_k^{zz}(i\omega_n)\Big|_{RPA} = \frac{g(i\omega_n)}{1 + V_k g(i\omega_n)}. \tag{D.18}$$

In order to analyze the collective excitations of a spin system beyond the RPA, the sum

over irreducible diagrams may be separated into its real and imaginary parts $\mathscr{G}_k^{zz}(\omega+i0^+) = \mathrm{Re}_k^{zz}(\omega)+i\mathrm{Im}_k^{zz}(\omega)$. This yields

$$G_k^{zz}(\omega+i0^+) = \frac{\mathrm{Re}_k^{zz}(\omega)+i\mathrm{Im}_k^{zz}(\omega)}{1+V_k\mathrm{Re}_k^{zz}(\omega)+iV_k\mathrm{Im}_k^{zz}(\omega)}. \tag{D.19}$$

We define the collective mode E_k to be a solution of

$$1+V_k\mathrm{Re}_k^{zz}(E_k) = 0. \tag{D.20}$$

The lifetime Γ_k^p associated with the p^{th} collective mode E_k^p follows from the p^{th} (complex) pole of $G(\omega)$, $z^p = E_k^p - i\Gamma_k^p$. It follows that

$$\Gamma_k^p = V_k\mathrm{Im}_k^{zz}(E_k^p). \tag{D.21}$$

Alternatively, we may work with a self energy by defining $\mathscr{G}_k^{zz} = g[1+\Sigma]^{-1}$ which yields

$$G_k^{zz}(i\omega_n) = \frac{g(i\omega_n)}{1+V_k g(i\omega_n)+\Sigma_k(i\omega_n)}. \tag{D.22}$$

RPA Green's Function

Here we examine the structure of the longitudinal RPA Green's function of an Ising system

$$G_k(i\omega_n) \equiv \frac{g(i\omega_n)}{1+V_k g(i\omega_n)}, \tag{D.23}$$

making use of the mean field (MF) operators discussed in Appendix A. Writing the Green's function as $G_k^{-1}(i\omega_n) = g^{-1}(i\omega_n)+V_k$ we see that the RPA Green's function essentially consists of a momentum dependent shift in the MF Green's function due to the interaction V_k. The MF Green's function (to be derived in Appendix E) is given by

$$g(i\omega_r) = -\sum_{n>m} c_{mn}^2 D_{mn}\frac{2E_{nm}}{E_{nm}^2-(i\omega_r)^2} - g_{el}\delta_{\omega_r,0}. \tag{D.24}$$

This function contains poles at the differences between each of the systems MF eigenstates, $E_{nm} = E_n - E_m$, as well as an additional elastic contribution,

$$g_{el} = \beta\left(\sum_m c_{mm}^2 D_m - \left[\sum_m c_{mm}D_m\right]^2\right), \tag{D.25}$$

that vanishes in the paramagnetic phase, and in the limit $T \to 0$. The c_{mn} are the mean field matrix elements of the S^z operator, and the population factors are $D_{mn} = D_m - D_n$, where $D_m = Z_0^{-1} e^{-\beta E_m}$.

Making use of the identity

$$\lim_{\varepsilon \to 0^+} \frac{1}{x \pm i\varepsilon} = \mathscr{P}\left(\frac{1}{x}\right) \mp i\pi\delta(x), \tag{D.26}$$

we take the real and imaginary parts of $g(\omega + i\varepsilon)$. We find

$$\mathrm{Re}[g(\omega)] = -\sum_{n>m} c_{mn}^2 D_{mn} \mathscr{P}\left[\frac{2E_{nm}}{E_{nm}^2 - \omega^2}\right] - g_{el}\delta_{\omega,0}, \tag{D.27}$$

where $\mathscr{P}$ denotes the principle value, and

$$\mathrm{Im}[g(\omega)] = -\pi \sum_{n>m} \left|\langle m|S^z|n\rangle_0\right|^2 D_{mn}\Big(\delta(E_{nm} - \omega) - \delta(E_{nm} + \omega)\Big). \tag{D.28}$$

Note that at zero temperature, the real part of g corresponds to the Van Vleck contribution to the susceptibility, that is, it is a contribution arising solely from the splitting of the energy levels of the system's eigenstates.

To understand the elastic contribution to the spectrum, it is advantageous to write

$$\mathrm{Im}[g(\omega)] = -\pi \sum_{nm} \left|\langle m|S^z|n\rangle_0\right|^2 D_{mn}\delta(E_{nm} - \omega), \tag{D.29}$$

where the summation over n and m is now unrestricted. If $\omega \neq 0$, all terms with $n = m$ vanish, as $D_{mn}\delta(\omega) = 0$; however, at $\omega = 0$ the $n = m$ terms lead to the elastic contribution to the spectrum, as we will show below. The Kramers-Kronig relation tells us

$$\mathrm{Re}[g(\omega)] = \mathscr{P}\int_{-\infty}^{\infty} \frac{d\Omega}{\pi} \frac{\mathrm{Im}[g(\Omega)]}{\Omega - \omega}. \tag{D.30}$$

The integration is straightforward except near $\omega = 0$ where we have

$$g_{el} = \lim_{\varepsilon \to 0} \int_{-\varepsilon}^{\varepsilon} \frac{d\Omega}{\pi} \frac{\mathrm{Im}[g(\Omega)]}{\Omega}. \tag{D.31}$$

For further discussion of the elastic contribution to the spectrum see the book *Rare Earth Magnetism*, by Jensen and Mackintosh [65].

We define the free field propagator to be

$$\mathscr{D}_k(i\omega_r) = \frac{1}{1+g(i\omega_r)V_k}. \tag{D.32}$$

If the Ising model is treated using the Hubbard-Stratonovich transformation, the expression above will be the propagator for the free auxiliary field, hence the name. Nomenclature aside, we divide the free propagator into two parts, $\mathscr{D}_k(i\omega_r) = D_k(i\omega_r) + D_k^0\delta_{i\omega_r,0}$, where

$$\begin{aligned} D_k(i\omega_r) &= \frac{\prod_{n>m}[E_{nm}^2-(i\omega_r)^2]}{\prod_p[(E_k^p)^2-(i\omega_r)^2]} \\ &= \frac{\prod_{n>m}[E_{nm}^2-(i\omega_r)^2]}{\prod_{n>m}[E_{nm}^2-(i\omega_r)^2]-V_k\sum_{n>m}c_{mn}^2D_{mn}2E_{nm}\prod_{p,q\neq m,n}[E_{pq}^2-(i\omega_r)^2]}, \end{aligned} \tag{D.33}$$

and

$$D_k^0 = \frac{g_{el}V_k\prod_{n>m}E_{nm}^4}{\prod_p(E_k^p)^2\left[\prod_p(E_k^p)^2-g_{el}V_k\prod_{n>m}E_{nm}^2\right]}. \tag{D.34}$$

It is convenient to factor the denominator of $D_k(i\omega_r)$ because, in the zero temperature limit, this yields the RPA modes of the system. At finite temperatures, there are additional poles corresponding to excitations between excited states. It is a matter of convenience to include the $i\omega_r = 0$ term in $D_k(i\omega_r)$, and then subtract it from D_k^0. Note that $D_k^0 \propto g_{el}$ vanishes as the temperature goes to zero, and in the paramagnetic phase of the system. The ratio of the product of the mean field energy levels to the product of RPA energy levels occurs quite frequently, hence we will designate it

$$R_k = \frac{\prod_{n>m}E_{nm}^2}{\prod_p(E_k^p)^2}. \tag{D.35}$$

In terms of R_k, we find

$$D_k^0 = \frac{g_{el}V_kR_k^2}{1-g_{el}V_kR_k}. \tag{D.36}$$

We now consider the inelastic part of the RPA Green's function $G = gD$, where g is given by equation (D.24) with $g_{el} = 0$ and D is given by equation (D.33). D has zeros at all the MF energy levels, while g has simple poles at all these levels. Hence, the poles of g contribute nothing to the pole structure of the longitudinal RPA Green's function. This is a rather trivial observation; however, it is worth noting that any function $F(z)$, with simple poles at the MF

energy levels, will not alter the pole structure of $F(z)D(z)$. This fact proves useful when examining corrections to the RPA result.

We now decompose the RPA Green's function into a sum over its constituent modes, in order to obtain the spectral density of each mode. The RPA Green's function is given by

$$G_k(i\omega_r) = \widetilde{G}_k(i\omega_r) - G_k^{el}\delta_{\omega_r,0}, \tag{D.37}$$

where

$$\widetilde{G}_k(i\omega_r) = -\frac{\sum_{n>m} c_{mn}^2 D_{mn} 2E_{nm} \prod_{t>s\neq nm}[E_{ts}^2 - (i\omega_r)^2]}{\prod_{n>m}[E_{nm}^2 - (i\omega_r)^2] - V_k \sum_{n>m} c_{mn}^2 D_{mn} 2E_{nm} \prod_{p,q\neq m,n}[E_{pq}^2 - (i\omega_r)^2]}, \tag{D.38}$$

and the elastic contribution is

$$G_k^{el} = g_{el}R_k\left[\frac{1 + 2V_kR_k\sum_{n>m} c_{mn}^2 D_{mn} E_{nm}^{-1}}{1 - g_{el}V_kR_k}\right]. \tag{D.39}$$

The denominator of $\widetilde{G}_k(i\omega_r)$ has been written out in full, rather than being expressed in terms of the RPA modes. This is to illustrate the fact that if one of the MF matrix elements c_{mn} vanishes, there will be a common factor of $E_{nm}^2 - (i\omega_r)^2$ in the numerator and denominator of $\widetilde{G}_k(i\omega_r)$. Hence, when a MF matrix element is zero, there will be a pole at the corresponding MF energy level in the RPA spectrum; however, this pole will carry no spectral weight. The inelastic part of the RPA Green's function has the form $\widetilde{G}_k(z) = \frac{P(z)}{Q(z)}$, where $P(z)$ and $Q(z)$ are polynomials in z, and $\deg[P(z)] < \deg[Q(z)]$. Assuming no degenerate modes, we may perform a partial fraction decomposition to obtain

$$\widetilde{G}_k(z \neq 0) = \sum_p \frac{P(E_k^p)}{Q'(E_k^p)}\left[\frac{1}{(z - E_k^p)} - \frac{1}{(z + E_k^p)}\right], \tag{D.40}$$

where

$$P(E_k^p) = P(-E_k^p) = \sum_{n>m} c_{mn}^2 D_{mn} 2E_{nm} \prod_{t>s\neq nm}[E_{ts}^2 - (E_k^p)^2] \tag{D.41}$$

$$Q'(E_k^p) = -Q'(-E_k^p) = 2E_k^p \prod_{s\neq p}\left[(E_k^p)^2 - (E_k^s)^2\right].$$

The spectral density is

$$A_k(\omega) = -\frac{1}{\pi}\mathrm{Im}[G_k(i\omega_r \to \omega + i\delta)] = \sum_p \frac{P(E_k^p)}{Q'(E_k^p)}\left[\delta(\omega - E_k^p) - \delta(\omega + E_k^p)\right], \tag{D.42}$$

and the dynamic structure factor is given by

$$S_k(\omega) = \frac{2\pi}{1-e^{-\beta\omega}} \sum_p \frac{P(E_k^p)}{Q'(E_k^p)} \left[\delta(\omega - E_k^p) - \delta(\omega + E_k^p) \right]. \tag{D.43}$$

Integrating over frequencies, we find the equal time correlation function to be given by

$$S_k(t=0) = \int_{-\infty}^{\infty} \frac{d\omega}{2\pi} S_k(\omega) = \sum_p \frac{P(E_k^p)}{Q'(E_k^p)} \frac{\sinh(\beta E_k^p)}{\cosh(\beta E_k^p) - 1} + \frac{1}{\beta} G_k^{el}, \tag{D.44}$$

where, as with the mean field Green's function, we have included the elastic contribution stemming from the zero frequency pole. We may compare this expression to its classical counterpart ($\omega << T$). We find

$$\chi_k = \beta S_k^c(t=0) = \sum_p \frac{2}{E_k^p} \frac{P(E_k^p)}{Q'(E_k^p)} + G_k^{el}. \tag{D.45}$$

As a consistency check of the formalism presented here, consider the imaginary time dynamic correlation function

$$\chi_k(i\omega_r) = -G_k(i\omega_r) = -\sum_p 2E_k^p \frac{P(E_k^p)}{Q'(E_k^p)} \left[\frac{1}{(i\omega_r)^2 - (E_k^p)^2} \right] + G_k^{el} \delta_{\omega_r,0}. \tag{D.46}$$

Summing over Matsubara frequencies should yield the equal time correlation function,

$$S_k(\tau=0) = \frac{1}{\beta} \sum_r \chi_k(i\omega_r) \overset{T\to 0}{=} \int_{-\infty}^{\infty} \frac{d\omega}{2\pi} \sum_p 2E_k^p \frac{P(E_k^p)}{Q'(E_k^p)} \left[\frac{1}{\omega^2 + (E_k^p)^2} \right] \Bigg|_{T=0}. \tag{D.47}$$

By performing the frequency summation, or the integral in the zero temperature limit, equation (D.44) may be recovered, as expected.

As a final note, we point out how the analytic structure of the Green's function changes when the effect of fluctuations beyond the Gaussian approximation (RPA) are included by renormalizing the system at its critical point. In the Gaussian approximation, the Green's function has the form

$$G_k(i\omega_n)\Big|_{RPA} \propto \frac{1}{(i\omega_n)^2 - E_k^2}. \tag{D.48}$$

Under renormalization, this changes to

$$G_k(i\omega_n) \propto \left[(i\omega_n)^2 - E_k^2\right]^{-1+\frac{\eta}{2}}. \tag{D.49}$$

This shows that at the critical point, rather than having the usual quasiparticle pole in the Green's function, there is a branch cut corresponding to a continuum of excitations. This implies the excitations at the quantum critical point are overdamped, and the system will show relaxational dynamics [28–30].

Appendix E

Spin Cumulants

Spin cumulants play a central role in the analysis of interacting spin systems. In this appendix, we calculate cumulants of up to four spin operators for a system with an arbitrary single ion Hamiltonian. Cumulants of this order are necessary for calculating corrections of order $\frac{1}{z}$ in the high density approximation developed in Chapter 6. We calculate the cumulants using the formalism discussed in Appendix A. Our focus will be on cumulants of the S^z operator; however, as any operator may be expanded in terms of mean field (MF) eigenstates, the results are quite general. Essentially, with a little modification, the results of this appendix are completely general expressions for the cumulants, or correlation functions, of operators acting on a system with a discrete set of energy levels.

The calculation of the cumulants is straightforward, but rather tedious, and the resulting equations are quite cumbersome. We present them here for reference, and note a significant simplification that occurs in the zero temperature limit. In writing out the cumulants we will make extensive use of the function (and products of these functions)

$$K^0_{nm}(i\omega_r) = \frac{1}{E_n - E_m - i\omega_r}, \tag{E.1}$$

the properties of which are discussed in Appendix A.

We begin by writing S^z in the MF basis

$$S^z = \sum_m c_{mm} L_{mm} + \sum_{m \neq n} c_{mn} L_{mn}. \tag{E.2}$$

The lowest order cumulant is given by

$$M_1(S^z) = \langle S^z \rangle_0 = \sum_m c_{mm} D_m. \tag{E.3}$$

Two Spin Cumulant

Defining $S_i \equiv S^z(\tau_i)$ and $L^i_{mn} \equiv L_{mn}(\tau_i)$, we find at second order

$$M_2(T_\tau S_1 S_2) = \sum_{m,n} c_{mm} c_{nn} \langle T_\tau L^1_{mm} L^2_{nn} \rangle_0 + \sum_{P\{1,2\}} \sum_{n>m} |c_{mn}|^2 \langle T_\tau L^1_{mn} L^2_{nm} \rangle_0 - \left[\sum_m c_{mm} D_m \right]^2 \quad \text{(E.4)}$$

where $P\{1,2,\ldots n\}$ denotes the set of all permutations. Contracting the MF operators we find

$$\langle T_\tau L^1_{mm} L^2_{nn} \rangle_0 = D_m \delta_{mn} \qquad \sum_{P\{1,2\}} \langle T_\tau L^1_{mn} L^2_{nm} \rangle_0 = -D_{nm} K_{nm}(\tau_{12}) \quad \text{(E.5)}$$

where we've set $\tau_{ij} \equiv \tau_i - \tau_j$ for brevity, and defined the MF propagator to be

$$K_{nm}(\tau) = K^0_{nm}(\tau) + K^0_{nm}(-\tau). \quad \text{(E.6)}$$

We now transform our cumulant to frequency space

$$M_2(\omega_{r_1}, \omega_{r_2}) = \mathscr{F}\{M_2(T_\tau S_1 S_2)\} = \prod_{i=1}^{2} \int_0^\beta d\tau_i e^{i\omega_{r_i}\tau_i} M_2(T_\tau S_1 S_2). \quad \text{(E.7)}$$

Note that

$$\prod_{i=1}^{2} \int_0^\beta d\tau_i e^{i\omega_{r_i}\tau_i} K_{nm}(\tau_{12}) = \beta \sum_{\lambda_s} K_{nm}(\lambda_s) \delta_{\omega_{r_1},\lambda_s} \delta_{\omega_{r_2},-\lambda_s} = \beta K_{nm}(\omega_{r_1}) \delta_{\omega_{r_1}+\omega_{r_2},0}, \quad \text{(E.8)}$$

where

$$K_{nm}(\omega_{r_1}) = \frac{2E_{nm}}{E^2_{mn} - (i\omega_{r_1})^2}. \quad \text{(E.9)}$$

Our final result for the second order cumulant is

$$\begin{aligned} M_2(\omega_{r_1}, \omega_{r_2}) =& \beta \sum_{n>m} |c_{mn}|^2 D_{nm} \frac{2E_{mn}}{E^2_{mn} - (i\omega_{r_1})^2} \delta_{\omega_{r_1}+\omega_{r_2},0} \\ &+ \beta^2 \left(\sum_m c^2_{mm} D_m - \left[\sum_m c_{mm} D_m \right]^2 \right) \prod_{i=1}^{2} \delta_{\omega_{r_i},0}. \end{aligned} \quad \text{(E.10)}$$

Performing a frequency summation, we obtain the MF correlation function of the S^z operator

$$\begin{aligned} g(\omega_{r_1}) &\equiv -\frac{1}{\beta}\sum_{r_2} M_2(\omega_{r_1},\omega_{r_2}) \\ &= -\sum_{n>m} |c_{mn}|^2 D_{mn} \frac{2E_{nm}}{E_{nm}^2 - (i\omega_{r_1})^2} - \beta\left(\sum_m c_{mm}^2 D_m - \left[\sum_m c_{mm} D_m\right]^2\right)\delta_{\omega_{r_1},0}, \end{aligned} \tag{E.11}$$

which can be written in terms of $K_{nm}(i\omega_r)$ as

$$-g(\omega_{r_1}) = \sum_{n>m} |c_{mn}|^2 D_{mn} K_{nm}(i\omega_r) + \beta\left(\sum_m c_{mm}^2 D_m - \left[\sum_m c_{mm} D_m\right]^2\right)\delta_{\omega_{r_1},0}. \tag{E.12}$$

In the zero temperature limit, this expression reduces to

$$-g(\omega_{r_1}) = \frac{\sum_{n>1} |c_{1n}|^2 2E_{n1} \prod_{m\neq n} E_{m1}^2 - (i\omega_{r_1})^2}{\prod_n E_{n1}^2 - (i\omega_{r_1})^2}. \tag{E.13}$$

Three Spin Cumulant

At third order we have

$$\begin{aligned} M_3(T_\tau S_1 S_2 S_3) =& \langle T_\tau S_1 S_2 S_3\rangle_0 - M_2(T_\tau S_1 S_2)\langle S_3\rangle_0 - M_2(T_\tau S_1 S_3)\langle S_2\rangle_0 \\ & - M_2(T_\tau S_2 S_3)\langle S_1\rangle_0 - \langle S_1\rangle_0\langle S_2\rangle_0\langle S_3\rangle_0 \end{aligned} \tag{E.14}$$

Expanding in the mean field basis, we find

$$\begin{aligned} \langle T_\tau S_1 S_2 S_3\rangle_0 =& \sum_m c_{mm}^3 \langle T_\tau L_{mm}^1 L_{mm}^2 L_{mm}^3\rangle_0 \\ &+ \sum_{P\{1,2,3\}}\left[\sum_{m\neq n} c_{mm}|c_{mn}|^2\langle T_\tau L_{mm}^1 L_{mn}^2 L_{nm}^3\rangle_0 + \sum_{m\neq n\neq p} c_{mn}c_{np}c_{pm}\langle T_\tau L_{mn}^1 L_{np}^2 L_{pm}^3\rangle_0\right]. \end{aligned} \tag{E.15}$$

In the case of a two level system, the final term in this expression is zero, and the third order cumulant vanishes altogether above the MF critical temperature. In principle, in a system with more than two levels, this cumulant may be non-zero, even in the paramagnetic phase of the system. In the summation in the third term, we sum over all m, and for each m we sum over all $n, p > m$ such that $n \neq p$. Using the formalism in Appendix A to contract the MF operators,

we find

$$\sum_{P\{1,2,3\}} \langle T_\tau L^1_{mm} L^2_{mn} L^3_{nm} \rangle_0 = -D_{mn} \sum_{P\{1,2,3\}} K^{mn}_{mn}(\tau_{12};\tau_{31}) \tag{E.16}$$
$$- D_m \Big[K_{mn}(\tau_{21}) + K_{mn}(\tau_{31}) + K_{mn}(\tau_{32}) \Big]$$
$$\sum_{P\{1,2,3\}} \langle T_\tau L^1_{mn} L^2_{np} L^3_{pm} \rangle_0 = -D_{pn} \sum_{P\{1,2,3\}} K^{pn}_{mn}(\tau_{31};\tau_{23}) + D_{pm} \sum_{P\{1,2,3\}} K^{pm}_{mn}(\tau_{21};\tau_{23}),$$

where we've defined

$$K_{mn}(\tau) \equiv K^0_{mn}(\tau) + K^0_{mn}(-\tau) \qquad\qquad K^{pq}_{mn}(\tau_1;\tau_2) \equiv K^0_{mn}(\tau_1) K^0_{pq}(\tau_2). \tag{E.17}$$

We now transform our cumulant to frequency space

$$M_3(\omega_{r_1},\omega_{r_2},\omega_{r_3}) = \mathscr{F}\{M_3(T_\tau S_1 S_2 S_3)\} = \prod_{i=1}^{3} \int_0^\beta d\tau_i e^{i\omega_{r_i}\tau_i} M_3(T_\tau S_1 S_2 S_3) \tag{E.18}$$
$$= \mathscr{F}\{\langle T_\tau S_1 S_2 S_3)\rangle_0\} - \beta M_2(\omega_1,\omega_2)\langle S_3\rangle_0 \delta_{\omega_{r_3},0}$$
$$- \beta M_2(\omega_1,\omega_3)\langle S_3\rangle_0 \delta_{\omega_{r_2},0} - \beta M_2(\omega_2,\omega_3)\langle S_3\rangle_0 \delta_{\omega_{r_1},0} - \beta^3 \langle S\rangle_0^3 \prod_{i=1}^{3} \delta_{\omega_i,0}.$$

For reference, we note that

$$\mathscr{F}\{K_{mn}(\tau_{12})\} = \beta^2 \sum_s K_{mn}(\lambda_s)\delta_{\omega_{r_1},\lambda_s}\delta_{\omega_{r_2},-\lambda_s}\delta_{\omega_{r_3},0} = \beta^2 K_{mn}(\omega_{r_1})\delta_{\omega_{r_1}+\omega_{r_2},0}\delta_{\omega_{r_3},0} \tag{E.19}$$

and

$$\mathscr{F}\{K^{pq}_{mn}(\tau_{12};\tau_{31})\} = \beta \sum_{st} K^0_{mn}(\lambda_s) K^0_{pq}(\lambda_t)\delta_{\omega_{r_1},\lambda_s-\lambda_t}\delta_{\omega_{r_2},-\lambda_s}\delta_{\omega_{r_3},\lambda_t} \tag{E.20}$$
$$= \beta K^{pq}_{mn}(-\omega_{r_2};\omega_{r_3})\delta_{\omega_{r_1}+\omega_{r_2}+\omega_{r_3},0},$$

where, in the last line, we define

$$K^0_{mn}(\omega_r) K^0_{pq}(\omega_s) \equiv K^{pq}_{mn}(\omega_r;\omega_s). \tag{E.21}$$

Making use of these expressions we find our Fourier transformed spin averages to be given by

$$\mathscr{F}\{\langle T_\tau L^1_{mm} L^2_{mm} L^3_{mm}\rangle_0\} = \beta^3 D_m \prod_{i=1}^{3} \delta_{\omega_{r_i},0}, \tag{E.22}$$

and

$$\widetilde{A_1} = \mathscr{F}\left\{ \sum_{P\{1,2,3\}} \langle T_\tau L^1_{mm} L^2_{mn} L^3_{nm} \rangle_0 \right\} = \beta D_{mn} \sum_{P\{\omega_{r_i}\}} K^{mn}_{nm}(\omega_{r_1};\omega_{r_2}) \delta_{\omega_{r_1}+\omega_{r_2}+\omega_{r_3},0} \tag{E.23}$$

$$- \beta^2 D_m \left[K_{mn}(\omega_{r_2}) \delta_{\omega_{r_2}+\omega_{r_3},0} \delta_{\omega_{r_1},0} + K_{mn}(\omega_{r_1}) \delta_{\omega_{r_1}+\omega_{r_3},0} \delta_{\omega_{r_2},0} + K_{mn}(\omega_{r_1}) \delta_{\omega_{r_1}+\omega_{r_2},0} \delta_{\omega_{r_3},0} \right]$$

$$A_2 = \mathscr{F}\left\{ \sum_{P\{1,2,3\}} \langle T_\tau L^1_{mn} L^2_{np} L^3_{pm} \rangle_0 \right\}$$

$$= \beta D_{pm} \sum_{P\{\omega_{r_i}\}} K^{nm}_{mp}(\omega_{r_1};\omega_{r_2}) \delta_{\omega_{r_1}+\omega_{r_2}+\omega_{r_3},0} + \beta D_{pn} \sum_{P\{\omega_{r_i}\}} K^{nm}_{pn}(\omega_{r_1};\omega_{r_2}) \delta_{\omega_{r_1}+\omega_{r_2}+\omega_{r_3},0}.$$

Note that we have made use of the fact $K^0_{mn}(-\omega_r) = -K^0_{nm}(\omega_r)$.

Some algebra will show that, in the low temperature limit, terms in $\langle T_\tau S_1 S_2 S_3 \rangle_0$ cancel with the lower order cumulants, significantly reducing the complexity of the expression. We are left with

$$\lim_{T\to 0} M_3(\omega_{r_1},\omega_{r_2},\omega_{r_3}) = \sum_{m\neq n} c_{mm}|c_{mn}|^2 A_1(\omega_{r_1},\omega_{r_2},\omega_{r_3}) + \sum_{m\neq n\neq p} c_{mn}c_{np}c_{pm} A_2(\omega_{r_1},\omega_{r_2},\omega_{r_3}) \tag{E.24}$$

with

$$A_1(\omega_{r_1},\omega_{r_2},\omega_{r_3}) = \beta D_{mn} \sum_{P\{\omega_{r_i}\}} K^{mn}_{nm}(\omega_{r_1};\omega_{r_2}) \delta_{\omega_{r_1}+\omega_{r_2}+\omega_{r_3},0} \tag{E.25}$$

$$A_2(\omega_{r_1},\omega_{r_2},\omega_{r_3}) = \beta D_{pm} \sum_{P\{\omega_{r_i}\}} K^{nm}_{mp}(\omega_{r_1};\omega_{r_2}) \delta_{\omega_{r_1}+\omega_{r_2}+\omega_{r_3},0}$$

$$+ \beta D_{pn} \sum_{P\{\omega_{r_i}\}} K^{nm}_{pn}(\omega_{r_1};\omega_{r_2}) \delta_{\omega_{r_1}+\omega_{r_2}+\omega_{r_3},0}.$$

This may be further reduced by considering the population factors in the A_is. We find

$$\lim_{T\to 0} M_3(\omega_{r_1},\omega_{r_2},\omega_{r_3}) = \sum_{n>1} (c_{11}-c_{nn})|c_{1n}|^2 A^0_1(\omega_{r_1},\omega_{r_2},\omega_{r_3}) \tag{E.26}$$

$$+ \sum_{\substack{n>1 \\ p>n}} \mathrm{Re}[c_{1n}c_{np}c_{p1}] A^0_2(\omega_{r_1},\omega_{r_2},\omega_{r_3}),$$

where

$$A_1^0(\omega_{r_1},\omega_{r_2},\omega_{r_3}) = \beta \sum_{P\{\omega_{r_i}\}} K_{n1}^{1n}(\omega_{r_1};\omega_{r_2})\delta_{\omega_{r_1}+\omega_{r_2}+\omega_{r_3},0} \tag{E.27}$$

$$A_2^0(\omega_{r_1},\omega_{r_2},\omega_{r_3}) = 2\beta \sum_{P\{\omega_{r_i}\}} \frac{E_{p1}E_{n1} - (i\omega_{r_1})(i\omega_{r_2})}{(E_{p1}^2 - (i\omega_{r_1})^2)(E_{n1}^2 - (i\omega_{r_2})^2)}\delta_{\omega_{r_1}+\omega_{r_2}+\omega_{r_3},0}.$$

In the terms involving transitions between three MF eigenstates, we have used the fact that $c_{np} = c_{pn}^*$ for any np to combine terms in the sum.

Four Spin Cumulant

We now calculate the fourth order cumulant. We start our reduction of the MF operators with L_{mn} such that m is minimal, unless otherwise noted. We find

$$\begin{aligned} M_4(T_\tau S_1 S_2 S_3 S_4) &= \langle T_\tau S_1 S_2 S_3 S_4\rangle_0 - \langle S_1\rangle_0\langle S_2\rangle_0\langle S_3\rangle_0\langle S_4\rangle_0 \\ &- M_2(T_\tau S_1 S_2)M_2(S_3 S_4) - M_2(T_\tau S_1 S_3)M_2(T_\tau S_2 S_4) - M_2(T_\tau S_1 S_4)M_2(T_\tau S_2 S_3) \\ &- M_3(T_\tau S_1 S_2 S_3)\langle S_4\rangle_0 - M_3(T_\tau S_1 S_2 S_4)\langle S_3\rangle_0 - M_3(T_\tau S_1 S_3 S_4)\langle S_2\rangle_0 - M_3(T_\tau S_2 S_3 S_4)\langle S_1\rangle_0 \\ &- M_2(T_\tau S_1 S_2)\rangle_0\langle S_3\rangle_0\langle S_4\rangle_0 - M_2(T_\tau S_1 S_3)\rangle_0\langle S_2\rangle_0\langle S_4\rangle_0 - M_2(T_\tau S_1 S_4)\rangle_0\langle S_2\rangle_0\langle S_3\rangle_0 \\ &- M_2(T_\tau S_2 S_3)\rangle_0\langle S_1\rangle_0\langle S_4\rangle_0 - M_2(T_\tau S_2 S_4)\rangle_0\langle S_1\rangle_0\langle S_3\rangle_0 - M_2(T_\tau S_3 S_4)\rangle_0\langle S_1\rangle_0\langle S_2\rangle_0 \end{aligned} \tag{E.28}$$

Expanding in terms of the MF operators, we find the fourth order spin correlation function to be given by

$$\begin{aligned} \langle T_\tau S_1 S_2 S_3 S_4\rangle_0 = &\sum_m c_{mm}^4 \langle T_\tau L_{mm}^1 L_{mm}^2 L_{mm}^3 L_{mm}^4\rangle_0 \\ &+ \sum_{m\neq n} c_{mm}^2 |c_{mn}|^2 \widetilde{B}_1 + \sum_{n>m} c_{mm}c_{nn}|c_{mn}|^2 \widetilde{B}_2 \\ &+ \sum_{n>m} |c_{mn}|^4 \widetilde{B}_3 + \sum_{m\neq n\neq p} c_{mm}c_{mn}c_{np}c_{pm}\widetilde{B}_4 \\ &+ \sum_{p>n>m} |c_{mn}|^2|c_{mp}|^2 \widetilde{B}_5 + \sum_m \sum_{n>m} \sum_{\substack{p>m \\ p\neq n}} \sum_{\substack{q>m \\ q\neq n,p}} c_{mn}c_{np}c_{pq}c_{qm}B_6, \end{aligned} \tag{E.29}$$

where

$$\widetilde{B}_1 = \sum_{P\{2,3,4\}} \langle T_\tau L^1_{mm} L^2_{mm} L^3_{mn} L^4_{nm} \rangle_0 + \sum_{P\{1,4\}} \langle T_\tau L^2_{mm} L^3_{mm} L^1_{mn} L^4_{nm} \rangle_0 \tag{E.30}$$
$$+ \sum_{P\{1,3\}} \langle T_\tau L^2_{mm} L^4_{mm} L^1_{mn} L^3_{nm} \rangle_0 + \sum_{P\{1,2\}} \langle T_\tau L^3_{mm} L^4_{mm} L^1_{mn} L^2_{nm} \rangle_0$$
$$\widetilde{B}_2 = \sum_{P\{1,2,3,4\}} \langle T_\tau L^1_{mm} L^2_{nn} L^3_{mn} L^4_{nm} \rangle_0$$
$$\widetilde{B}_3 = \langle T_\tau L^3_{mn} L^1_{nm} L^4_{mn} L^2_{nm} \rangle_0 + \langle T_\tau L^1_{mn} L^3_{nm} L^2_{mn} L^4_{nm} \rangle_0 + \sum_{P\{1,2\}} \sum_{P\{3,4\}} \langle T_\tau L^1_{mn} L^2_{nm} L^3_{mn} L^4_{nm} \rangle_0$$
$$\widetilde{B}_4 = \sum_{P\{1,2,3,4\}} \langle T_\tau L^1_{mm} L^2_{mn} L^3_{np} L^4_{pm} \rangle_0$$
$$\widetilde{B}_5 = \sum_{P\{1,2,3,4\}} \langle T_\tau L^1_{mn} L^2_{nm} L^3_{mp} L^4_{pm} \rangle_0$$
$$B_6 = \sum_{P\{1,2,3,4\}} \langle T_\tau L^1_{mn} L^2_{np} L^3_{pq} L^4_{qm} \rangle_0$$

The terms with repeated MF operators must be dealt with carefully, so as to not over count the possible unique time ordered averages of the operators. We place a tilde over the first five functions to differentiate them from the expressions obtained in the low temperature limit.

Contracting the MF operators leads to rather lengthy expressions which are listed here for reference. We begin by making the following definitions

$${}_{rs}K^{pq}_{mn}(\tau_{ab};\tau_{cd};\tau_{ef}) = K^0_{mn}(\tau_{ab}) K^0_{pq}(\tau_{cd}) K^0_{rs}(\tau_{ef}), \tag{E.31}$$

and

$$\widetilde{K}^{pq}_{mn}(\tau_{ab};\tau_{cd}) = K^{pq}_{mn}(\tau_{ab};\tau_{cd}) + K^{pq}_{mn}(\tau_{ba};\tau_{dc}) \tag{E.32}$$
$${}_{rs}\widetilde{K}^{pq}_{mn}(\tau_{ab};\tau_{cd};\tau_{ef}) = {}_{rs}K^{pq}_{mn}(\tau_{ab};\tau_{cd};\tau_{ef}) + {}_{rs}K^{pq}_{mn}(\tau_{ba};\tau_{dc};\tau_{fe}).$$

We find

$$\begin{aligned}\widetilde{B}_1 = &- D_{mn}\Big[{}_{mn}\widetilde{K}^{mn}_{mn}(\tau_{12};\tau_{23};\tau_{34}) + {}_{mn}\widetilde{K}^{mn}_{mn}(\tau_{12};\tau_{31};\tau_{43}) + {}_{mn}\widetilde{K}^{mn}_{mn}(\tau_{12};\tau_{34};\tau_{41}) \\ &\quad + {}_{mn}\widetilde{K}^{mn}_{mn}(\tau_{12};\tau_{24};\tau_{31}) + {}_{mn}\widetilde{K}^{mn}_{mn}(\tau_{12};\tau_{23};\tau_{41}) + {}_{mn}\widetilde{K}^{mn}_{mn}(\tau_{12};\tau_{24};\tau_{43}) \\ &\quad + {}_{mn}\widetilde{K}^{mn}_{mn}(\tau_{13};\tau_{34};\tau_{42}) + {}_{mn}\widetilde{K}^{mn}_{mn}(\tau_{13};\tau_{32};\tau_{24}) + {}_{mn}\widetilde{K}^{mn}_{mn}(\tau_{13};\tau_{32};\tau_{41}) \\ &\quad + {}_{mn}\widetilde{K}^{mn}_{mn}(\tau_{13};\tau_{41};\tau_{24}) + {}_{mn}\widetilde{K}^{mn}_{mn}(\tau_{14};\tau_{43};\tau_{32}) + {}_{mn}\widetilde{K}^{mn}_{mn}(\tau_{14};\tau_{42};\tau_{23})\Big] \\ &- D_m\Big[\widetilde{K}^{mn}_{mn}(\tau_{12};\tau_{31}) + \widetilde{K}^{mn}_{mn}(\tau_{12};\tau_{24}) + \widetilde{K}^{mn}_{mn}(\tau_{12};\tau_{23}) + \widetilde{K}^{mn}_{mn}(\tau_{12};\tau_{41}) \\ &\quad + \widetilde{K}^{mn}_{mn}(\tau_{13};\tau_{32}) + \widetilde{K}^{mn}_{mn}(\tau_{13};\tau_{41}) + \widetilde{K}^{mn}_{mn}(\tau_{13};\tau_{34}) + \widetilde{K}^{mn}_{mn}(\tau_{14};\tau_{42}) \\ &\quad + \widetilde{K}^{mn}_{mn}(\tau_{14};\tau_{43}) + +\widetilde{K}^{mn}_{mn}(\tau_{23};\tau_{34}) + \widetilde{K}^{mn}_{mn}(\tau_{23};\tau_{42}) + \widetilde{K}^{mn}_{mn}(\tau_{24};\tau_{43})\Big] \\ &- D_m\Big[K_{mn}(\tau_{12}) + K_{mn}(\tau_{13}) + K_{mn}(\tau_{14}) + K_{mn}(\tau_{23}) + K_{mn}(\tau_{24}) + K_{mn}(\tau_{34})\Big],\end{aligned} \tag{E.33}$$

and

$$\begin{aligned}\widetilde{B}_2 = \sum_{P\{1,2,3,4\}}\Big[&D_{mn}\ {}_{mn}K^{mn}_{mn}(\tau_{23};\tau_{12};\tau_{41}) + D_{mn}\ {}_{mn}K^{mn}_{mn}(\tau_{13};\tau_{21};\tau_{42}) \\ &+ D_m K^{mn}_{mn}(\tau_{23};\tau_{42}) + D_n K^{mn}_{mn}(\tau_{13};\tau_{41})\Big],\end{aligned} \tag{E.34}$$

and

$$\begin{aligned}\widetilde{B}_3 = D_{mn}\Bigg[&K^0_{mn}(\tau_{23})\Big(K^{nm}_{nm}(\tau_{24};\tau_{12})+K^{mn}_{mn}(\tau_{21};\tau_{42})\Big) \\ &+K^0_{mn}(\tau_{32})\Big(K^{nm}_{nm}(\tau_{34};\tau_{13})+K^{mn}_{mn}(\tau_{31};\tau_{43})\Big)+K^0_{mn}(\tau_{43})\Big(\widetilde{K}^{nm}_{nm}(\tau_{42};\tau_{14})+\widetilde{K}^{mn}_{mn}(\tau_{41};\tau_{24})\Big) \\ &+K^0_{mn}(\tau_{34})\Big(\widetilde{K}^{nm}_{nm}(\tau_{32};\tau_{13})+\widetilde{K}^{mn}_{mn}(\tau_{31};\tau_{23})\Big)+K^0_{mn}(\tau_{13})\Big(K^{nm}_{nm}(\tau_{14};\tau_{21})+K^{mn}_{mn}(\tau_{12};\tau_{41})\Big) \\ &+K^0_{mn}(\tau_{42})\Big(K^{nm}_{nm}(\tau_{43};\tau_{14})+K^{mn}_{mn}(\tau_{41};\tau_{34})\Big)++K^0_{mn}(\tau_{24})\Big(\widetilde{K}^{nm}_{nm}(\tau_{23};\tau_{12})+\widetilde{K}^{mn}_{mn}(\tau_{21};\tau_{32})\Big) \\ &\qquad+K^0_{mn}(\tau_{14})\Big(\widetilde{K}^{nm}_{nm}(\tau_{13};\tau_{21})+\widetilde{K}^{mn}_{mn}(\tau_{12};\tau_{31})\Big)\Bigg] \\ -D_n\Bigg[&\widetilde{K}^{nm}_{mn}(\tau_{43};\tau_{12})+\widetilde{K}^{nm}_{mn}(\tau_{34};\tau_{12})+K^0_{mn}(\tau_{24})K_{nm}(\tau_{13})+K^0_{mn}(\tau_{14})K_{nm}(\tau_{23}) \\ &\qquad+K_{mn}(\tau_{23})K^0_{nm}(\tau_{14})+K^{nm}_{mn}(\tau_{13};\tau_{24})+K^{nm}_{mn}(\tau_{42};\tau_{13})\Bigg] \\ +D_m\Bigg[&\widetilde{K}^{mn}_{mn}(\tau_{43};\tau_{12})+\widetilde{K}^{mn}_{mn}(\tau_{34};\tau_{12})+K^0_{mn}(\tau_{24})K_{mn}(\tau_{31})+K^0_{mn}(\tau_{14})K_{mn}(\tau_{32}) \\ &\qquad+K_{mn}(\tau_{32})K^0_{mn}(\tau_{41})+K_{mn}(\tau_{13})K^0_{mn}(\tau_{42})\Bigg].\end{aligned} \tag{E.35}$$

The $\widetilde{B}_1$ and $\widetilde{B}_3$ terms are more complicated then the rest, as the sum over the permutations of the imaginary time indices is restricted. For the remaining terms, as in $\widetilde{B}_2$, we may consider the sum of all possible permutations of the imaginary time index because each of the MF operators appearing in the averages is unique. For B_4, we begin our reduction with L_{np}, as the resulting equation is simpler in the low temperature limit. We find

$$\begin{aligned}\widetilde{B}_4 = \sum_{P\{1,2,3,4\}}\Bigg[&D_{mn\ mn}K^{mn}_{np}(\tau_{43};\tau_{12};\tau_{41})-D_{mp\ mp}K^{mp}_{np}(\tau_{23};\tau_{12};\tau_{41}) \\ &+D_m\Big(K^{mn}_{np}(\tau_{43};\tau_{42})-K^{mp}_{np}(\tau_{23};\tau_{42})\Big)\Bigg].\end{aligned} \tag{E.36}$$

The final two functions are given by

$$\widetilde{B}_5 = \sum_{P\{1,2,3,4\}} \Big[D_{mp\ mp} K^{mp}_{mn}(\tau_{21};\tau_{23};\tau_{42}) - D_{mn\ nm} K^{mp}_{mn}(\tau_{41};\tau_{43};\tau_{42}) \\ - D_{np\ np} K^{mp}_{mn}(\tau_{41};\tau_{23};\tau_{42}) + D_m K^{mp}_{mn}(\tau_{21};\tau_{43}) \Big], \tag{E.37}$$

$$B_6 = \sum_{P\{1,2,3,4\}} \Big[D_{mq\ qm} K^{np}_{mn}(\tau_{21};\tau_{32};\tau_{34}) + D_{qp} \Big({}_{qp}K^{mp}_{mn}(\tau_{21};\tau_{42};\tau_{34}) \\ - {}_{qp}K^{np}_{mn}(\tau_{41};\tau_{42};\tau_{34}) \Big) + D_{qn\ qn} K^{np}_{mn}(\tau_{41};\tau_{32};\tau_{34}) \Big].$$

In Fourier space, the fourth order cumulant becomes

$$M_4(\{\omega_{r_i}\}) = \prod_{i=1}^{4} \int_0^\beta d\tau_i e^{i\omega_{r_i}\tau_i} M_4(T_\tau S_1 S_2 S_3 S_4) \tag{E.38}$$
$$= \mathscr{F}\{\langle T_\tau S_1 S_2 S_3 S_4\rangle_0\} - \frac{\beta}{6} \sum_{P\{\omega_{r_i}\}} M_3(\omega_{r_1},\omega_{r_2},\omega_{r_3}) \langle S_4\rangle_0 \delta_{\omega_{r_4},0}$$
$$- \frac{\beta^2}{4} \sum_{P\{\omega_{r_i}\}} M_2(\omega_{r_1},\omega_{r_2}) \langle S\rangle_0^2 \delta_{\omega_{r_1}+\omega_{r_2}} \delta_{\omega_{r_3}} \delta_{\omega_{r_4}}$$
$$- \frac{1}{8} \sum_{P\{\omega_{r_i}\}} M_2(\omega_{r_1},\omega_{r_2}) M_2(\omega_{r_3},\omega_{r_4}) - \beta^4 \langle S\rangle_0^4 \prod_{i=1}^{4} \delta_{\omega_{r_i},0}$$

We find

$$\widetilde{B}_1 = \beta D_{mn} \sum_{P\{\omega_{r_i}\}} {}_{nm}K^{mn}_{mn}(\omega_{r_1};\omega_{r_1}+\omega_{r_2};\omega_{r_3}) \delta_{\sum \omega_{r_i},0} \tag{E.39}$$
$$+ \beta^2 D_m \sum_{P\{\omega_{r_i}\}} K^{nm}_{mn}(\omega_{r_1};\omega_{r_2}) \delta_{\omega_{r_1}+\omega_{r_2}+\omega_{r_3},0} \delta_{\omega_{r_4},0}$$
$$- \frac{\beta^3 D_m}{4} \sum_{P\{\omega_{r_i}\}} K_{mn}(\omega_{r_1}) \delta_{\omega_{r_1}+\omega_{r_2},0} \delta_{\omega_{r_3},0} \delta_{\omega_{r_4},0},$$

$$\widetilde{B}_2 = - \sum_{P\{\omega_{r_i}\}} \Big[2\beta D_{mn\ mn} K^{mn}_{nm}(\omega_{r_1};\omega_{r_2}+\omega_{r_3};\omega_{r_2}) \delta_{\omega_{r_1}+\omega_{r_2}+\omega_{r_3}+\omega_{r_4},0} \tag{E.40}$$
$$+ \beta^2 (D_m + D_n) K^{mn}_{nm}(\omega_{r_2};\omega_{r_3}) \delta_{\omega_{r_1},0} \delta_{\omega_{r_2}+\omega_{r_3}+\omega_{r_4},0} \Big],$$

$$\begin{aligned}\widetilde{B}_3 =&\beta D_{mn}\sum_{P\{\omega_{r_i}\}} {}_{mn}K^{nm}_{nm}(\omega_{r_1};\omega_{r_2};\omega_{r_3})\delta_{\sum\omega_{r_i},0} \\ &-\frac{\beta^2 D_n}{2}\sum_{P\{\omega_{r_i}\}} K^{mn}_{nm}(\omega_{r_1};\omega_{r_3})\delta_{\omega_{r_1}+\omega_{r_2},0}\delta_{\omega_{r_3}+\omega_{r_4},0} \\ &+\frac{\beta^2 D_m}{2}\sum_{P\{\omega_{r_i}\}} K^{mn}_{mn}(\omega_{r_1};\omega_{r_3})\delta_{\omega_{r_1}+\omega_{r_2},0}\delta_{\omega_{r_3}+\omega_{r_4},0},\end{aligned} \tag{E.41}$$

$$\widetilde{B}_4 = \sum_{P\{\omega_{r_i}\}}\Bigg[\beta\Bigg(D_{mn\ mn}K^{mn}_{np}(\omega_{r_1};\omega_{r_2};\omega_{r_2}+\omega_{r_3})+D_{mp\ pm}K^{mp}_{np}(\omega_{r_1};\omega_{r_1}+\omega_{r_2};\omega_{r_3})\Bigg)\delta_{\sum\omega_{r_i},0} \tag{E.42}$$

$$-\beta^2 D_m K^{pm}_{mn}(\omega_{r_1};\omega_{r_2})\delta_{\omega_{r_1}+\omega_{r_2}+\omega_{r_3},0}\delta_{\omega_{r_4},0}\Bigg]$$

$$\begin{aligned}\widetilde{B}_5 = \sum_{P\{\omega_{r_i}\}}\Bigg[&\beta\Bigg(D_{mp\ mp}K^{pm}_{nm}(\omega_{r_1};\omega_{r_2};\omega_{r_3})+D_{mn\ mn}K^{pm}_{nm}(\omega_{r_1};\omega_{r_2};\omega_{r_3}) \\ &-D_{np\ np}K^{pm}_{nm}(\omega_{r_1};\omega_{r_2};\omega_{r_1}+\omega_{r_3})\Bigg)\delta_{\sum\omega_{r_i},0} \\ &+\beta^2 D_m K^{mp}_{mn}(\omega_{r_1};\omega_{r_3})\delta_{\omega_{r_1}+\omega_{r_2},0}\delta_{\omega_{r_3}+\omega_{r_4},0}\Bigg]\end{aligned}$$

$$\begin{aligned}B_6 = \sum_{P\{\omega_{r_i}\}}\beta\Bigg[&D_{mq\ mq}K^{np}_{nm}(\omega_{r_1};\omega_{r_2}+\omega_{r_3};\omega_{r_2}) \\ &+D_{qp}\Bigg({}_{qp}K^{mp}_{nm}(\omega_{r_1};\omega_{r_2}+\omega_{r_3};\omega_{r_2})-{}_{qp}K^{pn}_{nm}(\omega_{r_1};\omega_{r_2};\omega_{r_3})\Bigg) \\ &+D_{qn\ qn}K^{pn}_{nm}(\omega_{r_1};\omega_{r_2};\omega_{r_2}+\omega_{r_3})\Bigg]\delta_{\sum\omega_{r_i},0}\end{aligned}$$

In the final term of $\widetilde{B}_4$, we have permuted the Matsubara frequencies, and made use of the fact that under the delta function $\omega_{r_3}=-\omega_{r_1}-\omega_{r_2}$, to obtain

$$\sum_{P\{\omega_{r_i}\}}\Bigg(K^{mn}_{np}(\omega_{r_1};\omega_{r_2})+K^{pm}_{np}(\omega_{r_1};\omega_{r_2})\Bigg)\delta_{\omega_{r_1}+\omega_{r_2}+\omega_{r_3},0}=-\sum_{P\{\omega_{r_i}\}}K^{pm}_{mn}(\omega_{r_1};\omega_{r_2})\delta_{\omega_{r_1}+\omega_{r_2}+\omega_{r_3},0}. \tag{E.43}$$

This facilitates taking the low temperature limit, which we now consider. Some tedious algebra will show that, as was the case with the previous cumulants, all the terms in M_4 involving lower

order cumulants cancel with terms in $\langle S_1 S_2 S_3 S_4 \rangle_0$. We are left with

$$\begin{aligned}\lim_{T\to 0} M_4(\{\omega_{r_i}\}) \approx & \sum_{m\neq n} c_{mm}^2 |c_{mn}|^2 B_1 + \sum_{n>m} c_{mm} c_{nn} |c_{mn}|^2 B_2 \\ & + \sum_{n>m} |c_{mn}|^4 B_3 + \sum_{m\neq n\neq p} c_{mm} c_{mn} c_{np} c_{pm} B_4 \\ & + \sum_{p>n>m} |c_{mn}|^2 |c_{mp}|^2 B_5 + \sum_m \sum_{n>m} \sum_{\substack{p>m \\ p\neq n}} \sum_{\substack{q>m \\ q\neq n,p}} c_{mn} c_{np} c_{pq} c_{qm} B_6,\end{aligned} \tag{E.44}$$

where

$$\begin{aligned}
B_1 =& \beta D_{mn} \sum_{P\{\omega_{r_i}\}} {}_{nm}K^{mn}_{mn}(\omega_{r_1}; \omega_{r_1}+\omega_{r_2}; \omega_{r_3}) \delta_{\sum \omega_{r_i},0} \\
B_2 =& -2\beta D_{mn} \sum_{P\{\omega_{r_i}\}} {}_{mn}K^{mn}_{nm}(\omega_{r_1}; \omega_{r_2}+\omega_{r_3}; \omega_{r_2}) \delta_{\sum \omega_{r_i},0} \\
B_3 =& \beta D_{mn} \sum_{P\{\omega_{r_i}\}} {}_{mn}K^{nm}_{nm}(\omega_{r_1}; \omega_{r_2}; \omega_{r_3}) \delta_{\sum \omega_{r_i},0} \\
B_4 =& \sum_{P\{\omega_{r_i}\}} \beta \left(D_{mn\ mn}K^{mn}_{np}(\omega_{r_1}; \omega_{r_2}; \omega_{r_2}+\omega_{r_3}) + D_{mp\ pm}K^{mp}_{np}(\omega_{r_1}; \omega_{r_1}+\omega_{r_2}; \omega_{r_3}) \right) \delta_{\sum \omega_{r_i},0} \\
B_5 =& \beta \sum_{P\{\omega_{r_i}\}} \Big[D_{mp\ mp}K^{pm}_{nm}(\omega_{r_1}; \omega_{r_2}; \omega_{r_3}) \delta_{\sum \omega_{r_i},0} + D_{mn\ mn}K^{pm}_{nm}(\omega_{r_1}; \omega_{r_2}; \omega_{r_3}) \delta_{\sum \omega_{r_i},0} \\
& - D_{np\ np}K^{pm}_{nm}(\omega_{r_1}; \omega_{r_2}; \omega_{r_1}+\omega_{r_3}) \delta_{\sum \omega_{r_i},0} \Big] \\
B_6 =& \beta \sum_{P\{\omega_{r_i}\}} \Big[D_{mq\ mq}K^{np}_{nm}(\omega_{r_1}; \omega_{r_2}+\omega_{r_3}; \omega_{r_2}) \delta_{\sum \omega_{r_i},0} \\
& + D_{qp} \left({}_{qp}K^{mp}_{nm}(\omega_{r_1}; \omega_{r_2}+\omega_{r_3}; \omega_{r_2}) - {}_{qp}K^{pn}_{nm}(\omega_{r_1}; \omega_{r_2}; \omega_{r_3}) \right) \delta_{\sum \omega_{r_i},0} \\
& + D_{qn\ qn}K^{pn}_{nm}(\omega_{r_1}; \omega_{r_2}; \omega_{r_2}+\omega_{r_3}) \delta_{\sum \omega_{r_i},0} \Big]
\end{aligned} \tag{E.45}$$

Making use of the population factors, this further reduces to

$$\lim_{T\to 0} M_4(\{\omega_{r_i}\}) \approx \sum_{n>1} c_{11}^2 |c_{1n}|^2 B_{1a}^0 + \sum_{n>1} c_{nn}^2 |c_{1n}|^2 B_{1b}^0 + \sum_{n>1} c_{11}c_{nn}|c_{1n}|^2 B_2^0 + \sum_{n>1} |c_{1n}|^4 B_3^0$$

$$+ \sum_{n\neq p>1} c_{11}c_{1n}c_{np}c_{p1}B_{4a}^0 + \sum_{m\neq p>1} c_{mm}c_{m1}c_{1p}c_{pm}B_{4b}^0 + \sum_{m\neq n>1} c_{mm}c_{mn}c_{n1}c_{1m}B_{4c}^0 \tag{E.46}$$

$$+ \sum_{p>n>1} |c_{1n}|^2|c_{1p}|^2 B_5^0(\{\omega_{r_i}\}) + \sum_{n>1}\sum_{\substack{p>1\\p\neq n}}\sum_{\substack{q>1\\q\neq n,p}} c_{1n}c_{np}c_{pq}c_{q1}B_6^0,$$

where

$$\begin{aligned}
B_{1a}^0 =& \beta \sum_{P\{\omega_{r_i}\}} {}_{n1}K_{1n}^{1n}(\omega_{r_1};\omega_{r_1}+\omega_{r_2};\omega_{r_3})\delta_{\sum\omega_{r_i},0} \\
B_{1b}^0 =& -\beta \sum_{P\{\omega_{r_i}\}} {}_{1n}K_{n1}^{n1}(\omega_{r_1};\omega_{r_1}+\omega_{r_2};\omega_{r_3})\delta_{\sum\omega_{r_i},0} \\
B_2^0 =& -2\beta \sum_{P\{\omega_{r_i}\}} {}_{1n}K_{n1}^{1n}(\omega_{r_1};\omega_{r_2}+\omega_{r_3};\omega_{r_2})\delta_{\sum\omega_{r_i},0} \\
B_3^0 =& \beta \sum_{P\{\omega_{r_i}\}} {}_{1n}K_{n1}^{n1}(\omega_{r_1};\omega_{r_2};\omega_{r_3})\delta_{\sum\omega_{r_i},0} \\
B_{4a}^0 =& \beta \sum_{P\{\omega_{r_i}\}} \left[{}_{1n}K_{np}^{1n}(\omega_{r_1};\omega_{r_2};\omega_{r_2}+\omega_{r_3}) + {}_{p1}K_{np}^{1p}(\omega_{r_1};\omega_{r_1}+\omega_{r_2};\omega_{r_3}) \right] \delta_{\sum\omega_{r_i},0} \\
B_{4b}^0 =& -\beta \sum_{P\{\omega_{r_i}\}} {}_{m1}K_{1p}^{m1}(\omega_{r_1};\omega_{r_2};\omega_{r_2}+\omega_{r_3})\delta_{\sum\omega_{r_i},0} \\
B_{4c}^0 =& -\beta \sum_{P\{\omega_{r_i}\}} {}_{1m}K_{n1}^{m1}(\omega_{r_1};\omega_{r_1}+\omega_{r_2};\omega_{r_3})\delta_{\sum\omega_{r_i},0} \\
B_5^0 =& \beta \sum_{P\{\omega_{r_i}\}} \left[{}_{1p}K_{n1}^{p1}(\omega_{r_1};\omega_{r_2};\omega_{r_3}) + {}_{1n}K_{n1}^{p1}(\omega_{r_1};\omega_{r_2};\omega_{r_3}) \right] \delta_{\sum\omega_{r_i},0} \\
B_6^0 =& \beta \sum_{P\{\omega_{r_i}\}} {}_{1q}K_{n1}^{np}(\omega_{r_1};\omega_{r_2}+\omega_{r_3};\omega_{r_2})\delta_{\sum\omega_{r_i},0}.
\end{aligned} \tag{E.47}$$